

RELAY COOPERATION IN MULTIACCESS NETWORKS

By

LALITHA SANKAR

**A Dissertation submitted to the
Graduate School—New Brunswick
Rutgers, The State University of New Jersey
in partial fulfillment of the requirements
for the degree of
Doctor of Philosophy
Graduate Program in Electrical and Computer Engineering**

**Written under the direction of
Prof. Narayan Mandayam
and approved by**

New Brunswick, New Jersey

October, 2007

ABSTRACT OF THE DISSERTATION

Relay Cooperation in Multiaccess Networks

by Lalitha Sankar

Dissertation Director: Prof. Narayan Mandayam

Cooperation in communication networks results when terminals use their energy and bandwidth resources to mutually enhance their transmissions. Cooperation can be induced in many ways and each approach entails a different tradeoff of power, bandwidth, complexity, and costs to achieve spatial diversity gains characteristic of antenna arrays. In this dissertation, we study a specific cooperative network - a *multiaccess relay channel* (MARC) where cooperation is induced via a dedicated relay node in a network where multiple users communicate with one destination.

We extend the relaying strategies of *decode-and-forward* (DF), *compress-and-forward* (CF), and *amplify-and-forward* (AF) to the MARC. Specifically, for DF we show that real-time decoding at the destination using a *sliding-window* incurs a rate loss relative to an offline *backward decoding* technique. We develop an *offset encoding* technique that improves *sliding window* decoding and achieves the corner points of the *backward decoding* rate region with significantly smaller delay.

Next we compare two approaches to inducing cooperation in a multiaccess channel. In one approach we allow the users to cooperate while in the other we induce cooperation via a relay when the users cannot or do not cooperate. Using the total transmit and processing power consumed at all nodes as a cost metric, we compare the DF and AF sum-rates and outage probabilities for the two networks. Our results

show that cooperation is most desirable in the regime where processing power is significantly smaller than the transmit power. We also show that relay cooperation is on average more energy efficient than user cooperation.

Finally, we develop a capacity result for the MARC. The MARC belongs to a class of multi-terminal networks whose capacity is, in general, not known. For a degraded Gaussian K -user MARC, we use *max-min optimization* techniques to show that DF achieves the K -user sum-capacity.

Acknowledgements

I would like to thank my thesis adviser, Professor Narayan Mandayam, for his advice and support at every stage of my doctoral program. I have benefitted tremendously from his care, guidance, and the numerous opportunities he created for me. I would also like to thank Dr. Gerhard Kramer of Bell Labs for his insight, inspiration, and guidance over a significant period of my doctoral studies. I am deeply grateful for his patience and efforts in teaching me the art of research and writing.

My thanks also go to Professor Roy Yates for his invaluable advice and insightful suggestions. I am particularly appreciative of the many hours he has spent discussing research with me and thank him for agreeing to be on my committee. I also wish to thank my committee members Professors Predrag Spasojevic and Vince Poor. I have immensely benefitted from my interactions with them.

I am fortunate to have been exposed to diverse viewpoints and ideas at WINLAB and also thank Professors Wade Trappe, Chris Rose, Dipankar Raychaudhuri, and Dick Frenkiel for making this possible. The collegial and enriching environment of WINLAB will always stay with me as a model worthy of emulation. Special thanks go to my friend Professor Larry Greenstein for his advice, encouragement, and for many lively political discussions.

My fellow students immensely enriched my graduate experience at WINLAB. I have wonderful memories of long discussions with Jasvinder Singh, Joydeep Acharya, Rito Roy, Hithesh Nama, Suhas Mathur, and Chandru Raman. Sumathi Gopal became a good friend and I thank her for many interesting conversations. My thanks also go to Ivana Marić, Ruoheng Liu, Dragan Samardzija, Sachin Ganu, Silvija Kokalj-Filipovic, Omer Ileri, Kemal Karakayali, Füzuzan Atay, and Pandurang Kamat for helping me understand and appreciate a diverse set of topics.

As always, I cannot thank my parents enough for their love and support and for

being incredible role models. My best friend and sister, Viji, has my utmost gratitude for always being there for me. My extended family deserves a special mention for their love and support as do my dear friends Yamuna, Priya, Shantha, and Bettina.

Finally, this thesis would not have been possible without the love, support, unshakeable faith, and immense patience, wisdom, and humor of my best friend and husband, Raj. Words cannot capture my joy and amazement at sharing my life with such an incredible human.

Dedication

To my parents

and

Raj

Table of Contents

Abstract	ii
Acknowledgements	iv
Dedication	vi
List of Figures	xi
1. Introduction	1
1.1. Motivation	1
1.2. Hierarchical Relay Cooperation	3
1.3. Outline of Dissertation	5
2. Multiaccess Relay Channel: Capacity Theorems and Cooperative Strategies	6
2.1. Introduction	6
2.2. Model and Preliminaries	7
2.2.1. Network Model	7
2.2.2. Fading Models	10
2.3. Outer Bounds	11
2.4. Achievable Strategies	12
2.4.1. Decode-and-Forward Strategy	12
2.4.2. Compress-and-Forward Strategy	14
2.4.3. Partial Decode-and-Forward Strategy	19
2.4.4. Mixed Strategy – PDF and CF	21
2.4.5. Amplify-and-Forward Strategy	24
2.5. Illustration of Results	25
2.5.1. No Fading or Line-of-sight Model	26

MARC	26
Half-Duplex MARC	29
2.5.2. Ergodic Phase Fading	30
MARC	30
Half-Duplex MARC	31
Effect of Transmit SNR	32
2.6. Conclusions	33
3. Offset Encoding for Multiaccess Relay Channels	34
3.1. Introduction	34
3.2. Preliminaries	36
3.2.1. Model and Notation	36
3.2.2. Random Code Construction	36
3.3. Decode-and-Forward	38
3.3.1. Backward Decoding	38
3.3.2. Sliding-Window Decoding	39
3.4. Offset Encoding	42
3.4.1. Two Users with Joint Decoding	43
3.4.2. K Users with Successive Decoding	45
3.5. Conclusions	48
4. User vs. Relay Cooperation in a Multiaccess Network	49
4.1. Introduction	49
4.2. Channel and Network Models	53
4.2.1. Network Model	53
4.2.2. Hierarchical Relay Network	56
4.2.3. Cooperative Network	56
4.2.4. Cost Metric: Total Power	58

4.2.5.	Fading Models	60
4.3.	Cooperative Strategies	61
4.3.1.	Partial- and Dynamic- Decode-and-Forward	61
	MARC with Time-Duplexed Sources	61
	Time-Duplexed MAC-GF – Two-Hop Scheme	66
	Time-Duplexed MAC-GF – Multi-Hop Scheme	69
4.3.2.	Amplify-and-Forward	72
	Two-hop User- and Relay-Cooperative Networks	73
	Multi-hop Cooperative Network	76
4.4.	Illustration of Results	79
4.4.1.	Achievable Rates: PDF	81
4.4.2.	Achievable Rates: AF	86
4.4.3.	Outage Probability: DDF	88
4.4.4.	Outage Probability: AF	92
4.4.5.	Relay Position	93
4.5.	Conclusions	97
5.	Sum-Capacity of Degraded Gaussian Multiaccess Relay Channels . . .	100
5.1.	Introduction	100
5.2.	Channel Model and Preliminaries	101
5.3.	Outer Bounds	103
5.4.	Decode-and-Forward	104
5.5.	Converse	114
5.5.1.	Average Transmit Power Constraint	123
5.6.	Concluding Remarks	123
	Appendix A. Partial Decode-and-Forward: Coding Theorem	125

Appendix B. DF Rate Region: Coding Theorems	131
B.1. Backward Decoding Analysis	131
B.2. Sliding-Window Joint Decoding Analysis	133
B.3. Sliding-Window Successive Decoding Analysis	135
Appendix C. MARC and MAC-GF: Rate and Outage Derivations	138
C.1. PDF Rate Region for User and Relay Cooperative Networks	138
C.1.1. Two-hop Scheme	138
C.1.2. Multi-hop Scheme	142
C.2. Hypoexponential Distribution	145
C.3. Half-Duplex Relay Channel – DDF Outage Analysis	146
C.3.1. Upper and Lower Bounds	148
C.4. Two-hop Cooperative Network – Outage Analysis under DDF	150
C.4.1. Upper and Lower Bounds	150
C.5. Multi-hop Cooperative Network – Outage Analysis under DDF	152
C.5.1. Upper and Lower Bounds	154
Appendix D. Degraded Gaussian MARC : Concavity Properties	156
D.1. Concavity of $I_{d,S}$	156
D.2. $B_{r,S}$ vs. $\underline{\gamma}_{\mathcal{K}}$	159
References	162
Curriculum Vitae	168

List of Figures

1.1. An example of a three-layer hierarchical relay network with source nodes (SN), forwarding nodes (FN) and access points (AP).	3
2.1. A K -user multiaccess relay channel.	8
2.2. A two-user Gaussian MARC with a full-duplex relay.	9
2.3. A two-user Gaussian MARC with a half-duplex relay.	10
2.4. Block Markov encoding for CF and a two-user MARC.	15
2.5. Block Markov Encoding for the PDF strategy for a two-user MARC. .	19
2.6. Block Markov encoding for the mixed PDF and CF strategy for a two-user MARC.	22
2.7. Two example geometries.	26
2.8. Inner and outer bounds on the sum rate $R_1 + R_2$ for Case 1 and the no fading model.	27
2.9. Inner and outer bounds on the sum rate $R_1 + R_2$ for Case 2 and the no fading model.	27
2.10. Inner and outer bounds on the sum rate $R_1 + R_2$ for the half-duplex MARC of Case 1.	29
2.11. Inner and outer bounds on the sum rate $R_1 + R_2$ for the half-duplex MARC of Case 2	30
2.12. Inner and outer bounds on the sum rate $R_1 + R_2$ for the MARC and half-duplex MARC of Case 2 under ergodic fading	31
3.1. A K -user multiaccess relay channel.	35
3.2. Regular encoding for a two-user MARC assuming the relay decodes correctly.	36

3.3. Example of a rate region achieved by DF and backward decoding for a two-user MARC.	38
3.4. Offset encoding for a K -user MARC assuming the relay decodes correctly.	40
3.5. Rate region with sliding-window decoding and offset encoding.	46
4.1. A two-user Gaussian MARC.	54
4.2. A two-user multiaccess channel with generalized feedback.	55
4.3. Time-duplexed transmission schemes for the MARC, the MAC-GF, and the MAC.	57
4.4. Encoding scheme for a two-hop AF strategy.	74
4.5. AF encoding for user k in a K -user multi-hop cooperative network.	77
4.6. Planar sector of a circle with the destination at the origin and 100 randomly chosen locations for a two-user multiaccess network.	80
4.7. Two user PDF sum-rate $R_1 + R_2$ vs. P_1 (sub-plot 1) and vs. P_{tot} (sub-plot 2) for $\eta = .01$	81
4.8. Two user PDF sum-rate $R_1 + R_2$ vs. P_{tot} for $\eta = .5$ (sub-plot 1) and $\eta = 1$ (sub-plot 2).	82
4.9. Two user PDF energy efficiency $(R_1 + R_2) / P_{tot}$ in bits/Joule vs. P_1 for $\eta = .01$ (sub-plot 1), $.5$ (sub-plot 2), and 1 (sub-plot 3).	82
4.10. Three user PDF sum-rate $R_1 + R_2 + R_3$ vs. P_1 (sub-plot 1) and vs. P_{tot} for $\eta = .01$ (sub-plot 2).	84
4.11. Three-user PDF sum-rate $R_1 + R_2 + R_3$ vs. P_{tot} for $\eta = .5$ (sub-plot 1) and $\eta = 1$ (sub-plot 2).	84
4.12. Three user PDF energy efficiency $(R_1 + R_2 + R_3) / P_{tot}$ vs. P_{tot} for $\eta = .01$ (sub-plot 1), $.5$ (sub-plot 2), and 1 (sub-plot 3).	85
4.13. Two user AF sum-rate $R_1 + R_2$ vs. P_1 (sub-plot 1) and vs. P_{tot} (sub-plot 2) for $\eta = .01$	87

4.14. Two user AF sum-rate $R_1 + R_2$ vs. P_{tot} for $\eta = .5$ (sub-plot 1) and $\eta = 1$ (sub-plot 2).	87
4.15. Two user AF energy efficiency $(R_1 + R_2)/P_{tot}$ vs. P_{tot} for $\eta = .01$ (sub-plot 1), $.5$ (sub-plot 2), and 1 (sub-plot 3).	89
4.16. Two user DDF outage probability P_{out} vs. P_1 (sub-plot 1) and vs. P_{tot} for $\eta = 0.01$ (sub-plot 2).	90
4.17. Two user DDF outage probability P_{out} vs. P_{tot} for $\eta = 0.5$ (sub-plot 1) and for $\eta = 1$ (sub-plot 2).	90
4.18. Three user DDF outage probability P_{out} vs. P_1 (sub-plot 1) and vs. P_{tot} for $\eta = 0.01$ (sub-plot 2).	91
4.19. Three user DDF outage probability P_{out} vs. total transmit SNR P_{tot} in dB for $\eta = 0.5$ (sub-plot 1) and $\eta = 1$ (sub-plot 2).	91
4.20. Two-hop three user DDF Outage Probability P_{out} vs. P_1 (sub-plot 1) and P_{tot} (sub-plot 2).	92
4.21. Two user AF outage probability P_{out} vs. P_1 (sub-plot 1) and vs. P_{tot} for $\eta = .01$ (sub-plot 2).	93
4.22. Two user AF outage probability P_{out} vs. P_{tot} for $\eta = 0.5$ (sub-plot 1) and for $\eta = 1$ (sub-plot 2).	94
4.23. Three user AF outage probability P_{out} vs. P_1 (sub-plot 1) and P_{tot} for $\eta = 0.01$ (sub-plot 2).	94
4.24. Three user AF outage probability P_{out} vs. P_{tot} for $\eta = 0.5$ (sub-plot 1) and $\eta = 1$ (sub-plot 2).	95
4.25. Two user PDF sum-rate $R_1 + R_2$ vs. P_1 (sub-plot 1) and P_{tot} for $\eta = 0.01$ (sub-plot 2) for relay position fixed at $(0.707, 0)$	95
4.26. Two user PDF energy efficiency $(R_1 + R_2)/P_{tot}$ vs. P_1 for $\eta = 0.01$ (sub-plot 1), $\eta = 0.5$ (sub-plot 2), and $\eta = 1$ (sub-plot 3) for relay position fixed at $(0.707, 0)$	96

4.27. Two user DF outage probability P_{out} vs. P_1 (sub-plot 1) and P_{tot} for $\eta = 0.01$ (sub-plot 2) for relay placed at $(0.707, 0)$	97
5.1. A two-user Gaussian degraded MARC.	101
5.2. A two-user stochastically degraded Gaussian MARC.	104
5.3. Five possible intersections of \mathcal{R}_r and \mathcal{R}_d for a two-user Gaussian MARC.	105
5.4. Illustration of Cases 1, 2, and 3.	108
C.1. Partial decode-and-forward encoding for a two-hop cooperative network.	139
C.2. PDF encoding for a L_k -hop cooperative network.	143
C.3. Plot of the probability distribution $p(\theta_k)$ for a collinear geometry with $d_{r,k} = .5$ and different values of \bar{P}_k	148
D.1. Rate region achieved at the destination for a two-user MARC and $\alpha_1 =$ $\alpha_2 = .5$	160

Chapter 1

Introduction

The growing demand for wireless applications is fueling research in the design and development of a variety of wireless network architectures ranging from wide-area cellular to decentralized ad-hoc and low-power sensor networks. The limitation of restricted power and bandwidth resources holds for all wireless networks, regardless of architecture. In [1], Telatar (and independently Foschini and Gans in [2]) showed that adding multiple antennas to wireless transmitters and receivers can yield dramatic gains in rate and reliability. However, restrictions in size and form factor of wireless devices largely limit the practical applicability of these results.

Cooperation is an alternative approach to this problem: cooperation results when nodes in a network share their bandwidth and power resources to mutually enhance their transmissions. This allows wireless devices constrained in size and processing capabilities to exploit the broadcast nature of the wireless medium to achieve the spatial diversity gains characteristic of multi-antenna channels [3]. In multi-terminal networks, cooperation can be induced in many ways with different approaches requiring different tradeoffs of power, bandwidth, and economic resources to achieve a desired fading diversity. In this thesis, we investigate one such approach, namely that of inducing cooperation using dedicated relay nodes.

1.1 Motivation

It is generally known that communications between a source-destination pair can benefit from cooperative forwarding by nodes overhearing the transmission [4]. A simple model for such a communication network is the relay channel introduced and studied by van der Meulen [5]. Two fundamental coding strategies for the relay channel were

developed by Cover and El Gamal [6] and are based on the idea that the relay aids the destination in decoding by transmitting a signal based on what it overhears. These coding techniques have been applied to a variety of multi-terminal wireless networks [7,8], and more recently, to quantify the rate and diversity benefits of node cooperation (see e.g., [3,9–11], [12–16] and the references therein).

In their seminal work on the throughput of wireless ad hoc networks [17], Gupta and Kumar showed that in a network of homogeneous cooperating nodes the per node throughput decreases (due to interference) with increasing number of nodes. They also showed that information-theoretic relaying schemes [6] can reverse this behavior [18] and thus provided added motivation for the information theory community to extend the relaying strategies of [6] to a variety of multi-terminal networks and channel models. For a detailed history and bibliography of cooperative communications see [4].

In the most general model of cooperation, some or all nodes in a network share their resources and some nodes called relays may be purely dedicated to aiding other nodes. The former cooperative approach has been referred to as *user cooperation* [3]; analogously, we can call the latter approach *relay cooperation*. The choice between the two models is significant because, in general, the nodes in a network can vary widely in their transmission and processing capabilities and independent nodes may not be willing to share with other nodes their limited power and bandwidth resources for forwarding and cooperation. In fact, it has been shown in an economic model that cooperating users need to be offered incentives (such as increased throughput or diversity) to share their resources voluntarily [19–21]. The user cooperation model may be better suited for special purpose homogeneous networks such as those used in military, sensor and monitoring applications; however, even in such networks where the network lifetime depends on the lifetime (battery resources) of the most connected node, it has been shown [22] and demonstrated [23] that designating some nodes as dedicated relay nodes can help preserve the lifetime of nodes that transmit data.

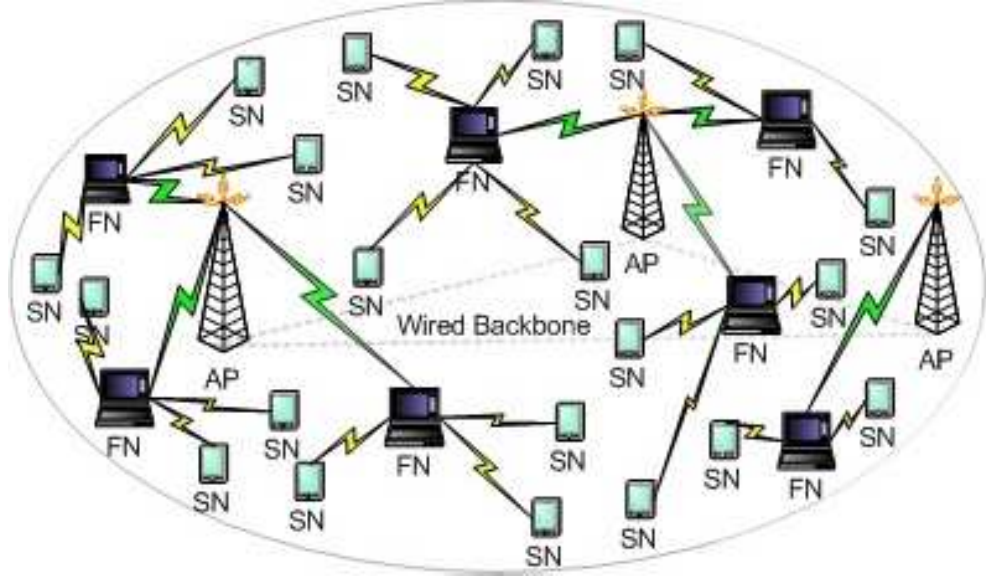


Figure 1.1: An example of a three-layer hierarchical relay network with source nodes (SN), forwarding nodes (FN) and access points (AP).

1.2 Hierarchical Relay Cooperation

Motivated by the above arguments, in this thesis, we study a specific relay cooperation model, namely, the multiaccess relay channel (MARC) where multiple sources transmit to a destination in the presence of a relay [24]. One can view the MARC as a building block of a large-scale *hierarchical relay network*, where a layer of one or more relay nodes enables cooperation between the layers containing source and destination nodes (see Fig. 1.1). Examples of such a *multi-tier* communication network [25] include hybrid wireless LAN/WAN networks and sensor networks where cooperation between user or sensor nodes is either undesirable or not possible, but an intermediate relay node can be used to aid communication between the sources and the destinations.

We present models for a discrete memoryless MARC and a Gaussian MARC. Because the MARC is a multiaccess generalization of the relay channel [5, 6], the achievable strategies developed for the relay channel extend to the MARC. In addition to the

cut-set outer bounds, we study the strategies of decode-and-forward (DF), compress-and-forward (CF), partial decode-and-forward (PDF), and amplify-and-forward (AF) [26–28]. We also present a memoryless model for a MARC with a *half-duplex* relay and extend the capacity theorems (inner and outer bounds) to this channel.

The DF rate for the relay channel can be achieved by a variety of encoding/decoding techniques. However, the DF rate region for the MARC depends on the decoding technique chosen at the destination. (Indeed, using an offline delay-intensive *backward decoding* technique at the destination achieves a larger rate region than a real-time *sliding-window* decoding technique.) We present an *offset encoding* technique that improves the rate region achieved by sliding-window decoding for K -user multiaccess channels. The technique offsets user transmissions by one block per user and achieves the corner points of the *backward decoding* rate region but with a significantly smaller delay.

Cooperation can be induced in practice in many ways and each approach may require a different tradeoff of power, bandwidth, processing, and economic resources. In order to design practical networks that derive maximal performance gains from cooperation, it is necessary to understand the similarities and differences between the user and relay cooperation models. We compare the performance of source cooperation in a multiaccess network to that of using a wireless relay. The former is modeled as a multiaccess channel with generalized feedback [7, Chap. 7] and the latter as a MARC. In general, it is hard to quantify the costs associated with the two cooperative approaches. We present a power-based cost metric to enable comparisons and determine the energy regimes where the two approaches to cooperation may be desirable.

Using the total transmit and processing power consumed as a cost metric, we compare the PDF and AF rates and the DF and AF outage probabilities for an area-averaged geometry. We show that both user and relay cooperation is energy efficient only in the regime where the processing power is negligible relative to the transmit power. We

also show that relay cooperation is (on average) more energy efficient than user cooperation. Finally, using a geometry-inclusive outage analysis, we show that for single antenna nodes, the relay network is limited in diversity to a maximum of 2 while a K -user cooperative network can achieve a maximum of K at the cost of using the channel K times. However, the K -fold diversity gains diminishes when one accounts for the processing costs of cooperation, i.e., the maximum diversity predicted by a diversity-multiplexing tradeoff analysis may not always be achievable in practical SNR regimes of interest without trading off power, delay, and complexity.

Finally, we develop a capacity result for the MARC. Cooperative networks belong to a large class of multi-terminal networks whose capacities have been a long-standing open problem in network information theory. In [6], Cover and El Gamal show that DF achieves capacity for a degraded relay channel. For a degraded MARC, unlike the relay channel, applying the degradedness condition does not simplify the outer bounds to match those for DF. Specifically for a degraded Gaussian MARC, we use a max-min optimization technique to show that DF achieves the K -user sum-capacity.

1.3 Outline of Dissertation

The rest of the dissertation is organized as follows. In Chapter 2 we present various MARC models and their inner and outer bounds. In Chapter 3 we present an off-set encoding technique that improves sliding-window decoding with DF for K -user multiaccess channels. In 4, we compare the performance of source cooperation in a multiaccess network with that of one that uses a wireless relay. Finally, in Chapter 5, we develop the sum-capacity of a degraded Gaussian MARC.

Chapter 2

Multiaccess Relay Channel: Capacity Theorems and Cooperative Strategies

2.1 Introduction

The multiaccess relay channel (MARC) is a network where several users communicate with a single destination in the presence of a relay [24]. Recently, there has been an increased focus on networks with one or more relays as models for wireless ad hoc and sensor networks, see for e.g., [9, 10, 12, 13, 18] and the references therein. Successful deployment of any such network lies in its ability to support multiple users simultaneously and not only one. We study the MARC as a specific model of a multi-user relay network.

Several coding strategies for the relay channel [5, 6] extend readily to the MARC [10, 26]. For example, the strategy of [6, Theorem 1], now often called *decode-and-forward* (DF), has a relay that decodes user messages before forwarding them to the destination [10, 26]. Similarly, the strategy in [6, Theorem 6], now often called *compress-and-forward* (CF), has the relay quantize its output symbols and transmit the resulting quantization bits to the destination [26]. For Gaussian channels, one can also consider an *amplify-and-forward* strategy where the relay forwards a scaled version of its output symbols to the destination [26].

In this chapter, we present models for a discrete memoryless and a Gaussian MARC with a *full-duplex* relay, i.e., a relay that can transmit and receive simultaneously in the same bandwidth. We also present a memoryless model for a MARC with a *half-duplex* relay and obtain the capacity theorems for this channel as a straightforward extension of those developed for the full-duplex case. We present a cut-set outer bound on the capacity region of the MARC and develop the rate regions for DF, CF, and AF. We also

present a *partial decode-and-forward* (PDF) strategy where the relay decodes only a part of the messages from the sources. This strategy generalizes DF and is particularly useful when there may be costs associated with relay cooperation. We also present a mixed strategy that combines DF and CF as a generalization of [6, Theorem 7]. For the Gaussian MARC, we focus on the line-of-sight and ergodic fading environments and study the rate regions achieved by the different strategies. Finally, we illustrate our results for two example geometries.

2.2 Model and Preliminaries

2.2.1 Network Model

The K -user MARC has K sources, one relay, and one destination (see Fig. 2.1). The sources emit the messages W_k , $k = 1, 2, \dots, K$, that are statistically independent and take on values uniformly in the sets $\{1, 2, \dots, M_k\}$. The channel is used N times so that the rate of W_k is $R_{W_k} = B_{W_k}/N$ bits per channel use where $B_{W_k} = \log_2 M_k$ bits. The channel input $X_{k,i}$ from source k at time i , $i = 1, 2, \dots, N$, is a function of W_k , while the relay's channel input $X_{r,i}$ is a causal function of its received signals $Y_r^{i-1} = (Y_{r,1}, Y_{r,2}, \dots, Y_{r,i-1})$. The destination uses the N channel outputs Y_d^N to decode the K messages as $(\hat{W}_1, \hat{W}_2, \dots, \hat{W}_K)$. We write $\mathcal{K} = \{1, 2, \dots, K\}$ for the set of sources, $\mathcal{T} = \{1, 2, \dots, K, r\}$ for the set of transmitters, and $\mathcal{D} = \{r, d\}$ for the set of receivers. We write $X_{\mathcal{S}} = \{X_k : k \in \mathcal{S}\}$ for all $\mathcal{S} \subseteq \mathcal{K}$, \mathcal{S}^c to denote the complement of \mathcal{S} in \mathcal{K} , and $|\mathcal{S}|$ for the cardinality of \mathcal{S} . The channel is time-invariant and memoryless with the conditional probability distribution

$$p(y_r, y_d | x_{\mathcal{K}}, x_r). \quad (2.1)$$

The capacity region $\mathcal{C}_{\text{MARC}}$ is the closure of the set of rate tuples $(R_{W_1}, R_{W_2}, \dots, R_{W_K})$ for which the destination can, for sufficiently large N , decode the K source messages with an arbitrarily small positive error probability.

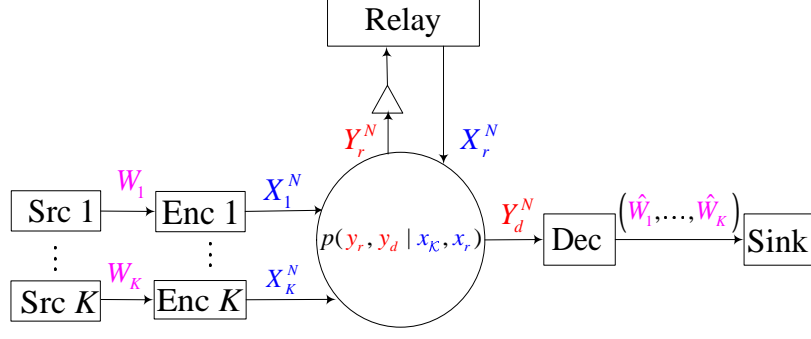


Figure 2.1: A K -user multiaccess relay channel.

As further notation, we write $R_S = \sum_{k \in S} R_k$ and we use the vector notation \underline{x}_k for length- n codewords of user k . We use the usual notation for entropy and mutual information [29, 30] and take all logarithms to the base 2 so that our rate units are bits. We write random variables (e.g. W_k) with uppercase letters and their realizations (e.g. w_k) with the corresponding lowercase letters. We drop subscripts on probability distributions if the arguments are lowercase versions of the random variables, e.g., we write (2.1) as $p(y_r, y_d | x_K, x_r)$.

For a Gaussian MARC (see Fig. 2.2), the received signals $Y_{r,i}$ and $Y_{d,i}$ are [24]

$$Y_{r,i} = \left(\sum_{k=1}^K h_{r,k,i} X_{k,i} \right) + Z_{r,i} \quad (2.2)$$

$$Y_{d,i} = \left(\sum_{k=1}^K h_{d,k,i} X_{k,i} \right) + h_{d,r,i} X_{r,i} + Z_{d,i} \quad (2.3)$$

where $Z_{r,i}$ and $Z_{d,i}$ are independent and identically distributed (i.i.d.) zero-mean, unit variance circularly symmetric (proper) complex Gaussian random variables and $h_{m,k,i}$ is the channel gain between receiver m and transmitter k at time i . Unless otherwise noted, we assume that a receiving node m knows only its own channel gains, i.e., it knows $h_{m,k,i}$ for all i and k , but it does not know $h_{m',k,i}$ for any $m' \neq m$. The transmitted signals from source k and the relay are constrained in power as

$$\sum_{i=1}^n E |X_{k,i}|^2 \leq nP_k \quad k \in \mathcal{T} \quad (2.4)$$

2. ergodic fading where $A_{m,k,i}$ are jointly i.i.d zero-mean, unit variance proper, complex Gaussian random variables for all i .

We write \underline{h} to denote the vector of fading gains, $h_{k,m,i}$, for all $k \in \mathcal{D}$, $m \in \mathcal{T}$, $k \neq m$, such that \underline{h} is a realization for a given channel use of a jointly independent and ergodic vector fading process \underline{H} .

Remark 2.1 *The no fading model can be viewed as a simplification of a Ricean channel with a large Ricean factor; i.e., we assume the line-of-sight component dominates the fading model thereby simplifying the model to a path-loss dependent Gaussian channel.*

2.3 Outer Bounds

An outer bound on the capacity region of a MARC is presented in [27] using the cut-set bounds in [30, Th. 14.10.1] as applied to the case of independent sources. We summarize the bounds below.

Proposition 2.2 *The capacity region $\mathcal{C}_{\text{MARC}}$ is contained in the union of the set of rate tuples (R_1, R_2, \dots, R_K) that satisfy, for all $\mathcal{S} \subseteq \mathcal{K}$,*

$$R_{\mathcal{S}} \leq \min (I(X_{\mathcal{S}}; Y_r Y_d | X_{\mathcal{S}^c} X_r U), I(X_{\mathcal{S}} X_r; Y_d | X_{\mathcal{S}^c} U)) \quad (2.8)$$

where the union is over all distributions

$$p(u) \cdot \left(\prod_{k=1}^K p(x_k | u) \right) \cdot p(x_r | x_{\mathcal{K}}, u) \cdot p(y_r, y_d | x_{\mathcal{K}}, x_r). \quad (2.9)$$

Remark 2.3 *The time-sharing random variable U ensures that the region in (2.8) is convex. One can apply Caratheodory's theorem [32] to this K -dimensional convex region to bound the cardinality of U as $|\mathcal{U}| \leq K + 1$.*

Remark 2.4 *For the Gaussian channel, one can verify that Gaussian signaling maximizes the outer bounds (see [6]). The bounds for the half-duplex case are obtained by conditioning the bounds in (2.8) on M_r and including the factor $p(m_r)$ in (2.9).*

2.4 Achievable Strategies

2.4.1 Decode-and-Forward Strategy

A DF code construction for the white Gaussian MARC is presented in [24]. This construction is extended to the d.m. MARC in [10] using regular Markov encoding at the sources and relay and *backward decoding* [7, p. 63] at the destination. We detail the encoding and decoding procedure in Chapter 3 and summarize the rate region below.

Proposition 2.5 *The rate region for DF is the union of the set of rate tuples (R_1, R_2, \dots, R_K) that satisfy,*

$$R_S \leq \min(I(X_S; Y_r | X_{S^c} V_K X_r U), I(X_S X_r; Y_d | X_{S^c} V_{S^c} U)) \quad \text{for all } S \subseteq \mathcal{K} \quad (2.10)$$

where the union is over all distributions that factor as

$$p(u) \cdot \left(\prod_{k=1}^K p(v_k | u) p(x_k | v_k, u) \right) \cdot p(x_r | v_K, u) \cdot p(y_r, y_d | x_T). \quad (2.11)$$

Proof: See Appendix B.1. ■

We remark that the time-sharing random variable U ensures that the region of Proposition 2.5 is convex. Further, the auxiliary random variable V_k enables cooperation between the relay and source k , for all k . Finally, one can also use a real-time *sliding-window* decoding technique at the destination to recover the corner points of the rate region achieved at the destination. This scheme has a significantly smaller delay than backward decoding where the destination waits for the entire message from all the sources before decoding. We develop this scheme in detail in Chapter 3.

The memoryless model presented in Section 2.2 for the half-duplex MARC allows us to use the rate results developed for the memoryless full-duplex MARC. Note further that we consider a *fixed* duplexing scheme where the listen and transmit fractions at the relay θ and $1 - \theta$ respectively are assumed known *a priori* at all nodes where $\theta = \Pr(M_r = L) = 1 - \Pr(M_r = T)$ and $\theta \in [0, 1]$. Thus, one can obtain the DF rate

bounds for a half-duplex MARC from Proposition 2.5 by conditioning the bounds in (2.10) over the half-duplex states of the relay as follows.

Corollary 2.6 *The DF rate region for a half-duplex MARC is the union of the set of rate tuples (R_1, R_2, \dots, R_K) that satisfy*

$$R_{\mathcal{S}} \leq \min(I(X_{\mathcal{S}}; Y_r | X_{\mathcal{S}^c} V_{\mathcal{K}} X_r M_r U), I(X_{\mathcal{S}} X_r; Y_d | X_{\mathcal{S}^c} V_{\mathcal{S}^c} M_r U)) \quad \text{for all } \mathcal{S} \subseteq \mathcal{K} \quad (2.12)$$

where the union is over all distributions

$$p(u) \cdot p(m_r) \cdot \left(\prod_{k=1}^K p(x_k, v_k | u, m_r) \right) \cdot p(x_r | u, m_r) \cdot p(y_r, y_d | x_{\mathcal{K}}, x_r) \quad (2.13)$$

such that the signaling at the relay satisfies (2.5) for $m_r \in \{L, T\}$ and

$$V_{\mathcal{K}} = \begin{cases} \emptyset & M_r = L \\ X_{\mathcal{K}} & M_r = T. \end{cases} \quad (2.14)$$

Note that the relay decodes the messages from the sources only in the *listen* fraction θ and cooperates with the sources in the *transmit* fraction $\bar{\theta} = 1 - \theta$.

Consider the Gaussian MARC with fixed channel gains. We write the signal transmitted by source k , for all $k \in \mathcal{K}$, and the relay in each channel as

$$X_k = \sqrt{\alpha_k P_k} V_k + \sqrt{(1 - \alpha_k) P_k} V_{k,0} \quad (2.15)$$

$$X_r = \sum_{k=1}^K \sqrt{\beta_k P_r} V_k + \sqrt{\bar{\beta} P_r} V_{r,0} \quad (2.16)$$

where V_k , $V_{k,0}$, and $V_{r,0}$ are independent and identically distributed (i.i.d) proper complex Gaussian random variables with zero mean and unit variance and the power fractions $\alpha_k, \beta_k \in [0, 1]$ such that

$$\bar{\beta} = 1 - \sum_{k=1}^K \beta_k. \quad (2.17)$$

Note that in general, α_k and β_k are complex. However, when the channel gains are not known at the transmitters one can show that it suffices to restrict α_k and β_k to be positive real numbers between 0 and 1 (see [33]).

For the MARC, substituting (2.15) and (2.16) in (2.10), we have

$$R_{\mathcal{S}} \leq \max_{\{\alpha_k, \beta_k\}_{k=1}^K} \min(I_{r,\mathcal{S}}, I_{d,\mathcal{S}}) \quad \text{for all } \mathcal{S} \subseteq \mathcal{K} \quad (2.18)$$

where

$$I_{r,\mathcal{S}} = C \left(\sum_{k \in \mathcal{S}} |h_{r,k}|^2 \alpha_k P_k \right) \quad (2.19)$$

$$I_{d,\mathcal{S}} = C \left((1 - \beta_{\mathcal{S}^c}) |h_{d,r}|^2 P_r + \sum_{k \in \mathcal{S}} \left(|h_{d,k}|^2 P_k + 2\sqrt{\bar{\alpha}_k \beta_k P_k P_r} \operatorname{Re}(h_{d,r} h_{d,k}^*) \right) \right) \quad (2.20)$$

where $\bar{\alpha}_k = 1 - \alpha_k$, $\beta_{\mathcal{S}^c} = \sum_{k \in \mathcal{S}^c} \beta_k$ and $C(x) = \log(1 + x)$.

For an ergodic fading channel where the transmitted signals experience all possible fading states over a message block, the DF rates are bounded as

$$R_{\mathcal{S}} \leq \max_{\{\alpha_k, \beta_k\}_{k=1}^K} \min(\mathbb{E}I_{r,\mathcal{S}}, \mathbb{E}I_{d,\mathcal{S}}) \quad (2.21)$$

where the expectation \mathbb{E} is over the joint fading process \underline{H} where $I_{r,\mathcal{S}}$ and $I_{d,\mathcal{S}}$ are given by (2.19) and (2.20) respectively. Further, one can use the fact that the transmitters do not have knowledge of the channel state to show that $1 - \alpha_k = \beta_k = 0$ maximize the rate bounds in (2.19) and (2.20) respectively [33].

Finally, for the half-duplex MARC, the rate region is achieved by simplifying (2.15) for the two modes as

$$X_k = \begin{cases} \sqrt{P_k} V_{k,0} & M_r = L \\ \sqrt{P_k} V_k & M_r = T \end{cases}. \quad (2.22)$$

The relay's signal X_r is then set to 0 for the listen fraction and to (2.16) for the transmit fraction. We obtain the DF rate region by substituting (2.22) and (2.16) in (2.12).

2.4.2 Compress-and-Forward Strategy

One can also consider a strategy where the relay compresses its received signal as in [6, Theorem 6]. The destination first decodes the compressed signal from the relay

	<u>Block 1</u>	<u>Block 2</u>	...	<u>Block B</u>	<u>Block B+1</u>
User 1	$\underline{x}_1(w_{1,1})$	$\underline{x}_1(w_{1,2})$...	$\underline{x}_1(w_{1,B})$	$\underline{x}_1(1)$
User 2	$\underline{x}_2(w_{2,1})$	$\underline{x}_2(w_{2,2})$...	$\underline{x}_2(w_{2,B})$	$\underline{x}_2(1)$
Relay	$\underline{x}_r(1)$	$\underline{x}_r(w_{r,1})$		$\underline{x}_r(w_{r,B-1})$	$\underline{x}_r(w_{r,B})$
	$\hat{y}_r(z_{r,1}, 1)$	$\hat{y}_r(z_{r,2}, w_{r,1})$...	$\hat{y}_r(z_{r,B}, w_{r,B-1})$	$\hat{y}_r(1, w_{r,B})$

Figure 2.4: Block Markov encoding for CF and a two-user MARC.

and uses that in conjunction with its own received signal to decode the source messages [34]. Note that the received and compressed signals at the relay carry messages from all the sources.

The encoding is done as follows. Consider the probability distribution

$$\left(\prod_{k=1}^K p(x_k) \right) \cdot p(x_r) \cdot p(\hat{y}_r | x_r, y_r) \cdot p(y_r, y_d | x_K, x_r). \quad (2.23)$$

For each user k , generate 2^{nR_k} codewords $\underline{x}_k(w_k)$, $w_k = 1, 2, \dots, 2^{nR_k}$, by choosing the letters $x_{k,i}(w_k)$, $i = 1, 2, \dots, n$, independently with distribution $p(x_k)$. Similarly, generate 2^{nR_r} codewords $\underline{x}_r(w_r)$, $w_r = 1, 2, \dots, 2^{nR_r}$, by choosing the letters $x_{r,i}(w_r)$ independently with distribution $p(x_r)$ for all i . For each $\underline{x}_r(w_r)$ generate $2^{nR'_r}$ codewords $\hat{y}_r(z_r)$, $z_r = 1, 2, \dots, 2^{nR'_r}$, by choosing the letters $\hat{y}_{r,i}(z_r, w_r)$ independently with distribution $p_{\hat{y}_r | X_r}(\cdot | x_{r,i}(w_r))$ for all i where $p(\hat{y}_r | x_r)$ is obtained from the distribution $p(\hat{y}_r | y_r, x_r)$ as

$$p(\hat{y}_r | x_r) = \sum_{x_K, y_r, y_d} p(x_K) p(\hat{y}_r | y_r, x_r) p(y_r, y_d | x_K, x_r). \quad (2.24)$$

Finally, we randomly partition the set $\{1, 2, \dots, 2^{nR_r}\}$ into 2^{nR_r} subsets and index them via w_r . The above code construction procedure is repeated $B + 1$ times, once for each block, and the b^{th} codebook is used in block b , $b = 1, 2, \dots, B + 1$. Note that the codebooks are independent across blocks and this fact simplifies the error analysis [8, 35].

A block Markov encoding strategy is employed where in block b , $b = 1, 2, \dots, B$, the k^{th} source transmits its independent message $w_{k,b} \in [1, 2^{nR_k}]$ via $\underline{x}_k(w_{k,b})$ while the relay transmits $\underline{x}_r(w_{r,b})$, $w_{r,b} \in [1, 2^{nR_r}]$, where R_r is the rate at which the relay forwards the compressed message $z_{r,b-1}$ from the previous block (see Fig. 2.4). In the same block, the relay also compresses its received signal \underline{y}_r as $\hat{\underline{y}}_r(z_{r,b}, w_{r,b})$, $z_{r,b} \in [1, 2^{nR_r}]$. The resulting rate region is given by the following theorem.

Theorem 2.7 *Compress-and-forward yields a rate region \mathcal{R}_{CF} given by the union of the set of rate tuples (R_1, R_2, \dots, R_K) , that satisfy*

$$R_S \leq I(X_S; \hat{Y}_r Y_d | X_{S^c} X_r U) \quad \text{for all } S \subseteq \mathcal{K} \quad (2.25)$$

where the union is over all joint distributions

$$p(u) \cdot \left(\prod_{k \in \mathcal{T}} p(x_k | u) \right) \cdot p(\hat{y}_r | y_r, x_r, u) \cdot p(y_d, y_r | x_{\mathcal{T}}) \quad (2.26)$$

and subject to the constraint

$$I(X_r; Y_d | U) \geq I(\hat{Y}_r; Y_r | X_r Y_d U). \quad (2.27)$$

Proof: For a constant U , the proof involves a relatively straightforward generalization of the decoding procedure in [6, Thm. 6] to the multiaccess problem of decoding K users at the destination [30, 14.3]. The time-sharing random variable U convexifies the rate region of Theorem 2.25. ■

Remark 2.8 *The constraint in (2.27) indicates that the rate achievable between the relay and destination limits the fidelity of the compressed signal.*

Corollary 2.9 *The CF rate region for a half-duplex relay is given by the union of the set of rate tuples (R_1, R_2, \dots, R_K) , that satisfy*

$$R_S \leq I(X_S; \hat{Y}_r Y_d | X_{S^c} X_r M_r U) \quad \text{for all } S \subseteq \mathcal{K} \quad (2.28)$$

where the union is over all distributions

$$p(u) \cdot p(m_r) \cdot \left(\prod_{k \in \mathcal{T}} p(x_k | m_r, u) \right) \cdot p(x_r | m_r, u) \cdot p(\hat{y}_r | y_r, \underline{x}_r, u) \cdot p(y_d, y_r | x_{\mathcal{K}}, x_r) \quad (2.29)$$

and subject to the constraint

$$I(X_r; Y_d | M_r U) \geq \theta I(\hat{Y}_r; Y_r | Y_d X_r M_r U). \quad (2.30)$$

Consider the Gaussian MARC with fixed channel gains. We generate proper complex Gaussian i.i.d. sequences $X_k \sim \mathcal{CN}(0, p_k)$, for all $k \in \mathcal{T}$, where p_k satisfies (2.4). Each letter in the quantized codeword $\underline{\hat{y}}_r$ is generated as

$$\hat{Y}_{r,i} = Y_{r,i} + Q_{r,i} \quad i = 1, 2, \dots, n \quad (2.31)$$

where $Q_{r,i} \sim \mathcal{CN}(0, D)$ is generated independent of $Y_{r,i}$ and $Y_{d,i}$ for all i . Using (2.2), (2.3), and (2.31), the constraint in (2.27) simplifies to yield the lower bound on the distortion D as

$$D \geq \frac{\left(\sum_{k \in \mathcal{K}} |h_{r,k}| p_k + 1 \right) \left(\sum_{k \in \mathcal{K}} |h_{d,k}| p_k + 1 \right) - \left| \sum_{k \in \mathcal{K}} h_{d,k} h_{r,k}^* p_k \right|^2}{(|h_{d,r}|^2 P_r)}. \quad (2.32)$$

Finally, the bounds in (2.25) simplify as

$$R_{\mathcal{S}} \leq \log \left(\frac{\left(\sum_{k \in \mathcal{S}} |h_{r,k}| p_k + D + 1 \right) \left(\sum_{k \in \mathcal{S}} |h_{d,k}| p_k + 1 \right) - \left| \sum_{k \in \mathcal{S}} h_{d,k} h_{r,k}^* p_k \right|^2}{D + 1} \right) \quad \text{for all } \mathcal{S} \subseteq \mathcal{K}. \quad (2.33)$$

We denote the region achieved by (2.33) as $\mathcal{R}_{CF}(\underline{p})$. Note that the minimum distortion in (2.32) increases with increasing K . This is due to the fact that the relay compresses the signal from all users simultaneously. Note further that in (2.33) the expression in the numerator depends only on the signal power of the users in \mathcal{S} ; however, the distortion D in the denominator depends on the transmit power of all users in \mathcal{K} . Thus, for a fixed user and relay transmit signal-to-noise ratio (SNR), the bounds on $R_{\mathcal{S}}$, for all \mathcal{S} , in (2.33) decreases as increasing number of sources transmit. In fact, the maximum

single-user rate for any source is achieved only when the remaining sources remain ‘silent’, i.e., do not transmit. Thus, to obtain the set of all achievable CF rate tuples \mathcal{R}_{G-CF} , one must consider all possible source power tuples, $\underline{p} = (p_1, p_2, \dots, p_K)$ where p_k satisfies (2.4) such that

$$\mathcal{R}_{G-CF} = co \left(\bigcup_{\underline{p}} \mathcal{R}_{CF}(\underline{p}) \right) \quad (2.34)$$

where $co(\cdot)$ denotes the convex hull operation.

Remark 2.10 *Note that since D depends on the transmit SNR at the sources, R_S is in general not a convex function of \underline{p} and thus, the rate region is a convex hull of the union of all rate regions, where the union is over all \underline{p} .*

Remark 2.11 *As (2.32) indicates, the distortion D decreases as the SNR between the relay and destination P_r (normalized by unit variance noise) increases. Note that as P_r increases, the CF strategy yields sum rates that approach the two-antenna multiple-access clustering capacity [10].*

Finally, the rate region for the ergodic channel is obtained by averaging (2.33) over all channel states subject to a fading averaged distortion in (2.32). We remark that implicit in this averaging is the assumption that the destination also knows the channel gains at the relay.

The rate region for the ergodic channel is obtained by averaging (2.33) over all channel states subject to averaging the constraint in (2.32) over the joint fading process \underline{H} . We remark that implicit in this averaging is the assumption that the destination also knows the channel gains at the relay and vice-versa. Finally, the code construction for the full-duplex Gaussian MARC detailed above can be extended in a straightforward manner to the half-duplex case.

	Block 1	Block 2	...	Block B	...	Block B+1
User 1	$\underline{x}_1(w_{1,1,1}, w_{1,2,1}, 1)$ $\underline{q}_1(w_{1,2,1}, 1)$ $\underline{v}_1(1)$	$\underline{x}_1(w_{1,1,2}, w_{1,2,2}, w_{1,2,1})$ $\underline{q}_1(w_{1,2,2}, w_{1,2,1})$ $\underline{v}_1(w_{1,2,1})$...	$\underline{x}_1(w_{1,1,B}, w_{1,2,B}, w_{1,2,B-1})$ $\underline{q}_1(w_{1,2,B}, w_{1,2,B-1})$ $\underline{v}_1(w_{1,2,B-1})$...	$\underline{x}_1(1, 1, w_{1,2,B})$ $\underline{q}_1(1, w_{1,2,B})$ $\underline{v}_1(w_{1,2,B})$
User 2	$\underline{x}_2(w_{2,1,1}, w_{2,2,1}, 1)$ $\underline{q}_2(w_{2,2,1}, 1)$ $\underline{v}_2(1)$	$\underline{x}_2(w_{2,1,2}, w_{2,2,2}, w_{2,2,1})$ $\underline{q}_2(w_{2,2,2}, w_{2,2,1})$ $\underline{v}_2(w_{2,2,1})$...	$\underline{x}_2(w_{2,1,B}, w_{2,2,B}, w_{2,2,B-1})$ $\underline{q}_2(w_{2,2,B}, w_{2,2,B-1})$ $\underline{v}_2(w_{2,2,B-1})$...	$\underline{x}_2(1, 1, w_{2,2,B})$ $\underline{q}_2(1, w_{2,2,B})$ $\underline{v}_2(w_{2,2,B})$
Relay	$\underline{x}_r(1, 1)$	$\underline{x}_r(w_{1,2,1}, w_{2,2,1})$...	$\underline{x}_r(w_{1,2,B-1}, w_{2,2,B-1})$...	$\underline{x}_r(w_{1,2,B}, w_{2,2,B})$

Figure 2.5: Block Markov Encoding for the PDF strategy for a two-user MARC.

2.4.3 Partial Decode-and-Forward Strategy

One can generalize DF by limiting the relay to decode only one of two streams transmitted by a source as in [6, theorem 7]. We refer to this strategy as a *partial decode-and-forward* strategy [28, 31]; this strategy is also called a *multipath decode-and-forward* to characterize the multipath nature of the data flow from the sources [4, Chap. 4]. In general, it may seem desirable to use the relay node to forward all messages from a source. In practice, however, the costs associated with using a relay node [21, 36] may limit their usage by the source nodes to transmitting data streams with higher reliability or QoS requirements.

We construct the codebooks at the sources and relay as follows. Consider the probability distribution

$$\left(\prod_{k=1}^K p(v_k) p(q_k|v_k) p(x_k|q_k) \right) \cdot p(x_r|v_K) \cdot p(y_r, y_d|x_K, x_r). \quad (2.35)$$

For each k , generate $2^{nR_{k,2}}$ codewords $\underline{v}_k(s_k)$, $s_k = 1, 2, \dots, 2^{nR_{k,2}}$, by choosing the letters $v_{k,i}(s_k)$, $i = 1, 2, \dots, n$, independently with distribution $p(v_k)$. Similarly, for every $\underline{v}_k(s_k)$ generate $2^{nR_{k,2}}$ codewords $\underline{q}_k(w_{k,2}, s_k)$, $w_{k,2} = 1, 2, \dots, 2^{nR_{k,2}}$, by choosing the letters $q_{k,i}(w_{k,2}, s_k)$ independently with distribution $p_{Q_k|V_k}(\cdot | v_{k,i}(s_k))$ for all i . For every $\underline{q}_k(w_{k,2}, s_k)$, generate a length- n relay codeword $\underline{x}_k(w_{k,1}, w_{k,2}, s_k)$, $w_{k,1} =$

$1, 2, \dots, 2^{nR_{k,1}}$, by choosing the letters $x_{k,i}(w_{k,1}, w_{k,2}, s_k)$ independently with probability distribution $p_{X_k|Q_k}(\cdot | q_{k,i}(w_{k,2}, s_k))$ for all i . Finally, generate one length- n codeword $\underline{x}_r(s_1, s_2, \dots, s_K)$ for each tuple (s_1, s_2, \dots, s_K) by choosing $x_{r,i}(s_1, s_2, \dots, s_K)$ independently with distribution $p_{X_r|V_1, V_2, \dots, V_K}(\cdot | v_{1,i}(s_1), \dots, v_{K,i}(s_K))$ for all i . The above code construction procedure is repeated $B + 1$ times, once for each block, and the b^{th} codebook is used in block b , $b = 1, 2, \dots, B + 1$. Note that the codebooks are independent across blocks and this fact simplifies the error analysis [8, 35].

A block Markov encoding strategy is employed where in block b , $b = 1, 2, \dots, B$, the k^{th} source transmits its independent message streams $w_{k,1,b} \in [1, 2^{nR_{k,1}}]$ and $w_{k,2,b} \in [1, 2^{nR_{k,2}}]$ via $\underline{x}_k(w_{k,1,b}, w_{k,2,b}, w_{k,2,b-1})$ while the relay transmits $\underline{x}_r(s_{1,b}, s_{2,b}, \dots, s_{K,b})$. The encoding is illustrated in Fig. 2.5 for a two-user MARC. In each block, the relay decodes the messages $w_{k,2}$, for all k , while the destination decodes $(w_{k,1}, w_{k,2})$. The k^{th} source rate is $R_k = R_{k,1} + R_{k,2}$ and we write $R_{\mathcal{S},k} = \sum_{m \in \mathcal{S}} R_{k,m}$, $m = 1, 2$. We use backward decoding at the destination to prove the following theorem.

Theorem 2.12 *The rate region for the PDF strategy is the union of the set of rate tuples (R_1, R_2, \dots, R_K) that, for all non-empty sets \mathcal{G}, \mathcal{S} with $\mathcal{G} \subseteq \mathcal{S} \subseteq \mathcal{K}$, satisfy*

$$R_{\mathcal{S},2} \leq I(Q_{\mathcal{S}}; Y_r | Q_{\mathcal{S}^c} V_{\mathcal{K}} X_r U) \quad (2.36)$$

$$R_{\mathcal{S},1} \leq I(X_{\mathcal{S}}; Y_d | X_{\mathcal{S}^c} V_{\mathcal{K}} Q_{\mathcal{K}} X_r U) \quad (2.37)$$

$$R_{\mathcal{S},1} + R_{\mathcal{G},2} \leq I(X_{\mathcal{S}} X_r; Y_d | X_{\mathcal{S}^c} Q_{\mathcal{G}^c} V_{\mathcal{G}^c} U) \quad (2.38)$$

where the union is over all input distributions of the form

$$p(u) \cdot \left[\prod_{k=1}^K p(v_k, q_k, x_k | u) \right] \cdot p(x_r | v_{\mathcal{K}}, u). \quad (2.39)$$

Proof: In Appendix A, we first develop the rate bounds for $K = 2$ and use this to demonstrate the generalization for arbitrary K . ■

Remark 2.13 *The rate bounds for the half-duplex channel can be obtained by conditioning the bounds in (2.36)-(2.38) on the relay's transmit and receive modes.*

For a Gaussian MARC, we consider Gaussian signaling at the sources and relay.

We write

$$X_k = \sqrt{(1 - \alpha_{k,1} - \alpha_{k,2}) P_k} V_{k,0} + \sqrt{\alpha_{k,2} P_k} Q_k + \sqrt{\alpha_{k,1} P_k} V_k \quad k \in \mathcal{K} \quad (2.40)$$

$$X_r = \sum_{k=1}^K \sqrt{\beta_k P_r} V_k + \sqrt{\left(1 - \sum_{k=1}^K \beta_k\right) P_r} V_{r,0} \quad (2.41)$$

where $V_{k,0}$, V_k , and Q_k for all k are i.i.d proper complex Gaussian random variables.

We first consider the case where the channel gains are fixed. One can simplify the rate bounds by substituting (2.40) and (2.41) in (2.36)-(2.38). Note that the signals $V_{k,0}$ for all k act as interference at the relay. In fact, for most geometries of interest where the relay is closer to the destination than the sources are, one can see that the PDF bounds are maximized for $\alpha_{k,1} + \alpha_{k,2} = 1$ for all k ; that is, PDF simplifies to DF. However, PDF can achieve larger rates for the half-duplex case as now the sources can transmit directly to the destination in the relay's *transmit* fraction, i.e., the sources set $\alpha_{k,1} + \alpha_{k,2} = 1$ in the θ fraction and $\alpha_{k,2} = 0$ in the $1 - \theta$ fraction. We detail this strategy in Chapter 4. Finally, one can achieve the rate bounds for the ergodic case by averaging the fixed fading rate bounds over all channel states.

2.4.4 Mixed Strategy – PDF and CF

One can also combine the PDF and CF strategies as in [6, Theorem 7]. The rate bounds in [6, Theorem 7] are obtained using successive decoding and can also be obtained using sliding-window decoding. For the MARC, we combine the techniques of backward and sliding-window decoding at the destination to achieve the rate region for this mixed strategy. Our motivation for doing so stems from the fact that the DF and PDF rate bounds achieved by backward decoding are at least as large as sliding window decoding as detailed in Chapter 3.

The encoding is done as follows. Consider the probability distribution

$$\left(\prod_{k=1}^K p(v_k) p(q_k | v_k) p(x_k | q_k) \right) \cdot p(x_r | v_{\mathcal{K}}) \cdot p(\hat{y}_r | y_r, x_r, q_{\mathcal{K}}, v_{\mathcal{K}}) \cdot p(y_r, y_d | x_{\mathcal{K}}, x_r). \quad (2.42)$$

	Block 1	Block 2	...	Block B	Block $B+1$
User 1	$\underline{x}_1(w_{1,1,1}, w_{1,2,1}, 1)$ $\underline{q}_1(w_{1,2,1}, 1)$ $\underline{v}_1(1)$	$\underline{x}_1(w_{1,1,2}, w_{1,2,2}, w_{1,2,1})$ $\underline{q}_1(w_{1,2,2}, w_{1,2,1})$ $\underline{v}_1(w_{1,2,1})$...	$\underline{x}_1(w_{1,1,B}, w_{1,2,B}, w_{1,2,B-1})$ $\underline{q}_1(w_{1,2,B}, w_{1,2,B-1})$ $\underline{v}_1(w_{1,2,B-1})$	$\underline{x}_1(1, w_{1,2,B})$ $\underline{q}_1(1, w_{1,2,B})$ $\underline{v}_1(w_{1,2,B})$
User 2	$\underline{x}_2(w_{2,1,1}, w_{2,2,1}, 1)$ $\underline{q}_2(w_{2,2,1}, 1)$ $\underline{v}_2(1)$	$\underline{x}_2(w_{2,1,2}, w_{2,2,2}, w_{2,2,1})$ $\underline{q}_2(w_{2,2,2}, w_{2,2,1})$ $\underline{v}_2(w_{2,2,1})$...	$\underline{x}_2(w_{2,1,B}, w_{2,2,B}, w_{2,2,B-1})$ $\underline{q}_2(w_{2,2,B}, w_{2,2,B-1})$ $\underline{v}_2(w_{2,2,B-1})$	$\underline{x}_2(1, w_{2,2,B})$ $\underline{q}_2(1, w_{2,2,B})$ $\underline{v}_2(w_{2,2,B})$
Relay	$\underline{x}_r(1, 1, 1)$ $\underline{\hat{y}}_r(z_{r,1}, 1, 1, 1)$	$\underline{x}_r(w_{r,1}, w_{1,2,1}, w_{2,2,1})$ $\underline{\hat{y}}_r(z_{r,2}, w_{r,1}, w_{1,2,1}, w_{2,2,1})$...	$\underline{x}_r(w_{r,B-1}, w_{1,2,B-1}, w_{2,2,B-1})$ $\underline{\hat{y}}_r(z_{r,B}, w_{r,B-1}, w_{1,2,B-1}, w_{2,2,B-1})$	$\underline{x}_r(w_{r,B}, w_{1,2,B}, w_{2,2,B})$ $\underline{\hat{y}}_r(1, w_{r,B}, w_{1,2,B}, w_{2,2,B})$

Figure 2.6: Block Markov encoding for the mixed PDF and CF strategy for a two-user MARC.

For each k , generate $2^{nR_{k,2}}$ codewords $\underline{v}_k(s_k)$, $s_k = 1, 2, \dots, 2^{nR_{k,2}}$, by choosing the letters $v_{k,i}(s_k)$, $i = 1, 2, \dots, n$, independently with distribution $p(v_k)$. Similarly, for every $\underline{v}_k(s_k)$ generate $2^{nR_{k,2}}$ codewords $\underline{q}_k(w_{k,2}, s_k)$, $w_{k,2} = 1, 2, \dots, 2^{nR_{k,2}}$, by choosing the letters $x_{k,i}(w_{k,2}, s_k)$ independently with distribution $p_{Q_k|V_k}(\cdot | v_{k,i}(s_k))$ for all i . Further, for every $\underline{q}_k(w_{k,2}, s_k)$ generate a length- n relay codeword $\underline{x}_k(w_{k,1}, w_{k,2}, s_k)$, $w_{k,1} = 1, 2, \dots, 2^{nR_{k,1}}$, by choosing the letters $x_{k,i}(w_{k,1}, w_{k,2}, s_k)$ independently with distribution $p_{X_k|Q_k}(\cdot | q_{k,i}(w_{k,2}, s_k))$ for all i . Generate one length- n relay codeword $\underline{x}_r(w_r, s_1, s_2, \dots, s_K)$, $w_r = 1, 2, \dots, 2^{nR_r}$, for each tuple (s_1, s_2, \dots, s_K) by choosing $x_{r,i}(w_r, s_1, s_2, \dots, s_K)$ independently with probability distribution $p_{X_r|V_1, V_2, \dots, V_K}(\cdot | v_{1,i}(s_1), \dots, v_{K,i}(s_K))$ for all i . Further, generate one length- n codeword $\underline{\hat{y}}_r(z_r, w_r, s_K, w_{K,2})$, $z_r = 1, 2, \dots, 2^{nR'_r}$, for each tuple $s_K = (s_1, s_2, \dots, s_K)$ and $w_{K,2} = (w_{1,2}, w_{2,2}, \dots, w_{K,2})$ by choosing $\hat{y}_{r,i}(z_r, w_r, w_{K,2}, s_{K,2})$ for all i independently with distribution $p_{\hat{Y}_r|Q_1, Q_2, \dots, Q_K, X_r}(\cdot | q_{1,i}(w_{1,2}), \dots, q_{K,i}(w_{K,2}), x_r(w_r, s_K))$. Finally, we randomly partition the set $\{1, 2, \dots, 2^{nR'_r}\}$ into 2^{nR_r} subsets and index them via w_r .

A block Markov encoding strategy is employed where in block b , $b = 1, 2, \dots, B$, the k^{th} source transmits its independent message streams $w_{k,1,b} \in [1, 2^{nR_{k,1}}]$ and $w_{k,2,b} \in$

$[1, 2^{nR_{k,2}}]$ via $\underline{x}_k(w_{k,1,b}, w_{k,2,b}, w_{k,2,b-1})$ while the relay transmits $\underline{x}_r(w_{r,b}, s_{1,b}, s_{2,b}, \dots, s_{K,b})$ where R_r is the rate at which the relay forwards the compressed message $w_{r,b}$ as the index of the partition to which $z_{r,b-1}$ belongs (see Fig. 2.6). Finally, the relay also compresses its received signal as $\hat{y}_r(z_{r,b}, w_{K,2}, s_{K,2})$.

In block b , the relay decodes the messages $w_{k,2,b}$, for all k . The destination first decodes $(w_{1,2,b}, w_{2,2,b}, \dots, w_{K,2,b})$ in block b using backward decoding starting from block $B + 1$. After decoding all $B + 1$ blocks, the destination uses sliding-window decoding to decode $z_{r,b}$ using blocks b and $b + 1$. The k^{th} source rate is $R_k = R_{k,1} + R_{k,2}$ and we write $R_{\mathcal{S},k} = \sum_{m \in \mathcal{S}} R_{k,m}$, $m = 1, 2$. We use backward decoding followed by sliding-window decoding at the destination to prove the following theorem.

Theorem 2.14 *The rate region for the mixed PDF-CF strategy is the union of the set of rate tuples (R_1, R_2, \dots, R_K) that, for all non-empty sets \mathcal{S} with $\mathcal{G} \subseteq \mathcal{S} \subseteq \mathcal{K}$, satisfy*

$$R_{\mathcal{S},2} \leq I(Q_{\mathcal{S}}; Y_r | Q_{\mathcal{S}^c} V_{\mathcal{K}} X_r U) \quad (2.43)$$

$$R_{\mathcal{S},2} \leq I(Q_{\mathcal{S}} V_{\mathcal{S}}; Y_d | Q_{\mathcal{S}^c} V_{\mathcal{S}^c} U) \quad (2.44)$$

$$R_{\mathcal{S},1} \leq I(X_{\mathcal{S}}; \hat{Y}_r Y_d | X_{\mathcal{S}^c} Q_{\mathcal{K}} V_{\mathcal{K}} X_r U) \quad (2.45)$$

where the union is over all input distributions in (2.42) subject to the constraint

$$I(X_r; Y_d | Q_{\mathcal{K}} V_{\mathcal{K}} U) \geq I(\hat{Y}_r; Y_r | Q_{\mathcal{K}} V_{\mathcal{K}} X_r Y_d U). \quad (2.46)$$

Proof: The proof is a straightforward extension of the proofs for Theorems 2.7 and 2.12. Thus, the bounds in (2.43) are obtained by decoding $w_{K,2}$ at the relay in every block while the bounds in (2.44) are obtained by decoding $w_{K,2}$ at the destination using backward decoding. This is followed by decoding $z_{r,b}$ in every block at the destination using successive decoding [6, Theorem 6]. Combining the resulting bounds at the destination with the bounds on the quantization rate at the relay yields the constraint (2.46). Finally, the bounds in (2.45) result from decoding $w_{K,1}$ at the destination using \hat{Y}_r and Y_d in every block. ■

One can extend the code constructions for PDF and CF for the Gaussian case to obtain the bounds for this case. Finally, the half-duplex bounds are obtained by conditioning (2.43)-(2.45) over the transmit and receive modes at the relay.

2.4.5 Amplify-and-Forward Strategy

For a Gaussian MARC, one can also consider a strategy where the relay amplifies its received signal before forwarding it to the destination. Thus, the transmitted signal at the relay in each time-symbol is $X_{r,i} = cY_{r,i-1}$ where the constant c results from applying the power constraint at the relay in (2.4). The resulting channel at the destination is a unit delay multiaccess inter-symbol interference (ISI) channel with the received signal in each time instant given as

$$Y_{d,i} = \left(\sum_{k=1}^K h_{d,k} X_{k,i} \right) + ch_{d,r} \left(\sum_{k=1}^K h_{r,k} X_{k,i-1} \right) + cZ_{r,i-1} + Z_{d,i} \quad (2.47)$$

For the case of fixed channel gains, the AF rate region is the capacity region of a unit-memory ISI MAC in (2.47) and is given by a *multiuser water-filling* solution [37]. We obtain the ergodic region by averaging this region over all possible channel instantiations.

For a set of K sources transmitting at power p_k , the scale factor c is given as

$$c = \sqrt{\frac{P_r}{1 + \sum_{k=1}^K h_{r,k} p_k}}. \quad (2.48)$$

Observe that c decreases with increasing K as the relay power is now shared over more users. Further, since the rate bounds R_S for all S at the destination depends on c , as with the CF strategy, we consider all possible power tuples \underline{p} in developing the AF rate region \mathcal{R}_{AF} . Thus, we write

$$\mathcal{R}_{AF} = co \left(\bigcup_{\underline{p}} \mathcal{R}_{CV}(\underline{p}) \right) \quad (2.49)$$

where $\mathcal{R}_{CV}(\underline{p})$ is the capacity region of an ISI channel for some \underline{p} and $co(\cdot)$ represents the convex hull of the union of such regions over all possible \underline{p} .

For the half-duplex case, we consider $\theta = 1/2$. The signals $Y_{d,1}$ and $Y_{d,2}$ in the two fractions are given as

$$Y_{d,1} = \left(\sum_{k=1}^K X_{k,1} \right) + Z_{d,1} \quad (2.50)$$

$$Y_{d,2} = \left(\sum_{k=1}^K h_{d,k} X_{k,2} \right) + c h_{d,r} \left(\sum_{k=1}^K h_{r,k} X_{k,1} \right) + c Z_{r,1} + Z_{d,2} \quad (2.51)$$

and result in a two-symbol multiaccess ISI channel. The rate bounds are given as [30, 10.5]

$$R_S \leq \max_{\{Q_k: \text{tr}(Q_k) \leq 2P_k\}_{k \in \mathcal{K}}} \frac{1}{2} \log \left| I_2 + \sum_{k \in \mathcal{S}} H_k Q_k H_k^\dagger \right| \quad (2.52)$$

where

$$H_k = \begin{bmatrix} h_{d,k} & 0 \\ c h_{d,r} h_{r,k}/c_s & h_{d,k}/c_s \end{bmatrix} \quad (2.53)$$

where $c_s = \sqrt{|h_{d,r}|^2 c^2 + 1}$ and H_k^\dagger is the conjugate transpose of H_k for all k and I_2 is a 2×2 identity matrix.

2.5 Illustration of Results

We illustrate our results for a two user MARC and the two example geometries shown in Fig. 2.7. While the two geometries chosen here illustrate the capacity achieving behavior of the DF and CF strategies, they are also reflective of the typical performance achieved by the various strategies considered here for an arbitrary placement of source and relay nodes. Case 1 is a geometry with a symmetric positioning of the sources with respect to the relay and destination while case 2 is a collinear geometry with both sources at the origin and the destination a unit distance away from the origin. In both cases, the relay moves along the line connecting the destination with the origin.

We plot the sum-rate in bits per channel use for each strategy as a function of the relay's distance from the origin. The noise normalized transmit SNR at the sources and relay is chosen as $P_1 = P_2 = P_r = 10$. We present and analyze the results separately for the no fading and ergodic fading model; to develop the we present the results for

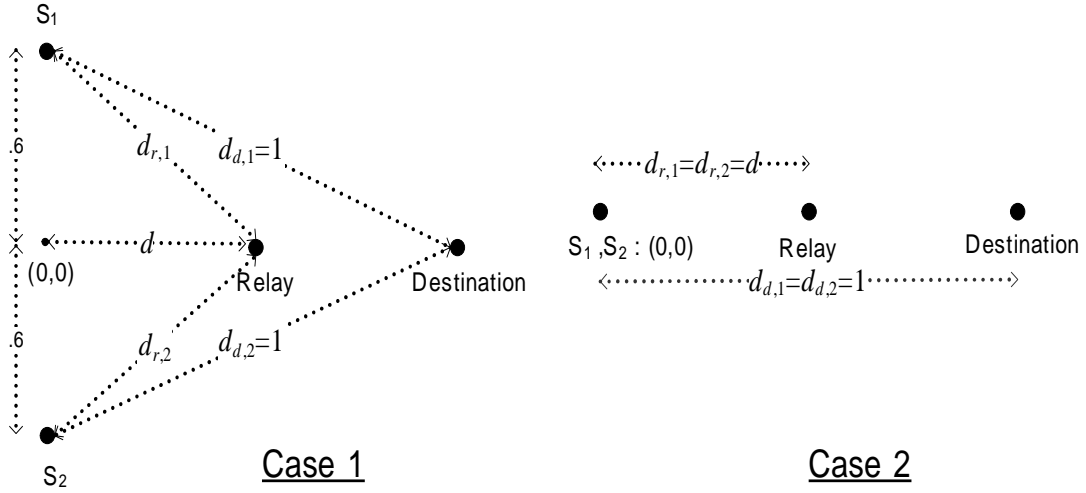


Figure 2.7: Two example geometries.

an ergodic phase fading channel, i.e., $A_{m,k,i} = e^{j\theta_{m,k,i}}$ where $\theta_{m,k,i}$ are i.i.d. uniformly between $[-\pi, \pi)$ for all $m \in \mathcal{D}$, $k \in \mathcal{T}$ and time-instants i . For the following analysis we use the free-space path loss exponent $\gamma = 2$ and evaluate all logarithms with respect to base 2 so that the resulting rates are in units of bits per channel use.

2.5.1 No Fading or Line-of-sight Model

MARC

The two user DF, CF, and AF sum-rates and the outer bounds of Proposition 2.2 are plotted in Figs. 2.8 and 2.9 for geometry 1 and 2 respectively. Recall that the DF and CF sum-rates for a Gaussian MARC are given by (2.18), (2.33) respectively. The direct multiple-access sum-rate between the sources and destination is also plotted as a straight-line since it is independent of the relay's position. The plots also include the optimal DF power fraction $\alpha_1 = \alpha_2 = \alpha$ allocated by the sources to transmitting a new message in (2.16) where the two fractions have the same value α at the maximum sum-rate point for the symmetric geometries in cases 1 and 2. We note that α does not apply to the CF and AF strategies where the relay does not decode the source messages.

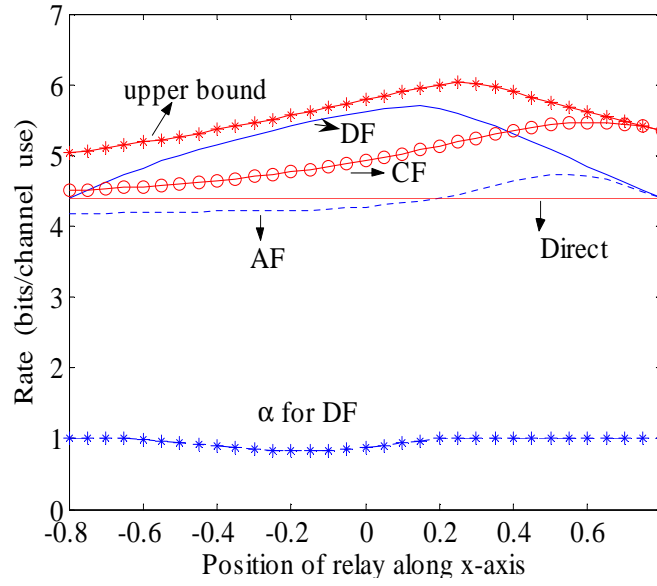


Figure 2.8: Inner and outer bounds on the sum rate $R_1 + R_2$ for Case 1 and the no fading model.

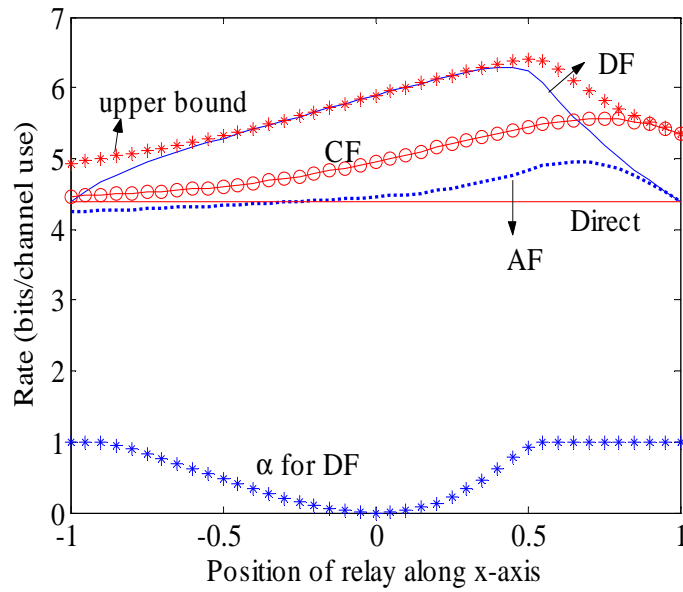


Figure 2.9: Inner and outer bounds on the sum rate $R_1 + R_2$ for Case 2 and the no fading model.

In Fig. 2.8, we observe that when the relay is closer to the destination, the CF strategy approaches the upper bound achieving capacity when the relay and destination enjoy an error-free channel. This can be verified analytically and results from the fact the distortion in the quantized signal decreases as the channel between the relay and destination becomes more reliable. In the limit, when the relay and destination are co-located, the destination has access to both channel outputs thus achieving the upper bound in (2.8).

The AF strategy performs only as well as the DF strategy when the relay is very close to the destination. The performance of the AF strategy suffers from the amplification of the received noise at the relay. Further as the relay moves away from the destination, the advantage of a high-rate channel between the relay and destination is also lost resulting in the AF strategy falling below the direct multiple-access sum-rate that is achievable in the absence of the relay.

The DF strategy approaches the outer bounds when the relay is physically close to the two sources. The resulting high rate channel between the relay and the sources forces maximum cooperation between the sources and the relay. This is clear from the optimal α curve in Figs. 2.8 and 2.9 where $\alpha = 1$ (no cooperation) results only when the rate achieved by the sources and relay at the destination exceeds the maximum rate achievable between the sources and relay.

For the collinear geometry considered in case 2, we observe from Fig. 2.9 that DF approaches the upper bound when the relay is physically close to the two sources. Finally, we note that the achievable rates for DF and CF are greater than the direct sum-rate when the relay is closer to the sources than the destination even if it does not physically lie between the sources and destination.

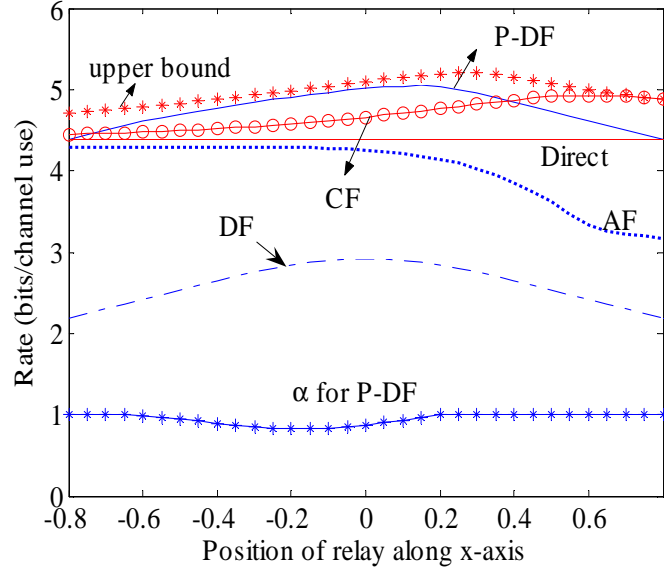


Figure 2.10: Inner and outer bounds on the sum rate $R_1 + R_2$ for the half-duplex MARC of Case 1.

Half-Duplex MARC

The achievable sum-rate bounds for DF, PDF, CF, and AF are shown in Fig. 2.10 and 2.11 for Case 1 and Case 2 respectively. Also shown is the outer bound on the sum-rate obtained by conditioning the bounds in (2.8) on the relay's half-duplex modes. For the sake of simplicity and to make comparisons between the CF, DF, PDF and AF strategies, we set $\theta = 1/2$. Analogous to the full-duplex MARC, we consider Gaussian signaling at the sources and relay for every strategy.

As expected, for both geometries the CF strategy approaches the upper bound as the relay approaches the destination. Here too, the CF strategy exploits the correlation between the received signals at the relay and destination and for the case where the relay is at the destination, the destination has reliable access to both channel outputs thus achieving capacity.

For case 2, we see that when the relay and sources are physically very close that the DF sum-rate approaches the outer bounds. The optimal α curve in Figs. 2.10 and

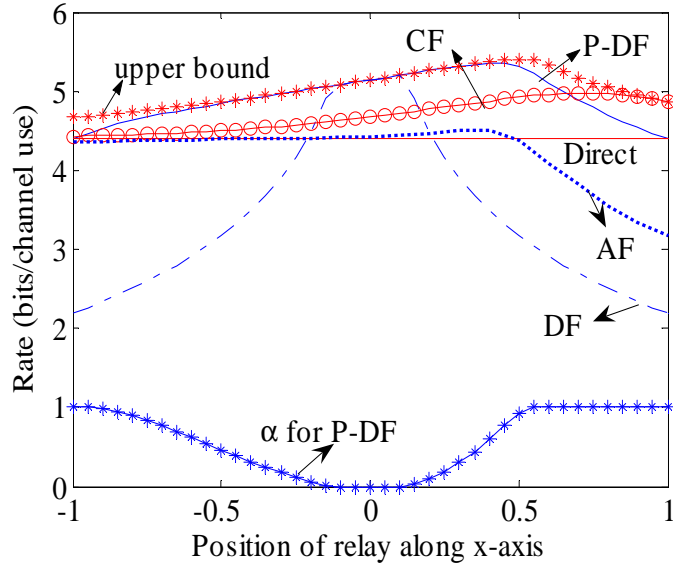


Figure 2.11: Inner and outer bounds on the sum rate $R_1 + R_2$ for the half-duplex MARC of Case 2

2.11 measures the fraction of power allocated to a new message at each source in the $(1 - \theta)$ fraction for the PDF strategy. The sources do not cooperate with relay in the CF and AF strategies while for the DF strategy, $\alpha_1 = \alpha_2 = 1$ since the sources do not send a new message in the $(1 - \theta)$ fraction. Note that $\theta = 1/2$ may not maximize the sum-rate achieved by the DF or the PDF strategy.

2.5.2 Ergodic Phase Fading

MARC

In [10], the authors show that for an ergodic fading channel, DF achieves the sum-capacity of a MARC when the relay lies in a region around the sources such that

$$\sum_{k \in \mathcal{S}} \frac{P_k}{d_{d,k}^\alpha} + \frac{P_r}{d_{d,r}^\alpha} \leq \sum_{k \in \mathcal{S}} \frac{P_k}{d_{r,k}^\alpha} \quad \text{for all } \mathcal{S} \subseteq \mathcal{K}. \quad (2.54)$$

Further, they also showed that due to the lack of channel state information at the transmitters and a uniform phase-fading channel the ergodic capacity is maximized when

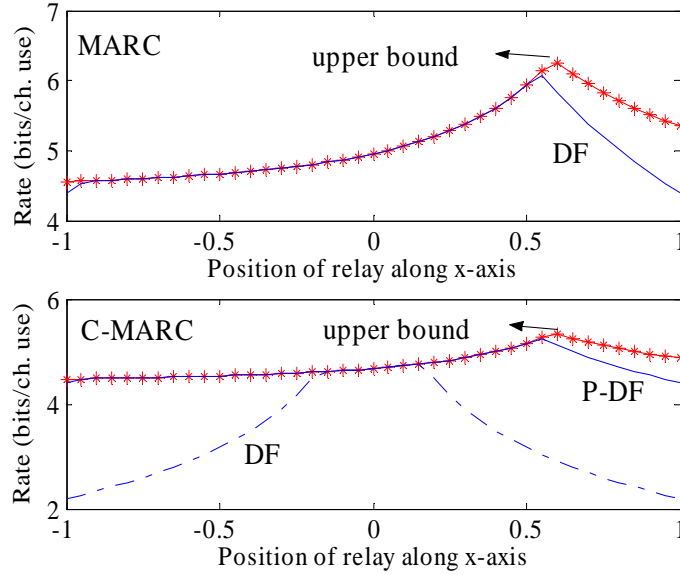


Figure 2.12: Inner and outer bounds on the sum rate $R_1 + R_2$ for the MARC and half-duplex MARC of Case 2 under ergodic fading

the sources do not cooperate with the relay, i.e., $\alpha_k = 0$ for all k .

Half-Duplex MARC

In an analogous manner, one can show that for a half-duplex MARC with fixed fractions θ and $1 - \theta$, the DF strategy achieves capacity when the relay lies in a region about the sources such that, for all $\mathcal{S} \subseteq \mathcal{K}$,

$$\left(1 + \sum_{k \in \mathcal{S}} \frac{P_k}{d_{d,k}^\gamma}\right)^\theta \cdot \left(1 + \frac{P_r}{d_{d,r}^\gamma} + \sum_{k \in \mathcal{S}} \frac{P_k}{d_{d,k}^\gamma}\right)^{(1-\theta)} \leq \left(1 + \sum_{k \in \mathcal{S}} \frac{P_k}{d_{r,k}^\gamma}\right)^\theta. \quad (2.55)$$

The resulting rate region for the half-duplex MARC under ergodic fading conditions is then given by the set of rate tuples (R_1, R_2, \dots, R_K) that satisfy

$$R_{\mathcal{S}} \leq \theta \log \left(1 + \sum_{k \in \mathcal{S}} \frac{P_k}{d_{d,k}^\gamma}\right) + (1 - \theta) \log \left(1 + \frac{P_r}{d_{d,r}^\gamma} + \sum_{k \in \mathcal{S}} \frac{P_k}{d_{d,k}^\gamma}\right) \quad \text{for all } \mathcal{S} \subseteq \mathcal{K}. \quad (2.56)$$

Further, for any θ , one can extend the analysis in [10] to show that the PDF strategy achieves capacity when the relay lies in a region about the sources such that

$$\left(1 + \sum_{k \in \mathcal{S}} \frac{P_k}{d_{d,k}}\right)^\theta \cdot \left(1 + \frac{P_r}{d_{d,r}} + \sum_{k \in \mathcal{S}} \frac{P_k}{d_{d,k}}\right)^{(1-\theta)} \leq \left(1 + \sum_{k \in \mathcal{S}} \frac{P_k}{d_{r,k}}\right)^\theta \cdot \left(1 + \sum_{k \in \mathcal{S}} \frac{P_k}{d_{d,k}}\right)^{(1-\theta)} \quad \text{for all } \mathcal{S} \subseteq \mathcal{K}. \quad (2.57)$$

This capacity achieving behavior of the DF and PDF strategy for the MARC and half-duplex MARC respectively under ergodic fading conditions is clearly demonstrated in Fig. 2.12 for the collinear geometry of case 2. The wide range of relay positions between $[-.9, .45]$ where the DF strategy achieves capacity for the MARC and between $[-.95, .45]$ for the half-duplex MARC clearly illustrates how clustering the sources and relay helps achieve the ergodic capacity. Further, for the half-duplex MARC the DF strategy also achieves capacity albeit over the smaller range $[-.15, .15]$ where the relay is very close to the sources.

Effect of Transmit SNR

One can similarly plot the DF, CF, and AF sum-rates for different values of transmit SNR at the sources and relay. In general, for a fixed transmit SNR at the relay, reducing the transmit SNR at the sources will reduce the maximum sum-rates achievable. On the other hand reducing only the transmit SNR at the relay will reduce the sum-rate gains achieved by relaying relative to the MAC sum-capacity. Further, the AF sum-rate decreases with decreasing transmit SNR at the sources due to noise amplification. However, one can verify from the rate expressions in Section 2.4 that the geometry-dependent performance of DF and CF does not change with transmit SNR; i.e., DF achieves or approaches capacity when the sources and the relay are clustered close together while CF does so when the relay is clustered close to the destination irrespective independent of transmit SNR.

2.6 Conclusions

We presented discrete and Gaussian memoryless models for a full-duplex multiaccess relay channel. We also presented a memoryless model for a MARC with a half-duplex relay. We extended the relaying strategies of DF, CF, and PDF developed by Cover and El Gamal for the relay channel [6] and studied their rate regions for both the no fading and ergodic fading channels. Finally, we illustrated the maximum sum-rates achieved by DF, CF, AF, and PDF for two example geometries and demonstrated the topology-dependent rate and capacity behavior for the no fading and ergodic phase-fading models.

Chapter 3

Offset Encoding for Multiaccess Relay Channels

3.1 Introduction

For the classic relay channel, several block-Markov encoding and decoding techniques achieve the DF rate in [6, Theorem 1] (see [10, Sec. I]):

- *irregular* encoding (different size codebooks at the source and relay) and *successive* decoding [6, Theorem 1],
- *regular* encoding (same size codebooks at the source and relay) and *sliding-window* decoding [8],
- regular encoding and *backward decoding* [7].

One can, in fact, use irregular encoding with any of the above decoding methods. The above techniques have all been generalized to multiple relay networks [10, 18, 35, 38, 39]. For the MARC, however, the different DF decoding methods do not always yield the same rate region. For example, we show that backward decoding can give larger rates than sliding-window decoding (see also [40, 41]). On the other hand, sliding-window decoding decodes blocks of message bits at regular intervals before all channel-symbol blocks are transmitted. This is useful: if the sliding window length is much smaller than the backward decoding delay, then sliding-window decoding is preferable for *streaming* applications.

To compare the methods, suppose the destination uses backward decoding for B message blocks transmitted in $B + 1$ channel-symbol blocks. The decoding delay is then $B + 1$ channel-symbol blocks for the first message block, where we measure delay from the start of the block to the time the block is decoded. Our main contribution is an

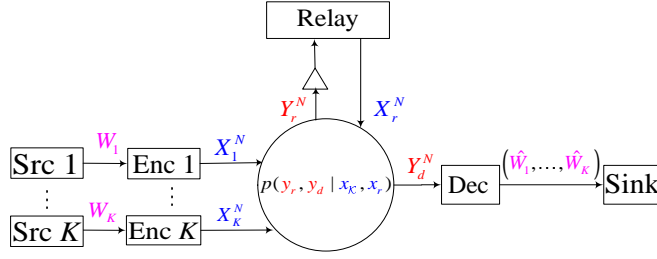


Figure 3.1: A K -user multiaccess relay channel.

offset encoding technique for sliding-window decoding that recovers the corner points of the destination's backward decoding rate regions with a delay of $K + 1$ channel-symbol blocks for every message block. The total number of channel-symbol blocks required is $B + K$. Note that K can be much smaller than B , e.g., if the relay serves only a small number of users at a time. For the non-corner boundary points of the backward decoding rate regions, we use a combination of offset encoding, no-offset encoding, and/or time sharing between different offset encoding methods. Note, however, that time-sharing increases decoding delay; rate-splitting methods might perhaps avoid this delay [42, 43].

This correspondence is organized as follows. In Section 3.2 we present the MARC model and summarize the DF random code construction of [10, Appendix A]. In Section 3.3, we review the backward decoding rate region and compute the sliding-window decoding rate region. The latter region is in general smaller than the former. In Section 3.4, we describe offset encoding and develop its rate region when combined with sliding-window decoding. Section 3.5 concludes the paper.

	Block 1	Block 2	Block 3	...	Block B	Block $B+1$
User 1	$\underline{x}_1(w_{1,1}, 1)$ $\underline{v}_1(1)$	$\underline{x}_1(w_{1,2}, w_{1,1})$ $\underline{v}_1(w_{1,1})$	$\underline{x}_1(w_{1,3}, w_{1,2})$ $\underline{v}_1(w_{1,2})$...	$\underline{x}_1(w_{1,B}, w_{1,B-1})$ $\underline{v}_1(w_{1,B-1})$	$\underline{x}_1(1, w_{1,B})$ $\underline{v}_1(w_{1,B})$
User 2	$\underline{x}_2(w_{2,1}, 1)$ $\underline{v}_2(1)$	$\underline{x}_2(w_{2,2}, w_{2,1})$ $\underline{v}_2(w_{2,1})$	$\underline{x}_2(w_{2,3}, w_{2,2})$ $\underline{v}_2(w_{2,2})$...	$\underline{x}_2(w_{2,B}, w_{2,B-1})$ $\underline{v}_2(w_{2,B-1})$	$\underline{x}_2(1, w_{2,B})$ $\underline{v}_2(w_{2,B})$
Relay	$\underline{x}_r(1, 1)$	$\underline{x}_r(w_{1,1}, w_{2,1})$	$\underline{x}_r(w_{1,2}, w_{2,2})$...	$\underline{x}_r(w_{1,B-1}, w_{2,B-1})$	$\underline{x}_r(w_{1,B}, w_{2,B})$

Figure 3.2: Regular encoding for a two-user MARC assuming the relay decodes correctly.

3.2 Preliminaries

3.2.1 Model and Notation

The K -user MARC model is the same that as detailed in Chapter 2. As further notation, we write $R_S = \sum_{k \in S} R_k$, $[m, n] = \{m, m+1, \dots, n\}$, and we use the vector notation \underline{x}_k for length- n codewords of user k . We use the usual notation for entropy and mutual information [29, 30] and take all logarithms to the base 2 so that our rate units are bits. We write random variables (e.g. W_k) with uppercase letters and their realizations (e.g. w_k) with the corresponding lowercase letters.

We assume familiarity of the reader with basic notions of backward decoding and joint decoding as described in [7, 8, 10, 35, 40].

3.2.2 Random Code Construction

A DF code construction is presented in [10, Appendix A] and we review it below. This construction is common to all the decoding methods considered below and it uses independent random variables V_k , $k = 1, 2, \dots, K$, to help the sources cooperate with the relay. The V_k have finite alphabets.

Random Code Construction:

Consider the probability distribution

$$\left(\prod_{k=1}^K p(v_k) p(x_k | v_k) \right) \cdot p(x_r | v_K). \quad (3.1)$$

We use regular encoding. For each k , generate 2^{nR_k} codewords $\underline{v}_k(s_k)$, $s_k = 1, 2, \dots, 2^{nR_k}$, by choosing the letters $v_{k,i}(s_k)$, $i = 1, 2, \dots, n$, independently with distribution $p(v_k)$. Similarly, for every $\underline{v}_k(s_k)$ generate 2^{nR_k} codewords $\underline{x}_k(w_k, s_k)$, $w_k = 1, 2, \dots, 2^{nR_k}$, by choosing the letters $x_{k,i}(w_k, s_k)$ independently with probability distribution $p_{X_k|V_k}(\cdot | v_{k,i}(s_k))$ for all i . Finally, generate one length- n relay codeword $\underline{x}_r(s_1, s_2, \dots, s_K)$ for each tuple (s_1, s_2, \dots, s_K) by choosing $x_{r,i}(s_1, s_2, \dots, s_K)$ independently with distribution $p_{X_r|V_1, V_2, \dots, V_K}(\cdot | v_{1,i}(s_1), \dots, v_{K,i}(s_K))$ for all i .

The above code construction procedure is repeated $B + 1$ times, once for each block, and the b^{th} codebook is used in block b , $b = 1, 2, \dots, B + 1$. Note that the codebooks are independent across blocks; this fact simplifies the error analysis [8, 35]. The encoding procedure of [10, Appendix A] proceeds as follows. We change this procedure in Sec. 3.4.

Regular Block Markov Encoding:

Encoder k parses w_k into B blocks $w_{k,1}, w_{k,2}, \dots, w_{k,B}$, each having nR_k bits, and transmits these messages over $B + 1$ channel-symbol blocks as shown in Fig. 3.2 for $K = 2$. More generally, user k transmits $\underline{x}_k(w_{k,b}, w_{k,b-1})$ in block b where $w_{k,0} = w_{k,B+1} = 1$ for all k . The relay sends the codeword $\underline{x}_r(s_{1,b}, s_{2,b}, \dots, s_{K,b})$ in block b where $s_{k,b}$ is the relay's estimate of $w_{k,b-1}$ from block $b - 1$. We set $s_{k,1} = 1$ for all k . We thus have $N = n(B + 1)$ and $B_{W_k} = nR_k B$ so the overall rate of user k is $R_{W_k} = R_k \cdot B / (B + 1)$ which approaches R_k for large B .

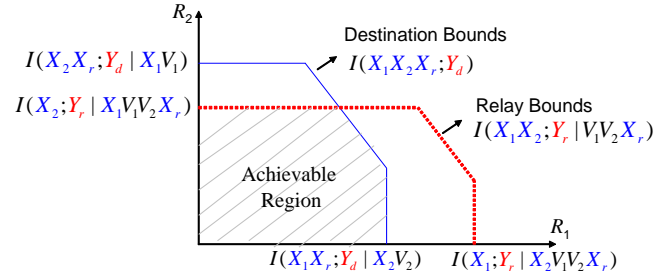


Figure 3.3: Example of a rate region achieved by DF and backward decoding for a two-user MARC.

3.3 Decode-and-Forward

3.3.1 Backward Decoding

Consider a 2-user MARC where the sources and the relay use the block-Markov encoding method described above. The relay decodes the messages reliably if (see Appendix B.1)

$$R_1 \leq I(X_1; Y_r | X_2 V_1 V_2 X_r) \quad (3.2)$$

$$R_2 \leq I(X_2; Y_r | X_1 V_1 V_2 X_r) \quad (3.3)$$

$$R_1 + R_2 \leq I(X_1 X_2; Y_r | V_1 V_2 X_r). \quad (3.4)$$

The destination decodes the message blocks in reverse order using its channel-symbol blocks $\underline{y}_{d,B+1}, \underline{y}_{d,B}, \dots, \underline{y}_{d,2}$. The resulting destination rate bounds are (see Appendix B.1)

$$R_1 \leq I(X_1 X_r; Y_d | X_2 V_2) \quad (3.5)$$

$$R_2 \leq I(X_2 X_r; Y_d | X_1 V_1) \quad (3.6)$$

$$R_1 + R_2 \leq I(X_1 X_2 X_r; Y_d). \quad (3.7)$$

Fig. 3.3 shows an example of the rate region defined by (3.2)-(3.7). For a K -user MARC, these bounds generalize as follows.

Theorem 3.1 *The capacity region of a K -user MARC includes the union of the set of rate tuples (R_1, R_2, \dots, R_K) that satisfy, for all $\mathcal{S} \subseteq \mathcal{K}$,*

$$R_{\mathcal{S}} \leq \min \left(\begin{array}{c} I(X_{\mathcal{S}}; Y_r | X_{\mathcal{S}^c} V_{\mathcal{K}} X_r U), \\ I(X_{\mathcal{S}} X_r; Y_d | X_{\mathcal{S}^c} V_{\mathcal{S}^c} U) \end{array} \right) \quad (3.8)$$

where the union is over all distributions that factor as

$$p(u) \cdot \left(\prod_{k=1}^K p(x_k, v_k | u) \right) \cdot p(x_r | v_{\mathcal{K}}, u) \cdot p(y_r, y_d | x_{\mathcal{K}}, x_r). \quad (3.9)$$

Proof: See Appendix B.1. ■

Remark 3.2 *The time-sharing random variable U ensures that the region of Theorem 3.1 is convex. For simplicity, we will develop the theory below for a constant U only.*

Remark 3.3 *The destination decodes the message blocks $w_{k,B}, w_{k,B-1}, \dots, w_{k,1}$ with delays of $2, 3, \dots, B+1$ channel-symbol blocks, respectively. Note that B must be large to ensure that the rate-loss factor $B/(B+1)$ due to block Markov encoding is close to 1.*

3.3.2 Sliding-Window Decoding

Suppose the destination uses sliding-window decoding, i.e., the destination decodes the message pair $(w_{1,b}, w_{2,b})$ transmitted in block b by using $\underline{y}_{d,b}$ and $\underline{y}_{d,b+1}$. For example, in Fig. 3.2, the destination decodes $(w_{1,2}, w_{2,2})$ by using $\underline{y}_{d,2}$ and $\underline{y}_{d,3}$. Observe that $(w_{1,b+1}, w_{2,b+1})$ is not known while decoding $(w_{1,b}, w_{2,b})$. One can check that the bounds in (3.5)-(3.7) are replaced by

$$R_1 \leq I(X_1; Y_d | X_2 V_1 V_2 X_r) + I(V_1 X_r; Y_d | V_2) \quad (3.10)$$

$$R_2 \leq I(X_2; Y_d | X_1 V_1 V_2 X_r) + I(V_2 X_r; Y_d | V_1) \quad (3.11)$$

$$R_1 + R_2 \leq I(X_1 X_2 X_r; Y_d). \quad (3.12)$$

The analysis used to obtain (3.10)-(3.12) is similar to that presented in Appendix B.2 and is hence omitted. In brief, the term $I(X_1; Y_d | X_2 V_1 V_2 X_r)$ in (3.10) results from $\underline{y}_{d,b}$

	Block 1	Block 2	Block 3	...	Block K	Block $K+1$
User 1	$\underline{x}_1(w_{1,1},1)$ $\underline{v}_1(1)$	$\underline{x}_1(w_{1,2},w_{1,1})$ $\underline{v}_1(w_{1,1})$	$\underline{x}_1(w_{1,3},w_{1,2})$ $\underline{v}_1(w_{1,2})$...	$\underline{x}_1(w_{1,K},w_{1,K-1})$ $\underline{v}_1(w_{1,K-1})$	$\underline{x}_1(w_{1,K+1},w_{1,K})$ $\underline{v}_1(w_{1,K})$
User 2	$\underline{x}_2(1,1)$ $\underline{v}_2(1)$	$\underline{x}_2(w_{2,1},1)$ $\underline{v}_2(1)$	$\underline{x}_2(w_{2,2},w_{2,1})$ $\underline{v}_2(w_{2,1})$...	$\underline{x}_2(w_{2,K-1},w_{2,K-2})$ $\underline{v}_2(w_{2,K-2})$	$\underline{x}_2(w_{2,K},w_{2,K-1})$ $\underline{v}_2(w_{2,K-1})$
	\vdots	\vdots	\vdots		\vdots	\vdots
User K	$\underline{x}_K(1,1)$ $\underline{v}_K(1)$	$\underline{x}_K(1,1)$ $\underline{v}_K(1)$	$\underline{x}_K(1,1)$ $\underline{v}_K(1)$...	$\underline{x}_K(w_{K,1},1)$ $\underline{v}_K(1)$	$\underline{x}_K(w_{K,2},w_{K,1})$ $\underline{v}_K(w_{K,1})$
Relay	$\underline{x}_r(1,1,\dots,1)$	$\underline{x}_r(w_{1,1},1,\dots,1)$	$\underline{x}_r(w_{1,2},w_{2,1},\dots,1)$...	$\underline{x}_r(w_{1,K-1},w_{2,K-2},\dots,1)$	$\underline{x}_r(w_{1,K},w_{2,K-1},\dots,w_{K,1})$

Figure 3.4: Offset encoding for a K -user MARC assuming the relay decodes correctly.

while the term $I(V_1 X_r; Y_d | V_2)$ is due to $\underline{y}_{d,b+1}$. In fact, the same bounds result if one increases the sliding window length to decode messages from many past blocks, unless this window includes block $B+1$. The bounds (3.11) and (3.12) are obtained similarly.

We next compare (3.5)-(3.7) and (3.10)-(3.12). Obviously, the bounds (3.7) and (3.12) are the same. But consider the right-hand side of (3.5) that expands as

$$I(X_1 X_r; Y_d | X_2 V_2) = I(X_1 V_1 X_r; Y_d | X_2 V_2) \quad (3.13)$$

$$= I(X_1; Y_d | X_2 V_1 V_2 X_r) + I(V_1 X_r; Y_d | X_2 V_2). \quad (3.14)$$

where (3.13) follows from the Markov chain $(V_1, V_2) - (X_1, X_2, X_r) - Y_d$ and (3.14) from the chain rule for mutual information. We further have

$$I(V_1 X_r; Y_d | X_2 V_2) = I(V_1 X_r; X_2 Y_d | V_2) \quad (3.15)$$

$$\geq I(V_1 X_r; Y_d | V_2) \quad (3.16)$$

where (3.15) follows from the Markov chain $X_2 - V_2 - (V_1, X_r)$. Note that (3.16) holds with equality if and only if

$$I(V_1 X_r; X_2 | V_2 Y_d) = 0. \quad (3.17)$$

Comparing (3.14) and (3.16) with (3.10), we see that the right-hand side of (3.5) is at least the right-hand side of (3.10). By symmetry, the right-hand side of (3.6) is at

least the right-hand side of (3.11). Hence, backward decoding is at least as good as sliding-window decoding.

We show by example that backward decoding can be strictly better than sliding-window decoding. Consider a MARC with $\{0, 1\}$ inputs X_1 , X_2 , and X_r . Suppose we have

$$Y_r = X_1 + X_2 \quad (3.18)$$

$$Y_d = X_1 + X_r \quad (3.19)$$

where we use integer addition. Any DF rate region must be in the capacity region of the user-to-relay multiaccess channel. This capacity region in bits per channel use is given by (see [30, p. 392])

$$R_1 \leq 1, \quad R_2 \leq 1, \quad R_1 + R_2 \leq 3/2. \quad (3.20)$$

One can check that backward decoding achieves this largest-possible DF region with independent and coin-tossing V_1, V_2, X_1, X_2 , and X_r . However, for sliding-window decoding the bounds (3.2)-(3.4) and (3.10)-(3.12) are

$$R_1 \leq H(X_1|V_1) \quad (3.21)$$

$$R_2 \leq \min (H(X_2|V_2), I(V_2 X_r; Y_d|V_1)) \quad (3.22)$$

$$R_1 + R_2 \leq \min (H(X_1 + X_2|V_1 V_2), H(X_1 + X_r)). \quad (3.23)$$

Suppose we desire $R_2 = 1$ so that (3.22) implies that X_2 is coin-tossing and independent of V_2 . For such V_2 and X_2 the bound (3.23) implies

$$\begin{aligned} R_1 + R_2 &\leq H(X_1 + X_2|V_1 V_2) \\ &= 1 + H(X_1|V_1)/2. \end{aligned} \quad (3.24)$$

We further have from (3.22) that

$$\begin{aligned} R_2 &\leq I(V_2 X_r; Y_d|V_1) \\ &= H(X_1 + X_r|V_1) - H(X_1|V_1) \\ &\leq \log_2 3 - H(X_1|V_1). \end{aligned} \quad (3.25)$$

The combination of $R_2 = 1$, (3.24) and (3.25) gives

$$R_1 \leq H(X_1|V_1)/2 \leq (\log_2(3) - 1)/2 \approx 0.292. \quad (3.26)$$

The same bound results if we add a time-sharing random variable U to all the entropies in (3.21)-(3.23). Sliding-window decoding cannot therefore achieve the backward decoding corner point $(R_1, R_2) = (1/2, 1)$.

For $K > 2$, the bounds (3.10)-(3.12) generalize to

$$R_{\mathcal{S}} \leq I(X_{\mathcal{S}}; Y_d | X_{\mathcal{S}^c} V_{\mathcal{S}} X_r) + I(V_{\mathcal{S}} X_r; Y_d | V_{\mathcal{S}^c}) \quad (3.27)$$

for all $\mathcal{S} \subseteq \mathcal{K}$. One can show that the bounds in (3.27) are in general more restrictive than the corresponding destination bounds in (3.8) for all $\mathcal{S} \subset \mathcal{K}$.

3.4 Offset Encoding

To improve sliding-window decoding, we offset the message blocks from the K sources by one block per source. Let π denote a permutation (order) of the source indices, i.e., $\pi = (\pi(1), \pi(2), \dots, \pi(K))$ where $\pi(i) \in \mathcal{K}$ for all i and $\{\pi(i) : i = 1, 2, \dots, K\} = \mathcal{K}$. We let user $\pi(i)$ start transmitting in block i , i.e., we set $w_{\pi(i),b} = 1$ for $b < i$ and $b \geq B + i$. The resulting message-to-codeword mappings with offset order $\pi = (1, 2, \dots, K)$ are shown in Fig. 3.4. Observe that offset encoding uses $B + K$ channel-symbol blocks so the overall rate-loss factor is $B/(B + K)$.

The relay decodes at the end of each block as before, except that $s_{\pi(i),b}$ is now the relay's estimate of $w_{\pi(i),b-i}$. We thus require

$$R_{\mathcal{S}} \leq I(X_{\mathcal{S}}; Y_r | X_{\mathcal{S}^c} V_{\mathcal{K}} X_r) \quad (3.28)$$

for all $\mathcal{S} \subseteq \mathcal{K}$ as in (3.8). In block b , the relay sends the codeword $\underline{x}_r(s_{\mathcal{K},b})$ where $s_{\mathcal{K},b} = \{s_{k,b} : k \in \mathcal{K}\}$.

The destination uses a sliding window of length $K + 1$ to decode the message blocks with the same index b . Hence, the combined encoding and decoding delay for

every message block is $K + 1$ channel-symbol blocks. We summarize the resulting rate bounds below and give the performance analysis in Appendices B.2 and B.3.

3.4.1 Two Users with Joint Decoding

Consider $K = 2$ and suppose the offset order is $\pi = (1, 2)$. Suppose the destination decodes $(w_{1,b}, w_{2,b})$ jointly by using $y_{d,b}$, $y_{d,b+1}$, and $y_{d,b+2}$. The analysis in Appendix B.2 shows that we can achieve (R_1, R_2) satisfying

$$R_1 \leq I(X_1 X_r; Y_d | X_2 V_2) \quad (3.29)$$

$$R_2 \leq I(X_2; Y_d | V_1 V_2 X_r) + I(V_2; Y_d) \quad (3.30)$$

$$R_1 + R_2 \leq I(X_1 X_2 X_r; Y_d). \quad (3.31)$$

Note that (3.29) is the same as (3.5) but (3.30) is different from (3.6). The difference arises because the destination does not know $w_{1,b+1}$ or $w_{1,b+2}$ when decoding $w_{2,b}$, in contrast with the situation of no offset discussed in Section 3.3.2. We can show that (3.6) is in general larger than (3.30) by expanding (3.6) as (see (3.13) and (3.14))

$$I(X_2 X_r; Y_d | X_1 V_1) = I(X_2 V_2 X_r; Y_d | X_1 V_1) \quad (3.32)$$

$$\begin{aligned} &= I(X_2; Y_d | X_1 V_1 V_2 X_r) \\ &\quad + I(V_2 X_r; Y_d | X_1 V_1) \end{aligned} \quad (3.33)$$

where (3.32) follows from the Markov chain $(V_1, V_2) - (X_1, X_2, X_r) - Y_d$ and (3.33) from the chain rule for mutual information. But the first mutual information term in (3.33) satisfies

$$I(X_2; Y_d | X_1 V_1 V_2 X_r) = I(X_2; X_1 Y_d | V_1 V_2 X_r) \quad (3.34)$$

$$\geq I(X_2; Y_d | V_1 V_2 X_r) \quad (3.35)$$

where (3.34) follows from the Markov chain $X_1 - (V_1, V_2, X_r) - X_2$. Similarly, the second mutual information term in (3.33) satisfies

$$I(V_2 X_r; Y_d | X_1 V_1) \geq I(V_2; Y_d | X_1 V_1) \quad (3.36)$$

$$= I(V_2; X_1 V_1 Y_d) \quad (3.37)$$

$$\geq I(V_2; Y_d) \quad (3.38)$$

where (3.37) follows from the independence of (X_1, V_1) and V_2 . It thus seems that we do not achieve all points in the backward decoding region. However, we next show that we can obtain the corner points of the destination's backward decoding region.

There are several types of corner points depending on whether the polytopes defined by the relay bounds (3.2)-(3.4) and the destination bounds (3.5)-(3.7) intersect. We focus on the destination bounds because the relay bounds are the same for both no-offset and offset encoding. Note, however, that if the polytopes intersect as in Fig. 3.3, then one of the corner points of the shaded region is not a corner point of the destination's backward decoding region. To achieve such points, it turns out that we can use either no-offset or offset encoding, as shown below. Alternatively, we could time-share between different offset orders, but this increases the decoding delay.

Consider the corner point

$$(R_1, R_2) = (I(X_1 X_r; Y_d | X_2 V_2), I(X_2 V_2; Y_d)) \quad (3.39)$$

labeled " $\pi = (1, 2)$ " in Fig. 3.5. We can achieve this point (ignoring the relay bounds (3.2)-(3.4)) provided that the sum of (3.29) and (3.30) is less restrictive than (3.31). But (3.31) expands as

$$R_1 + R_2 \leq I(X_1 X_2 X_r; Y_d) \quad (3.40)$$

$$= I(X_1 X_2 V_2 X_r; Y_d) \quad (3.41)$$

$$= I(X_1 X_r; Y_d | X_2 V_2) + I(X_2 V_2; Y_d). \quad (3.42)$$

where (3.41) follows from the Markov chain $V_2 - (X_1, X_2, X_r) - Y_d$. We further have

$$I(X_2 V_2; Y_d) = I(X_2; Y_d | V_2) + I(V_2; Y_d) \quad (3.43)$$

$$\leq I(X_2; V_1 X_r Y_d | V_2) + I(V_2; Y_d) \quad (3.44)$$

$$= I(X_2; Y_d | V_1 V_2 X_r) + I(V_2; Y_d) \quad (3.45)$$

where (3.45) follows from the Markov chain $X_2 - V_2 - (V_1, X_r)$. Thus, we achieve the corner point under consideration. For the offset order $\pi = (2, 1)$, we similarly obtain the corner point labeled “ $\pi = (2, 1)$ ” in Fig. 3.5. The shaded region in Fig. 3.5 shows the points achieved by no-offset encoding that are defined by (3.10)-(3.12). Interestingly, the union of rate-pairs achieved by the three methods (no-offset encoding, offset encoding with $\pi = (1, 2)$, offset encoding with $\pi = (2, 1)$) is precisely the backward decoding rate region. Alternatively, we can achieve the backward decoding rates by time-sharing between different offset orders, but this increases delay. Rate-splitting methods [42, 43] might let one avoid such delays.

Finally, we remark that the above shows that offset encoding improves sliding-window decoding, since one now achieves the corner point of the example in Section 3.3.2.

3.4.2 K Users with Successive Decoding

We wish to show that offset encoding recovers the destination’s backward decoding corner points for $K > 2$. However, the generalization of (3.29)-(3.31) is unwieldy and gives limited insight. Instead, we use successive decoding inside the sliding window to obtain the backward decoding corner points.

We begin by considering the set function (see (3.8))

$$f(\mathcal{S}) = \begin{cases} I(X_{\mathcal{S}} X_r; Y_d | X_{\mathcal{S}^c} V_{\mathcal{S}^c}), & \mathcal{S} \subseteq \mathcal{K}, \mathcal{S} \neq \emptyset \\ 0, & \mathcal{S} = \emptyset \end{cases} \quad (3.46)$$

for some distribution satisfying (3.9) with U a constant. We claim that $f(\cdot)$ is submodular [44, Ch. 44]. To see this, consider k_1 and k_2 in \mathcal{K} with $k_1 \neq k_2$, $k_1 \notin \mathcal{S}$, $k_2 \notin \mathcal{S}$,

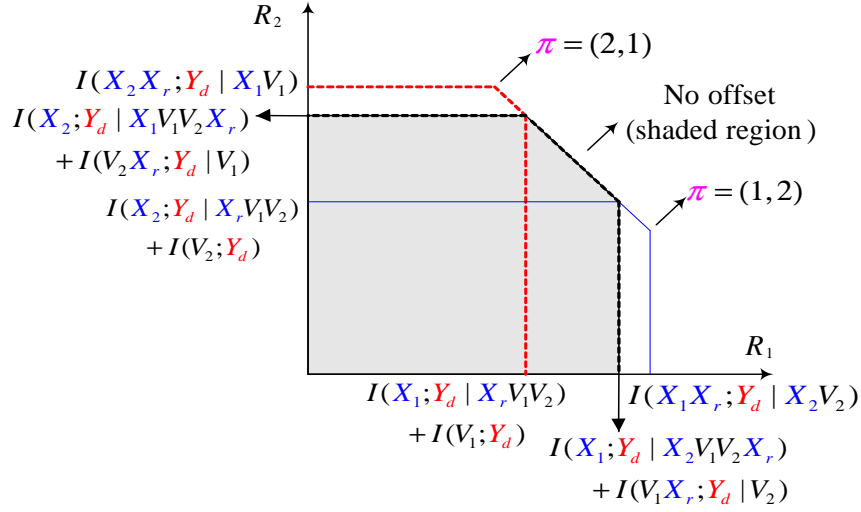


Figure 3.5: Rate region with sliding-window decoding and offset encoding.

and expand

$$\begin{aligned}
 & f(\mathcal{S} \cup \{k_1\}) + f(\mathcal{S} \cup \{k_2\}) \\
 &= I(X_{\mathcal{S}}X_{k_1}V_{k_1}X_r; Y_d | X_{(\mathcal{S} \cup \{k_1\})^c} V_{(\mathcal{S} \cup \{k_1\})^c}) \\
 & \quad + I(X_{\mathcal{S}}X_{k_2}V_{k_2}X_r; Y_d | X_{(\mathcal{S} \cup \{k_2\})^c} V_{(\mathcal{S} \cup \{k_2\})^c}) \tag{3.47}
 \end{aligned}$$

$$\begin{aligned}
 &= I(X_{k_1}V_{k_1}; Y_d | X_{(\mathcal{S} \cup \{k_1\})^c} V_{(\mathcal{S} \cup \{k_1\})^c}) \\
 & \quad + I(X_{\mathcal{S}}X_r; Y_d | X_{\mathcal{S}^c} V_{\mathcal{S}^c}) \\
 & \quad + I(X_{\mathcal{S}}X_{k_2}V_{k_2}X_r; Y_d | X_{(\mathcal{S} \cup \{k_2\})^c} V_{(\mathcal{S} \cup \{k_2\})^c}) \tag{3.48}
 \end{aligned}$$

where (3.47) follows from the Markov chain $V_{\mathcal{K}} - (X_{\mathcal{K}}, X_r) - Y_d$ and (3.48) from the chain rule for mutual information. We lower bound the first term in (3.48) as

$$\begin{aligned}
 & H(X_{k_1}V_{k_1} | X_{(\mathcal{S} \cup \{k_1\})^c} V_{(\mathcal{S} \cup \{k_1\})^c}) \\
 & \quad - H(X_{k_1}V_{k_1} | X_{(\mathcal{S} \cup \{k_1\})^c} V_{(\mathcal{S} \cup \{k_1\})^c} Y_d) \\
 &= H(X_{k_1}V_{k_1} | X_{(\mathcal{S} \cup \{k_1, k_2\})^c} V_{(\mathcal{S} \cup \{k_1, k_2\})^c}) \\
 & \quad - H(X_{k_1}V_{k_1} | X_{(\mathcal{S} \cup \{k_1\})^c} V_{(\mathcal{S} \cup \{k_1\})^c} Y_d) \tag{3.49}
 \end{aligned}$$

$$\geq I(X_{k_1}V_{k_1}; Y_d | X_{(\mathcal{S} \cup \{k_1, k_2\})^c} V_{(\mathcal{S} \cup \{k_1, k_2\})^c}) \tag{3.50}$$

where (3.49) follows from the independence of the (X_k, V_k) and (3.50) because conditioning cannot increase entropy. The expression (3.50) added to the final term in (3.48) is

$$I(X_{\mathcal{S} \cup \{k_1, k_2\}} X_r; Y_d | X_{(\mathcal{S} \cup \{k_1, k_2\})^C} V_{(\mathcal{S} \cup \{k_1, k_2\})^C}). \quad (3.51)$$

Inserting (3.50) into (3.48), we have

$$f(\mathcal{S} \cup \{k_1\}) + f(\mathcal{S} \cup \{k_2\}) \geq f(\mathcal{S}) + f(\mathcal{S} \cup \{k_1, k_2\}) \quad (3.52)$$

for both $\mathcal{S} \neq \emptyset$ and $\mathcal{S} = \emptyset$. The set function $f(\cdot)$ is therefore submodular by [44, Theorem 44.1, p. 767].

The above shows that the rate region defined by the destination bounds (see (3.8))

$$R_{\mathcal{S}} \leq I(X_{\mathcal{S}} X_r; Y_d | X_{\mathcal{S}^c} V_{\mathcal{S}^c}), \quad \mathcal{S} \subseteq \mathcal{K} \quad (3.53)$$

is a polymatroid associated with $f(\cdot)$ (see [44, p. 767]). But the non-zero corner points of this polymatroid are known to be given by (see [44, p. 777])

$$R_{\pi(k)} = \begin{cases} f(\{\pi(1), \dots, \pi(k)\}) \\ -f(\{\pi(1), \dots, \pi(k-1)\}), & k \leq \ell \\ 0, & k > \ell \end{cases} \quad (3.54)$$

where π is a permutation of the source indices, $k = 1, 2, \dots, K$, and $\ell = 1, 2, \dots, K$.

For example, consider $\pi = (1, 2, \dots, K)$ for which (3.54) evaluates to

$$R_k = \begin{cases} I(X_1 X_r; Y_d | X_{[2, K]} V_{[2, K]}), & k = 1 \\ I(X_k V_k; Y_d | X_{[k+1, K]} V_{[k+1, K]}), & 2 \leq k \leq \ell \\ 0, & k > \ell \end{cases} \quad (3.55)$$

where $X_{[K+1, K]}$ and $V_{[K+1, K]}$ are considered to be constants.

We are mainly interested in the corner points of the *base polytope* defined by $\ell = K$ in (3.54) (see [44, p. 767]) because the other corner points are achieved by discarding message bits. The expression (3.54) shows that there are up to $K!$ base polytope corner points, namely one point for each π .

Suppose the offset order is $\pi = (1, 2, \dots, K)$ as in Fig. 3.4. Consider the window with the channel-symbol blocks $\underline{y}_{d,1}, \underline{y}_{d,2}, \dots, \underline{y}_{d,K+1}$. In this window, the destination successively decodes $w_{K,1}, w_{K-1,1}, \dots, w_{1,1}$ by assuming that its past decoding steps were successful. In Appendix B.3, we show that one can approach the rate point $\underline{R} = (R_1, R_2, \dots, R_K)$ with

$$R_k = \begin{cases} I(X_1 X_r; Y_d | X_{[2,K]} V_{[2,K]}), & k = 1 \\ I(X_k V_k; Y_d | X_{[k+1,K]} V_{[k+1,K]}), & 2 \leq k \leq K \end{cases} \quad (3.56)$$

where $X_{[K+1,K]}$ and $V_{[K+1,K]}$ are considered to be constants. The codewords contributing to these rates are shown as shaded blocks in Fig. 3.4. But the rates (3.56) are precisely the rates in (3.55) for $\ell = K$. Hence we achieve the desired corner point. We can achieve the other corner points by changing the offset order π . Finally, we can achieve the non-corner points by time-sharing between offset orders. An interesting open problem is whether the union of rate points achieved by using all combinations of offset orderings and no-offsets gives the backward decoding rate region (see Fig. 3.5). If so, then there is no need to time share between offset orders.

3.5 Conclusions

We presented an offset encoding technique for DF that improves the rate region of sliding-window decoding. The technique achieves the corner points of the destination's backward decoding rate region but avoids the excessive delay associated with backward decoding. Offset encoding will clearly apply to other multi-terminal problems [41, 45–47].

Chapter 4

User vs. Relay Cooperation in a Multiaccess Network

4.1 Introduction

Cooperation results when nodes in a network share their power and bandwidth resources to mutually enhance their transmissions and receptions. Cooperation can be induced in several ways. In their seminal paper on *user cooperation* [3], Sendonaris *et al* demonstrate that rate and diversity gains can be achieved when a pair of users in a wireless multiaccess channel (MAC) cooperate. Alternately, one can induce cooperation by introducing a layer of dedicated relay nodes between the sources (user) and the destinations [28]. For example, in [9–13, 48] and the references therein, the rates achieved between a source-destination pair using one or more wireless relays is studied.

In this chapter, we compare two approaches to inducing cooperation in a multiaccess channel comprised of K sources and one destination. First, we allow source nodes to forward data for each other and second, we introduce a wireless relay node when cooperation between the sources nodes is either undesirable or not possible. We refer to networks employing the former approach as *user cooperative networks* and those employing the latter as *hierarchical relay networks*. We model the user cooperative network as a multiaccess channel with generalized feedback (MAC-GF) [7] and the hierarchical relay network as a MARC [45]. We assume single-antenna nodes and place *half-duplex* constraints on the transmit-receive capabilities of all nodes. Note that this requires time-duplexing sources in the cooperative network but not in the relay network [28, 49]. However, to achieve a fair comparison, we assume that the source nodes in both networks time-duplex their transmissions. We develop *partial decode-and-forward* (PDF) strategies, also called *multipath decode-and-forward* (MDF) [4],

for both networks. As the name suggests, in PDF, the cooperating node/relay decodes the user messages before forwarding them to the destination; further, the sources also send an additional message that is decoded only at the destination. Note that when the sources do not transmit an additional message stream to the destination, PDF simplifies to a *decode-and-forward* (DF) strategy and thus our analysis encompasses DF as a special case (see Appendix C.1). Further, for the user cooperative network we present a PDF strategy that allows an arbitrary number of half-duplex users to cooperate with each other. For a MARC with time-duplexed sources, the PDF strategy simplifies to that for a half-duplex relay channel [31]. Finally, we also consider *amplify-and-forward* (AF) strategies for both networks where each cooperating node or relay scales its received signal before forwarding it to the destination.

There are important differences between user cooperative and hierarchical relay networks that are not easy to analyze from an information-theoretic point of view. For example, in cooperative networks one likely needs economic incentives to induce cooperation [21]. On the other hand, hierarchical networks incur infrastructure costs [36]. While incentives and infrastructure costs are important elements that need to be considered in comparing the two networks, we use the total transmit and processing power consumed in each network as a cost metric for our comparisons. Thus, in addition to a transmit power, we also include in our costs the *processing power* consumed at each node for both cooperative and individual transmissions. To this end, we present a model for quantifying the processing power as a function of the transmission rate, and hence, the transmit signal-to-noise ratio (SNR). The model also introduces *processing scale factors* that can be roughly characterized as the ratio of the energy cost required for processing to that required for transmission. In [4, Chap. 6], the authors argue that cooperation is beneficial in the ‘*long-distance*’ regime where the energy costs of transmission offset the energy costs of reception. Thus, by accounting for both the transmit and processing power (energy) costs, we identify the regimes where cooperation is energy efficient and determine the *cross-over SNR* and *processing factor* thresholds that

characterize the cooperative regime.

Cooperation in wireless networks has been shown to achieve gains in achievable rates and fading diversity. However, the gains achieved are in general a function of the transmission parameters and network geometry. In an effort to generalize such results, we present an *area-averaged* comparison. Specifically, we consider a sector of a circular area with the destination at the center and users randomly distributed in the sector. For the case of relay cooperation we fix the position of the relay. We remark that this geometry encompasses a variety of centralized network architectures ranging from wireless LAN and cellular to sensor networks. Further, our choice of a sectorized area is motivated by the desire to maximize rate and diversity gains that result from both user cooperation between adjacent nodes and from using a single relay in a circular area. We present results for three kinds of wireless channel models, namely, the no-fading, the ergodic fading, and the quasi-static fading model to model line-of-sight, fast-fading, and slow fading environments respectively. For the first two models, we compare the maximum sum-rates achieved by PDF and AF for both networks using a bits/Joule metric. We also compare these results with the sum-capacity achieved by a MAC with time-duplexed sources and without user or relay cooperation. Our results demonstrate the effect of processing power in cooperation and are summarized by the following three observations:

- User or relay cooperation using PDF is most desirable in the regime where processing power is negligible relative to transmit power. Thus, while cooperation does not achieve multiplexing gains [9, 14, 15], decoding-based cooperative schemes can be relevant in the regime where transmit power costs dominate, i.e., in the *long-distance communication* regime [4, Chap. 6].
- For AF, a cooperative strategy with negligible processing costs, user cooperation achieves negligible gains in rate and energy efficiency relative to the time-duplexed MAC. Further, relaying is desirable relative to both user cooperation

and no cooperation in the regime where processing costs are comparable to transmit costs. This is because in this regime, the high processing costs at the users helps offset the additional transmit costs at the relay.

- On average, relay cooperation is more energy efficient than user cooperation. This is dominantly due to half-duplex nature of resource (power and bandwidth) sharing in user cooperative networks.

In general, the ratio of processing to transmission power depends on both the device functionality and the application supported. Thus, for short range mobile environments comprised of either energy constrained devices (such as sensors) or devices supporting high rate applications (such as laptops), it has been shown that the processing costs dominate transmission costs [4, 50, 51]. On the other hand, low-rate cellular-like communications are characterized by high transmission costs. Our results indicate that different cooperative schemes are appropriate for networks and devices operating in the different processing vs. transmit power regimes.

To understand the maximum diversity gains achievable by the two cooperative approaches, we compare the outage performance of the two networks for both DF and AF as a function of the total SNR at all transmitting nodes. We specifically consider the dynamic DF (DDF) protocol where the cooperating nodes or relay cooperate with the transmitting users only after successfully decoding their received signals [14]. In general, analytical expressions for outage probability are not easy to develop. However, as with multi-antenna networks [52], the benefits of cooperation can be quantified via an asymptotic diversity-multiplexing tradeoff analysis, see, for e.g. [9, 14, 15, 53]. In addition to the diversity-multiplexing tradeoff, one can also distinguish cooperative strategies and their characteristic distributed architectures via a *coding (SNR) gains* [54] that quantifies the network topology (quantified via distance-dependent path-gains) and coding scheme. To this end, we develop geometry-inclusive upper and lower bounds on the outage probability for both networks under DDF and AF. A geometry-inclusive

outage analysis is developed in [9, 54, 55] and [16] for the high SNR and the low SNR (wideband) regimes respectively. We here develop bounds using high SNR approximations and use numerical simulations to demonstrate the appropriateness of the analysis to the intermediate SNR regime.

For a fixed rate and for single antenna nodes, the diversity-multiplexing tradeoff analysis for both DDF and AF shows that the maximum diversity achievable for the relay network, irrespective of the number of users K , is 2 [14, 53, 56]. On the other hand in [14] the authors show that for specific cooperative strategies the K -user cooperative network can achieve a maximum diversity of K . Using a geometry-inclusive outage analysis we show that the maximum diversity predicted by the DM tradeoff analysis may not always be achievable in practical SNR regimes of interest without trading off delay and complexity. Finally, we present the outage results as a function of the total power to demonstrate the energy costs of achieving a desired diversity.

This chapter is organized as follows. In Section 4.2, we present the network and channel models and develop a power-based cost metric. In Section 4.3, we develop the PDF, DF, and AF strategies for both networks. We present the achievable rate regions for a non-fading and ergodic fading Gaussian channels and develop the geometry-inclusive outage probability analysis for a quasi-static fading model.

4.2 Channel and Network Models

4.2.1 Network Model

Our networks consist of K users (source nodes) numbered $1, 2, \dots, K$ and a destination node d . For the MARC there is one additional node, the relay node r (see Fig. 4.1). The input and output alphabets of node k are \mathcal{X}_k and \mathcal{Y}_k , respectively. We impose a *half-duplex* constraint on every node, i.e., each node can be in one of two modes, *listen* (L) or *transmit* (T) (LoT). We write $\mathcal{K} = \{1, 2, \dots, K\}$ for the set of users, $x_{\mathcal{S}} = \{x_m : m \in \mathcal{S}\}$, and $R_{\mathcal{S}} = \sum_{m \in \mathcal{S}} R_m$ for $\mathcal{S} \subseteq \mathcal{K}$. For the MARC, we write $\mathcal{T} = \mathcal{K} \cup \{r\}$

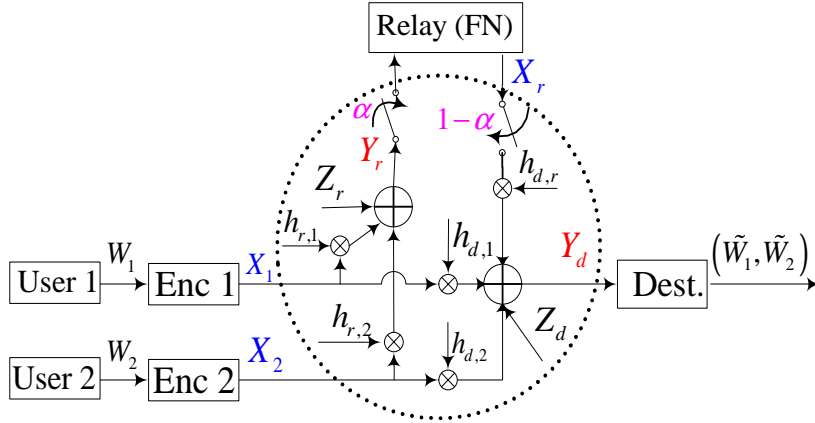


Figure 4.1: A two-user Gaussian MARC.

for the set of transmitters.

Let $X_{k,i} \in \mathcal{X}_k$ be the input of node k at time i . We model the two wireless multiaccess networks under study as additive Gaussian noise channels with fading. For such channels, the output of node m at time i is

$$Y_{m,i} = \begin{cases} \left(\sum_{k \neq m} h_{m,k,i} X_{k,i} \right) + Z_{m,i} & M_{m,i} = L \\ 0 & M_{m,i} = T \end{cases} \quad (4.1)$$

where the $Z_{m,i}$ are independent, proper, complex, zero-mean, unit variance Gaussian noise random variables, $M_{m,i}$ is the half-duplex mode at node m , and $h_{m,k,i}$ is the fading gain between transmitter k and receiver m at time i . We assume that both channels are used n times, i.e., $i = 1, 2, \dots, n$. Note that for both networks as well as the (non-cooperative) MAC, $X_{d,i} = 0$, i.e., $M_{d,i} = L$, for all i . Further, for the MAC, we also have $Y_{k,i} = 0$, i.e., $M_{k,i} = T$, for all i and for all $k \in \mathcal{K}$. We assume that the transmitted signals in both networks are constrained in power as

$$\sum_{i=1}^n E |X_{k,i}|^2 \leq nP_k \quad k \in \mathcal{T}. \quad (4.2)$$

We assume that the modes $M_{k,i}$ for all k are either known universally to all nodes at all times or shared, when needed, between all nodes with negligible overhead. We

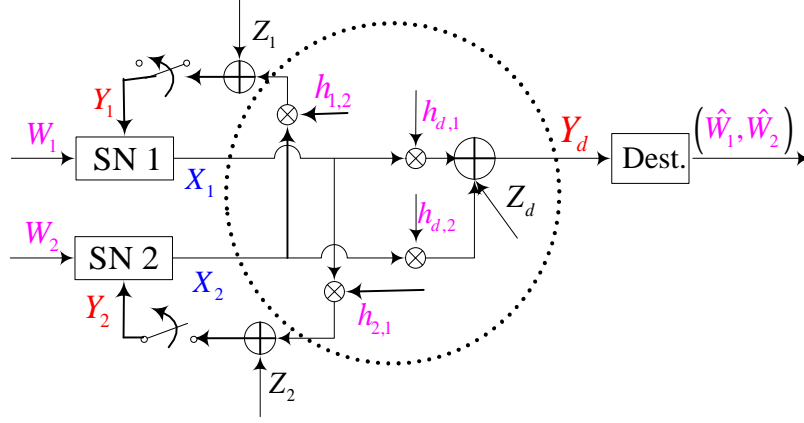


Figure 4.2: A two-user multiaccess channel with generalized feedback.

also assume that the nodes can adjust the duration of their modes to maximize a desired performance metric. Finally, we remark that one can generalize the model in (4.1) to include a sleep state as well as cost constraints for each mode [31].

The capacity region $\mathcal{C}_{\text{MARC}}$ of a K -user MARC is the closure of the set of rate tuples (R_1, R_2, \dots, R_K) for which the destination can, for sufficiently large N , decode the K source messages with an arbitrarily small positive error probability [24]. We define the capacity region $\mathcal{C}_{\text{MAC-GF}}$ of the MAC-GF similarly. Finally, we use the usual notation for entropy and mutual information [29, 30] and take all logarithms to the base 2 so that our rate units are bits. We write random variables (e.g. W_k) with uppercase letters and their realizations (e.g. w_k) with the corresponding lowercase letters. We drop subscripts on probability distributions if the arguments are lowercase versions of the random variables, e.g., we write the distribution of $H_{k,j}$ as $p(h_{k,j})$. We use h^* to denote the complex conjugate of a scalar h and H^\dagger to denote the complex conjugate transpose of a matrix H . Finally, throughout the sequel we use the words user and source interchangeably.

4.2.2 Hierarchical Relay Network

We model the hierarchical relay network as a Gaussian MARC with $K + 1$ inputs $X_{k,i}$, $k \in \mathcal{T}$, and two outputs $Y_{r,i}$ and $Y_{d,i}$ given by (4.1). Note that in this network the sources do not cooperate and thus, $Y_{k,i} = 0$, for all $k \in \mathcal{K}$. In general, all users in a MARC can transmit simultaneously while the relay half-duplexes its transmissions [45] (see Fig. 4.1). However, for comparison purposes as well as to simplify the exposition, we consider a time-duplexed model where each source transmits messages over the channel for a fixed period $T = 1/K$ of the total time. Further, the transmission period of source k , for all k , is sub-divided into two slots such that the relay listens in first slot and transmits in the second slot. We denote the time fractions for the two slots as θ_k and $\bar{\theta}_k = 1 - \theta_k$ for user k such that $\theta_k = \Pr(M_r = L) = 1 - \Pr(M_r = T)$. The time-duplexed two-hop scheme for the MARC is illustrated in Fig. 4.3 for user 2 where $\mathcal{C}_2 = \{r\}$ denotes the set of nodes that cooperate with user 2. We remark that the time-duplex multiaccess (TDMA) model considered here simplifies the analysis for the MARC to that for single-source relay channel and henceforth we refer to this model as a TD-MARC. Finally, note that Fig. 4.3 also includes the slotting schemes for a MAC and a MAC with time-duplexed sources (TD-MAC).

4.2.3 Cooperative Network

We model the cooperative network as a Gaussian MAC-GF (see Fig. 4.2). In [7], Willems developed a cooperative strategy, now often referred to as PDF, for a two-user MAC with cooperating sources. In general, there is a combinatorial explosion in the number of ways one can duplex K sources over their half-duplex states. In [45], we present a scheme where all K users cooperate with each other over $K + 1$ slots. In general, however, only a subset of sources with appropriate inter-user channels can benefit from cooperation. We now present two schemes that allow each user to be aided by an arbitrary number of users, up to K . In both schemes the users time-duplex their

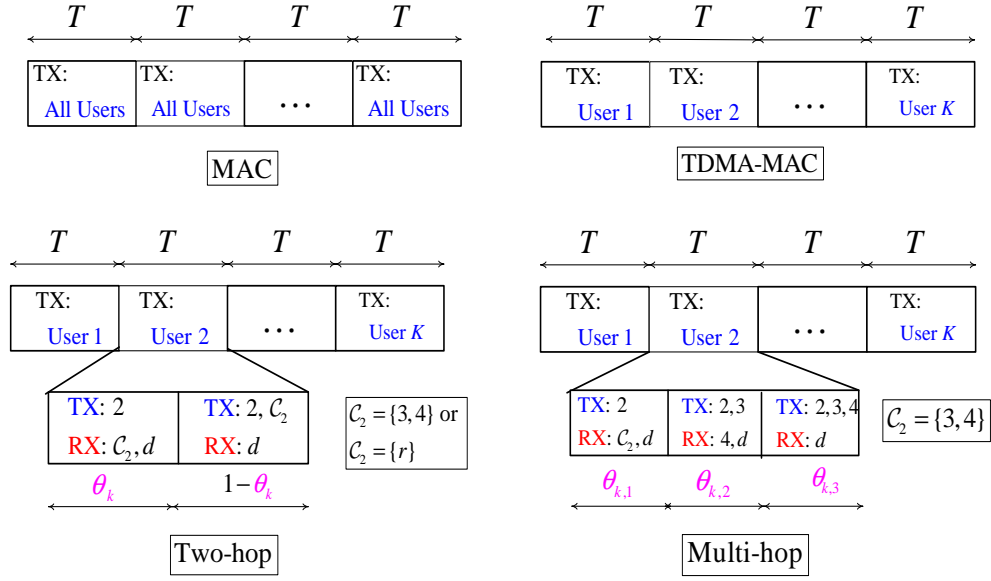


Figure 4.3: Time-duplexed transmission schemes for the MARC, the MAC-GF, and the MAC.

transmissions such that each user transmits its messages over a fixed period $T = 1/K$ of the total available time. The two schemes differ in the manner the period T is further sub-divided between the transmitting and the cooperating users.

In the first scheme, we restrict cooperation to a *two-hop scheme* such that the period over which user k , for all k , transmits is sub-divided into two slots. In the first slot only user k transmits while in the second slot both user k and the set C_k of users that cooperate with user k transmit as shown in Fig. 4.3 for user 2 and $C_2 = \{3, 4\}$. We remark that this scheme has the same number of hops as the MARC scheme described above except now one user at a time is aided by some set of other users, i.e., $C_k \subset \mathcal{K}$. We write θ_k and $1 - \theta_k$ to denote the time fractions associated with the first and second slots of user k such that $\theta_k = \Pr(M_j = L) = 1 - \Pr(M_j = T)$ for all $j \in C_k$.

The second scheme we consider is a *multi-hop scheme* where we divide the total transmission time for source k into L_k slots, $1 \leq L_k \leq K$. Thus, in each time-slot, except the first slot where only user k transmits, one additional user cooperates in the transmission until all L_k users transmit in slot L_k . We denote the l^{th} time fraction for

user k as $\theta_{k,l}$, $l = 1, 2, \dots, L$. Note that $L_k = |\mathcal{C}_k| - 1$ where \mathcal{C}_k is the set of users that cooperate with user k . The time-duplexed L_k -hop scheme is demonstrated in Fig. 4.3 for user 2 with $L_2 = 3$ and $\mathcal{C}_2 = \{3, 4\}$. We henceforth refer to this model as a MAC-GF with time-duplexed sources or simply a TDMA MAC-GF.

Remark 4.1 *Observe that the TDMA model described for the MARC is also a two-hop model with $\mathcal{C}_k = \{r\}$ for all k .*

Remark 4.2 *We remark that for both networks under AF, we assume equal length slots and consider a symbol-based slotted two-hop and multi-hop scheme.*

4.2.4 Cost Metric: Total Power

From (4.2) we see that the cooperative relay network has additional power relative to the other two networks due to an extra relay node. We incorporate a measure of fairness in our comparisons by using the total power consumed by each network as the cost metric. Further such a comparison also allows us to develop the energy regimes where cooperation is desirable.

We observe that in addition to a transmission power cost a node also consumes power in processing, i.e., encoding and decoding its transmissions and receptions respectively. In addition to its own transmission and processing costs, a node that relays for others consumes additional power in encoding and decoding packets for others. We account for this by introducing processing costs for both encoding and decoding as a function of the transmission and reception rates. To this end, we define encoding and decoding factors η_k and δ_k respectively and write the power required to process the transmissions of node j at node k as

$$P_{k,j}^{proc} = P_{k,0}^{proc} + (\eta_k I_k^{enc}(j) + \delta_k I_k^{dec}(j)) f(R_j) \quad \text{for all } k \in \mathcal{T}, j \in \mathcal{K} \quad (4.3)$$

where $I_k^{enc}(j)$ and $I_k^{dec}(j)$ are indicator functions that are set to 1 if user k encodes and decodes respectively for user j , $P_{k,0}^{proc}$ is the minimum processing power at user k that

in general depends on the device functionality and design, and $f(R_j)$ is a function of the transmission rate R_j at user j . Note that $P_{k,k}^{proc}$ is the power consumed by node k in processing its own transmissions while $P_{k,j}^{proc}$ is that required to cooperate with user j and thus, by definition, $P_{r,r}^{proc} = P_{r,0}^{proc}$. The function f modeling the processing cost typically depends on the encoding and decoding schemes used as well as the device functionality. For the Gaussian channel model considered here, since the rate R_k is proportional to the transmit SNR P_k , we choose f as

$$f = \log(1 + P_k) \quad \text{for all } k. \quad (4.4)$$

Note that in general the rate R_k depends on the cooperative scheme used. However, we justify the choice of f in (4.4) by observing that cooperative schemes, while enabling coherent combining gains, do not achieve multiplexing gains relative to non-cooperative communications. Finally, we assume that the destination in typical multi-access networks such as cellular or many-to-one sensor networks [57] has access to an unlimited energy source and ignore its processing costs in computing the total power consumed in the network.

We thus write the total power consumed at node k , $k \in \mathcal{T}$, as

$$P_{k,tot} = \begin{cases} P_k + P_{k,k}^{proc} + \sum_{j \in \mathcal{K}, j \neq k} I_k(j) P_{k,j}^{proc} & k \in \mathcal{K} \\ P_k + \sum_{j \in \mathcal{K}} I_k(j) P_{k,j}^{proc} & k = r \end{cases} \quad (4.5)$$

where $I_k(j)$ is an indicator function that takes the value 1 if node k cooperates with node j . The first $P_{k,k}^{proc}$ term corresponds to the power used to process its own message while the second summation term accounts for the power node k incurs in cooperating with all other source nodes. Observe that the relay node only incurs processing costs for those source nodes that it aids.

The total power consumed by all transmitting nodes in each network is given as

$$P_{tot} = \begin{cases} \sum_{k \in \mathcal{K}} P_{k,tot} & \text{MAC-GF or MAC} \\ \sum_{k \in \mathcal{T}} P_{k,tot} & \text{MARC.} \end{cases} \quad (4.6)$$

We remark that for the AF strategy, $P_r^{tot} = P_r + P_{r,0}^{proc}$ a cooperating node or the relay does not expend power in processing (encoding and/or decoding) signals for any user.

We write the power normalized rate in bits/s/Watt (= bits per Joule) as

$$R_{bpJ} = \frac{R}{P_{tot}} \text{ bits/Joule} \quad (4.7)$$

where P_{tot} is the total power consumed by all transmitters involved in achieving the rate R and is given by (4.6). We refer to the power normalized sum-rate achieved by a specific communication strategy as its *energy efficiency* in bits per Joule. Thus, for a K -user multiaccess network, the energy efficiency for a specific transmission scheme is given by the ratio of largest R_K achieved by the scheme to the total consumed power P_{tot} in (4.6). One can similarly compare the outage probability of a multiaccess network as a function of P_{tot} for different cooperative and non-cooperative communication strategies.

4.2.5 Fading Models

We model the fading gains as

$$h_{m,k,i} = \frac{A_{m,k,i}}{\sqrt{d_{m,k}^\gamma}} \quad (4.8)$$

where $d_{m,k}$ is the distance between the m^{th} receiver and the k^{th} source, γ is the path-loss exponent, and $A_{m,k,i}$ is a proper complex fading random variable. We assume that the fading gain $h_{m,k,i}$ is known only at receiver m . We consider three kinds of fading channels in this paper.

1. no fading $A_{m,k,i} = 1$ for all m, k, i .
2. ergodic Rayleigh fading where $A_{m,k,i}$ are jointly independent and identically distributed (i.i.d) zero-mean, unit variance proper, complex Gaussian random variables.
3. quasi-static Rayleigh fading where $A_{m,k,i}$ are jointly i.i.d zero-mean, unit variance proper, complex Gaussian random variables.

We assume that the fading gains are independent of the transmitted signals X_k , for all $k \in \mathcal{T}$. Finally, without loss of generality, we assume that no two nodes are co-located.

4.3 Cooperative Strategies

We now develop the cooperative strategies of PDF and AF for the two networks. For each network, we present the rate regions achieved by the two strategies for the no fading and ergodic fading channel models. Finally, for the quasi-static fading channel, we present an outage probability analysis.

4.3.1 Partial- and Dynamic- Decode-and-Forward

In [6], Cover and El Gamal present an achievable strategy for a single-source relay channel where the relay decodes the source messages before forwarding them to the destination. This strategy, now often called decode-and-forward (DF), extends easily to both a full-duplex [10, 58] and half-duplex MARC [28]. Note that for half-duplex channels, the cooperating node or relay decodes the message from the source in its ‘*listen*’ mode and forwards the decoded message in its ‘*transmit*’ mode. The source on the other hand transmits the same message in both modes. One can generalize this construction by allowing the source to also transmit a new message in the relay’s ‘*transmit*’ mode. We refer to the resulting strategy as partial decode-and-forward (PDF) (see [31, Sec. 3.3]).

MARC with Time-Duplexed Sources

For a MARC with time-duplexed sources the PDF strategy for each user simplifies to the PDF strategy for a single-source relay channel (see [31, Sec. 3.3]). In Appendix C.1, we develop the PDF rate bounds for a general single-source multi-relay channel

under a two-hop scheme. We specialize the bounds for the time-duplexed MARC below.

Achievable Rates: The rate bounds achieved by PDF for a Gaussian single-source relay channel under a half-duplex constraint are developed in Appendix C.1. We briefly describe the code construction below. We use Gaussian signaling at the sources and relay such that in slot k , in each use of the channel, user k transmits

$$X_k = \begin{cases} \sqrt{\alpha_k \bar{P}_k} U_k & \text{frac. } \theta_k \\ \sqrt{\alpha_k \bar{P}_k} Q_k + \sqrt{\bar{\alpha}_k \bar{P}_k} V_k & \text{frac. } \bar{\theta}_k \end{cases} \quad (4.9)$$

where $\theta_k = \Pr(M_j = L)$, U_k , Q_k , and V_k are i.i.d circularly symmetric complex Gaussian random variables with zero mean and unit variance and $\bar{\alpha}_k = 1 - \alpha_k$ and from (4.2) for time-duplexed users we have

$$\bar{P}_k = K P_k \quad (4.10)$$

$$\bar{P}_r = P_r / \bar{\theta}_k. \quad (4.11)$$

Finally, the relay's signal in its transmit fraction is

$$X_r = \sqrt{\bar{P}_r} V_k. \quad (4.12)$$

From (4.9), we see that source k transmits a new message via U_k in both fractions while allocating a fraction of its power to cooperating with the relay via V_k in the second fraction. In Appendix C.1, we show that when the channel gains are fixed, the rate R_k is achievable when

$$R_k \leq \max_{(\theta_k, \alpha_k)} \min(I_1^r(\theta_k, \alpha_k), I_2^r(\theta_k, \alpha_k)) \quad (4.13)$$

where

$$I_1^r(\theta_k, \alpha_k) = \theta_k \log(1 + |h_{r,k}|^2 \bar{P}_k) + \bar{\theta}_k \log(1 + \alpha_k |h_{d,k}|_k^2 \bar{P}_k) \quad (4.14)$$

$$\begin{aligned} I_2^r(\theta_k, \alpha_k) = & \theta_k \log(1 + |h_{d,k}|_k^2 \bar{P}_k) \\ & + \bar{\theta}_k \log\left(1 + |h_{d,k}|^2 \bar{P}_k + |h_{d,r}|^2 \bar{P}_r + 2 \operatorname{Re}\left(\sqrt{\bar{\alpha}_k \bar{P}_k \bar{P}_r} h_{d,k} h_{d,r}^*\right)\right) \end{aligned} \quad (4.15)$$

The sum-rate of the TD-MARC is then obtained as

$$R_{\mathcal{K}} = \frac{1}{K} \sum_{k=1}^K R_k. \quad (4.16)$$

For the ergodic fading case we write R_k as

$$R_k \leq \max_{(\theta_k, \alpha_k)} \min(\mathbb{E} I_1^r(\theta_k, \alpha_k), \mathbb{E} I_2^r(\theta_k, \alpha_k)) \quad (4.17)$$

where the expectation is over the joint fading distribution. Note that we assume that the channel state information (CSI) is only known at the receivers. Thus, we can use an analysis similar to that in ([33, Sec 4.2]) to show that $\alpha_k = 1$ maximizes the bounds for this case, i.e., the sources and the relay do not achieve coherent combining gains at the destination.

Outage Probability: For a quasi-static fading channel where the CSI is not available at the transmitters, an outage occurs when the rate transmitted falls below that supported by the channel. Observe that to achieve the spatial diversity gains of a 2×1 antenna array, it suffices to consider the DF strategy, i.e., in the k^{th} slot, for all k , user k and the relay use independent codebooks in the $\bar{\theta}_k$ fraction to retransmit the message transmitted in the θ_k fraction. The resulting code construction for user k simplifies as

$$X_k = \begin{cases} \sqrt{\alpha_k \bar{P}_k} U_k & \text{frac. } \theta_k \\ \sqrt{\alpha_k \bar{P}_k} Q_k & \text{frac. } \bar{\theta}_k \end{cases} \quad (4.18)$$

while the relay transmits

$$X_r = \sqrt{\alpha_k \bar{P}_k} V_k \quad (4.19)$$

where U_k , Q_k , and V_k are i.i.d circularly symmetric complex Gaussian random variables with zero mean and unit variance. One can use the same techniques as in Appendix C.1 to show that the achievable rate for a particular instantiation of the channel is bounded by

$$R_k \leq \min(I_1^r(\theta_k), I_2^r(\theta_k)) \quad (4.20)$$

where

$$I_1^r(\theta_k, \alpha_k) = \theta_k \log(1 + |h_{r,k}|^2 \bar{P}_k) \quad (4.21)$$

$$I_2^r(\theta_k, \alpha_k) = \theta_k \log(1 + |h_{d,k}|^2 \bar{P}_k) + \bar{\theta}_k \log(1 + |h_{d,k}|^2 \bar{P}_k + |h_{d,r}|^2 \bar{P}_r). \quad (4.22)$$

Specifically we focus on the *dynamic* DF protocol [14] where the relay ‘*listens*’ until it can successfully decode the message from user k . Thus, the fraction θ_k is a random variable defined as

$$\theta_k = \min \left(1, \left\lceil \frac{R_k}{\log(1 + |h_{r,k}|^2 \bar{P}_k)} \right\rceil \right) \quad (4.23)$$

where R_k is the rate at which user k transmits. The outage probability $P_o^{(k)}$ is then given as

$$P_o^{(k)} = \Pr(I_{2,DF}^r(\theta_k) < R_k). \quad (4.24)$$

where $I_{2,DF}^r(\theta_k)$ is

$$I_{2,DF}^r(\theta_k) = \theta_k \log(1 + |h_{d,k}|^2 \bar{P}_k) + \bar{\theta}_k \log(1 + |h_{d,k}|^2 \bar{P}_k + |h_{d,r}|^2 \bar{P}_r) \quad (4.25)$$

In [14], the authors determine the diversity-multiplexing tradeoff for a half-duplex relay channel under DDF and show that DDF achieves the diversity gains of a 2×1 antenna array for small multiplexing gains. In Appendix C.3, we develop upper and lower bounds on the outage probability. For simplicity, assuming large n , we relax the fractional requirement on θ_k and derive the probability distribution of θ_k as

$$p(\theta_k) = \begin{cases} \exp\left(\frac{-2^{R_k/\theta_k} d_{r,k}^\gamma}{\bar{P}_k}\right) \cdot R_k \ln 2 \cdot \exp\left(\frac{R_k \ln 2}{\theta_k}\right) \cdot \frac{d_{r,k}^\gamma}{\theta_k^2 \bar{P}_k} & 0 \leq \theta_k < 1 \\ 1 - \exp\left(\frac{-(2^R - 1) d_{r,k}^\gamma}{\bar{P}_k}\right) & \theta_k = 1. \end{cases} \quad (4.26)$$

Observe that the discrete distribution for fractional θ_k is obtained by integrating (4.26) over the appropriate range of θ_k .

We use the functional form of $p(\theta_k)$ to simplify the mixed distribution in (4.26) with a discrete distribution with two elements, θ_k^* and 1 where θ_k^* is the half-duplex fraction

at which its probability distribution $p(\theta_k)$ is maximized. We use this simplification to show that $P_o^{(k)}$ can be approximately bounded as

$$P_{o,2 \times 1} \leq P_o^{(k)} \leq K \frac{(2^R - 1)^2 d_{d,k}^\gamma d_{d,r}^\gamma}{2 \bar{P}_k^2} \simeq K P_{o,2 \times 1} \quad (4.27)$$

where $P_{o,2 \times 1}$ is the outage probability of a 2×1 *distributed* MIMO channel whose i^{th} antenna is at a distance $d_{d,i}$, $i = k, r$ from the destination. Without loss of generality, we assume that no two fading states have the same scale factors, i.e., $\bar{P}_k / d_{d,k}^\gamma \neq \bar{P}_k / d_{d,r}^\gamma$ for all k and θ_k . Under this assumption, we can apply lemma C.2 from Appendix C.2 to upper bound bound $P_{o,2 \times 1}$ as

$$P_{o,2 \times 1} \leq \frac{(2^R - 1)^2 d_{d,k}^\gamma d_{d,r}^\gamma}{2 \bar{P}_k^2} \quad (4.28)$$

and show that $P_{o,2 \times 1}$ asymptotically approaches the bound in (4.28) (see also [54, 55]).

Finally, the coding gains factor K relating the bounds on $P_o^{(k)}$ to the MIMO bounds is

$$K = \left(\frac{(2^{R/(1-\theta_k^*)} - 1)^2 \bar{P}_k}{(2^R - 1)^2 P_r^*} + \frac{2 d_{r,k}^\gamma}{d_{d,r}^\gamma} \right) \quad (4.29)$$

where $P_r^* = P_r / (1 - \theta_k^*)$, and $p(\theta_k = 1)$ is given by (4.26). We remark that for most geometries of interest, i.e., those where the source is closer to the relay than to the destination, $\theta_k^* \ll 1$. We demonstrate this in Fig. C.3 for a collinear geometry with $d_{d,k} = 1$ and $d_{d,r} = 0.5$. In this regime of interest, we also observe that the bounds on $P_o^{(k)}$ are relatively tight. Finally, throughout the sequel we assume $\bar{P}_k / d_{d,k}^\gamma \neq \bar{P}_k / d_{d,r}^\gamma$ for all k and θ_k . We justify this assumption by noting that such an assumption holds in general for arbitrary choices of node powers P_k , half-duplex fraction θ_k , and a random distribution of nodes over a fixed area.

Thus from (4.28) we see that for a fixed rate transmission, the maximum diversity achieved by DDF is 2, as predicted by the diversity-multiplexing tradeoff for DDF. Additionally, the factor K upper bounds the multiplicative factor (*coding gains*) by which $P_o^{(k)}$ differs from the MIMO lower bounds. Observe that the bounds in (4.27) get tighter as $d_{s,r} \rightarrow 0$, i.e., when user k and the relay form a cluster. Further K decreases

as P_r increases and/or $d_{r,k}$ decreases; note that decreasing $d_{r,k}$ also decreases θ_k^* as shown in Appendix C.3 thereby revealing the optimal node geometries for which $P_o^{(k)}$ is closest to the MIMO bounds. We remark that these bounds explain such behavior observed via simulations in ([49]) for a simple collinear geometry.

Finally, we observe that for single-antenna sources and destination, to achieve a maximum diversity greater than 2 requires a multi-antenna relay.

Time-Duplexed MAC-GF – Two-Hop Scheme

Achievable Rates: We consider the PDF strategy and develop the set of achievable rates for this case. Recall that in the two-hop scheme, only user k transmits in the first hop for a fraction of time θ_k while both user k and all the cooperating users in \mathcal{C}_k transmit in the remaining fraction $\bar{\theta}_k$. Thus, for this case the code construction at the transmitting user is the same as that for user k in (4.9) for the time-duplexed MARC. In its transmitting fraction $\bar{\theta}_k$, the cooperating user j transmits

$$X_j = \sqrt{\bar{P}_j / \bar{\theta}_k} V_k \quad \text{for all } j \in \mathcal{C}_k \quad (4.30)$$

where \bar{P}_k for all $k \in \mathcal{K}$ satisfies (4.2) and is obtained as

$$\bar{P}_k = P_k \cdot K / (N_k + 1) \quad (4.31)$$

where N_k is the total number of users whose messages are decoded and forwarded by user k . Note that $N_k \leq K - 1$ and is not related to $L_k = |\mathcal{C}_k|$. Comparing (4.10) and (4.31), we see that \bar{P}_k decreases when user k forwards data for an increasing number of other users. Finally, in the transmit fraction $\bar{\theta}_k$, user k splits its power between cooperating with the users in \mathcal{C}_k and transmitting a new message. In Appendix C.1, we show that for the case of fixed channel gains, the achievable rate R_k is

$$R_k \leq \max_{(\theta_k, \alpha)} \min (I_1^c(\theta_k, \alpha), I_2^c(\theta_k, \alpha)) \quad (4.32)$$

where

$$I_1^c(\theta_k, \alpha) = \theta_k \min_{j \in \mathcal{C}_k} (\log(1 + |h_{j,k}|^2 \bar{P}_k)) + \bar{\theta}_k \log(1 + \alpha_k |h_{d,k}|^2 \bar{P}_k) \quad (4.33)$$

$$I_2^c(\theta_k, \alpha) = \theta_k \log(1 + |h_{d,k}|^2 \bar{P}_k) + \bar{\theta}_k \log \left(1 + \alpha_k |h_{d,k}|^2 \bar{P}_k + \left| \sqrt{\alpha_k \bar{P}_k} h_{d,k} + \sum_{j \in \mathcal{C}_k} \sqrt{\bar{P}_j / \bar{\theta}_k} h_{d,j} \right|^2 \right). \quad (4.34)$$

Note that for $\mathcal{C}_k = \emptyset$, $\theta_k = \alpha_k = 1$ maximizes (4.32) thereby simplifying (4.32) to the point-to-point capacity bound $R_k \leq \log(1 + |h_{d,k}|^2 \bar{P}_k)$.

The sum-rate of the MAC-GF with time-duplexed sources is then obtained as

$$R_{\mathcal{K}} = \frac{1}{K} \sum_{k=1}^K R_k. \quad (4.35)$$

Finally, we remark that the rates achieved over an ergodic fading channel are obtained by averaging I_1^c and I_2^c over all channel fading states. Observe that due to lack of CSI at the transmitters, $\alpha_k = 0$ for all k for this case.

Outage Probability: We study the maximum diversity gains achieved by considering the DF strategy, i.e., user k , for all k , retransmits the same message in both fractions. Note that due to lack of transmitter CSI, the code construction for this case in contrast to that in (4.30), simplifies to using independent Gaussian random variables at the user and the cooperating nodes. Here again we study a DDF strategy where the fraction θ_k is chosen such that every node in the set \mathcal{C}_k of cooperating nodes decodes the message transmitted by user k . Thus, we have

$$\theta_k = \min \left(1, \max_{j \in \mathcal{C}_k} \left\lceil \frac{R_k}{\log(1 + |h_{j,k}|^2 \bar{P}_k)} \right\rceil \right). \quad (4.36)$$

An outage occurs when the transmitted rate R_k is larger than the rate bound achieved at the destination. The resulting outage probability for user k is

$$P_o^{(k)} = \Pr(I_{2,DF}^c < R_k) \quad (4.37)$$

where $I_{2,DF}^c$ is

$$I_{2,DF}^c(\theta_k) = \theta_k \log(1 + |h_{d,k}|^2 \bar{P}_k) + \bar{\theta}_k \log\left(1 + |h_{d,k}|^2 \bar{P}_k + \sum_{j \in \mathcal{C}_k} |h_{d,j}|^2 \frac{\bar{P}_j}{\bar{\theta}_k}\right). \quad (4.38)$$

Observe that for $\theta_k \rightarrow 1$, the first log term in (4.38) dominates the outage probability and thus we achieve a diversity approaching 1 which is the maximum achievable when the source transmits directly to the destination. On the other hand, as $\theta_k \rightarrow 0$, $I_{2,DF}^c(\theta_k)$ is dominated by the second log term in (4.38) and thus, the achievable diversity approaches L_k , the maximum diversity of a $L_k \times 1$ *distributed* MIMO channel whose i^{th} antenna, $i \in \mathcal{S}_k = \mathcal{C}_k \cup \{k\}$, is at a distance $d_{d,i}$ from the destination.

To the best of our knowledge, the diversity-multiplexing tradeoff for this two-hop scheme has not been evaluated. However, from (4.36) and (4.38), we see that irrespective of node geometry, one can choose P_k , and hence, \bar{P}_k sufficiently large such that θ_k is negligible. Thus, we can asymptotically approach the outage probability of a $L_k \times 1$ MIMO channel where $L_k = |\mathcal{C}_k| + 1$. In Appendix C.4, we derive an approximation to $P_o^{(k)}$ and show that

$$P_{o,L_k \times 1} \leq P_o^{(k)} \leq \frac{\left(2^{R_k/\bar{\theta}_k^*} - 1\right)^{L_k} \left(\bar{\theta}_k^*\right)^{L_k-1}}{(L_k!) (\bar{P}_k)^{L_k}} \prod_{j \in \mathcal{S}_k} \frac{d_{d,j}^\gamma}{\lambda_j} + \frac{(2^{R_k} - 1)^2 d_{d,k}^\gamma \left(\sum_{j \in \mathcal{C}_k} d_{j,k}^\gamma\right)}{\bar{P}_k^2} \quad (4.39)$$

where $\lambda_j = \bar{P}_j/\bar{P}_k$ for all $j \in \mathcal{S}_k$, $\theta_k^* = \arg \max_{\theta_k} p(\theta_k)$, and $\bar{\theta}_k^* = 1 - \theta_k^*$. Note that for the case where $L_k = 2$, our analysis simplifies to the outage analysis for the half-duplex relay channel. We now consider the case where $L_k > 2$ since this case suggests that the two-hop cooperative network can potentially achieve larger diversity gains than the time-duplexed relay network. Comparing the two terms in the summation in (C.74), we see that the first term dominates only when

$$\left(\sum_{j \in \mathcal{C}_k} d_{j,k}^\gamma\right) \leq \frac{C_0}{(\bar{P}_k)^{L_k-2}} \quad (4.40)$$

where C_0 is a constant independent of \bar{P}_k and is obtained by substituting (4.40) in (4.39) and equating the two terms in the summation. Thus, to achieve the maximum

diversity L_k , we need to choose P_k for all k large enough such that the finite distances $d_{j,k}$ for all $j \in \mathcal{C}_k$ satisfy (4.40). Alternately, for a fixed choice of P_k , for all k , we require user k and its cooperating users in \mathcal{C}_k to be clustered close enough to satisfy (4.40).

Thus, we see that except when the inter-node distances between user k and its cooperating users are *clustered*, i.e., satisfy (4.40), the maximum diversity gain achieved by DDF for a two-hop cooperative network does not exceed that of a single-antenna relay network. We demonstrate this distance-dependent behavior in Section 4.4.

Time-Duplexed MAC-GF – Multi-Hop Scheme

Achievable Rates: As with the other two cases, here too we consider the PDF strategy and develop the set of achievable rates for this scheme. Recall that in the multi-hop scheme, following the first fraction $\theta_{k,1}$ where only user k transmits, in each of the fractions $\theta_{k,l}$, $l = 2, 3, \dots, L_k$, one additional user cooperates in the transmission until all L_k users transmit in slot L_k . Note that $\theta_{k,l}$, for all l , satisfy

$$\sum_{l=1}^{L_k} \theta_{k,l} = 1. \quad (4.41)$$

Thus, for this case user k transmits

$$X_k = \begin{cases} \sqrt{\alpha_k \bar{P}_k} U_k & \theta_{k,l}, l = 1, 2, \dots, L_k - 1 \\ \sqrt{\alpha_k \bar{P}_k} Q_k + \sqrt{\bar{\alpha}_k \bar{P}_k} V_k & \bar{\theta}_{k,L_k}. \end{cases} \quad (4.42)$$

Thus, user k transmits the same signal in the first $L_k - 1$ fractions until all the $L_k - 1$ users decode its message reliably. Let $\pi_k(\cdot)$ be a permutation on \mathcal{C}_k such that user $\pi_k(l)$ begins its transmissions in the fraction $\theta_{k,l}$, for all $l = 2, 3, \dots, L_k$. We further define $\pi_k(1) = k$ and $\pi_k(i:j) = \{\pi_k(i), \pi_k(i+1), \dots, \pi_k(j)\}$. The signal $X_{\pi_k(l)}$ transmitted by user $\pi_k(l)$ from $\theta_{k,l}$ onwards is

$$X_{\pi_k(l)} = \sqrt{\frac{\bar{P}_{\pi_k(l)}}{\theta_{k,l}}} V_k \quad \text{for all } \pi_k(l) \in \mathcal{C}_k \quad (4.43)$$

where \bar{P}_k for all $k \in \mathcal{K}$ is given by (4.31) and $\bar{\theta}_{k,l}$ is the total transmission fraction of user $\pi_k(l)$, $l = 1, 2, \dots, L_k$, and is given as

$$\bar{\theta}_{k,l} = \sum_{j=l}^{L_k} \theta_{k,j} = 1 - \sum_{j=1}^{l-1} \theta_{k,j}. \quad (4.44)$$

Note that, as expected, the total transmission fraction for user k is $\bar{\theta}_{k,1} = 1$ and

$$\sum_{j=l}^{L_k} \theta_{k,j} = \Pr(\pi_k(l) = T) = 1 - \Pr(\pi_k(l) = L) \quad \text{for all } l. \quad (4.45)$$

We write $\underline{\theta}_k$ to denote the vector of time fractions with entries $\theta_{k,l}$ for all $l = 1, 2, \dots, L_k$.

In Appendix C.1, we show that for the case of fixed channel gains, the achievable rate R_k for this scheme is

$$R_k \leq \max_{\pi_k(2:L_k)} \max_{(\underline{\theta}_k, \alpha)} \min(I_1^c(\underline{\theta}_k, \alpha), I_2^c(\underline{\theta}_k, \alpha)) \quad (4.46)$$

where

$$\begin{aligned} I_1^c(\underline{\theta}_k, \alpha) = & \min_{l \in \{2, 3, \dots, L_k\}} \sum_{j=1}^{l-1} \theta_{k,j} \log \left(1 + \left| \sum_{m=1}^j h_{\pi_k(l), \pi_k(m)} \sqrt{\frac{\bar{P}_{\pi_k(m)}}{\bar{\theta}_{k,m}}} \right|^2 \right) \\ & + \theta_{k,L_k} \log(1 + \alpha_k |h_{d,k}|^2 \bar{P}_k) \end{aligned} \quad (4.47)$$

$$\begin{aligned} I_2^c(\underline{\theta}_k, \alpha) = & \theta_{k,1} \log(1 + |h_{d,k}|^2 \bar{P}_k) + \sum_{l=2}^{L_k-1} \theta_{k,l} \log \left(1 + \left| \sum_{j=\pi_k(1)}^{\pi_k(l)} \sqrt{\frac{\bar{P}_j}{\bar{\theta}_{k,j}}} h_{d,j} \right|^2 \right) \\ & + \theta_{k,L_k} \log \left(1 + \alpha_k |h_{d,k}|^2 \bar{P}_k + \left| \sum_{j=\pi_k(2)}^{\pi_k(L_k)} \sqrt{\frac{\bar{P}_j}{\bar{\theta}_{k,j}}} h_{d,j} \right|^2 \right). \end{aligned} \quad (4.48)$$

Note that for $\mathcal{C}_k = \emptyset$, $\theta_{k,1} = \alpha_k = 1$ maximizes (4.32) thereby simplifying (4.32) to the point-to-point capacity bound $R_k \leq \log(1 + |h_{d,k}|^2 \bar{P}_k)$. As before, the sum-rate of the MAC-GF with time-duplexed sources is then obtained as

$$R_{\mathcal{K}} = \frac{1}{K} \sum_{k=1}^K R_k. \quad (4.49)$$

Finally, we remark that the rates achieved over an ergodic fading channel are obtained by averaging I_1^c and I_2^c over all channel fading states. Observe that due to lack of CSI at the transmitters, $\alpha_k = 0$ for all k for this case.

Outage Probability: We study the maximum diversity gains achieved by considering the DF strategy, i.e., we set $\alpha_k = 1$ such that user k retransmits the same message in all fractions. However, due to lack of transmitter CSI, the code construction for this case in contrast to that in (4.30), simplifies to using i.i.d. zero-mean unit variance Gaussian random variables at both user k and the cooperating nodes. Note that the transmit power at user k , \bar{P}_k , is given by (4.31). Here again we consider the DDF strategy. However, unlike the two-hop case where the choice of θ_k is dictated by the node with the worst receive SNR, we now choose the fraction $\theta_{k,l}$ small enough to ensure that at least one node, denoted as $\pi_k(l+1)$, decodes the message from user k . Thus the fraction $\theta_{k,l}$, for $l = 1, 2, \dots, L_k - 1$, is given as

$$\theta_{k,l} = \begin{cases} \min_{j \in \mathcal{C}_k} \min \left\{ 1, \left\lceil \frac{R_k}{\log(1 + |h_{m,j}|^2 \bar{P}_k)} \right\rceil \right\} & l = 1 \\ \min_{j \in \mathcal{C}'_k(l)} \min \left\{ 1, \left\lceil \frac{R_k - \sum_{m=1}^{l-1} \theta_{k,m} \log(1 + \sum_{i=1}^m |h_{j,\pi_k(i)}|^2 \bar{P}_{\pi_k(i)} / \bar{\theta}_{k,i})}{\log(1 + \sum_{i=1}^l |h_{j,\pi_k(i)}|^2 \bar{P}_{\pi_k(i)} / \bar{\theta}_{k,i})} \right\rceil \right\} & 2 \leq l \leq \bar{L}_k \end{cases} \quad (4.50)$$

where $\bar{L}_k = L_k - 1$, $\mathcal{C}'_k(l) = \mathcal{C}_k \setminus \{\pi_k(l)\}_{l=2}^l$, i.e., the minimization of $\theta_{k,l}$ in (4.50) is over the set \mathcal{C}'_k that results from excluding from \mathcal{C}'_k the set of users chosen to transmit in the $l - 1$ preceding fractions. Finally, θ_{k,L_k} is

$$\theta_{k,L_k} = 1 - \sum_{l=1}^{L_k-1} \theta_{k,l}. \quad (4.51)$$

In general, computing the probability distribution of $p(\theta_{k,l})$ is not straightforward. However, in Appendix C.5 we show that it suffices to consider specific values of $p(\theta_{k,l})$ to obtain upper and lower bounds on $P_o^{(k)}$.

An outage occurs when the transmitted rate R_k is larger than the rate bound achieved at the destination. The resulting outage probability for user k is

$$P_o^{(k)} = \Pr(I_{2,DF}^c < R_k) \quad (4.52)$$

where $I_{2,DF}^c$ is

$$I_{2,DF}^c(\theta_k) = \theta_{k,1} \log(1 + |h_{d,k}|^2 \bar{P}_k) + \sum_{l=2}^{L_k} \theta_{k,l} \log \left(1 + \sum_{j=1}^l |h_{d,\pi_k(j)}|^2 \frac{\bar{P}_{\pi_k(j)}}{\bar{\theta}_{k,j}} \right) \quad (4.53)$$

and $\bar{\theta}_{k,l}$ is defined in (4.44). In general, it is not easy to obtain closed form expressions for the probability distribution of $\theta_{k,l}$, for all l . However, in Appendix C.5, we show that for small $\theta_{k,l}^*$, $l = 1, 2, \dots, L_k - 1$, $P_o^{(k)}$ is bounded as

$$P_{o,L_k \times 1} \leq P_o^{(k)} \leq \frac{\left(2^{R_k/\bar{\theta}_{k,L_k}^*} - 1\right)^{L_k} (\theta_{k,L_k}^*)^{L_k-1}}{(L_k!) (\bar{P}_k)^{L_k}} \cdot \prod_{j \in \mathcal{S}_k} \frac{d_{d,j}^\gamma}{\lambda_j} + \frac{(2^{R_k} - 1)^{L_k} \left(\prod_{j \in \mathcal{C}_k} d_{j,k}^\gamma\right) d_{d,k}^\gamma}{\bar{P}_k^{L_k}}. \quad (4.54)$$

where from lemma C.2 we show that

$$P_{o,L_k \times 1} \leq \frac{(2^{R_k} - 1)^{L_k}}{(L_k!) (\bar{P}_k)^{L_k}} \prod_{j \in \mathcal{S}_k} \frac{d_{d,j}^\gamma}{\lambda_j} \quad (4.55)$$

and asymptotically approaches it. Thus, we see that DDF achieves a maximum diversity of L_k for a L_k -hop cooperative network. However, achieving this diversity comes at a cost of increasing transmission and decoding delays.

4.3.2 Amplify-and-Forward

The cooperative strategy of amplify-and-forward is relevant for nodes that are limited in processing capabilities. Thus, instead of decoding their received signals, the cooperating node or relay, amplifies its received signal and forwards the resulting amplified signal to the destination. We first develop the achievable rates and outage analysis for a two-hop network where user k , for all $k \in \mathcal{K}$, is aided by the $L_k - 1$ users in the set \mathcal{C}_k . Note that for $L_k = 2$ and $\mathcal{C}_k = \{r\}$, the analysis specializes to that for a time-duplexed MARC. Without loss of generality, we consider $\theta_k = 1/2$ for the two-hop scheme and $\theta_{k,l} = 1/L_k$, $l = 1, 2, \dots, L_k$, for the L_k -hop scheme.

The AF outage analysis and diversity-multiplexing tradeoff for a half-duplex relay channel was first studied in [9] under the assumption that the source and relay transmit over orthogonal channels. The diversity-multiplexing tradeoff for the more general choice of non-orthogonal signaling schemes at the source and relay is studied in [14].

For the same channel, the AF ergodic fading rate and outage probability is studied in [59] for both orthogonal and non-orthogonal signaling schemes at the source and the relay. For a K -user multi-hop cooperative network, the authors in [14] present an AF protocol that achieves the diversity-multiplexing tradeoff of a $K \times 1$ MIMO channel. Finally, in [54], Laneman develops a coding-gain and geometry-inclusive AF outage analysis for a half-duplex multi-relay channel for the case of orthogonal signaling at the source and cooperating relays.

For a half-duplex MARC, the AF rate region is presented in [28]. For a MARC with time-duplexed users, the AF rate and outage analysis simplifies to that for a half-duplex relay channel. For a MAC-GF with time-duplexed users, we present an AF rate and outage analysis for both the two-hop and the multi-hop scheme. We also present a simple AF protocol for the multi-hop scheme. For the ergodic channel we assume that the channel gains are the same in both fractions and that the destination also knows the fading gains at the cooperating nodes. Finally, we also present upper and lower bounds on the outage probability for both the two-hop and the multi-hop scheme. Due to the difficulty in obtaining abalytically precise outage expressions, we apply a geometry-inclusive high SNR upper bounds developed in [55] and lower bound the outage by the outage of an equivalent MIMO channel.

Two-hop User- and Relay-Cooperative Networks

Achievable Rates: Consider the transmission of user k in the k^{th} time-slot (see Fig. 4.4). We first study the no fading case. The signals $Y_{d,1}$ and $Y_{d,2}$ received at the destination in the first and second fractions respectively are

$$Y_{d,1} = h_{d,k}X_{k,1} + Z_{d,1} \quad (4.56)$$

$$Y_{d,2} = h_{d,k}X_{k,2} + \left(\sum_{j \in \mathcal{C}_k} h_{d,j}X_{j,2} \right) + Z_{d,2} \quad (4.57)$$

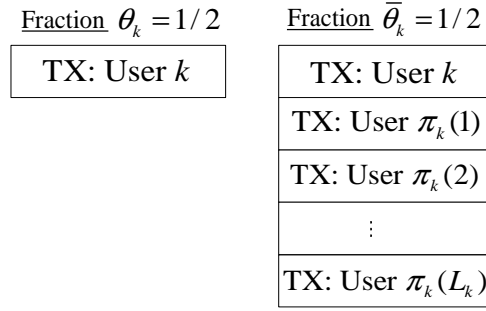


Figure 4.4: Encoding scheme for a two-hop AF strategy.

where $X_{j,2}$ is the transmitted signal at node j in the second fraction and it depends on $Y_{j,1}$, its received signal in the first fraction via a scale factor c_j as

$$X_{j,2} = c_j Y_{j,1} = c_j (h_{j,k} X_{k,1} + Z_{j,1}). \quad (4.58)$$

where

$$|c_j|^2 = \frac{2\bar{P}_j}{|h_{j,k}|^2 \bar{P}_k + 1}. \quad (4.59)$$

For ease of analysis, we write

$$c_s = \sqrt{1 + \left(\sum_{j \in \mathcal{C}_k} |c_j h_{d,j}|^2 \right)} \quad (4.60)$$

and simplify (4.56) and (4.57) as (see also [59])

$$\underline{Y}_d = H \underline{X}_k + \underline{Z}_d \quad (4.61)$$

where

$$\underline{Y}_d = \begin{bmatrix} Y_{d,1} & Y_{d,2}/c_s \end{bmatrix}^T \quad (4.62)$$

$$\underline{X}_k = \begin{bmatrix} X_{k,1} & X_{k,2} \end{bmatrix}^T \quad (4.63)$$

$$\underline{Z}_d = \begin{bmatrix} Z_{d,1} & \left(\sum_{j \in \mathcal{C}_k} \frac{c_j}{c_s} h_{d,j} Z_{j,1} \right) + \frac{Z_{d,2}}{c_s} \end{bmatrix}^T \quad (4.64)$$

and

$$H = \begin{bmatrix} h_{d,k} & 0 \\ \sum_{j \in \mathcal{C}_k} \frac{c_j}{c_s} h_{d,j} h_{j,k} & h_{d,k}/c_s \end{bmatrix}. \quad (4.65)$$

For the two-symbol channel in (4.61), we maximize the achievable rate R_k by choosing X_k as Gaussian distributed and subject to the power constraint in (4.2). We thus achieve all R_k that satisfy [1, Sec. 3.1]

$$R_k \leq \max_{Q_k = E(\underline{X}_k \underline{X}_k^\dagger): \text{tr}(Q) \leq 2\bar{P}_k} \frac{1}{2} \log |I_2 + H Q_k H^\dagger|. \quad (4.66)$$

Remark 4.3 *The AF analysis for the half-duplex relay channel is obtained by setting $\mathcal{C}_k = \{r\}$.*

Remark 4.4 *Note that the above analysis assumes that the destination, in addition to knowing $h_{d,k}$ and $h_{d,j}$ for all $j \in \mathcal{C}_k$, also knows the channel gains $h_{j,k}$ for all j .*

Remark 4.5 *One can also consider a relatively simpler orthogonal relaying scheme where user k transmits on an orthogonal channel to that used by the cooperating users in \mathcal{C}_k , i.e., $X_{k,2} = 0$. Note that the resulting AF rate will be smaller.*

Finally for the ergodic fading case, the achievable rate is bounded as

$$R_k \leq \mathbb{E} \frac{1}{2} \log |I_2 + \bar{P}_k H H^\dagger| \quad (4.67)$$

where the expectation is over all the jointly independent fading processes $\{h_{l,m}\}$, for all $l \in \mathcal{C}_k \cup \{k\}$, $m = d$ or $l \in \mathcal{C}_k$, $m = k$. Note that due to lack of transmitter CSI the bound in (4.67) is maximized when user k transmits i.i.d Gaussian signals in the two fractions.

Outage Analysis: Due to a lack of CSI at the transmitters, we maximize the mutual information, and hence minimize the outage probability, by choosing $X_{k,1}$ and $X_{k,2}$ as independent Gaussian signals [33]. We circumvent the difficulty in developing an exact expression for the outage probability P_{out} by presenting high SNR upper and lower bounds on P_{out} . Expanding (4.66) and ignoring fading terms to the fourth power (see also [59]), we can write the outage probability P_{out} as

$$P_{out} = \Pr \left(\frac{1}{2} \log \left(1 + |h_{d,k}|^2 \bar{P}_k \left(1 + \frac{1}{c_s} \right) + \frac{\bar{P}_k}{c_s^2} \left| \sum_{j \in \mathcal{C}_k} \frac{c_j}{c_s} h_{d,j} h_{j,k} \right|^2 \right) < R_k \right) \quad (4.68)$$

where R_k is the rate at which user k transmits. In general, an analytic expression for P_{out} is involved. However, one can lower bound P_{out} by the outage probability of a $L_k \times 1$ distributed MIMO channel with $L_k - 1$ antennas transmitting the same signal.

Thus, we have

$$P_{out} \geq \Pr \left(\log \left(1 + |h_{d,k}|^2 \bar{P}_k + \bar{P}_k \left| \sum_{j \in \mathcal{C}_k} h_{d,j} \right|^2 \right) < R_k \right) \quad (4.69)$$

$$= \Pr \left(\log \left(1 + |h_{d,k}|^2 \bar{P}_k + \bar{P}_k |h'_d|^2 \right) < R_k \right) \quad (4.70)$$

$$\sim \frac{(2^{R_k} - 1)^2 d_{d,k}^\gamma}{2\bar{P}_k^2 \left(\sum_{j \in \mathcal{C}_k} 1/d_{d,j}^\gamma \right)} \quad (4.71)$$

where (4.70) follows from the fact that the sum, h'_d , of complex Gaussian random variables $h_{d,j}$, for all j , is also Gaussian distributed while (4.71) follows from applying lemma C.2 in the high SNR regime. The expression $f(x) \sim g(x)$ implies $\lim_{x \rightarrow \infty} f/g = 1$.

On the other hand, one can upper bound P_{out} by the outage probability of an orthogonal AF protocol with $|\mathcal{C}_j| = 1$. The bounds for the latter network in the high SNR regime are developed in [54] and we summarize them below as

$$P_{out} \leq \frac{(2^{2R_k} - 1)^2 d_{d,k}^\gamma d'}{2\bar{P}_k^2} \quad (4.72)$$

where

$$d' = \max_{j \in \mathcal{C}_k} (d_{j,k}^\gamma + d_{d,j}^\gamma). \quad (4.73)$$

Thus, we see that the maximum diversity achievable by a two-hop AF scheme in the high SNR regime is at most 2 and is independent of the number of cooperating users in \mathcal{C}_k . At the other extreme of the low SNR wideband regime, the authors in [16] show that for a half-duplex relay channel AF does not achieve the high SNR diversity gains and propose an outage capacity achieving *bursty* AF scheme.

Multi-hop Cooperative Network

We consider a simple L_k -hop cooperative AF protocol where user k is aided by user $\pi_k(l)$, $l = 1, 2, \dots, L_k$, in the l^{th} fraction, i.e., user $\pi_k(l)$ forwards in the fraction $\theta_{k,l}$

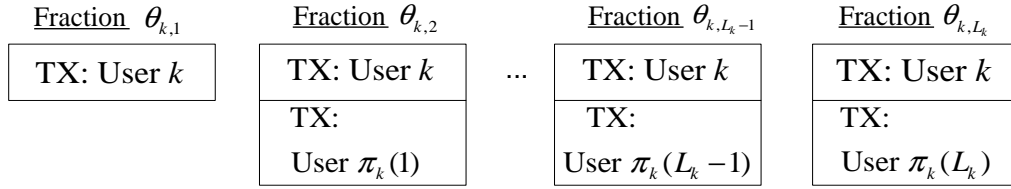


Figure 4.5: AF encoding for user k in a K -user multi-hop cooperative network.

a scaled version of the signal it receives from user k in the first fraction (see Fig. 4.5).

Note that $\pi_k(1) = k$ and $\theta_{k,l} = 1/L_k$ for all l . We denote the received signal at the destination in the l^{th} fraction as $Y_{d,l}$ and write

$$Y_{d,l} = h_{d,k}X_{k,l} + h_{d,\pi_k(l)}X_{\pi_k(l),l} + Z_{d,l} \quad l = 1, 2, \dots, L_k \quad (4.74)$$

where the signal $X_{\pi_k(l),l}$ transmitted by user $\pi_k(l)$ in the l^{th} fraction depends on signal $Y_{\pi_k(l),1}$ that it receives in the first fraction as

$$X_{\pi_k(l),l} = c_{\pi_k(l)}Y_{\pi_k(l),1} = c_{\pi_k(l)}(h_{\pi_k(l),k}X_{k,1} + Z_{\pi_k(l),1}) \quad (4.75)$$

and

$$|c_{\pi_k(l)}|^2 = \frac{L_k \bar{P}_{\pi_k(l)}}{|h_{\pi_k(l),k}|^2 \bar{P}_k + 1}. \quad (4.76)$$

Achievable Rates: We simplify (4.56) as

$$\underline{Y}_d = H \underline{X}_k + \underline{Z}_d \quad (4.77)$$

where

$$\underline{Y}_d = \begin{bmatrix} Y_{d,1} & Y_{d,2}/c'_2 & \dots & Y_{d,L_k}/c'_{L_k} \end{bmatrix}^T \quad (4.78)$$

$$\underline{X}_k = \begin{bmatrix} X_{k,1} & X_{k,2} & \dots & X_{k,L_k} \end{bmatrix}^T \quad (4.79)$$

$$\underline{Z}_d = \begin{bmatrix} Z_{d,1} & \frac{c_{\pi_k(2)}h_{d,\pi_k(2)}Z_{\pi_k(2),1} + Z_{d,2}}{c'_2} & \dots & \frac{c_{\pi_k(L_k)}h_{d,\pi_k(L_k)}Z_{\pi_k(L_k),1} + Z_{d,L_k}}{c'_{L_k}} \end{bmatrix}^T \quad (4.80)$$

and

$$c'_l = \sqrt{1 + c_{\pi_k(l)}^2 |h_{d,\pi_k(l)}|^2} \quad \text{for all } l = 2, 3, \dots, L_k \quad (4.81)$$

such that the entries $h_{i,j}$ of the matrix H , for all $i, j = 1, 2, \dots, L_k$, are

$$h_{i,j} = \begin{cases} c_{\pi_k(i)} h_{\pi_k(i),k} h_{d,\pi_k(i)} / c'_i & j = 1 \\ h_{d,k} / c'_i & i = j \\ 0 & \text{o.w.} \end{cases} \quad (4.82)$$

For the L_k -symbol vector channel in (4.77), we choose X_k as Gaussian distributed to maximize the achievable rate R_k . We thus achieve all R_k that satisfy

$$R_k \leq \max_{Q_k = E(\underline{X}_k \underline{X}_k^\dagger) : \text{tr}(Q) \leq 2\bar{P}_k} \frac{1}{L_k} \log |I_{L_k} + H Q_k H^\dagger|. \quad (4.83)$$

Remark 4.6 Due to a pre-log factor of $1/L_k$, note that the above scheme is desirable only when the rate gains are significant relative to direct transmission. Further, here too we assume that the destination, in addition to knowing $h_{d,k}$ and $h_{d,j}$ for all $j \in \mathcal{C}_k$, also knows the channel gains $h_{j,k}$ for all j .

Remark 4.7 One can also consider an orthogonal relaying scheme where user k and the cooperating users in \mathcal{C}_k use orthogonal channels to transmit to the destination, i.e., $X_{k,j} = 0$, $j = 2, 3, \dots, L_k$ (see [54]).

Finally for the ergodic fading case, the achievable rate is bounded as

$$R_k \leq \mathbb{E} \frac{1}{L_k} \log |I_{L_k} + \bar{P}_k H H^\dagger| \quad (4.84)$$

where the expectation is over all the jointly independent fading processes $\{h_{l,m}\}$, for all (l, m) such that $l \in \mathcal{C}_k \cup \{k\}$, $m = d$ or $l \in \mathcal{C}_k$, $m = k$. Note that due to lack of CSI the bounds in (4.84) are maximized when user k , for all k , transmits i.i.d Gaussian signals in the two fractions.

Outage Analysis: Due to a lack of CSI at the transmitters, we assume independent and identically distributed Gaussian signaling in each fraction at user k . Then, for a transmission rate R_k , setting $Q_k = \bar{P}_k I_{L_k}$ in (4.83), we write the outage probability P_{out} as

$$P_{out} = \Pr \left(\frac{1}{L_k} \log |I_{L_k} + \bar{P}_k H H^\dagger| < R_k \right). \quad (4.85)$$

An expression for P_{out} is not easy to evaluate analytically. However, we can lower bound P_{out} with the outage probability of a $L_k \times 1$ distributed MIMO channel with i.i.d Gaussian signaling across the L_k transmit antennas. Thus, we have

$$P_{out} \geq \Pr \left(\log \left(1 + |h_{d,k}|^2 \bar{P}_k + \bar{P}_k \sum_{j \in \mathcal{C}_k} h_{d,j}^2 \right) < R_k \right) \quad (4.86)$$

$$\sim \frac{(2^{R_k} - 1)^{L_k} \prod_{l=1}^{L_k} d_{d,\pi_k(l)}^\gamma}{(L_k!) \bar{P}_k^{L_k}} \quad (4.87)$$

where (4.87) follows from applying lemma C.2 in the high SNR regime and the approximation $f(x) \sim g(x)$ is in the sense of $f(x)/g(x) \rightarrow 1$ as $x \rightarrow \infty$ [60]. On the other hand, one can upper bound P_{out} by the outage probability of an orthogonal AF protocol where user k and its cooperating users transmit on orthogonal channels, i.e., only user $\pi_k(l)$ transmits in the fraction $\theta_{k,l}$. A high SNR upper bound on the outage probability of this orthogonal scheme is developed in [54] and we summarize it below as

$$P_{out} \leq \frac{(2^{L_k R_k} - 1)^{L_k} d_{d,k}^\gamma \prod_{j \in \mathcal{C}_k} (d_{d,j}^\gamma + d_{j,k}^\gamma)}{L_k! \bar{P}_k^{L_k}}. \quad (4.88)$$

Comparing (4.87) and (4.88), we see that the L_k -hop AF scheme can achieve a maximum diversity of L_k in the high SNR regime at the expense of user k repeating the signal L_k times. We remark however that in the SNR ranges where the distance factors in the numerator are comparable to the SNR in the denominator, the diversity gains will reduce. We demonstrate such an observation using numerical results in the following section.

4.4 Illustration of Results

We consider a planar geometry with the users distributed randomly in a sector of a circle of unit radius and angle $\pi/3$. We place the destination at the center of the circle, denoted as the origin, and for the relay network, we place the relay at $(0.5, 0)$ as shown in Fig. 4.6. The K users are distributed randomly over the sector excluding a dead zone around the destination of radius 0.3. We plot the K -user sum-rate of the relay and user

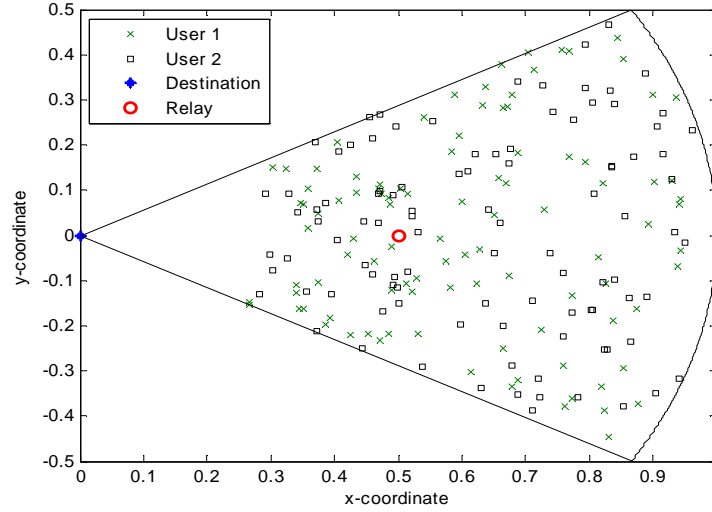


Figure 4.6: Planar sector of a circle with the destination at the origin and 100 randomly chosen locations for a two-user multiaccess network.

cooperative networks and include the sum-capacity of a TD-MAC as a baseline for our comparisons. We remark that the sum-rate optimization for both networks chooses a cooperative strategy for user k , for all k , only when the rate achieved by cooperation exceeds the TDMA rate for user k .

For all networks, we compute the achievable rates for the no fading channel and outage probabilities for the quasi-static channel model assuming a random distribution of users and average the results over 100 such random placements. Further, for the quasi-static fading channel, we also average the outage probability over all time-duplexed users. One can make similar comparisons for the ergodic fading case too.

We assume that all K users have the same transmit power constraint, i.e., $P_k = P_1$ for all $k \in \mathcal{K}$. For the relay network we choose the relay's transmit power $P_r = fP_1$ where the scale factor f takes the values 0.5 and 1. To compare the energy efficiency of the networks, we compute the total transmit and processing power assuming that the same processing factors for encoding and decoding, i.e., $\eta_k = \delta_k = \eta$ and the baseline

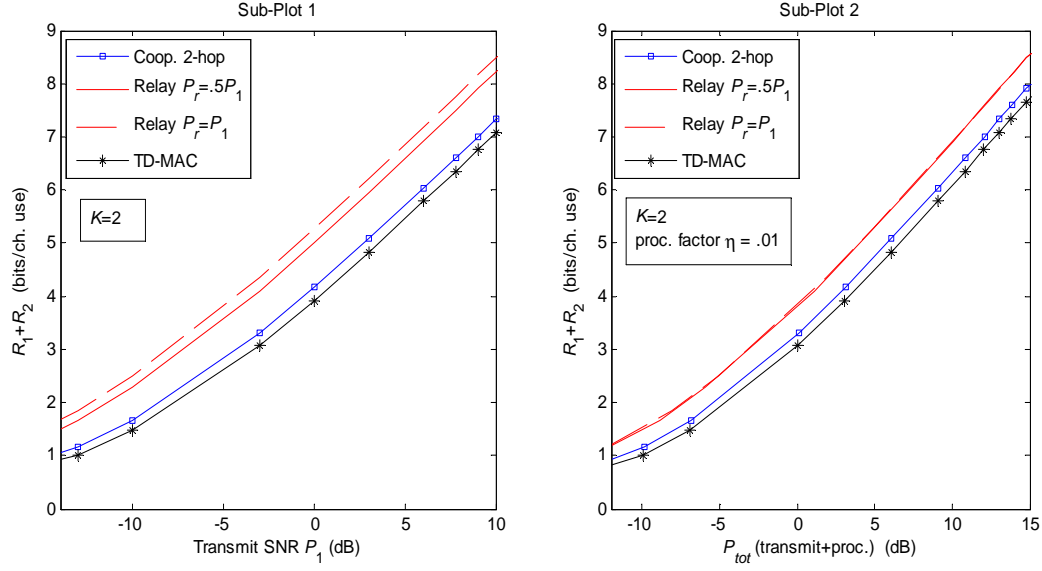


Figure 4.7: Two user PDF sum-rate $R_1 + R_2$ vs. P_1 (sub-plot 1) and vs. P_{tot} (sub-plot 2) for $\eta = .01$.

processing power $P_{k,0}^{proc} = 0$ for all $k \in \mathcal{T}$. For the following analysis we use the free-space path loss exponent $\gamma = 4$. Finally, we compare the rate and outage performance for $\eta = .01, .5$, and 1, thereby modeling the extremes of the processing cost regime as well as a mid-point. For the quasi-static fading model, we consider a symmetric transmission rate, i.e., all users transmit at a fixed rate $R = 0.25$.

We present the rate and outage plots for $K = 2$ and $K = 3$ as a function of the transmit SNR P_1 in dB, where the transmit SNR is the transmit power P_1 normalizing by the unit variance noise at the receivers. We also plot the rate and outage probability as a function of the noise normalized total transmit and processing SNR P_{tot} in dB where P_{tot} is given by (4.5) and (4.6). For $K = 3$, we compare the performance of both the two-hop and three-hop cooperative schemes.

4.4.1 Achievable Rates: PDF

The first sub-plot in Fig. 4.7 compares the area-averaged PDF sum-rates $R_1 + R_2$ as a function of P_1 for the user and relay cooperative network with that for the TD-MAC.

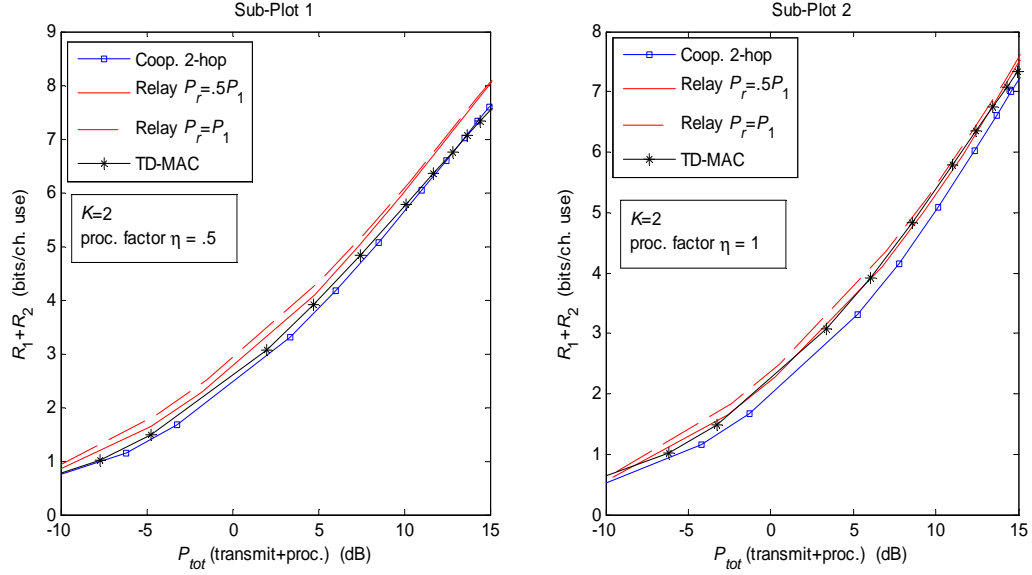


Figure 4.8: Two user PDF sum-rate $R_1 + R_2$ vs. P_{tot} for $\eta = .5$ (sub-plot 1) and $\eta = 1$ (sub-plot 2).

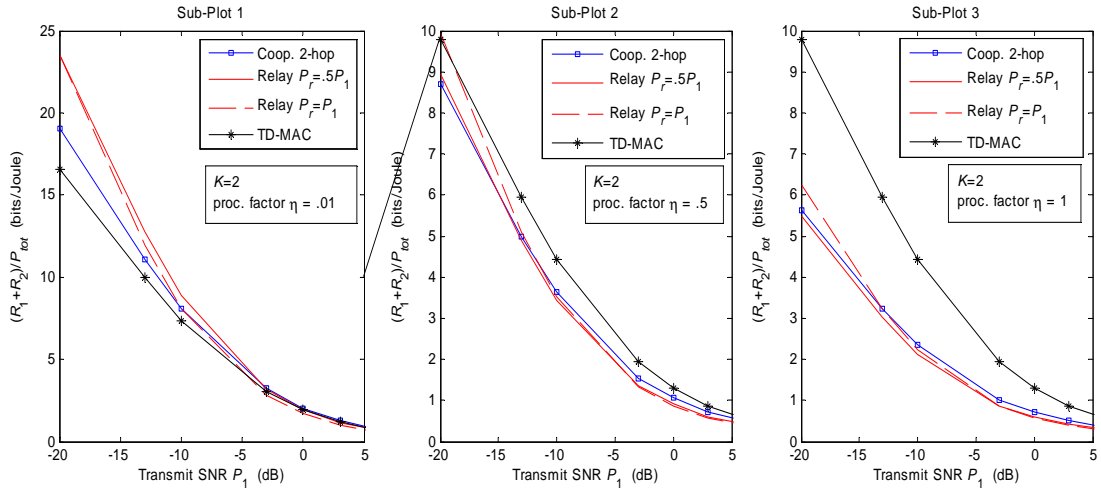


Figure 4.9: Two user PDF energy efficiency $(R_1 + R_2) / P_{tot}$ in bits/Joule vs. P_1 for $\eta = .01$ (sub-plot 1), $.5$ (sub-plot 2), and 1 (sub-plot 3).

The plot shows that for the relay network modeled as a time-duplexed MARC, the achievable sum-rate increases with increasing relay power and these rates are larger than those achieved by the other three networks. Note further that the plot verifies the known result that neither user nor relay cooperation achieves multiplexing gains [9,14]. However, this plot does not account for the additional power at the relay. In sub-plot 2, we plot $R_1 + R_2$ as a function of P_{tot} for $\eta = .01$. This plot shows that with increasing relay power the rate gains achieved by cooperation is not sufficient to overcome the energy costs of cooperation. In fact, the plot shows that the increased rates achieved by the relay network for $f = 1$ requires proportionately larger total power relative to that for $f = .5$. Further, from the two sub-plots in Fig. 4.8 one can see that with increasing η , i.e., increasing processing power, while the rate gains achieved by both kinds of cooperative networks diminishes relative to the TD-MAC; the sum-rate performance of the relay network degrades more gracefully than that for the user cooperative network. Thus, we see that in the low transmit SNR regime relaying can still achieve gains, albeit small, relative to the TD-MAC for $\eta = 1$, i.e., for the case where processing power is comparable to the transmit power.

In Fig 4.9, we compare the energy efficiency of each network in bits per Joule as a function of the transmit SNR P_1 in dB for $\eta = 0.01, 0.5$, and 1 in sub-plots 1, 2, and 3 respectively. Recall that we model the energy efficiency of each network as its sum-rate normalized with respect to the total power. One can clearly verify that the energy efficiency, irrespective of η , of all the networks increases as the transmit SNR decreases [61]. Further, for any η , as P_1 increases, the energy costs of cooperation dominate any gains in sum-rate achieved by cooperation thus driving the energy efficiency of the two cooperative approaches below that of the TD-MAC. In other words, one can identify *cross-over* powers for both cooperative networks above which it is energy efficient to abandon cooperation and transmit directly. Note that the total power range in each sub-plot is chosen to ensure the same range of sum-rates. Comparing the three sub-plots, we see that with increasing η the total power required to achieve the same sum-rate

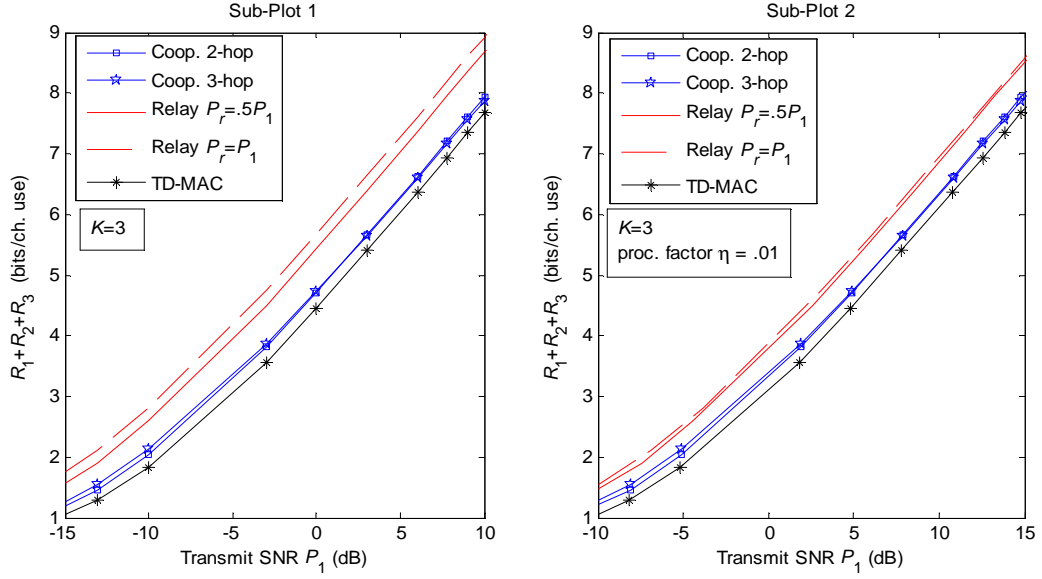


Figure 4.10: Three user PDF sum-rate $R_1 + R_2 + R_3$ vs. P_1 (sub-plot 1) and vs. P_{tot} for $\eta = .01$ (sub-plot 2).

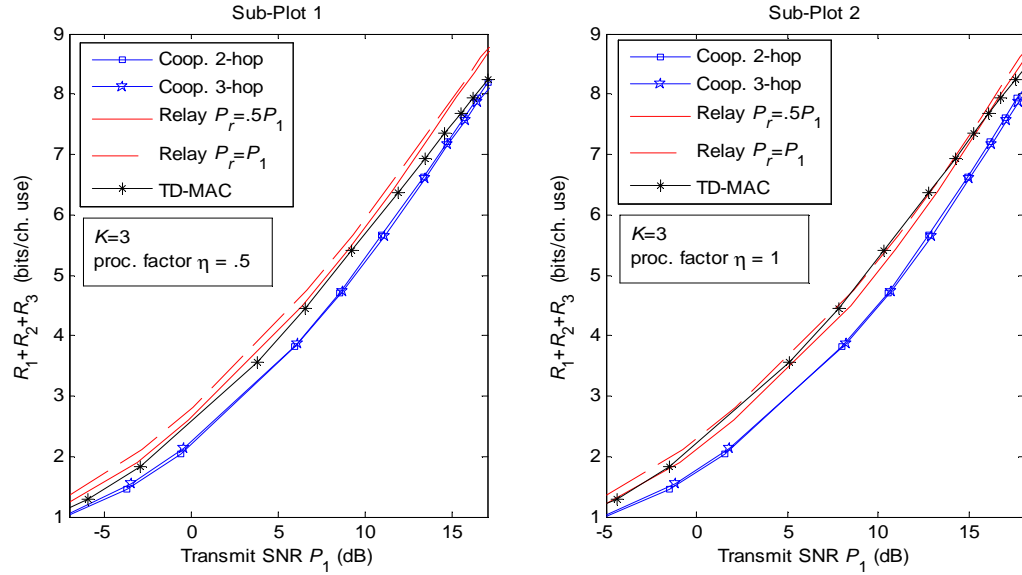


Figure 4.11: Three-user PDF sum-rate $R_1 + R_2 + R_3$ vs. P_{tot} for $\eta = .5$ (sub-plot 1) and $\eta = 1$ (sub-plot 2).

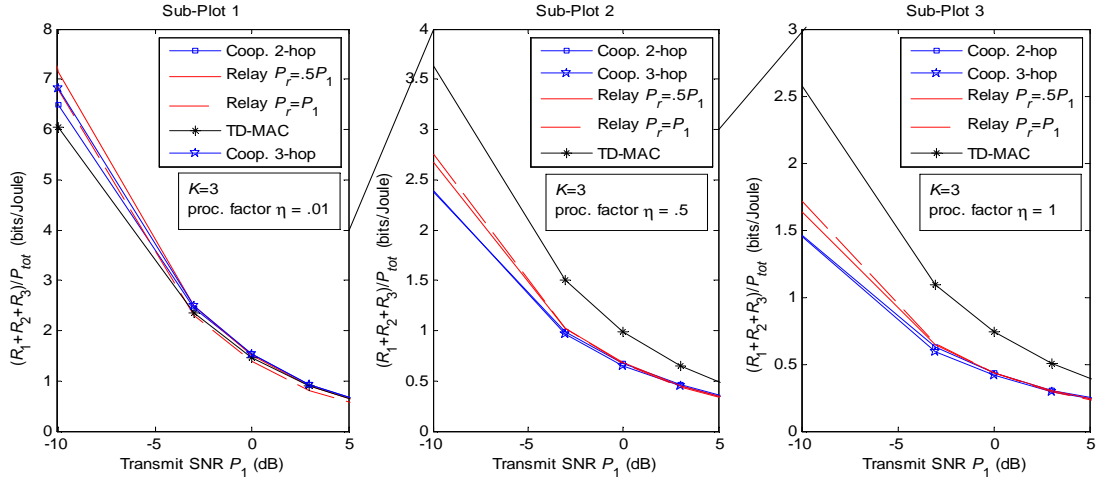


Figure 4.12: Three user PDF energy efficiency $(R_1 + R_2 + R_3) / P_{tot}$ vs. P_{tot} for $\eta = .01$ (sub-plot 1), $.5$ (sub-plot 2), and 1 (sub-plot 3).

increases. Further, as η increases from $.01$ to 1 the cross-over power decreases for both kinds of cooperative networks. Note that for all three values of η , the cross-over SNR for the user cooperative network is smaller than that for the relay network. This is a direct result of the fact that in the cooperative network the users also bear the additional processing costs of cooperative encoding and decoding. From the continuity of the rate expressions as a function of power, one can see that the energy efficiency in general decreases with increasing η for all networks as demonstrated by the lines connecting the y-axis ticks from one sub-plot to another.

Next, we demonstrate the performance of the multi-hop cooperative scheme by considering a three-user multiaccess network. In Fig. 4.10 we compare the achievable three-user sum-rate $R_1 + R_2 + R_3$ as a function of both P_1 and P_{tot} . The plots demonstrate negligible gains between the two- and three-hop cooperative schemes. Recall that for the multi-hop case, we choose the set \mathcal{C}_k of users cooperating with user k as that which maximizes R_k . Thus, the rate gains from multi-hopping are typically limited to those users that are farther away from the destination than are their cooperating users. This in turn implies that with increasing K the rate gains achieved by the distant users

is offset by the reduction in rate experienced by the users closer to the destination as a result of sharing their transmit power for cooperation. Further, comparing the rate gains that result from relay cooperation in Figs. 4.7 and 4.10 for $K = 2$ and $K = 3$ respectively, we see that sharing the relay between more users also reduces the cooperative rate gains. These observations are further illustrated in sub-plot 2 where we compare the sum-rates as a function of P_{tot} . This plot clearly shows that with increasing P_r , the rate gains resulting from relay cooperation do not scale faster than the processing power costs thereby suggesting that it is efficient to employ relay cooperation only in the low transmit and processing power regime and for small K .

Finally, Fig. 4.12 demonstrates that relay and user cooperation are energy efficient only in the low transmit and processing power regimes. In fact, from Fig. 4.12 as well as the continuity of the rate expressions one can show that there exists a processing factor η_0 beyond which the energy efficiency curves for both user and relay cooperation falls below that for TD-MAC, i.e., it is more energy efficient to directly transmit to the destination than it is to cooperate.

4.4.2 Achievable Rates: AF

In Fig. 4.13 and 4.15 we compare the sum-rate and energy efficiency of the relay and user cooperative networks under AF. From the first sub-plot in Fig. 4.13 we see that relay cooperation achieves rate gains as the transmit power decreases relative to the TD-MAC sum-capacity; we note that the gains achieved by user cooperation while non-zero are relatively insignificant. The gains for both networks however are limited to the relatively low SNR regime. Further, from sub-plot 2, we see that in this regime, the transmission is also energy-efficient. A similar behavior is demonstrated for $\eta = .5$ and $\eta = 1$ in Fig. 4.14.

Recall that since AF does not involve encoding or decoding by the cooperating

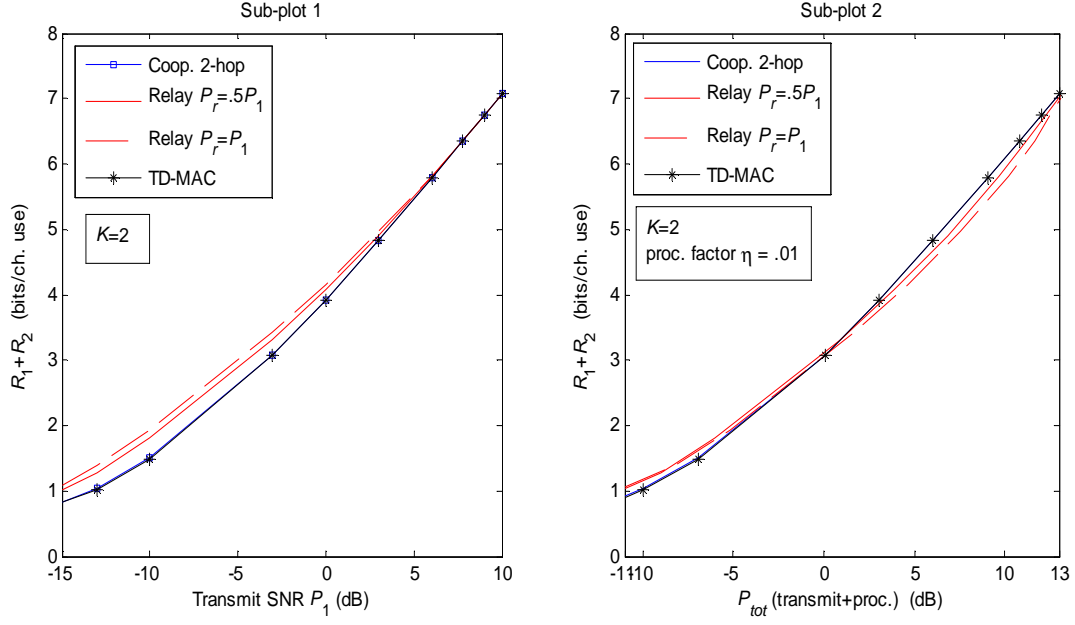


Figure 4.13: Two user AF sum-rate $R_1 + R_2$ vs. P_1 (sub-plot 1) and vs. P_{tot} (sub-plot 2) for $\eta = .01$.

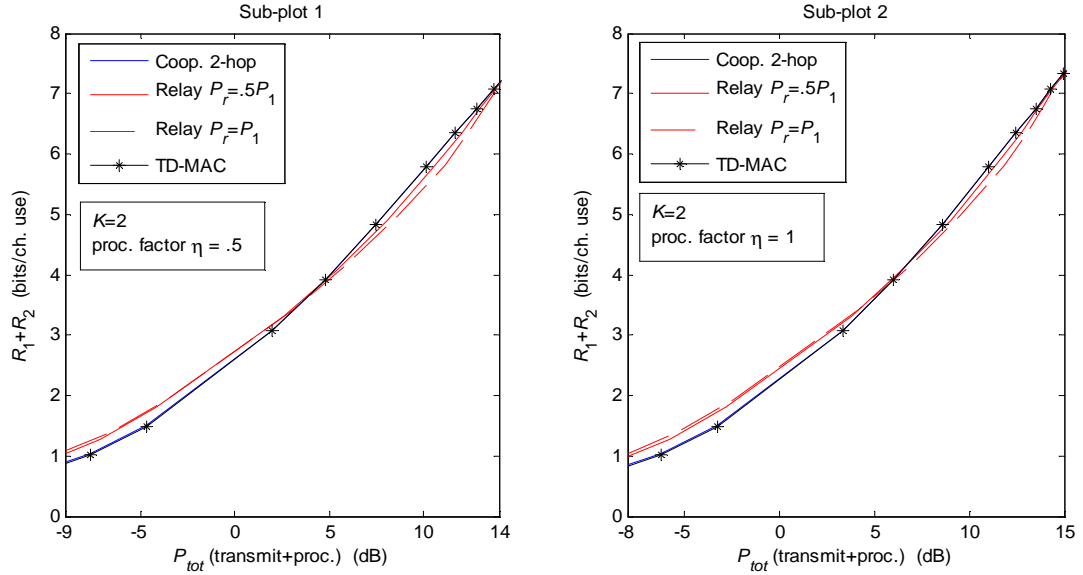


Figure 4.14: Two user AF sum-rate $R_1 + R_2$ vs. P_{tot} for $\eta = .5$ (sub-plot 1) and $\eta = 1$ (sub-plot 2).

users, the energy costs of cooperation for the TD-MAC and the user cooperative network are the same while that for the relay network includes the additional cost of transmission at the relay, i.e., P_r . This cost of relaying is demonstrated in the first sub-plot of Fig. 4.15 where we see that the energy cost of relay transmissions shadows the rate gains achieved thus driving the energy efficiency of the relay network below that of the user cooperative and the TD-MAC network. However, as η increases to .05 and 1 in sub-plots 2 and 3 respectively we see that relaying is more energy-efficient relative to the other two networks in the low transmit SNR regime. Further, the cross-over power P_1 of the relay network also increases with increasing η . This is due to the fact as the processing factor increases, the fixed cost of transmission at the relay is dominated by the increasing cost of processing (encoding) at the users. Thus, while the energy efficiency of all networks decreases with increasing η , the effect of P_r reduces with increasing η thus making relay cooperation more energy efficient in the high processing factor regime. One can make a similar comparison for a three-user MAC and compare the performance of the three-hop scheme. However, from (4.77), one can see that with increasing K the pre-log factor $1/L_k$ for user k will quickly outweigh the logarithmic rate gains.

4.4.3 Outage Probability: DDF

In Fig. 4.16 we compare the two user DDF outage probability, P_{out} , of the two cooperative networks and the TD-MAC as a function of P_1 in sub-plot 1 and as a function of P_{tot} for $\eta = 0.01$ in sub-plot 2. Recall that P_{out} is an average of the outage probability of both users over all random user locations. As expected, we see that both the relay and the user cooperative network achieve a maximum diversity of 2 relative to the unit diversity of the TD-MAC as seen from the slope of the outage curves for a fixed symmetric rate $R = 0.25$. Further sub-plot 1 also demonstrates a SNR gain achieved by the relay network relative to the user cooperative network. Further as demonstrated in sub-plot 2 and both sub-plots in Fig. 4.17 this SNR gain is not diminished even when

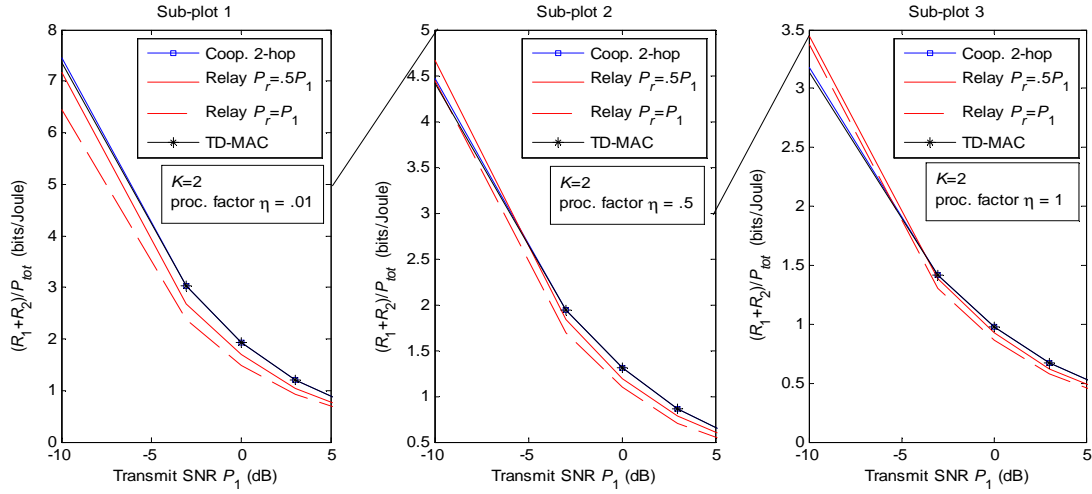


Figure 4.15: Two user AF energy efficiency $(R_1 + R_2)/P_{tot}$ vs. P_{tot} for $\eta = .01$ (sub-plot 1), $.5$ (sub-plot 2), and 1 (sub-plot 3).

we account for the energy costs of cooperation by plotting P_{out} as a function of the total (transmit and processing) SNR P_{tot} . Note further that accounting for the processing costs translates the outage curves for all three networks.

We compare the outage probability of a three user MAC in Figs. 4.18 and 4.19. The figures clearly validates our analysis that the two hop cooperative scheme on average does not achieve the maximum diversity gains of 3. On the other hand, the slope of P_{out} for the three-hop scheme approaches the maximum diversity of 3 but does not achieve coding gains relative to the relay network. Further, accounting for the processing costs, we see that the diversity gains of the three-hop scheme significantly diminish with increasing processing factor η . In fact, with increasing η the two-hop relay network demonstrates increased SNR gains relative to the two and three-hop cooperative networks.

In Section 4.3.1 we showed that a two-hop K -user cooperative network can achieve the maximum diversity of K when all K sources form a cluster. We demonstrate this in Fig. 4.20 for a clustered geometry where the three users are randomly located in a circle of radius 0.1 and centered at $(0.7, 0)$. We plot the outage probability averaged over the

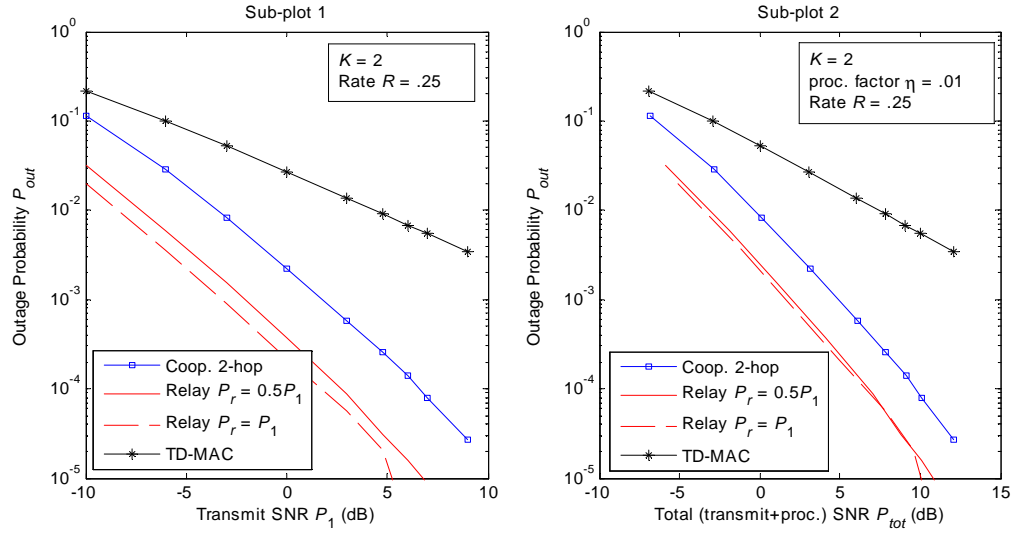


Figure 4.16: Two user DDF outage probability P_{out} vs. P_1 (sub-plot 1) and vs. P_{tot} for $\eta = 0.01$ (sub-plot 2).

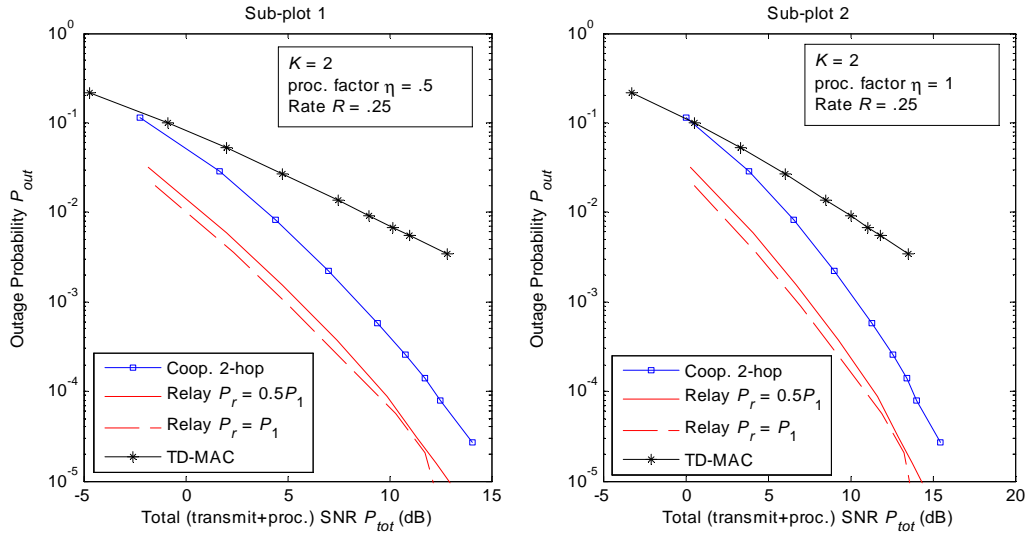


Figure 4.17: Two user DDF outage probability P_{out} vs. P_{tot} for $\eta = 0.5$ (sub-plot 1) and for $\eta = 1$ (sub-plot 2).

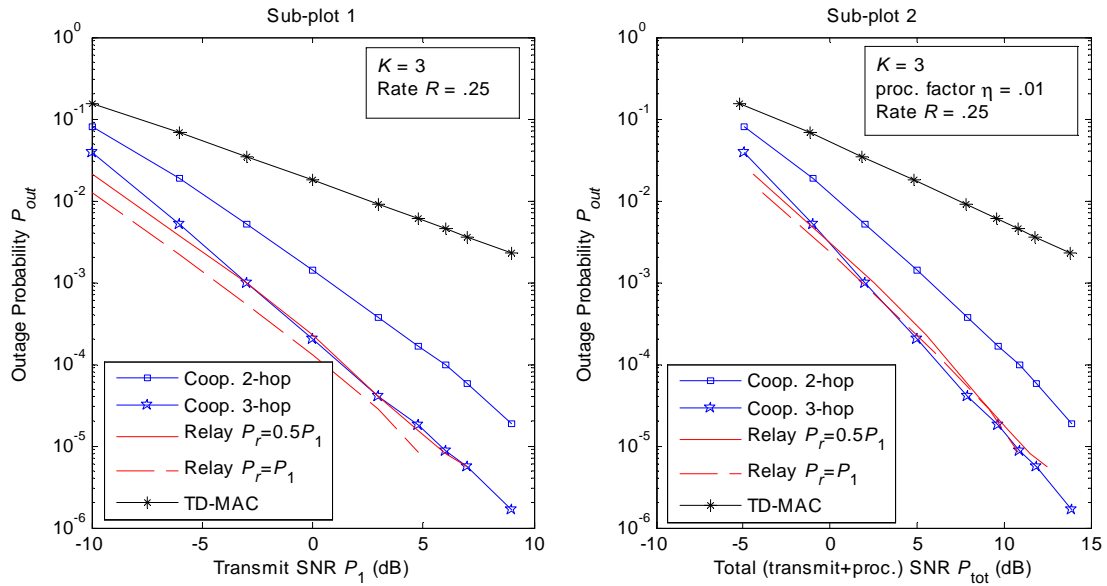


Figure 4.18: Three user DDF outage probability P_{out} vs. P_1 (sub-plot 1) and vs. P_{tot} for $\eta = 0.01$ (sub-plot 2).

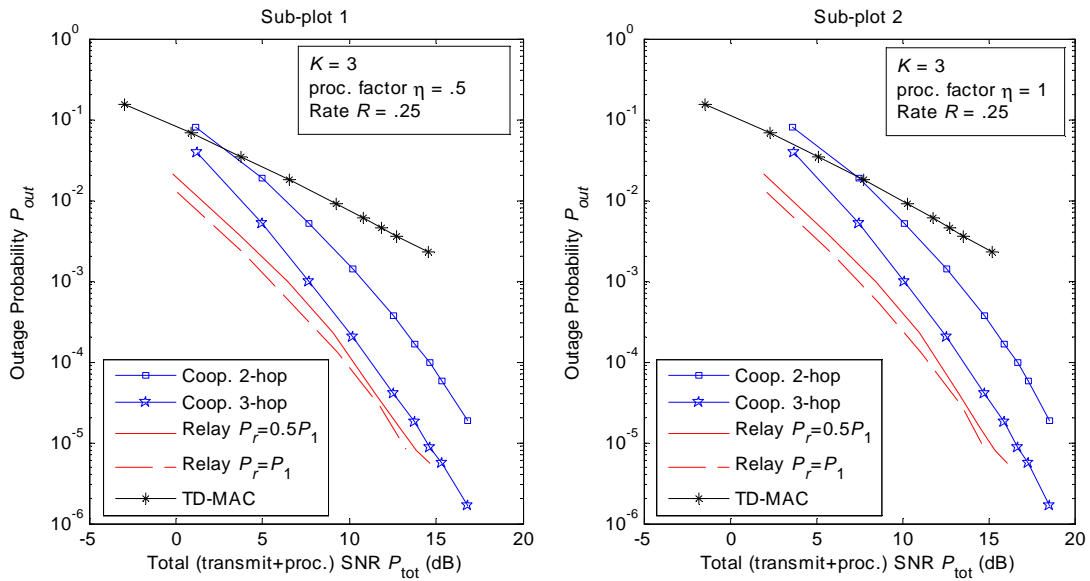


Figure 4.19: Three user DDF outage probability P_{out} vs. total transmit SNR P_{tot} in dB for $\eta = 0.5$ (sub-plot 1) and $\eta = 1$ (sub-plot 2).

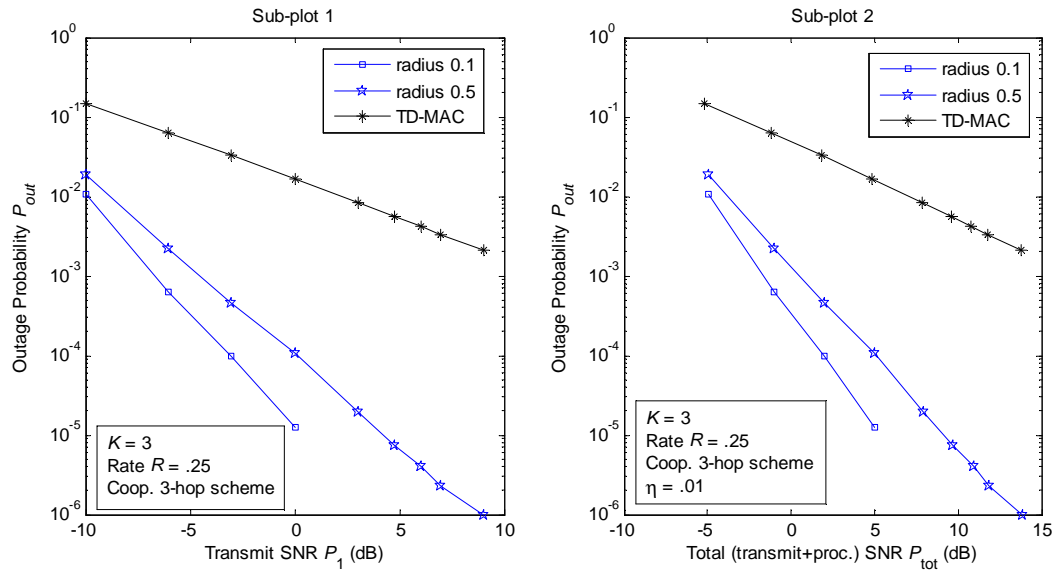


Figure 4.20: Two-hop three user DDF Outage Probability P_{out} vs. P_1 (sub-plot 1) and P_{tot} (sub-plot 2).

location of the three users and over 10 such random placements of the users. We also plot the outage when the clustering radius is increased to 0.5. The decrease in diversity order from 3 to 2 as the radius increases agree with our analysis and demonstrate the need for user clustering to achieve a diversity order of 3 for the chosen SNR range.

4.4.4 Outage Probability: AF

In Figs. 4.21 and 4.22 we plot the two user AF outage probability for the cooperative user and relay networks and compare them with that for the non-cooperative TD-MAC. As predicted, we see that both kinds of cooperative networks achieve the same maximum diversity of 2. However, from sub-plot 2 in Fig 4.21 and the two sub-plots in Fig. 4.22 we see that the relay network achieves an average coding gain of 3 dB relative to the user cooperative network. In Figs. 4.23 and 4.24 we compare the outage probabilities of a three user cooperative, relay, and TD-MAC network. Observe that the two-hop AF scheme only achieves a maximum diversity of 2 as shown in Section 4.3.2. The three-hop scheme on the other hand achieves a maximum diversity approaching

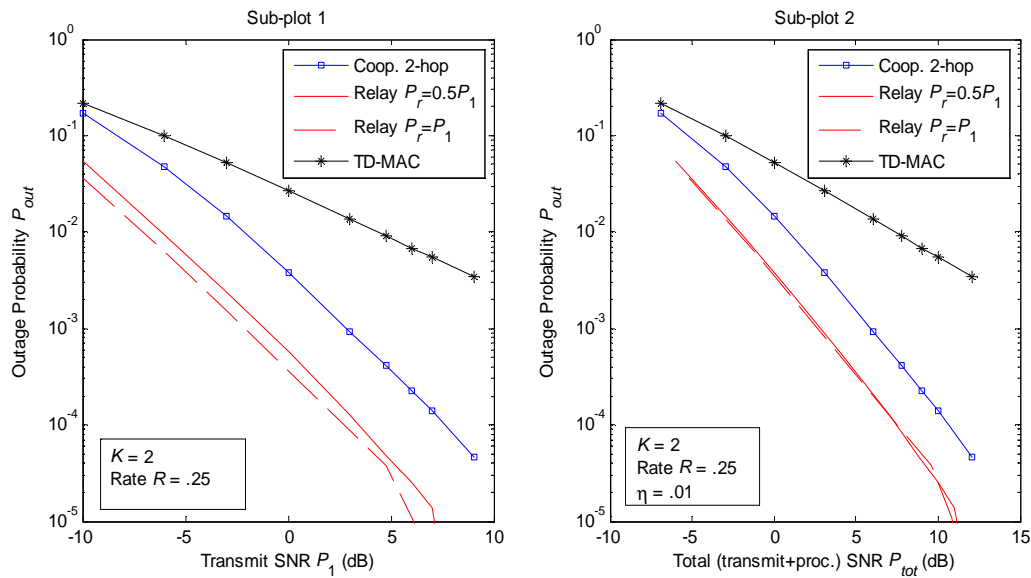


Figure 4.21: Two user AF outage probability P_{out} vs. P_1 (sub-plot 1) and vs. P_{tot} for $\eta = .01$ (sub-plot 2).

3. However, it does not uniformly achieves coding gains relative to the AF outage probability (2-hop) achieved by the relay network.

4.4.5 Relay Position

We briefly discuss the effect of relay position on the rate and outage performance of the relay network. We presented numerical results for a fixed relay position at at $(0.5, 0)$, i.e, at half the sector radius and on the line bisecting the sector. A natural question that arises is whether a different placement of the relay may yield different results. For instance, given the uniform node distribution over a circular sector, more nodes are likely to be closer to the circumference than to the center and thus placing the relay at $(1/\sqrt{2}, 0)$, i.e. at a radius that divides the area in half, may result in a larger rates and smaller outage probabilities. In Figs. 4.25 and 4.26 we illustrate the sum-rate and energy efficiency respectively for this choice of relay position. Comparing Fig. 4.7 and 4.25 we see that the rate gains achieved by the relay network relative to the cooperative

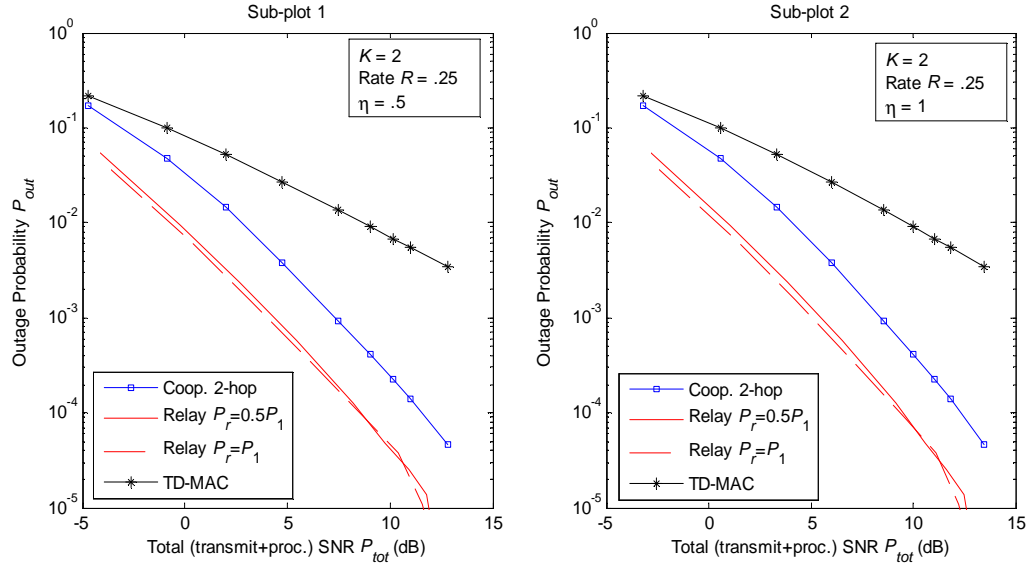


Figure 4.22: Two user AF outage probability P_{out} vs. P_{tot} for $\eta = 0.5$ (sub-plot 1) and for $\eta = 1$ (sub-plot 2).

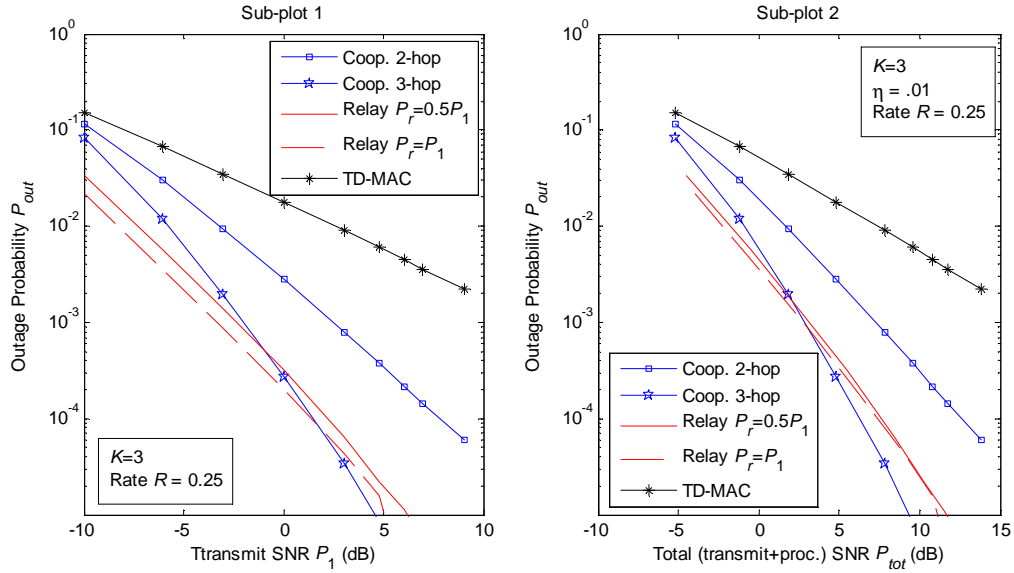


Figure 4.23: Three user AF outage probability P_{out} vs. P_1 (sub-plot 1) and P_{tot} for $\eta = 0.01$ (sub-plot 2).

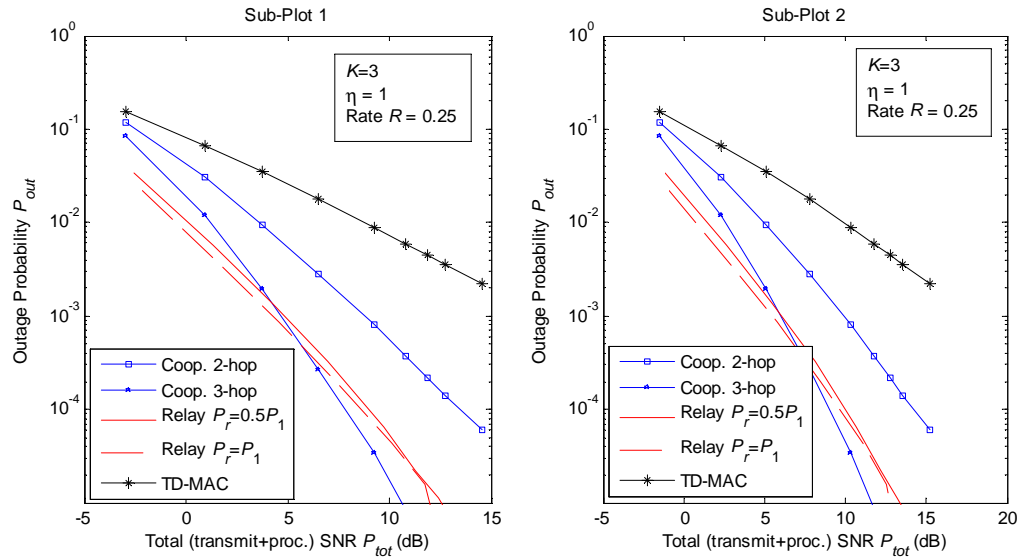


Figure 4.24: Three user AF outage probability P_{out} vs. P_{tot} for $\eta = 0.5$ (sub-plot 1) and $\eta = 1$ (sub-plot 2).

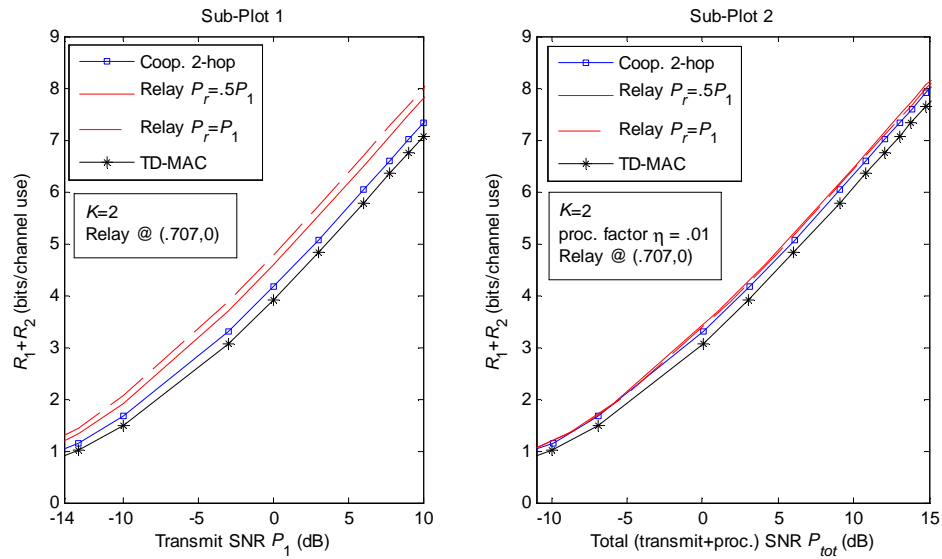


Figure 4.25: Two user PDF sum-rate $R_1 + R_2$ vs. P_1 (sub-plot 1) and P_{tot} for $\eta = 0.01$ (sub-plot 2) for relay position fixed at $(0.707, 0)$.

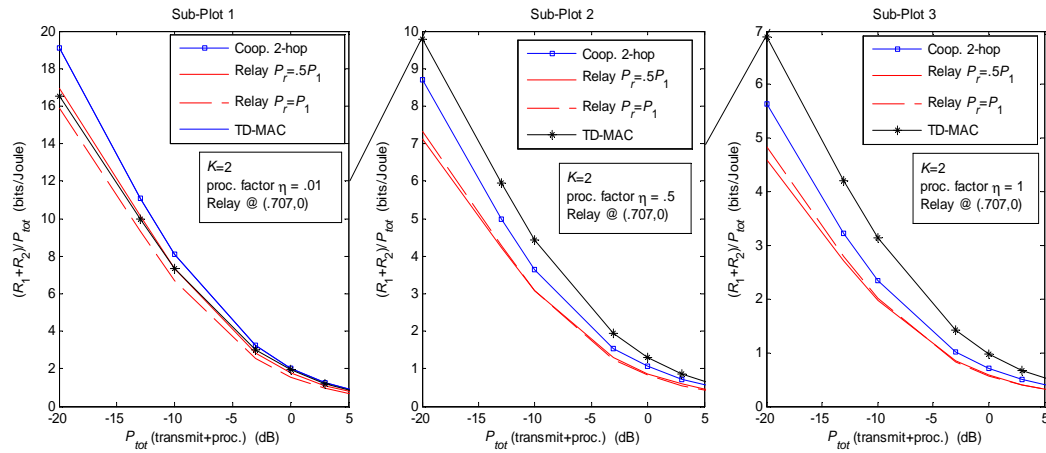


Figure 4.26: Two user PDF energy efficiency $(R_1 + R_2)/P_{tot}$ vs. P_1 for $\eta = 0.01$ (sub-plot 1), $\eta = 0.5$ (sub-plot 2), and $\eta = 1$ (sub-plot 3) for relay position fixed at $(0.707, 0)$.

network diminish. Further, from Fig. 4.26 we see that both user cooperation and non-cooperative time-duplexing are more energy efficient communication approaches than relaying.

The larger rates achieved by placing the relay closer to the destination at $(0.5, 0)$ than at $(0.707, 0)$ is due to the distance dependent fading gains seen by the relay's signal at the destination. While it is known that when the relay is clustered close to the sources DDF achieves or approaches the channel capacity, we note that the resulting capacity is not the largest rate achieved over all relay positions; the latter is achieved at a point midway between the sources and relay as illustrated in [28, 31].

One can demonstrate a similar behavior for the AF scheme. The effect on the DDF outage probability is demonstrated in Fig. 4.27. Comparing with Fig. 4.16, we see that the coding gains for the relay network reduces by 3 dB when the relay is moved farther away from the destination. In practice, the relay position may need to be chosen to maximize the average achievable rates and diversity order.

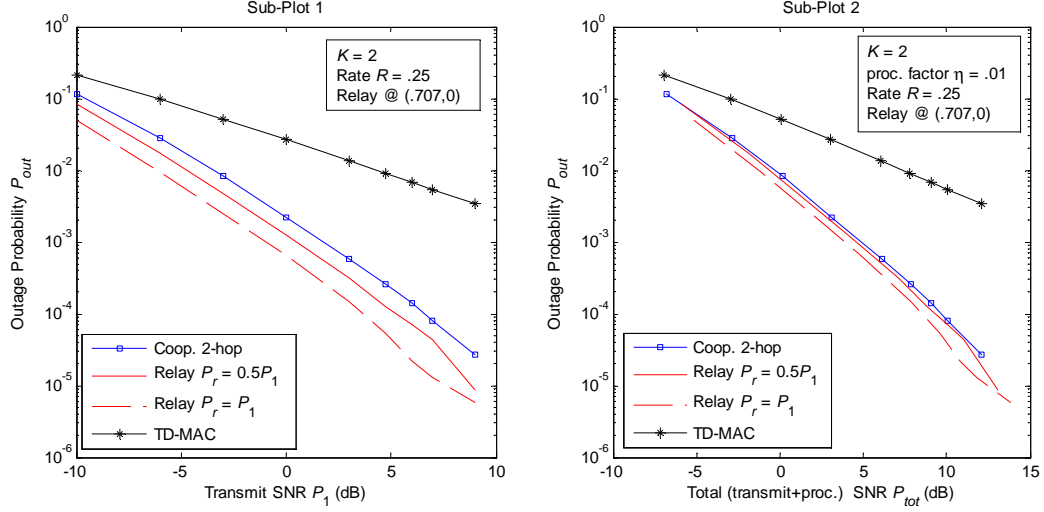


Figure 4.27: Two user DF outage probability P_{out} vs. P_1 (sub-plot 1) and P_{tot} for $\eta = 0.01$ (sub-plot 2) for relay placed at $(0.707, 0)$.

4.5 Conclusions

We compared the rate and diversity performance of user and relay cooperation in a multiaccess network. We chose the total transmit and processing power as a cost metric for the comparison and developed a model for processing power costs as a function of the transmitted rate, and hence, transmitted power. We considered a time-duplexed transmission model for both cooperative networks and the MAC and developed a two-hop scheme for both the relay and user cooperative network. We also presented a multi-hop scheme for the user cooperative network for the case of multiple cooperating users. For the cooperative strategies of PDF (DF for outage) and AF, we developed the achievable rate bounds as well as upper and lower bounds on the outage probability. We also presented numerical results for both the achievable rates and outage probability averaged over random user locations within a circular sector. Our results demonstrated that due to the processing (encoding and decoding) costs associated with PDF and DF, both user and relay cooperative networks are energy efficient only in the regime where transmit costs dominate processing costs, i.e., the *long distance communications* regime. On

the other hand, AF is desirable for the relay network only when the processing costs are comparable to the transmit costs. Further, for both strategies, we showed that using a relay is on average more energy efficient than user cooperation. Finally, we also showed that as a result of sharing fixed power and bandwidth resources the gains from either kind of cooperation decreases with increasing number of users.

We also compared the diversity gains achieved by user and relay cooperation by developing upper and lower bounds on the outage probability for DDF and AF. Our analytical results, verified by numerical simulations, showed that a two-hop relay network can achieve a maximum diversity of 2 for both DDF and AF. A two-hop user cooperative network aided by $K - 1$ users achieves a K -fold diversity gain only when the cooperating users are physical proximal, i.e., clustered. On the other hand, the K -hop scheme achieves a maximum diversity order of K ; however the cooperative energy costs of this scheme make it unattractive relative to the 2-hop AF strategy for the relay network; in fact the K -hop scheme is desirable only in the low processing costs regime where it achieves coding gains relative to the relay network. We make similar observations for AF except now a two-hop relay and user cooperative network only achieve a maximum diversity of 2. On the other hand, despite a K -fold diversity increase, the performance of the K -hop scheme for the user cooperative network suffers from increased energy costs and diminished codings gains in the high processing costs regime relative to the outage performance of the relay network.

In conclusion, we see that cooperation is desirable only when the energy costs of cooperation are negligible compared to the total energy costs. Further, multi-hop schemes for the user cooperative network that achieve full diversity are desirable in practice only if the associated processing costs are not prohibitive, i.e., in the regime where they achieve positive coding gains relative to the relay and non-cooperative networks. The simple processing cost model presented here captures the effect of transmit rate on processing power. One can also tailor this model to explicitly include delay, complexity, and device-specific processing costs. Finally, one can also compare the

energy-efficiency and diversity performance of a wide variety of cooperative schemes ranging in complexity from a simple multi-hopping scheme to the processing-intensive compress-and-forward strategy over different SNR regimes.

Chapter 5

Sum-Capacity of Degraded Gaussian Multiaccess Relay Channels

5.1 Introduction

Capacity results for relay channels are known only for a few special cases such as the degraded relay channel [6] and its multi-relay generalization [35, 62], the semi-deterministic relay channel [63], orthogonal relay channels [64, 65], the Gaussian relay without delay channel [66, 67], and ergodic phase-fading relay channels [68]. Specifically, for the classic single-user relay channel [6] and its multi-relay generalization [35], applying the degradedness condition simplifies the outer bounds on the capacity to coincide with the inner bounds achieved by DF. Applying the degradedness condition for a MARC, however, does not result in such a simplification.

For a K -user degraded Gaussian MARC, we use optimization techniques to show that DF achieves the K -user sum-capacity. We first obtain the largest K -user DF sum-rate by maximizing the minimum of the sum-rates achieved at the relay and at the destination. The maximization is over all possible source and relay power fractions that achieve coherent combining gains at the destination. We solve the max-min optimization problem using techniques analogous to the classic minimax problem in detection theory [69, II.C] and refer to the resulting sum-rate optimal power policy at each source and the relay as a *max-min rule*.

One can obtain an outer bound on the capacity region of a MARC by specializing the cut-set bounds of [30, Th. 14.10.1] for the case of independent sources [28]. As with DF, the outer bound on the K -user sum-rate is also obtained by taking a minimum over two bounds where the first bound results from a cut with both the relay and the

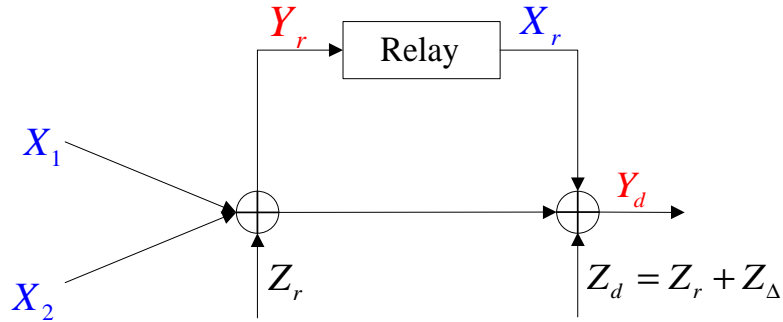


Figure 5.1: A two-user Gaussian degraded MARC.

destination as receivers while the second bound results from a cut with only the destination as a receiver. For the degraded case the first bound simplifies to using only the relay's signal; however, this bound is at least as large as the DF bound achieved at the relay. The second outer bound on the other hand matches that achieved by DF at the destination. We show that the cut-set bound on the K -user sum-rate can also be maximized using max-min techniques and the resulting bound is the same as that achieved by DF. Finally, we show that the max-min rule for DF also maximizes the sum-rate outer bound.

This chapter is organized as follows. In Section 5.2 we present a model for a degraded Gaussian MARC. In Section 5.3 we review the cut-set bounds on the capacity region of a MARC. In Section 5.4 we determine the maximum K -user DF sum-rate. We develop the converse in Section 5.5. Finally, in Section 5.6, we discuss the result and conclude.

5.2 Channel Model and Preliminaries

A K -user degraded Gaussian MARC has K user (source) nodes, one relay node, and one destination node (see Fig. 5.1). The sources emit the messages W_k , $k = 1, 2, \dots, K$, that are statistically independent and take on values uniformly in the sets $\{1, 2, \dots, M_k\}$. The channel is used n times so that the rate of W_k is $R_k = B_k/n$ bits

per channel use where $B_k = \log_2 M_k$ bits. In each use of the channel, the input to the channel from source k is X_k while the relay's input is X_r . The channel outputs Y_r and Y_d , respectively, at the relay and the destination are

$$Y_r = \sum_{k=1}^K X_k + Z_r \quad (5.1)$$

$$Y_d = \sum_{k=1}^K X_k + X_r + Z_d \quad (5.2)$$

$$= Y_r + X_r + Z_\Delta \quad (5.3)$$

where Z_r and Z_Δ are independent Gaussian random variables with zero-mean and variance N_r and N_Δ respectively such that the noise variance at the destination is

$$N_d = N_r + N_\Delta. \quad (5.4)$$

We remark that we assume a relay that operates in a full-duplex manner, i.e., it can transmit and receive simultaneously in the same bandwidth. Further, its input X_r in each channel use is a causal function of its outputs from previous channel uses. We write $\mathcal{K} = \{1, 2, \dots, K\}$ for the set of sources, $\mathcal{T} = \mathcal{K} \cup \{r\}$ for the set of transmitters, $\mathcal{R} = \{r, d\}$ for the set of receivers, $X_{\mathcal{S}} = \{X_k : k \in \mathcal{S}\}$ for all $\mathcal{S} \subseteq \mathcal{K}$, and \mathcal{S}^c to denote the complement of \mathcal{S} in \mathcal{K} .

The transmitted signals from source k and the relay have a per symbol power constraint

$$E |X_k|^2 \leq P_k \quad k \in \mathcal{T}. \quad (5.5)$$

One can equivalently express (5.3) as a Markov chain

$$(X_1, X_2, \dots, X_K) - (Y_r, X_r) - Y_d. \quad (5.6)$$

Finally, for $K = 1$, we note (5.6) simplifies to the degraded condition in [6, (10)].

The capacity region \mathcal{C}_{MARC} is the closure of the set of rate tuples (R_1, R_2, \dots, R_K) for which the destination can, for sufficiently large n , decode the K source messages with an arbitrarily small positive error probability. As further notation, we write $R_{\mathcal{S}} =$

$\sum_{k \in \mathcal{S}} R_k$ and $Y_{\mathcal{R}} = (Y_r, Y_d)$. We write $\underline{0}$ and $\underline{1}$ to denote vectors whose entries are all zero and one respectively and \underline{e} to denote a *unit vector*, i.e., a vector with only one non-zero entry that is set to unity. We use the usual notation for entropy and mutual information [29, 30] and take all logarithms to the base 2 so that our rate units are bits.

The degraded Gaussian MARC defined in (5.1)-(5.3) is a *physically degraded* channel, i.e., it has one independent observation at the relay and a degraded copy of that observation at the destination. Except for a few cases, such as the broadcast channel, physically degraded wireless channels have limited practical relevance. A degraded model with perhaps more practical relevance is a *stochastically degraded* Gaussian MARC shown in Fig. 5.2 where $Z'_r \neq Z_r$ though they have the same variance N_r . For example, a stochastically degraded Gaussian MARC may be used to model multiaccess relay networks where the received signal strength is dominated by path-loss. The independence of Z'_r and Z_r adds an additional degree of freedom to the channel observations at the relay and destination and thus, the capacity of a stochastically degraded Gaussian MARC is at least as large as its physically degraded counterpart. The difference between a stochastically and a physically degraded Gaussian MARC, however, makes the converse obtained for the latter inapplicable for the former. Thus, in addition to solving a theoretical model, capacity results for the physically degraded Gaussian MARC can provide insights into signaling schemes for the stochastically degraded case.

5.3 Outer Bounds

An outer bound on the capacity region of a MARC is presented in [27] using the cut-set bounds in [30, Th. 14.10.1] as applied to the case of independent sources. We summarize the bounds below.

Proposition 5.1 *The capacity region $\mathcal{C}_{\text{MARC}}$ is contained in the union of the set of rate*

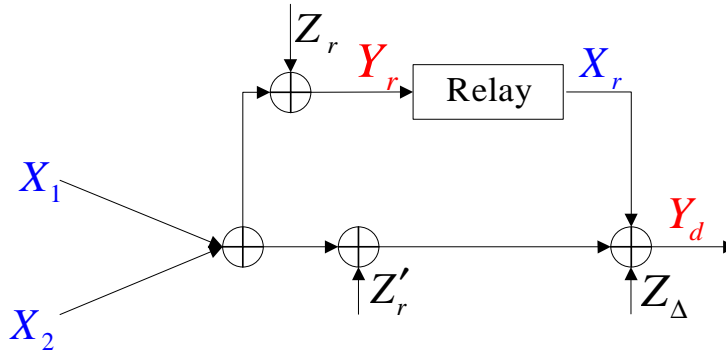


Figure 5.2: A two-user stochastically degraded Gaussian MARC.

tuples (R_1, R_2, \dots, R_K) that satisfy, for all $\mathcal{S} \subseteq \mathcal{K}$,

$$R_{\mathcal{S}} \leq \min \left(\begin{array}{c} I(X_{\mathcal{S}}; Y_r, Y_d | X_{\mathcal{S}^c}, X_r, U), \\ I(X_{\mathcal{S}}, X_r; Y_d | X_{\mathcal{S}^c}, U) \end{array} \right) \quad (5.7)$$

where the union is over all distributions

$$p(u) \cdot \left(\prod_{k=1}^K p(x_k | u) \right) \cdot p(x_r | x_{\mathcal{K}}, u) \cdot p(y_r, y_d | x_{\mathcal{K}}, x_r).$$

Remark 5.2 The time-sharing random variable U ensures that the region in (5.7) is convex. One can apply Caratheodory's theorem [32] to this K -dimensional convex region to bound the cardinality of U as $|\mathcal{U}| \leq K + 1$.

5.4 Decode-and-Forward

A DF code construction is presented in [10, Appendix A] (see also [58]) and we extend it here for the degraded Gaussian MARC. The rate region achieved by DF is presented in [10, 58, Appendix A] and we summarize the result below.

Proposition 5.3 The rate region for DF is the union of the set of rate tuples (R_1, R_2, \dots, R_K) that satisfy, for all $\mathcal{S} \subseteq \mathcal{K}$,

$$R_{\mathcal{S}} \leq \min \left(\begin{array}{c} I(X_{\mathcal{S}}; Y_r | X_{\mathcal{S}^c} V_{\mathcal{K}} X_r U), \\ I(X_{\mathcal{S}} X_r; Y_d | X_{\mathcal{S}^c} V_{\mathcal{S}^c} U) \end{array} \right) \quad (5.8)$$

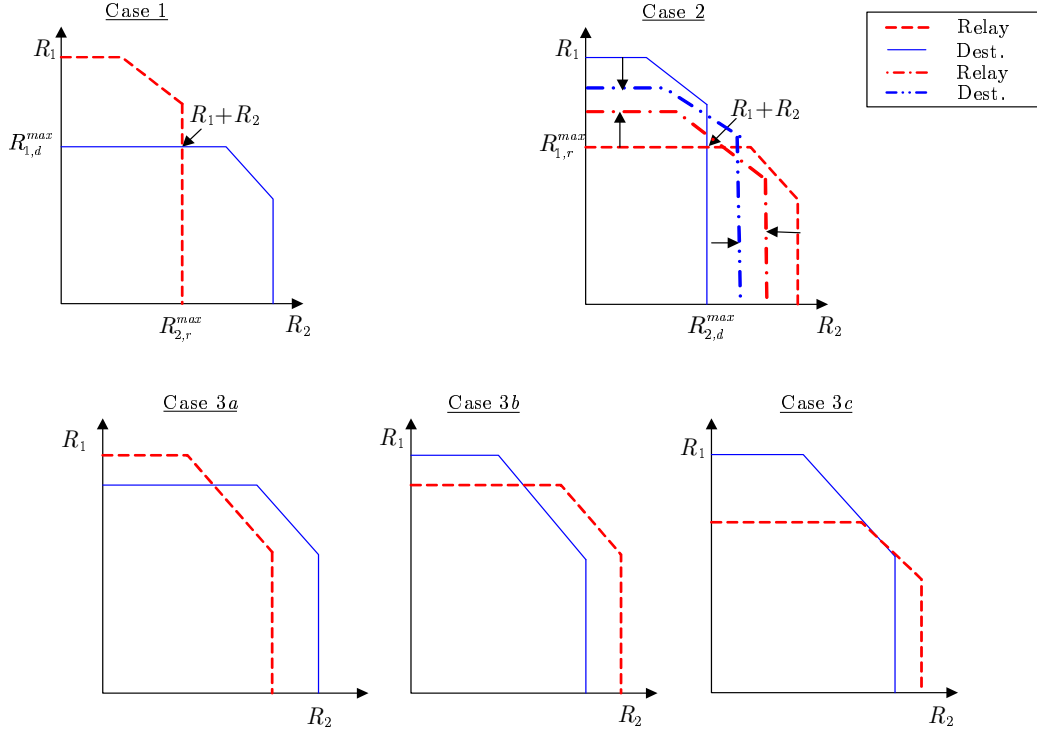


Figure 5.3: Five possible intersections of \mathcal{R}_r and \mathcal{R}_d for a two-user Gaussian MARC.

where the union is over all distributions that factor as

$$p(u) \cdot \left(\prod_{k=1}^K p(v_k|u) p(x_k|v_k, u) \right) \cdot p(x_r|v_{\mathcal{K}}, u) \cdot p(y_r, y_d|x_{\mathcal{T}}). \quad (5.9)$$

Proof: See [58]. ■

Remark 5.4 *The time-sharing random variable U ensures that the region of Theorem 5.3 is convex.*

Remark 5.5 *We remark that independent random variables V_k , $k = 1, 2, \dots, K$, are used in the code construction to help the sources cooperate with the relay.*

For the degraded Gaussian MARC, we employ the following code construction. We generate zero-mean, unit variance, independent and identically distributed (i.i.d) Gaussian random variables V_k , $V_{k,0}$, and $V_{r,0}$, for all $k \in \mathcal{K}$, such that the channel

inputs from source k and the relay are

$$X_k = \sqrt{\alpha_k P_k} V_{k,0} + \sqrt{(1 - \alpha_k) P_k} V_k \quad k \in \mathcal{K} \quad (5.10)$$

$$X_r = \sum_{k=1}^K \sqrt{\beta_k P_r} V_k + \sqrt{\left(1 - \sum_{k=1}^K \beta_k\right) P_r} V_{r,0} \quad (5.11)$$

where

$$\alpha_k \in [0, 1] \text{ and } \beta_k \in [0, 1] \text{ for all } k. \quad (5.12)$$

We write

$$\underline{\alpha}_{\mathcal{K}} = (\alpha_1, \alpha_2, \dots, \alpha_K) \quad (5.13)$$

$$\underline{\beta}_{\mathcal{K}} = (\beta_1, \beta_2, \dots, \beta_K) \quad (5.14)$$

and define Γ to be the set of $(\underline{\alpha}_{\mathcal{K}}, \underline{\beta}_{\mathcal{K}})$ that satisfy (5.12). Substituting (5.10) and (5.11) in (5.8), for any choice of $\underline{\alpha}_{\mathcal{K}}$ and $\underline{\beta}_{\mathcal{K}}$, we obtain

$$R_{\mathcal{S}} \leq \min \left(I_{r,\mathcal{S}}(\underline{\alpha}_{\mathcal{K}}), I_{d,\mathcal{S}}(\underline{\alpha}_{\mathcal{K}}, \underline{\beta}_{\mathcal{K}}) \right) \text{ for all } \mathcal{S} \subseteq \mathcal{K} \quad (5.15)$$

where $I_{r,\mathcal{S}}$ and $I_{d,\mathcal{S}}$, the bounds at the relay and destination respectively, are

$$I_{r,\mathcal{S}} = C \left(\frac{\sum_{k \in \mathcal{S}} \alpha_k P_k}{N_r} \right) \quad (5.16)$$

$$I_{d,\mathcal{S}} = C \left(\frac{\sum_{k \in \mathcal{S}} P_k}{N_d} + \frac{\left(1 - \sum_{k \in \mathcal{S}^c} \beta_k\right) P_r}{N_d} + 2 \sum_{k \in \mathcal{S}} \sqrt{(1 - \alpha_k) \beta_k} \frac{P_k P_r}{N_d N_d} \right) \quad (5.17)$$

and $C(x) = \frac{1}{2} \log(1 + x)$. For a fixed $(\underline{\alpha}_{\mathcal{K}}, \underline{\beta}_{\mathcal{K}})$, the DF rate bounds are given by (5.15). Note that one can use the concavity of the log function to show that $I_{r,\mathcal{S}}$ for all \mathcal{S} , is a concave function of $\underline{\alpha}_{\mathcal{K}}$. In Appendix D.1 we show that $I_{d,\mathcal{S}}$ is a concave function of $\underline{\alpha}_{\mathcal{K}}$ and $\underline{\beta}_{\mathcal{K}}$. The DF rate region, \mathcal{R}_{DF} , achieved over all $(\underline{\alpha}_{\mathcal{K}}, \underline{\beta}_{\mathcal{K}}) \in \Gamma$, is given by the following theorem.

Theorem 5.6 *The DF rate region \mathcal{R}_{DF} for a degraded Gaussian MARC is*

$$\mathcal{R}_{DF} = \bigcup_{\underline{\alpha}_{\mathcal{K}}, \underline{\beta}_{\mathcal{K}}} \left(\mathcal{R}_r(\underline{\alpha}_{\mathcal{K}}) \cap \mathcal{R}_d(\underline{\alpha}_{\mathcal{K}}, \underline{\beta}_{\mathcal{K}}) \right) \quad (5.18)$$

where the rate region \mathcal{R}_t , $t = r, d$, is

$$\mathcal{R}_t = \{(R_1, R_2, \dots, R_K) : 0 \leq R_S \leq I_{t,S}\}. \quad (5.19)$$

Proof: The rate region \mathcal{R}_{DF} follows directly from Proposition 5.8 and the code construction in (5.10)-(5.11). ■

Corollary 5.7 *The rate region \mathcal{R}_{DF} is convex.*

Proof: To show that \mathcal{R}_{DF} is convex, it suffices to show that $I_{r,S}$ and $I_{d,S}$, for all S , are concave functions over the convex set Γ of $(\underline{\alpha}_{\mathcal{K}}, \underline{\beta}_{\mathcal{K}})$. This is because the concavity of $I_{r,S}$ and $I_{d,S}$, for all S , ensures that a convex sum of any collection of rate tuples in \mathcal{R}_{DF} also belongs to \mathcal{R}_{DF} , i.e., satisfies (5.19) for $t = r, d$. The concavity of $I_{r,S}$ follows directly from the concavity of the log function with respect to $\underline{\alpha}_{\mathcal{K}}$. Finally, in Appendix D.1, we show that $I_{d,S}$ is a concave function of $(\underline{\alpha}_{\mathcal{K}}, \underline{\beta}_{\mathcal{K}})$. ■

The region \mathcal{R}_{DF} in (5.18) is a union of the intersection of the regions \mathcal{R}_r and \mathcal{R}_d achieved at the relay and destination respectively, where the union is over all $(\underline{\alpha}_{\mathcal{K}}, \underline{\beta}_{\mathcal{K}}) \in \Gamma$. Since \mathcal{R}_{DF} is convex, each point on the boundary of \mathcal{R}_{DF} is obtained by maximizing the weighted sum $\sum_{k \in \mathcal{K}} \mu_k R_k$ over all Γ , and for all $\mu_k > 0$. Specifically, we determine the optimal policy $(\underline{\alpha}_{\mathcal{K}}^*, \underline{\beta}_{\mathcal{K}}^*)$ that maximizes the sum-rate $R_{\mathcal{K}}$ when $\mu_k = 1$ for all k .

From (5.18), we see that every point on the boundary of \mathcal{R}_{DF} results from the intersection of $\mathcal{R}_r(\underline{\alpha}_{\mathcal{K}})$ and $\mathcal{R}_d(\underline{\alpha}_{\mathcal{K}}, \underline{\beta}_{\mathcal{K}})$ for some $(\underline{\alpha}_{\mathcal{K}}, \underline{\beta}_{\mathcal{K}})$. In Fig. 5.3, we illustrate the five possible choices for the sum-rate resulting from such an intersection for a two-user MARC. Cases 1 and 2 result when no rate pair on the sum-rate plane achieved at one receiver lies within or on the boundary of the rate region achieved at the other receiver. On the other hand, cases 3a, 3b, and 3c result when there is more than one

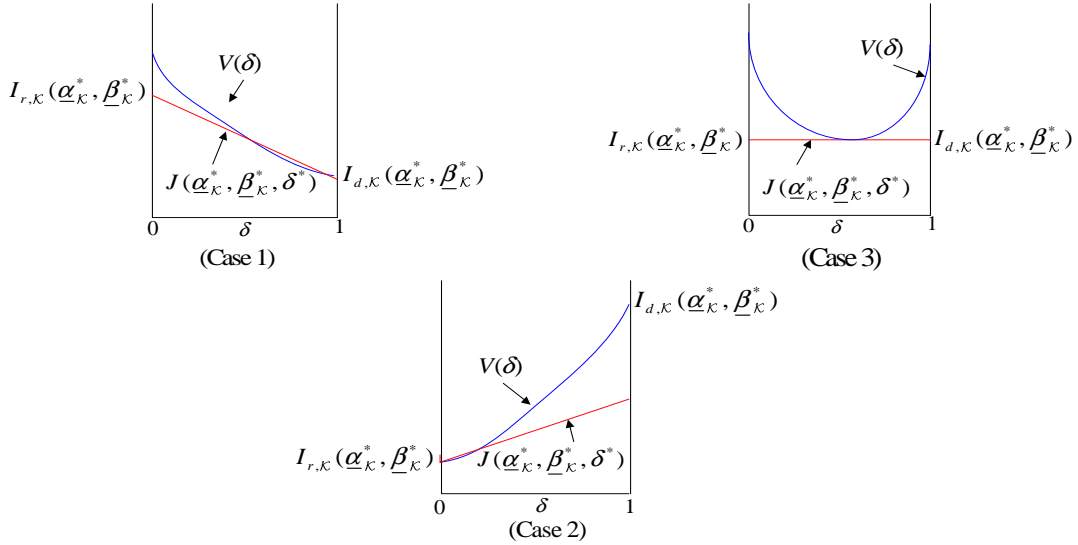


Figure 5.4: Illustration of Cases 1, 2, and 3.

such rate pair. We now argue that it suffices to consider only cases 3a, 3b, and 3c to maximize the sum-rate. The argument uses the fact that, for any $\underline{\beta}_K$, the bounds $I_{r,S}$ and $I_{d,S}$, for all S , are monotonically increasing and decreasing functions, respectively, of $\underline{\alpha}_K$. Consider an (α_1, α_2) that results in the rate region shown in Fig. 5.3 for Case 2. The sum-rate for this case is then given by $R_{1,r}^{\max} + R_{2,d}^{\max}$ where $R_{k,t}^{\max}$ is the maximum single-user rate achieved by user k at receiver t . From the monotonic behavior of the rate bounds at the two receivers, one can find an (α_1, α'_2) that increases $R_{2,d}^{\max}$ while decreasing $R_{1,r}^{\max}$ sufficiently to effect a transition towards one of cases 3a, 3b, or 3c. Observe further that the sum-rate increases as a result as shown in Fig. 5.3. Similar arguments can also be applied to the pair $R_{2,r}^{\max}$ and $R_{1,d}^{\max}$ to increase the sum-rate. Finally, one can also extend these arguments to the K -user case to show that it suffices to consider only the three cases where the rate tuples on the sum-rate plane achieved at one receiver lie within or on the boundary of the rate region achieved at the other receiver. We henceforth enumerate cases 3a, 3b, and 3c as cases 1, 2, and 3 respectively.

The largest bound on the K -user DF sum-rate R_K is then given as

$$\max_{(\underline{\alpha}_K, \underline{\beta}_K) \in \Gamma} \min \left(I_{r,K}(\underline{\alpha}_K), I_{d,K}(\underline{\alpha}_K, \underline{\beta}_K) \right). \quad (5.20)$$

The *max-min* problem in (5.20) is a dual of the classic *minimax* problem in detection theory [69, II.C]. This allows us to apply techniques used to obtain a minimax solution to maximize the bounds in (5.20) over all $(\underline{\alpha}_{\mathcal{K}}, \underline{\beta}_{\mathcal{K}})$ in Γ (see also [70]). We refer to a sum-rate optimal $(\underline{\alpha}_{\mathcal{K}}, \underline{\beta}_{\mathcal{K}})$ as a *max-min rule*. Consider the function

$$J(\underline{\alpha}_{\mathcal{K}}, \underline{\beta}_{\mathcal{K}}, \delta) = \delta I_{r,\mathcal{K}}(\underline{\alpha}_{\mathcal{K}}) + (1 - \delta) I_{d,\mathcal{K}}(\underline{\alpha}_{\mathcal{K}}, \underline{\beta}_{\mathcal{K}}) \quad \delta \in [0, 1]. \quad (5.21)$$

Observe that J is linear in δ ranging in value from $I_{d,\mathcal{K}}$ for $\delta = 0$ to $I_{r,\mathcal{K}}$ for $\delta = 1$. Thus, the optimization in (5.20) is equivalent to maximizing the minimum of the two end points of the line J over Γ . Maximizing $J(\underline{\alpha}_{\mathcal{K}}, \underline{\beta}_{\mathcal{K}}, \delta)$ over $(\underline{\alpha}_{\mathcal{K}}, \underline{\beta}_{\mathcal{K}})$, we obtain a continuous convex function

$$V(\delta) = \max_{(\underline{\alpha}_{\mathcal{K}}, \underline{\beta}_{\mathcal{K}}) \in \Gamma} J(\underline{\alpha}_{\mathcal{K}}, \underline{\beta}_{\mathcal{K}}, \delta) \quad \delta \in [0, 1]. \quad (5.22)$$

From (5.21) and (5.22), we see that for any $(\underline{\alpha}_{\mathcal{K}}, \underline{\beta}_{\mathcal{K}})$, $J(\underline{\alpha}_{\mathcal{K}}, \underline{\beta}_{\mathcal{K}}, \delta)$ either lies strictly below or is tangential to $V(\delta)$. The following proposition summarizes a well-known solution to the max-min problem in (5.20) [70].

Proposition 5.8 $(\underline{\alpha}_{\mathcal{K},\delta^*}, \underline{\beta}_{\mathcal{K},\delta^*})$ is a *max-min rule* where

$$\delta^* = \arg \min_{\delta \in [0,1]} V(\delta). \quad (5.23)$$

The maximum bound on $R_{\mathcal{K}}$, $V(\delta^*)$, is completely determined by the following three cases (see Fig. 5.4).

$$\text{Case 1: } \delta^* = 0 : V(\delta^*) = I_{d,\mathcal{K}}(\underline{\alpha}_{\mathcal{K},\delta^*}, \underline{\beta}_{\mathcal{K},\delta^*}) < I_{r,\mathcal{K}}(\underline{\alpha}_{\mathcal{K},\delta^*}) \quad (5.24)$$

$$\text{Case 2: } \delta^* = 1 : V(\delta^*) = I_{r,\mathcal{K}}(\underline{\alpha}_{\mathcal{K},\delta^*}) < I_{d,\mathcal{K}}(\underline{\alpha}_{\mathcal{K},\delta^*}, \underline{\beta}_{\mathcal{K},\delta^*}) \quad (5.25)$$

$$\text{Case 3: } 0 < \delta^* < 1 : V(\delta^*) = I_{r,\mathcal{K}}(\underline{\alpha}_{\mathcal{K},\delta^*}) = I_{d,\mathcal{K}}(\underline{\alpha}_{\mathcal{K},\delta^*}, \underline{\beta}_{\mathcal{K},\delta^*}). \quad (5.26)$$

We apply Proposition 5.8 to determine the maximum bound on $R_{\mathcal{K}}$. We study each case separately and determine the optimal power fractions at the sources and relay, i.e., the max-min rule $(\underline{\alpha}_{\mathcal{K},\delta^*}, \underline{\beta}_{\mathcal{K},\delta^*})$, for each case.

Case 1: $\delta^ = 0$* : This case occurs when the maximum bound achievable at the destination, $I_{d,\mathcal{K}}(\underline{\alpha}_{\mathcal{K},\delta^*}, \underline{\beta}_{\mathcal{K},\delta^*})$ is smaller than the bound at the relay $I_{r,\mathcal{K}}(\underline{\alpha}_{\mathcal{K},\delta^*})$. From (5.17), we observe that $I_{d,\mathcal{K}}(\underline{\alpha}_{\mathcal{K}}, \underline{\beta}_{\mathcal{K}})$ decreases monotonically with α_k for all k and achieves a maximum at $\underline{\alpha}_{\mathcal{K},\delta^*} = \underline{0}$ of

$$I_{d,\mathcal{K}}(\underline{\alpha}_{\mathcal{K},\delta^*}, \underline{\beta}_{\mathcal{K}}) = C \left(\frac{\sum_{k \in \mathcal{K}} P_k + P_r + 2 \sum_{k \in \mathcal{K}} \sqrt{\beta_k P_k P_r}}{N_d} \right). \quad (5.27)$$

Further, since $I_{d,\mathcal{K}}$ is a concave function of $\underline{\beta}_{\mathcal{K}}$, from Appendix D.1 we see that it is maximized by setting

$$c = \sum_{k=1}^K \beta_k = 1 \quad (5.28)$$

such that from (D.18) we have

$$\beta_{k,\delta^*} = \frac{P_k}{\sum_{k \in \mathcal{K}} P_k}. \quad (5.29)$$

Substituting $\underline{\alpha}_{\mathcal{K},\delta^*} = \underline{0}$ in (5.16), we obtain

$$I_{r,\mathcal{K}}(\underline{\alpha}_{\mathcal{K},\delta^*}) = 0 \quad (5.30)$$

which contradicts the assumption in (5.24), thus making this case infeasible. The infeasibility of this case implies that the largest rate region that is achievable at the destination cannot be enclosed within the region achieved at the relay. Note that we did not need to determine $\underline{\beta}_{\mathcal{K}}^*$ to demonstrate the infeasibility of this case.

Case 2: $\delta^ = 1$* : This case occurs when the maximum bound achievable at the relay, $I_{r,\mathcal{K}}(\underline{\alpha}_{\delta^*})$ is smaller than the bound at the destination $I_{d,\mathcal{K}}(\underline{\alpha}_{\mathcal{K},\delta^*}, \underline{\beta}_{\mathcal{K},\delta^*})$. From (5.16), we observe that $I_{r,\mathcal{K}}$ increases monotonically with α_k for all k and achieves a maximum at

$$\underline{\alpha}_{\mathcal{K},\delta^*} = \underline{1} \quad (5.31)$$

of

$$I_{r,\mathcal{K}}(\underline{\alpha}_{\mathcal{K},\delta^*}) = C \left(\frac{\sum_{k \in \mathcal{K}} P_k}{N_r} \right). \quad (5.32)$$

Comparing (5.16) and (5.17) at $\underline{\alpha}_{\mathcal{K},\delta^*} = \underline{1}$, we obtain the condition for this case as

$$\frac{\sum_{k \in \mathcal{K}} P_k}{N_r} \leq \frac{\sum_{k \in \mathcal{K}} P_k + P_r}{N_d}. \quad (5.33)$$

Expanding (5.33), we have, for any $\mathcal{S} \subset \mathcal{K}$,

$$\frac{\sum_{k \in \mathcal{S}} P_k}{N_r} \leq \frac{\sum_{k \in \mathcal{S}} P_k + P_r}{N_d} - \frac{\sum_{k \in \mathcal{S}^c} P_k (N_d - N_r)}{N_d N_r} \quad (5.34)$$

$$< \frac{\sum_{k \in \mathcal{S}} P_k + P_r}{N_d} \quad (5.35)$$

where (5.35) follows from (5.4). This implies that $\underline{\alpha}_{\mathcal{K},\delta^*} = \underline{1}$ also maximizes the bound on $R_{\mathcal{S}}$ for all \mathcal{S} . The largest rate region achieved in this case is the set of (R_1, R_2, \dots, R_K) tuples that satisfy

$$R_{\mathcal{S}} \leq C \left(\frac{\sum_{k \in \mathcal{S}} P_k}{N_r} \right) \text{ for all } \mathcal{S} \subset \mathcal{K}. \quad (5.36)$$

Observe that for $\underline{\alpha}_{\mathcal{K},\delta^*} = \underline{1}$, source k , for all k , does not allocate any power to transmit V_k and thus we do not achieve coherent combining gains at the destination. The optimal power policy at the relay is then $\underline{\beta}_{\mathcal{K},\delta^*} = \underline{0}$, i.e., the relay forwards the decoded messages from all sources via a single codeword $X_r = V_{r,0}$ in (5.11). Intuitively, one expects this case to occur when the relay has a relatively high signal-to-noise ratio (SNR) at the destination. The condition in (5.33) confirms this observation as

$$\frac{P_r}{N_d} \geq \sum_{k \in \mathcal{K}} P_k \left(\frac{1}{N_r} - \frac{1}{N_d} \right). \quad (5.37)$$

Case 3: Equal bounds case: $0 < \delta^* < 1$: This case occurs when the maximum rate bound achievable at the relay and destination are related as

$$I_{r,\mathcal{K}}(\underline{\alpha}_{\delta^*}) = I_{d,\mathcal{K}}(\underline{\alpha}_{\delta^*}, \underline{\beta}_{\delta^*}) \quad (5.38)$$

The max-min solution for this case falls in one of two possible categories. The first is the relatively straightforward case where $\underline{\alpha}_{\mathcal{K},\delta^*} = \underline{1}$ is the max-min rule that satisfies (5.38). Observe that the maximum sum-rate achieved is the same as that in case 5.4.

We now study the second and more interesting case where $\underline{\alpha}_{\mathcal{K},\delta^*} \neq \underline{1}$. For ease of notation, we drop δ from the subscript and write the max-min rule as $(\underline{\alpha}_{\mathcal{K}}, \underline{\beta}_{\mathcal{K}}^*)$. From (5.17), we see that for $\underline{\alpha}_{\mathcal{K}} \neq \underline{1}$, $I_{d,\mathcal{K}}$ is maximized by a $\underline{\beta}_{\mathcal{K}}^*$ with entries β_k^* that, for all $k \in \mathcal{K}$, satisfy

$$\sum_{k \in \mathcal{K}} \beta_k^* = 1. \quad (5.39)$$

In Appendix D.1 we show that, for a fixed $\underline{\alpha}_{\mathcal{K}}$ and for $\underline{\beta}_{\mathcal{K}}$ subject to (5.39), $I_{d,\mathcal{K}}$ is a concave function of $\underline{\beta}_{\mathcal{K}}$ that achieves a maximum at

$$\beta_k^* = \begin{cases} \frac{(1-\alpha_k)P_k}{\sum_{k=1}^K (1-\alpha_k)P_k} & \underline{\alpha}_{\mathcal{K}} \neq \underline{1} \\ 0 & \underline{\alpha}_{\mathcal{K}} = \underline{1} \end{cases} \quad \text{for all } k \in \mathcal{K}. \quad (5.40)$$

The rate region at the destination for a fixed $\underline{\alpha}_{\mathcal{K}}$ is then a union over all $\underline{\beta}_{\mathcal{K}}$ subject to (5.39) (see Fig. D.1). Observe that the optimal power fraction β_k^* that the relay allocates to cooperating with user k is proportional to the power allocated by user k to achieve coherent combining gains at the destination.

Thus, from (5.26) and (5.39), one can formulate the optimization problem for this case as

$$\begin{aligned} & \text{maximize} && I_{r,\mathcal{K}}(\underline{\alpha}) \\ & \text{subject to} && I_{r,\mathcal{K}}(\underline{\alpha}) = I_{d,\mathcal{K}}(\underline{\alpha}, \underline{\beta}) \\ & && \sum_{k \in \mathcal{K}} \beta_k = 1. \end{aligned} \quad (5.41)$$

Using Lagrange multipliers one can show that it suffices to consider $\beta_k = \beta_k^*$ in the maximization. Observe that since the optimal β_k^* is a function of $\underline{\alpha}_{\mathcal{K}}$, $I_{d,\mathcal{K}}(\underline{\alpha}_{\mathcal{K}}, \underline{\beta}_{\mathcal{K}}^*)$ simplifies to a function of $\underline{\alpha}_{\mathcal{K}}$ as

$$I_{d,\mathcal{K}}(\underline{\alpha}_{\mathcal{K}}, \underline{\beta}_{\mathcal{K}}^*) = C \left(\frac{\sum_{k \in \mathcal{K}} P_k + P_r + 2 \sqrt{\sum_{k \in \mathcal{K}} (1 - \alpha_k^*) P_k P_r}}{N_d} \right). \quad (5.42)$$

We further simplify $I_{d,\mathcal{K}}(\underline{\alpha}_{\mathcal{K}}, \underline{\beta}_{\mathcal{K}}^*)$ and $I_{r,\mathcal{K}}(\underline{\alpha}_{\mathcal{K}})$ as follows. We write

$$P_{\max} = \max_{k \in \mathcal{K}} P_k \quad \text{and} \quad \lambda_k = P_k / P_{\max}. \quad (5.43)$$

$$q_{\mathcal{K}} \triangleq \sqrt{\sum_{k \in \mathcal{K}} (1 - \alpha_k^*) \lambda_k}. \quad (5.44)$$

Using (5.43) and (5.44), we have

$$I_{r,\mathcal{K}}(q_{\mathcal{K}}) = C \left(\frac{\left(\sum_{k \in \mathcal{K}} P_k \right) - q_{\mathcal{K}} P_{\max}}{N_r} \right). \quad (5.45)$$

$$I_{d,\mathcal{K}}(q_{\mathcal{K}}) = C \left(\frac{\left(\sum_{k \in \mathcal{K}} P_k \right) + P_r + 2q_{\mathcal{K}} \sqrt{P_{\max} P_r}}{N_d} \right). \quad (5.46)$$

Observe that $I_{r,\mathcal{K}}(q_{\mathcal{K}})$ and $I_{d,\mathcal{K}}(q_{\mathcal{K}})$ are monotonically increasing and decreasing functions of $q_{\mathcal{K}}$ and thus, the maximization in (5.41) simplifies to determining a $q_{\mathcal{K}}$ such that

$$\frac{\sum_{k \in \mathcal{K}} P_k - q_{\mathcal{K}}^2 P_{\max}}{N_r} = \frac{\sum_{k \in \mathcal{K}} P_k + P_r + 2q_{\mathcal{K}} \sqrt{P_{\max} P_r}}{N_d}. \quad (5.47)$$

We remark that the condition in (5.47) has the geometric interpretation that the bounds on $R_{\mathcal{K}}$ are maximized when the K -user sum rate plane achieved at the relay is tangential to the concave sum-rate surface achieved at the destination at its maximum value.

From (5.12), since $\alpha_k \leq 1$ for all k , the condition for this case simplifies as

$$\frac{\sum_{k \in \mathcal{K}} P_k}{N_r} \geq \frac{\sum_{k \in \mathcal{K}} P_k + P_r}{N_d}. \quad (5.48)$$

Strict inequality in (5.48) requires that $\alpha_k^* < 1$ for at least one $k \in \mathcal{K}$. To determine the optimal $\underline{\alpha}_{\mathcal{K}}^*$, we write the solutions to the quadratic in (5.47) as

$$q_{\mathcal{K},1} = \frac{-K_1 + \sqrt{K_1^2 - (K_2 - K_3) K_0}}{K_0} \quad (5.49)$$

$$q_{\mathcal{K},2} = \frac{-K_1 - \sqrt{K_1^2 - (K_2(\mathcal{K}) - K_3(\mathcal{K})) K_0}}{K_0} \quad (5.50)$$

where

$$K_0 = P_{\max} / N_r \quad (5.51)$$

$$K_1 = \sqrt{P_{\max} P_r} / N_d \quad (5.52)$$

$$K_2(\mathcal{K}) = \frac{\sum_{k \in \mathcal{K}} P_k}{N_d} + \frac{P_r}{N_d} \quad (5.53)$$

$$K_3(\mathcal{K}) = \frac{\sum_{k \in \mathcal{K}} P_k}{N_r}. \quad (5.54)$$

From (5.48), we have

$$K_3(\mathcal{K}) - K_2(\mathcal{K}) \geq 0. \quad (5.55)$$

Using (5.55) in (5.49) and (5.50), we obtain a unique solution $q_{\mathcal{K},1} \geq 0$ since $q_{\mathcal{K},2} < 0$.

The max-min rule for this case is then the set $A_{\mathcal{K}}$ of $\underline{\alpha}_{\mathcal{K}}^*$ satisfying

$$A_{\mathcal{K}} = \left\{ \underline{\alpha}_{\mathcal{K}}^* : \sum_{k \in \mathcal{K}} (1 - \alpha_k^*) \lambda_k = q_{\mathcal{K},1}^2 \right\} \quad (5.56)$$

and a unique $\underline{\beta}_{\mathcal{K}}^*$ with entries β_k^* as in (5.40). The maximum achievable sum-rate for this case is then obtained from (5.49) and (5.16) as

$$C \left(\left(\sum_{k \in \mathcal{K}} P_k / N_r \right) - q_{\mathcal{K},1}^2 P_{\max} / N_r \right). \quad (5.57)$$

5.5 Converse

Consider the outer bounds in Proposition 5.1. For a degraded Gaussian MARC we apply (5.6), the Markov relationship $U - (X_{\mathcal{K}}, X_r) - (Y_r, Y_d)$, and the fact that conditioning does not increase entropy to simplify (5.7) as

$$R_{\mathcal{S}} \leq \min \begin{pmatrix} I(X_{\mathcal{S}}; Y_r | X_r X_{\mathcal{S}^c}), \\ I(X_{\mathcal{S}} X_r; Y_d | X_{\mathcal{S}^c}) \end{pmatrix} \text{ for all } \mathcal{S} \subseteq \mathcal{K} \quad (5.58)$$

and a joint distribution

$$\left(\prod_{k=1}^K p(x_k) \right) \cdot p(x_r | x_{\mathcal{K}}) \cdot p(y_r, y_d | x_{\mathcal{K}}, x_r). \quad (5.59)$$

We write $B_{r,\mathcal{S}}$ and $B_{d,\mathcal{S}}$ to denote, respectively, the first and second bound on $R_{\mathcal{S}}$ in (5.58).

Expanding the bounds on $R_{\mathcal{S}}$ in (5.58), we have

$$R_{\mathcal{S}} \leq \min (h(Y_r | X_r X_{\mathcal{S}^c}) - h(Z_r), h(Y_d | X_{\mathcal{S}^c}) - h(Z_d)). \quad (5.60)$$

For a fixed covariance matrix of the input random variables $X_{\mathcal{K}}$ and X_r , one can apply a conditional entropy maximization theorem [71, Lemma 1] to show that

$$h(Y_r | X_r X_{\mathcal{S}^c}) \quad (5.61)$$

$$h(Y_d | X_{\mathcal{S}^c}) \quad (5.62)$$

are maximized by choosing the distribution in (5.59) as jointly Gaussian.

Consider the bound $B_{r,S}$. Expanding Y_r , we have

$$R_S \leq C \left(\frac{Evar(\sum_{k \in S} X_k | X_r X_{S^c})}{N_r} \right). \quad (5.63)$$

For Gaussian signals, using chain rule, we have

$$Evar(\sum_{m \in S} X_k | X_r X_{S^c}) = \frac{\det(K_{\underline{A}|\underline{C}})}{\det(K_{\underline{B}|\underline{C}})} \quad (5.64)$$

where

$$\underline{A} = \begin{bmatrix} \sum_{m \in S} X_k \\ X_r \end{bmatrix} \quad (5.65)$$

$$\underline{B} = [X_r] \quad (5.66)$$

$$\underline{C} = [X_{S^c}] \quad (5.67)$$

and for random vectors \underline{X} and \underline{Y} , $K_{\underline{X}|\underline{Y}}$ is

$$K_{\underline{X}|\underline{Y}} = E \left[(\underline{X} - E(\underline{X}|\underline{Y})) (\underline{X} - E(\underline{X}|\underline{Y}))^T \right] \quad (5.68)$$

where \underline{X}^T is the transpose of \underline{X} . Note that the expectation $E(\underline{X}|\underline{Y})$ is with respect to \underline{X} for a fixed value of $\underline{Y} = \underline{y}$ while the expectation outside the square brackets in (5.68) is over all random variables. We use the fact that X_S and X_{S^c} are independent to expand (5.64) as

$$Evar(\sum_{k \in S} X_k | X_r X_{S^c}) = var(\sum_{k \in S} X_k) - \frac{E^2 \left(\sum_{k \in S} X_k \tilde{X}_{r,S} \right)}{P_{r,S}} \quad (5.69)$$

where $\tilde{X}_{r,S} = (X_r - E(X_r | X_{S^c}))$ is a Gaussian random variable with variance

$$P_{r,S} = E\tilde{X}_{r,S}^2 = Evar(X_r | X_{S^c}). \quad (5.70)$$

Substituting (5.69) in (5.63) and using (5.5) to bound $\text{var}(X_k)$ for all k , we obtain,

$$R_S \leq C \left(\frac{\sum_{k \in S} \text{var} X_k - \frac{1}{P_{r,S}} E^2 \left(\sum_{k \in S} X_k \tilde{X}_{r,S} \right)}{N_r} \right) \quad (5.71)$$

$$\leq C \left(\frac{\left(\sum_{k \in S} P_k \right) - \frac{1}{P_{r,S}} E^2 \left(\sum_{k \in S} X_k \tilde{X}_{r,S} \right)}{N_r} \right). \quad (5.72)$$

We define, for all $k \in \mathcal{K}$,

$$\sqrt{\gamma_k P_k P_r} \triangleq E(X_k X_r). \quad (5.73)$$

Note that by definition,

$$\gamma_k \in [0, 1] \quad \text{for all } k. \quad (5.74)$$

Using the independence of X_k for all k and (5.73), we write

$$E \left(\sum_{k \in S} X_k \tilde{X}_r \right) = \sum_{k \in S} E(X_k X_r) = \sum_{k \in S} \sqrt{\gamma_k P_k P_r}. \quad (5.75)$$

Next we use (5.73) to evaluate $P_{r,S}$. We start by considering the random variable

$$\hat{X}_r = X_r - E(X_r | X_K). \quad (5.76)$$

Using (5.73) and the independence of X_k for all k , we can write the variance of \hat{X}_r as

$$E \hat{X}_r^2 = E \text{var}(X_r | X_K) \quad (5.77)$$

$$= (1 - \gamma_K) P_r. \quad (5.78)$$

where we used (5.68) to simplify (5.77) to (5.78). Continuing thus, we consider the

random variable $\bar{X}_r = \hat{X}_r - E(\hat{X}_r | X_{K-1})$. Using the independence of X_k for all k ,

we thus have

$$E \bar{X}_r^2 = E \hat{X}_r^2 - E E^2(\hat{X}_r | X_{K-1}) \quad (5.79)$$

$$= E \text{var}(X_r | X_{K-1} X_K) \quad (5.80)$$

$$= (1 - \gamma_{K-1} - \gamma_K) P_r. \quad (5.81)$$

Generalizing this, we have

$$Evar(X_r|X_{\mathcal{S}^c}) = \left(1 - \sum_{k \in \mathcal{S}^c} \gamma_k\right) P_r \triangleq \bar{\gamma}_{\mathcal{S}^c} P_r \quad \text{for all } \mathcal{S} \subseteq \mathcal{K}. \quad (5.82)$$

Finally, we substitute (5.82) and (5.75) in (5.71) to simplify the first bound as

$$R_{\mathcal{S}} \leq \begin{cases} C \left(\sum_{k \in \mathcal{S}} \frac{P_k}{N_r} \right) & \sum_{k \in \mathcal{S}^c} \gamma_k = 1 \\ C \left(\sum_{k \in \mathcal{S}} \frac{P_k}{N_r} - \frac{\left(\sum_{k \in \mathcal{S}} \sqrt{\gamma_k P_k} \right)^2}{N_r \bar{\gamma}_{\mathcal{S}^c}} \right) & \text{o.w.} \end{cases} \quad (5.83)$$

Observe that for $K = 1$, we have $V_1 = X_r$ and $\gamma_1 = 1$, and thus, (5.83) simplifies to the first outer bound in [6, theorem 5]. Finally, from (5.82), observe that γ_k , for all k , satisfy

$$\sum_{k \in \mathcal{K}} \gamma_k \leq 1. \quad (5.84)$$

Consider the bound $B_{d,\mathcal{S}}$ in (5.58). Expanding Y_d using (5.2), we have

$$R_{\mathcal{S}} \leq C \left(\frac{Evar\left(\sum_{k \in \mathcal{S}} X_k + X_r | X_{\mathcal{S}^c}\right)}{N_d} \right) \quad (5.85)$$

$$= C \left(\frac{\sum_{k \in \mathcal{S}} \left(P_k + 2E\left(X_k \tilde{X}_r\right) \right) + Evar(X_r | X_{\mathcal{S}^c})}{N_d} \right) \quad (5.86)$$

Using (5.5), (5.82,) and (5.75), we simplify (5.86) as

$$R_{\mathcal{S}} \leq C \left(\frac{\sum_{k \in \mathcal{S}} P_k + \bar{\gamma}_{\mathcal{S}^c} P_r + 2 \sum_{k \in \mathcal{S}} \sqrt{\gamma_k P_k P_r}}{N_d} \right). \quad (5.87)$$

Observe that for $K = 1$, (5.87) simplifies to the second bound in [6, theorem 5].

Combining (5.83) and (5.87), we have

$$R_{\mathcal{S}} \leq \min(B_{1,\mathcal{S}}, B_{2,\mathcal{S}}) \quad \text{for all } \mathcal{S} \subseteq \mathcal{K} \quad (5.88)$$

where $B_{r,\mathcal{S}}$ and $B_{d,\mathcal{S}}$ are the bounds in (5.83) and (5.87) respectively. Comparing (5.83) and (5.16), we see that $B_{r,\mathcal{S}}$ is, in general, not equal to the DF bound $I_{r,\mathcal{S}}$. Further,

$B_{r,S}$ is not a concave function of $\underline{\gamma}_{\mathcal{K}}$. However, in Appendix D.2, we show that for a fixed $\underline{\gamma}_{\mathcal{S}^c}$, $B_{r,S}$ is a concave function of $\underline{\gamma}_{\mathcal{S}}$. On the other hand, as shown for $I_{d,S}$, one can verify that $B_{d,S}$ in (5.87) is a concave function of $(\underline{\alpha}_{\mathcal{K}}, \underline{\beta}_{\mathcal{K}})$.

We obtain the outer bound rate region \mathcal{R}_{OB} as follows. From (5.88) we see that for any choice of $\underline{\gamma}_{\mathcal{K}}$, the rate region is an intersection of the regions enclosed by the bounds $B_{r,S}$ and $B_{d,S}$ for all S . Since $B_{r,S}$ is not a concave function of $\underline{\gamma}_{\mathcal{K}}$, one must also consider all possible convex combinations of $\underline{\gamma}_{\mathcal{K}}$ to obtain \mathcal{R}_{OB} . For the K -dimensional convex region \mathcal{R}_{OB} , we can apply Caratheodory's theorem [32] to express every rate tuple (R_1, R_2, \dots, R_K) in \mathcal{R}_{OB} as a convex combination of at most $K + 1$ rate tuples, where each rate tuple is obtained for a specific choice of $\underline{\gamma}_{\mathcal{K}}$. We denote a collection of $K + 1$ power fractions as $\{\underline{\gamma}_{\mathcal{K}}\}_{K+1}$ such that the rate tuple achieved by the m^{th} vector $\underline{\gamma}_{\mathcal{K}}^{(m)}$ is weighted by the m^{th} entry of the weight vector $\underline{\eta}$, for all $m \in \mathcal{K} \cup \{K + 1\}$. Note that the entries of $\underline{\eta}$ satisfy

$$\sum_{m=1}^{K+1} \eta_m = 1. \quad (5.89)$$

Finally, we denote the set of all $\underline{\zeta} = (\{\underline{\gamma}_{\mathcal{K}}\}_{K+1}, \underline{\eta})$ satisfying (5.74) and (5.89) as Γ_{OB} .

Theorem 5.9 *The outer bound region \mathcal{R}_{OB} for a degraded Gaussian MARC is given as*

$$\mathcal{R}_{OB} = \bigcup_{\underline{\zeta} \in \Gamma_{OB}} (\mathcal{R}_1(\underline{\zeta}) \cap \mathcal{R}_2(\underline{\zeta})) \quad (5.90)$$

where the rate region \mathcal{R}_j^{ob} , $j = r, d$, is

$$\mathcal{R}_j^{ob}(\underline{\zeta}) = \{(R_1, R_2, \dots, R_K) : 0 \leq R_S \leq \overline{B}_{j,S}(\underline{\zeta})\} \quad (5.91)$$

and the bound $\overline{B}_{j,S}$ is obtained as

$$\overline{B}_{j,S}(\underline{\zeta}) = \sum_{m=1}^{K+1} \eta_m B_{j,S}(\underline{\gamma}_{\mathcal{K}}^{(m)}). \quad (5.92)$$

The region \mathcal{R}_{OB} in (5.18) is a union of the intersection of the regions \mathcal{R}_r^{ob} and \mathcal{R}_d^{ob} , where the union is over all convex combinations of $\underline{\gamma}_{\mathcal{K}}$. Since \mathcal{R}_{OB} is convex, we obtain

the boundary of \mathcal{R}_{OB} by maximizing the weighted sum $\sum_{k \in \mathcal{K}} \mu_k R_k$ over all $-\mathcal{O}_B$ and for all $\mu_k > 0$. Specifically, we determine the sum-rate $R_{\mathcal{K}}$ when $\mu_k = 1$ for all k . Comparing (5.83) and (5.87), we see that $B_{r,\mathcal{S}}$ and $B_{d,\mathcal{S}}$ are monotonically increasing and decreasing functions respectively of $\underline{\gamma}_{\mathcal{S}}$ for a fixed $\underline{\gamma}_{\mathcal{S}^c}$. Then using arguments similar to those used for DF we restrict our maximization analysis to the three cases in Proposition 5.8 and write the largest outer bounds on the K -user sum-rate $R_{\mathcal{K}}$ as

$$\max_{\underline{\gamma} \in \Gamma_{OB}} \min\{\overline{B}_{r,\mathcal{K}}, \overline{B}_{d,\mathcal{K}}\}. \quad (5.93)$$

From (5.83) and (5.87), we see that $B_{r,\mathcal{K}}$ and $B_{d,\mathcal{K}}$ can be simplified as

$$B_{r,\mathcal{K}} = C \left(\frac{\sum_{k \in \mathcal{K}} P_k}{N_r} - \frac{x^2 P_{\max}}{N_r} \right) \quad (5.94)$$

$$B_{d,\mathcal{K}} = C \left(\frac{\sum_{k \in \mathcal{K}} P_k}{N_d} + \frac{P_r}{N_d} + \frac{2x\sqrt{P_{\max}P_r}}{N_d} \right) \quad (5.95)$$

where we define

$$x \triangleq \sum_{k=1}^K \sqrt{\gamma_k \lambda_k} \quad (5.96)$$

and λ_k , for all k , is defined in (D.29) as the ratio of P_k to $P_{\max} = \max_{k \in \mathcal{K}} P_k$. In Appendix D.2 we show that $B_{r,\mathcal{K}}$ is a concave function of x . Further, one can similarly verify that $B_{d,\mathcal{K}}$ is also a concave function of x . Thus, the max-min problem in (5.93) simplifies to

$$\max_x \min\{B_{r,\mathcal{K}}(x), B_{d,\mathcal{K}}(x)\} \quad (5.97)$$

where the maximization is over all x that result choosing γ_k , for all k , that satisfies (5.74) and (5.84).

Remark 5.10 Note that in general $B_{r,\mathcal{K}}$ is not a concave function of $\underline{\gamma}_{\mathcal{K}}$. However, from the dependence of $B_{r,\mathcal{K}}$ on $\underline{\gamma}_{\mathcal{K}}$ in (5.83), we see that it suffices to limit the analysis to a set Γ_{ob} of non-negative $\underline{\gamma}_{\mathcal{K}}$ that satisfy (5.94) and the constraint $\sum_{k \in \mathcal{K}} \gamma_k \leq 1$.

Remark 5.11 Note that one can define $\gamma_k \triangleq (1 - \alpha_k) \beta_k$ for $\alpha_k \in [0, 1]$, $\beta_k \in [0, 1]$ and $\sum_{k \in \mathcal{K}} \beta_k \leq 1$. Substituting this in (5.83) and (5.87), we have $B_{d,\mathcal{K}} = I_{d,\mathcal{K}}$ while $B_{r,\mathcal{K}} \geq I_{r,\mathcal{K}}$ with equality for $\beta_k = \beta_k^*$ in (5.40).

We now apply Proposition 5.8 to solve (5.97). Then, for any $\delta \in [0, 1]$, we write

$$J^{ob}(x, \delta) = \delta B_{r, \mathcal{K}}(x) + (1 - \delta) B_{d, \mathcal{K}}(x) \quad (5.98)$$

$$V^{ob}(\delta) = \max_x J^{ob}(x, \delta) \quad (5.99)$$

and denote x^{ob} as the max-min rule that minimizes $V^{ob}(\delta)$ at δ^* . We now study the three cases and determine the max-min rule and the maximum sum-rate in each case.

Case 4: $\delta^ = 0$: $B_{d, \mathcal{K}}(x^{ob}) < B_{r, \mathcal{K}}(x^{ob})$:* Since $B_{d, \mathcal{K}}$ is a concave function of γ_k , for all k , following steps similar to those in Appendix D.1, one can show that it is maximized by

$$\gamma_k^{(ob)} = \frac{P_k}{\sum_{k \in \mathcal{K}} P_k} \quad \text{for all } k \in \mathcal{K}. \quad (5.100)$$

The maximum sum-rate $B_{d, \mathcal{K}}(\underline{\alpha}_{\mathcal{K}}^{ob}, \underline{\beta}_{\mathcal{K}}^{ob})$ is

$$B_{d, \mathcal{K}}(\underline{\alpha}_{\mathcal{K}}^{ob}, \underline{\beta}_{\mathcal{K}}^{ob}) = C \left(\frac{\sum_{k \in \mathcal{K}} P_k + P_r + 2 \sqrt{\sum_{k \in \mathcal{K}} P_k P_r}}{N_d} \right). \quad (5.101)$$

Observe that the resulting x^{ob} is given as

$$x^{ob} = \sqrt{\sum_{k \in \mathcal{K}} \lambda_k}. \quad (5.102)$$

Finally, substituting x^{ob} in (5.94), we obtain

$$B_{r, \mathcal{K}}(x^{ob}) = B_{r, \mathcal{K}}(\underline{\gamma}_{\mathcal{K}}^{ob}) = 0 \quad (5.103)$$

which contradicts the assumption of this case, thus making this case infeasible.

Case 5: $\delta^ = 1$: $B_{r, \mathcal{K}}(x^{ob}) < B_{d, \mathcal{K}}(x^{ob})$:* From (5.94), we see that $B_{r, \mathcal{K}}$ achieves a maximum at $x^{ob} = 0$ of

$$B_{r, \mathcal{K}}(\underline{\alpha}_{\mathcal{K}}^{ob}, \underline{\beta}_{\mathcal{K}}) = C \left(\frac{\sum_{k \in \mathcal{K}} P_k}{N_r} \right). \quad (5.104)$$

From (5.96) we see that $x^{ob} = 0$ is achieved for $\underline{\gamma}_{\mathcal{K}}^{ob} = \underline{0}$. The analysis from here on is exactly the same as in DF for case 5.4 and the rate region achieved by the outer bounds

is the same as \mathcal{R}_{DF} in case 5.4. Thus, we obtain the capacity region for this case as the set of (R_1, R_2, \dots, R_K) tuples that satisfy

$$R_{\mathcal{S}} \leq C \left(\frac{\sum_{k \in \mathcal{S}} P_k}{N_r} \right) \quad \text{for all } \mathcal{S} \subseteq \mathcal{K}. \quad (5.105)$$

Finally, we remark that the condition under which the case occurs is the same as that for DF case 5.4 and the subsequent observations hold here too. Further, $\gamma_k = 0$ implies that the sum-rate optimal strategy involves independent signaling at the sources and the relay.

Case 6: Equal bounds case: $0 < \delta^* < 1 : B_{r,\mathcal{K}}(x^{ob}) = B_{d,\mathcal{K}}(x^{ob})$: As in case 5.4, the max-min solution x^{ob} for this case also falls in one of two possible categories. The first is the relatively straightforward case where the bounds are equal for $x^{ob} = 0$, i.e., $\underline{\gamma}_{\mathcal{K}}^{ob} = \underline{0}$ and the maximum sum-rate achieved is the same as that in case 5.5. We now study the second and more interesting case where $x^{ob} \neq 0$. Observe that this corresponds to the requirement that $\underline{\gamma}_{\mathcal{K}}^{ob}$ lies on the simplex

$$\sum_{k \in \mathcal{K}} \gamma_k^{ob} = 1. \quad (5.106)$$

From (5.94) and (5.95), we see that $B_{r,\mathcal{K}}(x)$ and $B_{d,\mathcal{K}}(x)$ are monotonically decreasing and increasing functions of x respectively and thus intersect at most once over the range of x . The optimal x^{ob} then satisfies

$$C \left(\frac{\sum_{k \in \mathcal{K}} P_k}{N_r} - \frac{(x^{ob})^2 P_{\max}}{N_r} \right) = C \left(\frac{\left(\sum_{k \in \mathcal{K}} P_k \right) + P_r + 2x^{ob} \sqrt{P_{\max} P_r}}{N_d} \right). \quad (5.107)$$

Observe that the condition in (5.107) is the same as that for DF case 5.4, and thus, we have

$$x^{ob} = q_{\mathcal{K},1} = \frac{-K_1 + \sqrt{K_1^2 - (K_2 - K_3) K_0}}{K_0} \quad (5.108)$$

where the constants K_0, K_1, K_2 , and K_3 are as defined in (5.51)-(5.54) and $q_{\mathcal{K},1}$ satisfies the DF condition for case 5.4. The resulting max-min bound is then given by

(5.57). The $\underline{\gamma}_{\mathcal{K}}^{ob}$ that achieves this maximum satisfies

$$\sum_{k=1}^K \sqrt{\gamma_k^{ob} \lambda_k} = x^{ob}. \quad (5.109)$$

For the definition

$$\gamma_k^{ob} \triangleq (1 - \alpha_k^{ob}) \beta_k^{ob} \quad (5.110)$$

such that $\alpha_k^{ob} \in [0, 1]$, $\beta_k^{ob} \in [0, 1]$, for all k , and

$$\sum_{k \in \mathcal{K}} \beta_k = 1 \quad (5.111)$$

(5.109) simplifies to

$$\sum_{k=1}^K \sqrt{(1 - \alpha_k^{ob}) \beta_k^{ob} \lambda_k} = x^{ob}. \quad (5.112)$$

Further for the choice of

$$\beta_k^{ob} = \beta_k^* = \begin{cases} \frac{(1 - \alpha_k) P_k}{\sum_{k=1}^K (1 - \alpha_k) P_k} & \underline{\alpha}_{\mathcal{K}} \neq 1 \\ 0 & \underline{\alpha}_{\mathcal{K}} = \underline{1} \end{cases} \quad \text{for all } k \in \mathcal{K}. \quad (5.113)$$

we can find an $\underline{\alpha}_{\mathcal{K}}^{ob}$ that satisfies

$$\sum_{k=1}^K (1 - \alpha_k^{ob}) \lambda_k = (x^{ob})^2 = q_{\mathcal{K},1}^2. \quad (5.114)$$

Thus, the set of $\underline{\alpha}_{\mathcal{K}}^{ob}$ that maximize $B_{r,\mathcal{K}} = B_{d,\mathcal{K}}$ is the same as the set $A_{\mathcal{K}}$ of $\underline{\alpha}_{\mathcal{K}}^*$ that maximizes the DF sum-rate. This implies that the set of $\underline{\gamma}_{\mathcal{K}}^{ob}$ that maximize the sum-rate outer bound for this case also contains those correlation coefficients that maximize the DF bounds.

Thus, we've shown that the maximum K -user sum-rate outer bounds, for each of the two feasible cases that result from the max-min optimization, can be achieved by DF for a specific choice of the power fractions that the sources and the relay allocate to achieving cooperative (coherent combining) gains.

5.5.1 Average Transmit Power Constraint

We determined the sum-capacity for a degraded Gaussian MARC under a per symbol transmit power constraint at the sources and relay. One can also consider an average power constraint at every transmitter. The achievable strategy remains unchanged; for the converse we start with the convex sums of the outer bounds in (5.7) over n channel uses. The bounds $B_{r,S}$ and $B_{d,S}$ are now written as convex sums over n channel uses such that $B_{j,\mathcal{K}}^{(i)}$ is the bound achieved in the i^{th} channel use for all $i = 1, 2, \dots, n$. The analysis in Section 5.4 can be applied to develop $B_{j,\mathcal{K}}^{(i)}$ for each i under the assumption that the power transmitted in that channel use is subject to an average constraint over all n uses. Finally, we can use the concavity of $B_{j,\mathcal{K}}^{(i)}$, $j = r, d$, as a function of a single variable x_i to simplify the bounds to those developed in Section 5.5, and thus, obtain the same sum-capacity result.

5.6 Concluding Remarks

We determined the sum-capacity of a degraded Gaussian MARC. For the inner bounds, we considered the achievable strategy of DF and determined the largest K -user sum-rate using max-min optimization techniques. For the converse, we considered the cut-set outer bounds for the case of independent sources and showed that the K -user sum-rate outer bounds can also be maximized using max-min optimization techniques. In fact the max-min optimization for both the inner and outer bounds simplified to two feasible cases.

We showed that both the inner and outer bounds on the K -user sum-rate are a minimum of two bounds, one obtained using Y_r and the other using Y_d ; however, the inner and outer bounds that use Y_r are not exactly the same. This difference is due to the fact that the input distributions for the inner and outer bounds are different. In fact, the input distribution for the inner bound uses auxiliary random variables $V_{\mathcal{K}}$ to model the correlation between the inputs at the sources and the relay and is more restrictive

than the distribution for the outer bound. Despite this difference, the reason we achieve sum-capacity is due to the form taken by the solutions for the two feasible cases. The maximum sum-rate for the first feasible case for both the inner and outer bound is achieved when the sources and the relay do not allocate any power to achieving coherent combining gains at the destination. Thus, for this case, $V_K = 0$, and the two bounds match. In fact, the sum-capacity is the largest value that the bound achieved using Y_r takes and corresponds to a geometry where the relay has a relatively high SNR channel to the destination.

The largest sum-rate for the second case is achieved by maximizing the bounds at the relay and destination when they are equal. In general, for this case $V_K \neq 0$, i.e., a non-empty subset of sources and the relay allocate power to achieve cooperative combining gains at the destination. The largest DF sum-rate is then achieved by a relay power policy that maximizes the cooperative gains achieved at the destination, i.e., X_r is a unique weighted sum of V_k for all k where the weight for each k is proportional to the power allocated by source k to cooperating with the relay. Further, the maximum sum-rate admits several solutions for the power fractions allocated at the sources for cooperation subject to a constraint that results from the equating the two bounds on the sum-rate. For the converse, we showed that the maximum outer bound on the K -user sum-rate is the same as the maximum DF sum-rate. We also showed that the outer bound is maximized by a set of source-relay cross-correlation coefficients (source and relay power fractions) subject to the same constraint as DF. Further, we showed that a subset of such a set also maximizes the DF sum-rate and thus we achieve the sum-capacity for this subset. Finally, since the DF max-min rule requires a unique correlation between X_r and V_K , conditioning the outer bound that uses Y_r on X_r alone suffices to achieve the sum-capacity.

Appendix A

Partial Decode-and-Forward: Coding Theorem

We derive the PDF rate bounds for discrete memoryless MARCs, $K = 2$, and backward decoding. The random code construction and the encoding are described in Section 2.4.3 and we use (strongly) typical sequence decoders. Define the set of typical sequences of length n with respect to ϵ and $P_{X,Y}(\cdot)$ as

$$T_\epsilon^{(n)}(X, Y) = \left\{ (\underline{x}, \underline{y}) : \left| \frac{n(a, b|\underline{x}, \underline{y})}{n} - P_{X,Y}(a, b) \right| \leq \frac{\epsilon}{|\mathcal{X}| \cdot |\mathcal{Y}|} \right\} \quad (\text{A.1})$$

where $n(a, b|\underline{x}, \underline{y})$ is the number of times the pair (a, b) occurs in the sequence of pairs $(x_1, y_1), (x_2, y_2), \dots, (x_n, y_n)$. \mathcal{X} and \mathcal{Y} are the alphabets of X and Y with cardinalities $|\mathcal{X}|$ and $|\mathcal{Y}|$, respectively. We refer to [72, Ch. 2] for properties of such sequences.

Encoding: Consider block b .

1. Source 1 transmits $\underline{x}_1(w_{1,1,b}, w_{1,2,b}, w_{1,2,b-1})$ while source 2 transmits $\underline{x}_2(w_{2,1,b}, w_{2,2,b}, w_{2,2,b-1})$ where $w_{1,2,0}, w_{2,2,0}, w_{1,1,B+1}, w_{2,1,B+1}, w_{1,2,B+1}$, and $w_{2,2,B+1}$ are set to 1.
2. The relay transmits $\underline{x}_r(s_{1,b}, s_{2,b})$ where $(s_{1,b}, s_{2,b})$ is the message pair decoded at the relay in block $(b - 1)$.

Decoding:

1. *At the relay:* The relay decodes $(w_{1,2,b}, w_{2,2,b})$ in block b , $b = 1, 2, \dots, B$, by using $\underline{y}_{r,b}$ and by assuming that its message estimates in the previous blocks are correct (see [6]). More precisely, the relay decodes by finding a $(\tilde{w}_{1,2,b}, \tilde{w}_{2,2,b})$

such that

$$\begin{aligned} &(\underline{q}_1(\tilde{w}_{1,2,b}, w_{1,2,b-1}), \underline{q}_2(\tilde{w}_{2,2,b}, w_{2,2,b-1}), \underline{v}_1(w_{1,2,b-1}), \\ &\quad \underline{v}_2(w_{2,2,b-1}), \underline{x}_r(w_{1,2,b-1}, w_{2,2,b-1}), \underline{y}_{r,b}) \in \\ &\quad T_\epsilon^{(n)}(Q_1, Q_2, V_1, V_2, X_r, Y_r). \end{aligned} \quad (\text{A.2})$$

We assume that the correct codewords are identified as being typical since this is a high probability event for large n . With this assumption the relay makes an error only if it identifies a $(\tilde{w}_{1,2,b}, \tilde{w}_{2,2,b}) \neq (w_{1,2,b}, w_{2,2,b})$ that satisfies (A.2). This error event can be further split into three disjoint error events. The first error event has a $\tilde{w}_{1,2,b} \neq w_{1,2,b}$ and $\tilde{w}_{2,2,b} = w_{2,2,b}$ satisfying (A.2). Using [10, Lemma 1] and the union bound, the probability of this event is at most

$$2^{n(R_{1,2} - I(Q_1; Y_r | Q_2 V_1 V_2 X_r) + 6\epsilon)}. \quad (\text{A.3})$$

Thus, for reliable decoding we set

$$R_{1,2} < I(Q_1; Y_r | Q_2 V_1 V_2 X_r). \quad (\text{A.4})$$

The second error event has $\tilde{w}_{1,2,b} = w_{1,2,b}$ and a $\tilde{w}_{2,2,b} \neq w_{2,2,b}$ satisfying (A.2).

By symmetry to (A.4), we set

$$R_{2,2} < I(Q_2; Y_r | Q_1 V_1 V_2 X_r). \quad (\text{A.5})$$

The third error event has a $\tilde{w}_{1,2,b} \neq w_{1,2,b}$ and a $\tilde{w}_{2,2,b} \neq w_{2,2,b}$ satisfying (A.2).

We again use [10, Lemma 1] to bound the probability of this event by

$$2^{n(R_{1,2} + R_{2,2} - I(Q_1 Q_2; Y_r | V_1 V_2 X_r) + 6\epsilon)}. \quad (\text{A.6})$$

Reliable decoding thus requires

$$R_{1,2} + R_{2,2} < I(Q_1 Q_2; Y_r | V_1 V_2 X_r). \quad (\text{A.7})$$

2. *At the destination:* The destination collects all of its $B+1$ output blocks. Starting from the last block, the destination decodes $(w_{1,1,b+1}, w_{2,1,b+1}, w_{1,2,b}, w_{2,2,b})$, $b =$

$B, B - 1, \dots, 1$ by using $\underline{y}_{d,b+1}$ and by assuming that its previously decoded message estimates are correct (see [6]). More precisely, the destination decodes by finding a $(\tilde{w}_{1,1,b+1}, \tilde{w}_{2,1,b+1}, \tilde{w}_{1,2,b}, \tilde{w}_{2,2,b})$ such that

$$\begin{aligned} &(\underline{x}_1(\tilde{w}_{1,1,b+1}, w_{1,2,b+1}, \tilde{w}_{1,2,b}), \underline{x}_2(\tilde{w}_{2,1,b+1}, w_{2,2,b+1}, \tilde{w}_{2,2,b}), \underline{q}_1(w_{1,2,b+1}, \tilde{w}_{1,2,b}), \\ &\quad \underline{q}_2(w_{2,2,b+1}, \tilde{w}_{2,2,b}), \underline{v}_1(\tilde{w}_{1,2,b}), \underline{v}_2(\tilde{w}_{2,2,b}), \underline{x}_r(\tilde{w}_{1,2,b}, \tilde{w}_{2,2,b}), \underline{y}_{d,b+1}) \\ &\in T_\epsilon^{(n)}(X_1, X_2, Q_1, Q_2, V_1, V_2, X_r, Y_d). \quad (\text{A.8}) \end{aligned}$$

As before we assume that the correct codewords are identified as being typical. Specifically, fifteen kinds of errors occur in decoding the message tuple $(\tilde{w}_{1,1,b+1}, \tilde{w}_{2,1,b+1}, \tilde{w}_{1,2,b}, \tilde{w}_{2,2,b})$. We first consider the singleten error events, i.e., only one of the four messages is decoded incorrectly using (A.8). We have four such events, corresponding to either $\tilde{w}_{1,1,b+1} \neq w_{1,1,b+1}$ or $\tilde{w}_{2,1,b+1} \neq w_{2,1,b+1}$, or $\tilde{w}_{1,2,b} \neq w_{1,2,b}$, or $\tilde{w}_{2,2,b} \neq w_{2,2,b}$. Using [10, Lemma 1] and the union bound, we follow the same decoding steps as for the relay decoder to show that

$$R_{1,1} < I(X_1; Y_d | Q_1 Q_2 V_1 V_2 X_r) \quad (\text{A.9})$$

$$R_{2,1} < I(X_2; Y_d | X_1 Q_1 Q_2 V_1 V_2 X_r) \quad (\text{A.10})$$

$$R_{1,2} < I(X_1 X_r Q_1 V_1; Y_d | X_2 Q_2 V_2 X_r) \quad (\text{A.11})$$

$$= I(X_1 X_r; Y_d | X_2 Q_2 V_2) \quad (\text{A.12})$$

$$R_{2,2} < I(X_2 X_r; Y_d | X_1 Q_1 V_1) \quad (\text{A.13})$$

ensures reliable communications where (A.12) and (A.13) result from the Markov chain $(V_k, Q_k) - (X_k, X_r) - (Y_r, Y_d)$ for $k = 1$ and 2 respectively. We next consider the six error events where a pair of messages is decoded incorrectly, i.e., the incorrect message pair satisfies (A.8). We use the union bound and [10,

Lemma 1] to show that reliable communications requires

$$R_{1,1} + R_{2,1} < I(X_1 X_2; Y_d | Q_1 V_1 Q_2 V_2 X_r) \quad (\text{A.14})$$

$$R_{1,1} + R_{1,2} < I(X_1 X_r; Y_d | X_2 Q_2 V_2) \quad (\text{A.15})$$

$$R_{1,1} + R_{2,2} < I(X_1 X_2 X_r; Y_d | Q_1 V_1) \quad (\text{A.16})$$

$$R_{2,1} + R_{1,2} < I(X_1 X_2 X_r; Y_d | Q_2 V_2) \quad (\text{A.17})$$

$$R_{2,1} + R_{2,2} < I(X_2 X_r; Y_d | X_1 Q_1 V_1) \quad (\text{A.18})$$

$$R_{1,2} + R_{2,2} < I(X_1 X_2 X_r; Y_d) \quad (\text{A.19})$$

where the bounds (A.14)-(A.19) are obtained by bounding the error probability of the events

$$(\tilde{w}_{1,1,b+1}, \tilde{w}_{2,1,b+1}) \neq (w_{1,1,b+1}, w_{2,1,b+1}) \quad (\text{A.20})$$

$$(\tilde{w}_{1,1,b+1}, \tilde{w}_{1,2,b}) \neq (w_{1,1,b+1}, w_{1,2,b}) \quad (\text{A.21})$$

$$(\tilde{w}_{1,1,b+1}, \tilde{w}_{2,2,b}) \neq (w_{1,1,b+1}, w_{2,2,b}) \quad (\text{A.22})$$

$$(\tilde{w}_{2,1,b+1}, \tilde{w}_{1,2,b}) \neq (w_{2,1,b+1}, w_{1,2,b}) \quad (\text{A.23})$$

$$(\tilde{w}_{2,1,b+1}, \tilde{w}_{2,2,b}) \neq (w_{2,1,b+1}, w_{2,2,b}) \text{ and} \quad (\text{A.24})$$

$$(\tilde{w}_{1,2,b}, \tilde{w}_{2,2,b}) \neq (w_{1,2,b}, w_{2,2,b}) \quad (\text{A.25})$$

respectively for the case when both messages in a pair are decoded incorrectly. Note that (A.15) and (A.18), simplify to the bounds on R_1 and R_2 respectively. Further, comparing (A.12) and (A.15), we see that the bounds for the case when either $w_{1,2,b}$ or the pair $(w_{1,1,b+1}, w_{1,2,b})$ are decoded incorrectly are the same. One can similarly see that the bounds in (A.13) and (A.18) that result from incorrectly decoding $w_{2,2,b}$ and $(w_{2,1,b+1}, w_{2,2,b})$ respectively are also the same. For the case where three of the four messages in $(\tilde{w}_{1,1,b+1}, \tilde{w}_{2,1,b+1}, \tilde{w}_{1,2,b}, \tilde{w}_{2,2,b})$ are decoded incorrectly, i.e., an incorrect triple satisfies the typicality requirement in (A.8), we obtain four possible error events. Using the same decoding steps as

before, we can show that reliable communications requires

$$R_{1,1} + R_{2,1} + R_{1,2} < I(X_1 X_2 X_r; Y_d | Q_2 V_2) \quad (\text{A.26})$$

$$R_{1,1} + R_{2,1} + R_{2,2} < I(X_1 X_2 X_r; Y_d | Q_1 V_1) \quad (\text{A.27})$$

$$R_{1,1} + R_{1,2} + R_{2,2} < I(X_1 X_2 X_r; Y_d) \quad (\text{A.28})$$

$$R_{2,1} + R_{1,2} + R_{2,2} < I(X_1 X_2 X_r; Y_d) \quad (\text{A.29})$$

where the bounds (A.26)-(A.29) are obtained by bounding the error probability of the events

$$(\tilde{w}_{1,1,b+1}, \tilde{w}_{2,1,b+1}, \tilde{w}_{1,2,b}) \neq (w_{1,1,b+1}, w_{2,1,b+1}, w_{1,2,b}) \quad (\text{A.30})$$

$$(\tilde{w}_{1,1,b+1}, \tilde{w}_{2,1,b+1}, \tilde{w}_{2,2,b}) \neq (w_{1,1,b+1}, w_{2,1,b+1}, w_{2,2,b}) \quad (\text{A.31})$$

$$(\tilde{w}_{1,1,b+1}, \tilde{w}_{1,2,b}, \tilde{w}_{2,2,b}) \neq (w_{1,1,b+1}, w_{1,2,b}, w_{2,2,b}) \text{ and} \quad (\text{A.32})$$

$$(\tilde{w}_{2,1,b+1}, \tilde{w}_{1,2,b}, \tilde{w}_{2,2,b}) \neq (w_{2,1,b+1}, w_{1,2,b}, w_{2,2,b}) \quad (\text{A.33})$$

respectively for the case where all three messages in a triple are decoded incorrectly. Comparing (A.26) and (A.17), we see that the bounds for the case when either $w_{1,2,b}$ or the pair $(w_{1,1,b+1}, w_{1,2,b})$ are decoded incorrectly are the same. A similar observation results from comparing (A.27) and (A.16). Finally, we consider the event where there exists a tuple $(\tilde{w}_{1,1,b+1}, \tilde{w}_{2,1,b+1}, \tilde{w}_{1,2,b}, \tilde{w}_{2,2,b})$ satisfying (A.8) such that all four message are decoded incorrectly. Reliable communications then require

$$R_{1,1} + R_{1,2} + R_{2,1} + R_{2,2} = R_1 + R_2 < I(X_1 X_2 X_r; Y_d). \quad (\text{A.34})$$

Comparing (A.34) with (A.28) and (A.29), we again see that decoding a tuple with $w_{k,2,b}$ yields the same bounds as decoding a tuple with both $(w_{k,1,b+1}, w_{k,2,b})$ for $k = 1, 2$. One can generalize this observation for any $K > 2$; thus, for any disjoint $\mathcal{A}, \mathcal{G} \subset \mathcal{K}$ we have $R_{1,\mathcal{A}} + R_{2,\mathcal{G}} = R_{1,\mathcal{A} \cup \mathcal{G}} + R_{2,\mathcal{G}}$ and hence it suffices to consider sets \mathcal{S} and \mathcal{G} such that $\mathcal{G} \subseteq \mathcal{S}$.

Finally, combining the bounds in (A.9)-(A.13), (A.14)-(A.19), (A.26)-(A.29), and (A.34) the bounds simplify to those in (2.36)-(2.38). The analysis carries over in a straightforward way to weakly-typical (or entropy-typical) sequences [30, p. 51], the addition of a time-sharing random variable U [30, p. 396], and $K > 2$.

Appendix B

DF Rate Region: Coding Theorems

B.1 Backward Decoding Analysis

We derive the DF rate bounds for discrete memoryless MARCs, $K = 2$, and backward decoding. The random code construction and the encoding are described in Section 3.2.2 and we use (strongly) typical sequence decoders. Define the set of typical sequences of length n with respect to ϵ and $P_{X,Y}(\cdot)$ as

$$T_\epsilon^{(n)}(X, Y) = \left\{ (\underline{x}, \underline{y}) : \left| \frac{n(a, b|\underline{x}, \underline{y})}{n} - P_{X,Y}(a, b) \right| \leq \frac{\epsilon}{|\mathcal{X}| \cdot |\mathcal{Y}|} \text{ for all } (a, b) \text{ and } n(a, b|\underline{x}, \underline{y}) = 0 \text{ if } P_{X,Y}(a, b) = 0 \right\}. \quad (\text{B.1})$$

where $n(a, b|\underline{x}, \underline{y})$ is the number of times the pair (a, b) occurs in the sequence of pairs $(x_1, y_1), (x_2, y_2), \dots, (x_n, y_n)$. \mathcal{X} and \mathcal{Y} are the alphabets of X and Y with cardinalities $|\mathcal{X}|$ and $|\mathcal{Y}|$, respectively. We refer to [72, Ch. 2] for properties of such sequences.

Decoding:

1. *At the relay:* The relay decodes $(w_{1,b}, w_{2,b})$ in block b , $b = 1, 2, \dots, B$, by using $\underline{y}_{r,b}$ and by assuming that its message estimates in the previous blocks are correct (see [6]). More precisely, the relay decodes by finding a $(\tilde{w}_{1,b}, \tilde{w}_{2,b})$ such that

$$(\underline{x}_1(\tilde{w}_{1,b}, w_{1,b-1}), \underline{x}_2(\tilde{w}_{2,b}, w_{2,b-1}), \underline{v}_1(w_{1,b-1}), \underline{v}_2(w_{2,b-1}), \underline{x}_r(w_{1,b-1}, w_{2,b-1}), \underline{y}_{r,b}) \in T_\epsilon^{(n)}(X_1, X_2, V_1, V_2, X_r, Y_r). \quad (\text{B.2})$$

We assume that the correct codewords are identified as being typical since this is a high probability event for large n . With this assumption the relay makes an error only if it identifies a $(\tilde{w}_{1,b}, \tilde{w}_{2,b}) \neq (w_{1,b}, w_{2,b})$ that satisfies (B.2). This

error event can be further split into three disjoint error events. The first error event has a $\tilde{w}_{1,b} \neq w_{1,b}$ and $\tilde{w}_{2,b} = w_{2,b}$ satisfying (B.2). Using [10, Lemma 1] and the union bound, the probability of this event is at most

$$2^{n(R_1 - I(X_1; Y_r | X_2 V_1 V_2 X_r) + 6\epsilon)}. \quad (\text{B.3})$$

Thus, for reliable decoding we set

$$R_1 < I(X_1; Y_r | X_2 V_1 V_2 X_r). \quad (\text{B.4})$$

The second error event has $\tilde{w}_{1,b} = w_{1,b}$ and a $\tilde{w}_{2,b} \neq w_{2,b}$ satisfying (B.2). By symmetry to (B.4), we set

$$R_2 < I(X_2; Y_r | X_1 V_1 V_2 X_r). \quad (\text{B.5})$$

The third error event has a $\tilde{w}_{1,b} \neq w_{1,b}$ and a $\tilde{w}_{2,b} \neq w_{2,b}$ satisfying (B.2). We again use [10, Lemma 1] to bound the probability of this event by

$$2^{n(R_1 + R_2 - I(X_1 X_2; Y_r | V_1 V_2 X_r) + 6\epsilon)}. \quad (\text{B.6})$$

Reliable decoding thus requires

$$R_1 + R_2 < I(X_1 X_2; Y_r | V_1 V_2 X_r). \quad (\text{B.7})$$

2. *At the destination:* The destination collects all of its $B+1$ output blocks. Starting from the last block, the destination decodes $(w_{1,b}, w_{2,b})$, $b = B, B-1, \dots, 1$ by using $\underline{y}_{d,b+1}$ and by assuming that its previously decoded message estimates are correct (see [6]). More precisely, the destination decodes by finding a $(\tilde{w}_{1,b}, \tilde{w}_{2,b})$ such that

$$\begin{aligned} & (\underline{x}_1(w_{1,b+1}, \tilde{w}_{1,b}), \underline{x}_2(w_{2,b+1}, \tilde{w}_{2,b}), \underline{v}_1(\tilde{w}_{1,b}), \underline{v}_2(\tilde{w}_{2,b}), \underline{x}_r(\tilde{w}_{1,b}, \tilde{w}_{2,b}), \underline{y}_{d,b+1}) \\ & \in T_\epsilon^{(n)}(X_1, X_2, V_1, V_2, X_r, Y_d). \end{aligned} \quad (\text{B.8})$$

As before we assume that the correct codewords are identified as being typical. Again, three kinds of error events can occur in decoding $(w_{1,b}, w_{2,b})$. Using [10,

Lemma 1] and the union bound, we follow the same decoding steps as for the relay decoder to show that

$$R_1 < I(X_1 X_r; Y_d | X_2 V_2) \quad (\text{B.9})$$

$$R_2 < I(X_2 X_r; Y_d | X_1 V_1) \quad (\text{B.10})$$

$$R_1 + R_2 < I(X_1 X_r X_2; Y_d) \quad (\text{B.11})$$

ensures reliable communications.

Combining (B.4), (B.5), (B.7), and (B.9)-(B.11), we have the bounds (3.2)-(3.7). The analysis carries over in a straightforward way to weakly-typical (or entropy-typical) sequences [30, p. 51], the addition of a time-sharing random variable U [30, p. 396], and $K > 2$.

B.2 Sliding-Window Joint Decoding Analysis

We derive the DF rate bounds for $K = 2$, offset encoding, and sliding-window decoding. Without loss of generality, we consider the offset order $\pi = (1, 2)$. Section 3.2.2 describes the random code construction.

Encoding: Consider block b .

1. Source 1 transmits $\underline{x}_1(w_{1,b}, w_{1,b-1})$ while source 2 transmits $\underline{x}_2(w_{2,b-1}, w_{2,b-2})$ where $w_{2,-1}, w_{2,0}, w_{1,0}, w_{1,B+1}, w_{1,B+2}$, and $w_{2,B+1}$ are set to 1.
2. The relay transmits $\underline{x}_r(s_{1,b}, s_{2,b})$ where $(s_{1,b}, s_{2,b})$ is the message pair decoded at the relay in block $(b - 1)$.

Decoding:

1. *At the relay:* The relay decoder error analysis is the same as that described in Appendix B.1 up to changes in the message indices. We therefore have the same rate bounds (B.4), (B.5), and (B.7).

2. *At the destination:* The destination decodes $(w_{1,b}, w_{2,b})$ by using $\underline{y}_{d,b}$, $\underline{y}_{d,b+1}$, and $\underline{y}_{d,b+2}$ and by assuming that no errors were made up to block b . More precisely, the destination decodes by finding a $(\tilde{w}_{1,b}, \tilde{w}_{2,b})$ such that three events occur:

$$\begin{aligned} \mathcal{E}_1 : \quad & (\underline{v}_1(w_{1,b-1}), \underline{v}_2(w_{2,b-2}), \underline{x}_1(\tilde{w}_{1,b}, w_{1,b-1}), \underline{x}_2(w_{2,b-1}, w_{2,b-2}), \\ & \underline{x}_r(w_{1,b-1}, w_{2,b-2}), \underline{y}_{d,b}) \in T_\epsilon^{(n)}(V_1, V_2, X_1, X_2, X_r, Y_d) \end{aligned} \quad (\text{B.12})$$

$$\begin{aligned} \mathcal{E}_2 : \quad & (\underline{v}_1(\tilde{w}_{1,b}), \underline{v}_2(w_{2,b-1}), \underline{x}_2(\tilde{w}_{2,b}, w_{2,b-1}), \underline{x}_r(\tilde{w}_{1,b}, w_{2,b-1}), \underline{y}_{d,b+1}) \\ & \in T_\epsilon^{(n)}(V_1, V_2, X_2, X_r, Y_d) \end{aligned} \quad (\text{B.13})$$

$$\mathcal{E}_3 : \quad (\underline{v}_2(\tilde{w}_{2,b}), \underline{y}_{d,b+2}) \in T_\epsilon^{(n)}(V_2, Y_d). \quad (\text{B.14})$$

Note that the codebooks in different blocks are generated independently (see Section 3.2.2) so the above three error events are independent (see [8, 35]). As before, we consider three disjoint error events that can occur in decoding $(w_{1,b}, w_{2,b})$. The first event has a $\tilde{w}_{1,b} \neq w_{1,b}$ and $\tilde{w}_{2,b} = w_{2,b}$ satisfying (B.12)-(B.14). We upper bound the probability of this error event using [10, Lemma 1] and the union bound as

$$\begin{aligned} & \sum_{\tilde{w}_{1,b} \neq w_{1,b}} \Pr(\mathcal{E}_1 \cap \mathcal{E}_2 \cap \mathcal{E}_3) \\ &= \sum_{\tilde{w}_{1,b} \neq w_{1,b}} \Pr(\mathcal{E}_1) \cdot \Pr(\mathcal{E}_2) \cdot \Pr(\mathcal{E}_3) \end{aligned} \quad (\text{B.15})$$

$$\leq 2^{n(R_1 - I(X_1; Y_d | X_2 V_1 V_2 X_r) - I(V_1 X_r; Y_d | X_2 V_2) + 12\epsilon)} \quad (\text{B.16})$$

$$= 2^{n(R_1 - I(X_1 X_r; Y_d | X_2 V_2) + 12\epsilon)} \quad (\text{B.17})$$

where we used $\Pr(\mathcal{E}_3) \leq 1$ for (B.16) and (3.13)-(3.14) for (B.17). Thus, we set

$$R_1 < I(X_1 X_r; Y_d | X_2 V_2). \quad (\text{B.18})$$

Consider next the case where $\tilde{w}_{1,b} = w_{1,b}$ but $\tilde{w}_{2,b} \neq w_{2,b}$. The expression (B.15) with the summation over $\tilde{w}_{2,b} \neq w_{2,b}$ instead of $\tilde{w}_{1,b} \neq w_{1,b}$ is upper bounded as

$$2^{n(R_2 - I(X_2; Y_d | V_1 V_2 X_r) - I(V_2; Y_d) + 12\epsilon)} \quad (\text{B.19})$$

where we used $\Pr(\mathcal{E}_1) \leq 1$. We thus require

$$R_2 < I(X_2; Y_d | V_1 V_2 X_r) + I(V_2; Y_d). \quad (\text{B.20})$$

Finally, consider the case $\tilde{w}_{1,b} \neq w_{1,b}$ and $\tilde{w}_{2,b} \neq w_{2,b}$. The expression (B.15) with the summation now over both $\tilde{w}_{1,b} \neq w_{1,b}$ and $\tilde{w}_{2,b} \neq w_{2,b}$ is upper bounded as

$$\begin{aligned} & 2^{n(R_1+R_2)} \cdot 2^{-nI(X_1; Y_d | X_2 V_1 V_2 X_r) + n6\epsilon} \\ & \cdot 2^{-nI(X_2 V_1 X_r; Y_d | V_2) + n6\epsilon} \cdot 2^{-nI(V_2; Y_d) + n6\epsilon} \end{aligned} \quad (\text{B.21})$$

$$= 2^{n(R_1+R_2-I(X_1 X_2 X_r; Y_d) + 18\epsilon)} \quad (\text{B.22})$$

where we have used the chain rule for mutual information and the Markov chain $(V_1, V_2) - (X_1, X_2, X_r) - Y_d$. For reliable decoding, we thus require

$$R_1 + R_2 < I(X_1 X_2 X_r; Y_d). \quad (\text{B.23})$$

Combining (B.18), (B.20), and (B.23), we obtain (3.29)-(3.31). Again, the analysis carries over in a straightforward way to weakly-typical sequences, the addition of a time-sharing random variable U , and $K > 2$.

B.3 Sliding-Window Successive Decoding Analysis

We derive DF rate bounds for $K \geq 2$, offset encoding, and sliding-window decoding. We further focus on the message blocks $w_{k,b}$ with $b = 1$. However, the destination decoder now performs successive rather than joint decoding. Without loss of generality, we consider the offset order $\pi = (1, 2, \dots, K)$. Section 3.2.2 describes the random code construction, and the encoding and relay decoding are the same as in Appendix B.2.

Decoding at the destination: Consider the window with the channel-symbol blocks $\underline{y}_{d,1}, \underline{y}_{d,2}, \dots, \underline{y}_{d,K+1}$. As explained in Section 3.4.2, the destination successively decodes in the reverse order $w_{K,1}, w_{K-1,1}, \dots, w_{1,1}$ (see the shaded blocks in Fig. 3.4 for

the cases $k = K$, $k = 2$, and $k = 1$). The destination further assumes that its past decoding steps were successful, and we perform our analysis with the same assumption. For $k = K, K - 1, \dots, 2$, the destination finds a $\tilde{w}_{k,1}$ such that two events occur:

$$\mathcal{E}_{1,k} : (\underline{v}_k(\tilde{w}_{k,1}), \underline{v}_{[k+1,K]}(1), \underline{x}_{[k+1,K]}(1, 1), \underline{y}_{d,k+1}) \in T_\epsilon^{(n)}(V_k, V_{[k+1,K]}, X_{[k+1,K]}, Y_d) \quad (\text{B.24})$$

$$\mathcal{E}_{2,k} : (\underline{x}_k(\tilde{w}_{k,1}, 1), \underline{v}_{[k,K]}(1), \underline{x}_{[k+1,K]}(1, 1), \underline{y}_{d,k}) \in T_\epsilon^{(n)}(X_k, V_{[k,K]}, X_{[k+1,K]}, Y_d) \quad (\text{B.25})$$

where $\underline{v}_{[i,j]}(1) = \{v_i(1), v_{i+1}(1), \dots, v_j(1)\}$ and similarly for $\underline{x}_{[i,j]}(1, 1)$ and $\underline{v}_{\mathcal{K}}(1)$ below. As before, we assume that variables with vacuous index sets are appropriate constants, e.g., we assume that all the entries of $\underline{v}_{[K+1,K]}$ are the same constant $V_{[K+1,K]}$.

The events $\mathcal{E}_{1,k}$ and $\mathcal{E}_{2,k}$ are independent and we assume that the correct codewords are identified as being typical. The destination thus makes an error only if it identifies a $\tilde{w}_{k,1} \neq w_{k,1}$ that satisfies both (B.24) and (B.25). We upper bound the probability of this event using [10, Lemma 1] as

$$\sum_{\tilde{w}_{k,1} \neq w_{k,1}} \Pr(\mathcal{E}_{1,k}) \cdot \Pr(\mathcal{E}_{2,k}) \leq 2^{n(R_k - I(X_k V_k; Y_d | X_{[k+1,K]} V_{[k+1,K]}) + 12\epsilon)}. \quad (\text{B.26})$$

For $1 < k \leq K$, we therefore require

$$R_k < I(X_k V_k; Y_d | X_{[k+1,K]} V_{[k+1,K]}). \quad (\text{B.27})$$

For $k = 1$, we add $\underline{x}_r(\cdot)$ to (B.24) and (B.25) as follows:

$$\begin{aligned} \mathcal{E}_{1,1} : & (\underline{v}_1(\tilde{w}_{1,1}), \underline{v}_{[2,K]}(1), \underline{x}_{[2,K]}(1, 1), \underline{x}_r(\tilde{w}_{1,1}, 1, \dots, 1), \underline{y}_{d,2}) \\ & \in T_\epsilon^{(n)}(V_1, V_{[2,K]}, X_{[2,K]}, X_r, Y_d) \end{aligned} \quad (\text{B.28})$$

$$\begin{aligned} \mathcal{E}_{2,1} : & (\underline{x}_1(\tilde{w}_{1,1}, 1), \underline{v}_{\mathcal{K}}(1), \underline{x}_{[2,K]}(1, 1), \underline{x}_r(1, 1, \dots, 1), \underline{y}_{d,1}) \\ & \in T_\epsilon^{(n)}(X_1, V_{\mathcal{K}}, X_{[2,K]}, X_r, Y_d). \end{aligned} \quad (\text{B.29})$$

The resulting bound is

$$R_1 < I(X_1 X_r; Y_d | X_{[2,K]} V_{[2,K]}). \quad (\text{B.30})$$

For example, for $K = 2$ the two rate bounds are

$$R_2 < I(X_2 V_2; Y_d) \quad (\text{B.31})$$

$$R_1 < I(X_1 X_r; Y_d | X_2 V_2) \quad (\text{B.32})$$

and one can approach the corner point (3.39). One can check that the above analysis generalizes to $b > 1$.

Appendix C

MARC and MAC-GF: Rate and Outage Derivations

C.1 PDF Rate Region for User and Relay Cooperative Networks

We derive the PDF rate bounds for both two-hop and multi-hop Gaussian single-source multi-relay channels using typical sequence decoding. We summarize the typicality definition for a collection of L random variables (X_1, X_2, \dots, X_L) as follows [30, Chap 10, p. 384].

Definition C.1 *The set $A_\epsilon^{(n)}$ of ϵ -typical n -sequences $(\underline{x}_1, \underline{x}_2, \dots, \underline{x}_L)$ with respect to ϵ and $P_{X_1, X_2, \dots, X_L}(\cdot)$ is defined by*

$$A_\epsilon^{(n)}(X_1, X_2, \dots, X_L) = A_\epsilon^{(n)} = \{(\underline{x}_1, \underline{x}_2, \dots, \underline{x}_L) : \left| \frac{-1}{n} \log p(s) - H(S) \right| < \epsilon, \\ \text{for all } S \subseteq \{X_1, X_2, \dots, X_L\}\}. \quad (\text{C.1})$$

We develop the rate bounds for user k and write \mathcal{C}_k to denote the set of users that act as relays for user k such that $|\mathcal{C}_k| = L_k - 1$. We assume that the total number of channel uses for user k over all fractions, denoted as n , is sufficiently large to invoke typicality arguments. Note that the number of channel uses in a fraction θ_k is simply $n\theta_k$, where we assume that θ_k is chosen such that $n\theta_k$ is a positive integer.

C.1.1 Two-hop Scheme

Encoding: We use Gaussian signaling at the sources and relay such that in slot k user k transmits

$$X_k = \begin{cases} \sqrt{\alpha_k \bar{P}_k} U_k & \text{frac. } \theta_k \\ \sqrt{\alpha_k \bar{P}_k} Q_k + \sqrt{\bar{\alpha}_k \bar{P}_k} V_k & \text{frac. } \bar{\theta}_k \end{cases} \quad (\text{C.2})$$

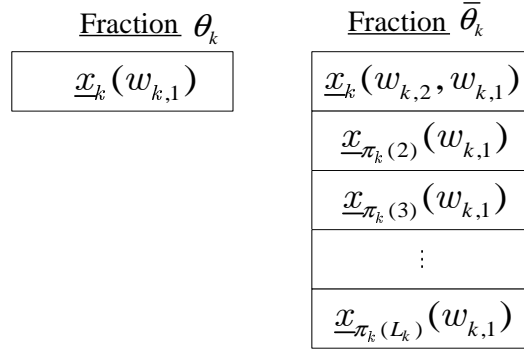


Figure C.1: Partial decode-and-forward encoding for a two-hop cooperative network.

where U_k , Q_k , and V_k are independent and identically distributed (i.i.d) circularly symmetric complex Gaussian random variables with zero mean and unit variance and $\bar{\alpha}_k = 1 - \alpha_k$. The power \bar{P}_k satisfies (4.2) and is defined for the MARC and MAC-GF, respectively, in (4.10) and (4.31). Thus user k uses the signals in (C.2) to transmit the message $w_{k,1} \in \{1, 2, \dots, 2^{nR_{k,1}}\}$ in the fraction θ_k at a rate $R_{k,1}$. In the fraction $\bar{\theta}_k$, user k retransmits $w_{k,1}$ via V_k and also sends a new message $w_{k,2} \in \{1, 2, \dots, 2^{nR_{k,2}}\}$ at rate $R_{k,2}$ via Q_k . Note that $w_{k,2}$ is only decoded by the destination.

Let $\pi_k(\cdot)$ be a permutation on \mathcal{C}_k such that user $\pi_k(l)$ begins its transmissions in the fraction $\bar{\theta}_k$, for all $l = 2, 3, \dots, L_k$. We further define $\pi_k(1) = k$ and $\pi_k(i:j) = \{\pi_k(i), \pi_k(i+1), \dots, \pi_k(j)\}$. We remark that, unlike the multi-hop scheme, the order of the user indexes in \mathcal{C}_k does not affect the achievable rate for the two-hop scheme. However, for ease of use, we use the same notation for both schemes. Thus for the two-hop scheme, user $\pi_k(l)$, for all $l = 2, 3, \dots, L_k$, decodes $w_{k,1}$ in the fraction θ_k and retransmits it in fraction $\bar{\theta}_k$ such that its transmitted signal $X_{\pi_k(l)}$ is

$$X_{\pi_k(l)} = \begin{cases} \sqrt{\frac{\bar{P}_k}{\bar{\theta}_k}} V_k & \text{for all } l = 2, 3, \dots, L_k. \end{cases} \quad (\text{C.3})$$

The resulting encoding scheme is shown in Fig. C.1. Note that we write \underline{x}_m to denote a codeword transmitted by node m .

Decoding:

1. *At the nodes in \mathcal{C}_k :* The node $\pi_k(l)$ decodes $w_{k,1}$ in the fraction θ_k by using $\underline{y}_{\pi_k(l)}$. More precisely, node $\pi_k(l)$ decodes by finding a $\tilde{w}_{k,1}$ such that

$$(\underline{x}_k(\tilde{w}_{k,1}), \underline{y}_{\pi_k(l)}) \in A_\epsilon^{(n\theta_k)}(X_k, Y_{\pi_k(l)}). \quad (\text{C.4})$$

Using [30, Thm. 14.2.3] and the union bound, the probability of this event is at most

$$2^{n(R_{k,1} - \theta_k I(X_k; Y_{\pi_k(l)}) + 3\epsilon)}. \quad (\text{C.5})$$

For Gaussian signaling in (C.2) over a Gaussian channel, reliable decoding then requires [30, Th. 14.2.3]

$$R_{k,1} \leq \theta_k \log \left(1 + |h_{\pi_k(l),k}|^2 \overline{P}_k \right) \quad \text{for all } l = 2, 3, \dots, L_k. \quad (\text{C.6})$$

2. *At the destination:* The destination uses its received signals from both fractions to jointly decode $(w_{k,1}, w_{k,2})$. Focussing on the typical error events, we see that the destination makes an error only if it identifies a $(\tilde{w}_{k,1}, \tilde{w}_{k,2}) \neq (w_{k,1}, w_{k,2})$ using joint typical decoding. More precisely, the destination decodes by finding a $(\tilde{w}_{k,1}, \tilde{w}_{k,2})$ such that two events occur:

$$\mathcal{E}_1 : (\underline{x}_k(\tilde{w}_{k,1}), \underline{y}_d) \in A_\epsilon^{(n\theta_k)}(X_k, Y_d) \quad (\text{C.7})$$

$$\begin{aligned} \mathcal{E}_2 : & (\underline{x}_1(\tilde{w}_{k,1}, \tilde{w}_{k,2}), \underline{x}_{\pi_k(1)}(\tilde{w}_{k,1}), \underline{x}_{\pi_k(2)}(\tilde{w}_{k,1}), \dots, \underline{x}_{\pi_k(L_k)}(\tilde{w}_{k,1}), \\ & \underline{y}_d) \in A_\epsilon^{(n\bar{\theta}_k)}(X_k, X_{\pi_k(1)}, X_{\pi_k(2)}, \dots, X_{\pi_k(L_k)}, Y_d). \end{aligned} \quad (\text{C.8})$$

Note that the codebooks in different fractions are generated independently so the above two events are independent (see [8, 35]). We consider three disjoint error events that can occur in decoding $(w_{k,1}, w_{k,2})$. The first event has a $\tilde{w}_{k,1} \neq w_{k,1}$ and $\tilde{w}_{k,2} = w_{k,2}$ satisfying (C.7)-(C.8). We upper bound the probability of this error event using [30, 14.3, p. 393] and the union bound as

$$\sum_{\tilde{w}_{k,1} \neq w_{k,1}} \Pr(\mathcal{E}_1 \cap \mathcal{E}_2) \quad (\text{C.9})$$

$$= \sum_{\tilde{w}_{k,1} \neq w_{k,1}} \Pr(\mathcal{E}_1) \cdot \Pr(\mathcal{E}_2) \quad (\text{C.10})$$

$$\leq 2^{n(R_{k,1} - \theta_k I(X_1; Y_d) - \bar{\theta}_k I(X_1 X_{C_k}; Y_d) + 3\epsilon\bar{\theta}_k + 3\epsilon\theta_k)} \quad (\text{C.11})$$

where $X_{\mathcal{C}_k} = \{X_l : l \in \mathcal{C}_k\}$. Then from (C.2) and (C.3), for reliable decoding we set

$$R_{k,1} < \theta_k \log (1 + |h_{d,k}|^2 \bar{P}_k) + \bar{\theta}_k \log \left(1 + \alpha |h_{d,k}|^2 \bar{P}_k + \left| (1 - \alpha) h_{d,k} \sqrt{\bar{P}_k} + \sum_{l=2}^{L_k} h_{d,\pi_k(l)} \sqrt{\frac{\bar{P}_l}{\bar{\theta}_k}} \right|^2 \right). \quad (\text{C.12})$$

The second error event has $\tilde{w}_{k,1} = w_{k,1}$ and a $\tilde{w}_{k,2} \neq w_{k,2}$ satisfying (C.7)-(C.8). We again use [30, 14.3, p. 393] to bound the probability of this event by

$$2^{n(R_{k,2} - \bar{\theta}_k I(X_k; Y_d | X_{\mathcal{C}_k}) + 6\epsilon \bar{\theta}_k)}. \quad (\text{C.13})$$

Reliable decoding thus requires

$$R_{k,2} < \bar{\theta}_k \log (1 + \alpha |h_{d,k}|^2 \bar{P}_k). \quad (\text{C.14})$$

Finally, consider the case $\tilde{w}_{k,1} \neq w_{k,1}$ and $\tilde{w}_{k,2} \neq w_{k,2}$. The expression (C.9) with the summation now over both $\tilde{w}_{k,1} \neq w_{k,1}$ and $\tilde{w}_{k,2} \neq w_{k,2}$ is upper bounded as

$$2^{n(R_{k,1} + R_{k,2})} \cdot 2^{-n\theta_k I(X_k; Y_d) + 3\epsilon \theta_k n} \cdot 2^{-n\theta_k I(X_1; Y_d) - n\bar{\theta}_k I(X_1 X_{\mathcal{C}_k}; Y_d) + 3n\epsilon \theta_k + 3n\epsilon \bar{\theta}_k} \quad (\text{C.15})$$

For reliable decoding, we thus require

$$R_1 < \theta_k \log (1 + |h_{d,k}|^2 \bar{P}_k) + \bar{\theta}_k \log \left(1 + \alpha_k |h_{d,k}|^2 \bar{P}_k + \left| \bar{\alpha}_k h_{d,k} \sqrt{\bar{P}_k} + \sum_{l=2}^{L_k} h_{d,\pi_k(l)} \sqrt{\frac{\bar{P}_l}{\bar{\theta}_k}} \right|^2 \right). \quad (\text{C.16})$$

Combining (C.12), (C.14), and (C.16), we have the bounds (4.32), (4.33), and (4.34). Finally, for the case when $\mathcal{C}_k = \{r\}$, i.e., the time-duplexed MARC, we obtain the bounds in (4.13), (4.14), and (4.15).

C.1.2 Multi-hop Scheme

Encoding: In this scheme, user k transmits

$$X_k = \begin{cases} \sqrt{\alpha_k \bar{P}_k} V_{k,l} & \theta_{k,l}, l = 1, 2, \dots, L_k - 1 \\ \sqrt{\alpha_k \bar{P}_k} Q_k + \sqrt{\bar{\alpha}_k \bar{P}_k} V_{k,L_k} & \bar{\theta}_{k,L_k} \end{cases} \quad (\text{C.17})$$

where $V_{k,l}$, Q_k , for all $l = 1, 2, \dots, L_k$, are i.i.d zero-mean unit variance Gaussian random variables. User k transmits the message $w_{k,1} \in \{1, 2, \dots, 2^{nR_{k,1}}\}$ over the fractions $\theta_{k,l}$, $l = 1, 2, \dots, L_k - 1$, at a rate $R_{k,1}$. Note that it uses independent signals in each fraction to transmit the same message; as shown in the sequel this simplifies the decoding analysis. In the fraction θ_{k,L_k} , user k retransmits $w_{k,1}$ via V_{k,L_k} and also sends a new message $w_{k,2} \in \{1, 2, \dots, 2^{nR_{k,2}}\}$ at rate $R_{k,2}$ via Q_k . Note that $w_{k,2}$ is only decoded by the destination. Finally, user $\pi_k(l)$, for all $l = 2, 3, \dots, L_k$, decodes $w_{k,1}$ in the fraction $\theta_{k,l}$ and retransmits it starting from $\theta_{k,l}$ such that its transmitted signal $X_{\pi_k(l)}(\theta_{k,j})$ in the fraction $\theta_{k,j}$ is

$$X_{\pi_k(l)}(\theta_{k,j}) = \sqrt{\frac{\bar{P}_{\pi_k(l)}}{\bar{\theta}_{k,l}}} V_{k,j} \quad \text{for } j = l, l+1, \dots, L_k \quad (\text{C.18})$$

where \bar{P}_k for all $k \in \mathcal{K}$ is given by (4.31) and $\bar{\theta}_{k,l}$ is the total transmission fraction of user $\pi_k(l)$ given as

$$\bar{\theta}_{k,l} = \sum_{j=l}^{L_k} \theta_{k,j} = 1 - \sum_{j=1}^{l-1} \theta_{k,j}. \quad (\text{C.19})$$

Fig. C.2 illustrates the multi-hop encoding scheme.

Decoding:

1. *At the nodes in \mathcal{C}_k :* The node $\pi_k(l)$ decodes $w_{k,1}$ upto the fraction $\theta_{k,l-1}$ by using $\underline{y}_{\pi_k(l)}$. More precisely, node $\pi_k(l)$ decodes by finding a $\tilde{w}_{k,1}$ such that the following $(l-1)$ events occurs:

$$\begin{aligned} \mathcal{E}_j : & (\underline{x}_{\pi_k(1)}(\tilde{w}_{k,1}), \underline{x}_{\pi_k(2)}(\tilde{w}_{k,1}), \dots, \underline{x}_{\pi_k(j)}(\tilde{w}_{k,1}), \underline{y}_d) \in \\ & A_e^{(n\theta_{k,j})}(X_{\pi_k(1)}, X_{\pi_k(2)}, \dots, X_{\pi_k(l-1)}, Y_d). \end{aligned} \quad j = 1, 2, \dots, \pi_k(l-1)$$

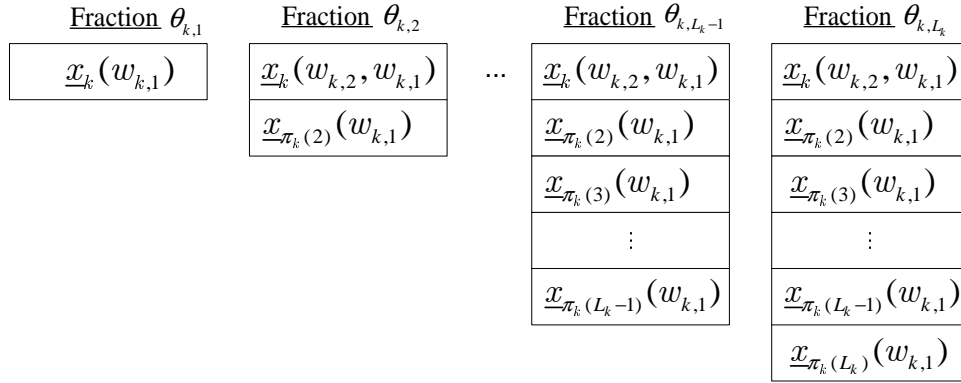


Figure C.2: PDF encoding for a L_k -hop cooperative network.

Note that the source codebooks in different fractions are generated independently so the above $l - 1$ events are independent (see [8, 35]). We upper bound the probability of this error event using [30, 14.3, p. 393] and the union bound as

$$\sum_{\tilde{w}_{k,1} \neq w_{k,1}} \Pr \left(\bigcap_{j=1}^{l-1} \mathcal{E}_j \right) \quad (\text{C.20})$$

$$= \sum_{\tilde{w}_{k,1} \neq w_{k,1}} \prod_{j=1}^{l-1} \Pr(\mathcal{E}_j) \quad (\text{C.21})$$

$$\leq 2^{n(R_{k,1} - \sum_{j=1}^{l-1} \theta_{k,l}(I(X_{\pi_k(1:j)}; Y_d) + 3\epsilon))} \quad (\text{C.22})$$

For the signaling in (C.17), reliable decoding then requires

$$R_{k,1} \leq \sum_{j=1}^{l-1} \theta_{k,j} \log \left(1 + \left| \sum_{m=1}^j h_{\pi_k(l), \pi_k(m)} \frac{\overline{P}_{\pi_k(m)}}{\theta_{k,m}} \right|^2 \right) \quad l = 2, 3, \dots, L_k. \quad (\text{C.23})$$

2. *At the destination:* The destination uses its received signals from all fractions to jointly decode $(w_{k,1}, w_{k,2})$. Focussing on the typical error events, we see that the destination makes an error only if it identifies a $(\tilde{w}_{k,1}, \tilde{w}_{k,2}) \neq (w_{k,1}, w_{k,2})$ using joint typical decoding. More precisely, the destination decodes by finding

a $(\tilde{w}_{k,1}, \tilde{w}_{k,2})$ such that the following L_k events occur:

$$\mathcal{E}_1 : (\underline{x}_k(\tilde{w}_{k,1}), \underline{y}_d) \in A_\epsilon^{(n\theta_{k,1})}(X_k, Y_d) \quad (\text{C.24})$$

$$\begin{aligned} \mathcal{E}_j : & (\underline{x}_k(\tilde{w}_{k,1}), \underline{x}_{\pi_k(2)}(\tilde{w}_{k,1}), \dots, \underline{x}_{\pi_k(j)}(\tilde{w}_{k,1}), \underline{y}_d) \\ & \in A_\epsilon^{(n\theta_{k,j})}(X_k, X_{\pi_k(2)}, X_{\pi_k(3)}, \dots, X_{\pi_k(j)}, Y_d). \quad j = 2, \dots, L_k - 1 \end{aligned} \quad (\text{C.25})$$

$$\begin{aligned} \mathcal{E}_{L_k} : & (\underline{x}_1(\tilde{w}_{k,1}, \tilde{w}_{k,2}), \underline{x}_{\pi_k(2)}(\tilde{w}_{k,1}), \dots, \underline{x}_{\pi_k(L_k)}(\tilde{w}_{k,1}), \underline{y}_d) \\ & \in A_\epsilon^{(n\theta_{k,L_k})}(X_k, X_{\pi_k(2)}, X_{\pi_k(3)}, \dots, X_{\pi_k(L_k)}, Y_d). \end{aligned} \quad (\text{C.26})$$

As before, due to the independence of the codebooks in the different fractions the above L_k events are independent. The decoding analysis of $(w_{k,1}, w_{k,2})$ can be further broken down into three disjoint error events. The first event has a $\tilde{w}_{k,1} \neq w_{k,1}$ and $\tilde{w}_{k,2} = w_{k,2}$ satisfying (C.24)-(C.26). We upper bound the probability of this error event using [30, 14.3, p. 393] and the union bound as

$$\sum_{\tilde{w}_{k,1} \neq w_{k,1}} \Pr \left(\bigcap_{j=1}^{L_k} \mathcal{E}_j \right) \quad (\text{C.27})$$

$$= \sum_{\tilde{w}_{k,1} \neq w_{k,1}} \prod_{j=1}^{L_k-1} \Pr(\mathcal{E}_j) \quad (\text{C.28})$$

$$\leq 2^{n(R_{k,1} - \sum_{j=1}^{L_k} \theta_{k,l} I(X_{\pi_k(1:j)}; Y_d) + 3\epsilon)} \quad (\text{C.29})$$

For the signaling in (C.17), reliable decoding then requires

$$R_{k,1} \leq \sum_{j=1}^{L_k} \theta_{k,j} \log \left(1 + \left| \sum_{m=1}^j h_{d,\pi_k(m)} \sqrt{\frac{\bar{P}_{\pi_k(m)}}{\bar{\theta}_{k,m}}} \right|^2 \right) \quad (\text{C.30})$$

The second error event has a $\tilde{w}_{k,1} = w_{k,1}$ and a $\tilde{w}_{k,2} \neq w_{k,2}$ satisfying (C.24)-(C.26). We again use [30, 14.3, p. 393] to bound the probability of this event by

$$2^{n(R_{k,2} - \theta_{k,L_k} I(X_k; Y_d | X_{C_k}) + 6\epsilon \theta_{k,L_k})}. \quad (\text{C.31})$$

Reliable decoding thus requires

$$R_{k,2} < \theta_{k,L_k} \log \left(1 + \alpha_k |h_{d,k}|^2 \bar{P}_k \right). \quad (\text{C.32})$$

Finally, consider the case $\tilde{w}_{k,1} \neq w_{k,1}$ and $\tilde{w}_{k,2} \neq w_{k,2}$. The expression (C.27) with the summation now over both $\tilde{w}_{k,1} \neq w_{k,1}$ and $\tilde{w}_{k,2} \neq w_{k,2}$ is upper bounded as

$$2^{n(R_{k,1}+R_{k,2})} \cdot 2^{-n(\sum_{j=1}^{L_k} \theta_{k,l}(I(X_{\pi_k(1:j)}; Y_d) - 3\epsilon))} \quad (\text{C.33})$$

For reliable decoding, we thus require

$$R_1 < \sum_{l=1}^{L_k-1} \theta_{k,l} \log \left(1 + \left| \sum_{m=1}^l h_{d,\pi_k(m)} \sqrt{\frac{\bar{P}_k}{\bar{\theta}_{k,l}}} \right|^2 \right) + \bar{\theta}_{k,L_k} \log \left(1 + \alpha_k |h_{d,k}|^2 \bar{P}_k + \left| \bar{\alpha}_k h_{d,k} \sqrt{\bar{P}_k} + \sum_{m=2}^{L_k} h_{d,\pi_k(m)} \sqrt{\frac{\bar{P}_l}{\bar{\theta}_k}} \right|^2 \right). \quad (\text{C.34})$$

Combining (C.30), (C.32), and (C.34), we obtain the bounds (4.46), (4.47), and (4.48).

C.2 Hypoexponential Distribution

Consider a collection of independent identically distributed unit mean exponential random variables E_l , $l \in \mathcal{L} = \{1, 2, \dots, L\}$. We denote a weighted sum of E_l , for all l , as

$$H = \sum_{l=1}^L E_l c_l. \quad (\text{C.35})$$

We assume that the coefficients c_l are unique, i.e., no two coefficients are equal to each other. The following lemma summarizes the probability distribution of H [73, p. 11].

Lemma C.2 *The random variable H has a hypoexponential distribution given as [73, p. 11]*

$$p_H(h) = \begin{cases} \sum_{l=1}^L \frac{c_l}{c_l} e^{-h/c_l} & h \geq 0 \\ 0 & o.w. \end{cases} \quad (\text{C.36})$$

where the constants C_l , for all l , are given as

$$C_l = \begin{cases} 1 & L = 1 \\ \frac{(-c_l)^{L-1}}{\prod_{j=1, j \neq l}^L (c_j - c_l)} & L > 1. \end{cases} \quad (\text{C.37})$$

The cumulative distribution function of H is bounded as

$$F_H(\eta) \leq \frac{\eta^L}{L! \left(\prod_{l=1}^L c_l \right)}. \quad (\text{C.38})$$

C.3 Half-Duplex Relay Channel – DDF Outage Analysis

The outage probability for user k transmitting at a fixed rate R_k is

$$P_o^{(k)} = \Pr(I_2^{DF} < R_k) \quad (\text{C.39})$$

where

$$I_2^{DF} = \theta_k \log(1 + |h_{d,k}|^2 \bar{P}_k) + \bar{\theta}_k \log(1 + |h_{d,k}|^2 \bar{P}_k + |h_{d,r}|^2 P_r) \quad (\text{C.40})$$

where $\bar{P}_r = P_r / \bar{\theta}_k$ and

$$\theta_k = \min \left(1, \frac{R_k}{\log(1 + |h_{r,k}|^2 \bar{P}_k)} \right). \quad (\text{C.41})$$

Recall that $h_{k,j} = a_{k,j} / d_{k,j}^{\gamma/2}$ where $a_{k,j}$ is a circularly symmetric complex Gaussian random variable with zero-mean and unit variance, $d_{k,j}$ is the distance between nodes k and j , and γ is the path-loss exponent. Thus, $|h_{k,j}|^2$ is exponentially distributed as

$$p(|h_{k,j}|^2 = x) = d_{k,j}^{\gamma} e^{-x/d_{k,j}^{\gamma}}. \quad (\text{C.42})$$

Substituting (C.42) in (C.41), we see that $\theta_k = 0$ for $d_{r,k} = 0$, i.e., when user k and the relay are co-located. Observe that for this case, (C.39) simplifies to the outage bounds of a 2×1 MIMO channel.

In general, however, θ_k is a random variable and its probability distribution $p(\theta_k)$ can be computed using (C.42) for any $d_{r,k} > 0$. From (C.41) we see that θ_k is a mixed distribution with a discrete component at $\theta_k = 1$. Using (C.42), we write the probability distribution of θ_k as

$$p(\theta_k) = \begin{cases} f_r(\theta_k, R_k) \cdot g_r(\theta_k, R_k) & 0 \leq \theta_k < 1 \\ 1 - \exp\left(\frac{-(2^R - 1)d_{r,k}^{\gamma}}{\bar{P}_k}\right) & \theta_k = 1 \end{cases} \quad (\text{C.43})$$

where

$$f_r(\theta_k, R_k) = \exp\left(\frac{-2^{R_k/\theta_k} d_{r,k}^\gamma}{\bar{P}_k}\right) \cdot R_k \ln 2 \quad (\text{C.44})$$

$$g_r(\theta_k, R_k) = \exp\left(\frac{R_k \ln 2}{\theta_k}\right) \cdot \frac{d_{r,k}^\gamma}{\theta_k^2 \bar{P}_k}. \quad (\text{C.45})$$

Observe that for finite SNR $p(\theta_k = 1)$ is non-zero for all $d_{r,k} > 0$. Further $p(\theta_k = 1)$ decreases with \bar{P}_k as

$$p(\theta_k = 1) = \left(1 - \exp\left(\frac{-(2^{R_k} - 1)d_{r,k}^\gamma}{\bar{P}_k}\right)\right) \leq \frac{(2^{R_k} - 1)d_{r,k}^\gamma}{\bar{P}_k}. \quad (\text{C.46})$$

We assume a unit variance white Gaussian noise, we henceforth refer to \bar{P}_k as the transmit signal-to-noise ratio (SNR). Observe that for a fixed \bar{P}_k , the functions f_r and g_r are monotonically increasing and decreasing functions of θ_k . At $\theta_k = 0$, the doubly exponential function f_r dominates the product resulting in $p(\theta_k = 0) = 0$. Further, as θ_k increases from 0, $p(\theta_k)$ first increases due to f_r and then decreases as f_r approaches a constant while g_r continues to decrease. Note that the θ_k^* that maximizes $p(\theta_k)$ depend on both $d_{r,k}$ and \bar{P}_k for a fixed R_k . Finally, for a fixed $d_{r,k}$, θ_k^* decreases with increasing transmit SNR \bar{P}_k . This is because the function f_r increases at least as fast as $1/(1 - 2^{R_k/\theta_k} d_{r,k}^\gamma/\bar{P}_k)$ while the function g_r only decreases at a rate proportional to $1/\bar{P}_k$ for any θ_k . This causes both θ_k^* and the width of the peak about θ_k^* to decrease with \bar{P}_k . This is demonstrated in Fig.C.3 for a collinear geometry with $d_{r,k} = .5$ and $d_{d,1} = 1$. We will exploit this behavior to obtain an approximation. Finally, we remark that the maximum $\theta_k^* < 1$ can be obtained analytically by differentiating (C.43) and satisfies

$$\frac{2^{R/\theta_k^*} R_k d_{r,k}^\gamma \ln 2}{\bar{P}_k} - R_k \ln 2 - 2 \frac{(\theta_k^*)^3 \bar{P}_k}{d_{r,k}^\gamma} = 0 \quad (\text{C.47})$$

Further, for finite R_k that does not scale with the SNR \bar{P}_k , in the high SNR regime, θ_k^* approximately satisfies

$$(\theta_k^*)^{-3} 2^{R_k/\theta_k^*} R_k \ln 2 \simeq 2 \bar{P}_k^2 / d_{r,k}^{2\gamma} \quad (\text{C.48})$$

Observe from (C.48) that the term $(\theta_k^*)^{-3} 2^{R_k/\theta_k^*}$ exponentially increases with decreasing θ_k while the term on the right hand side of the equality only increases quadratically

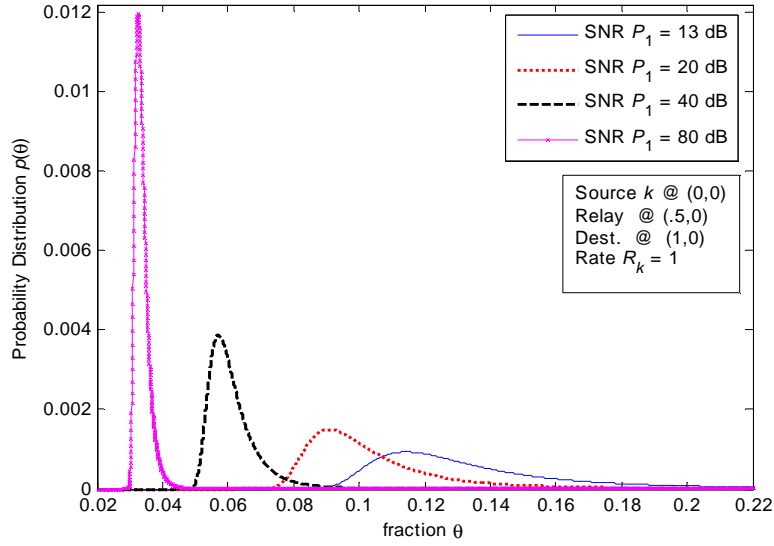


Figure C.3: Plot of the probability distribution $p(\theta_k)$ for a collinear geometry with $d_{r,k} = .5$ and different values of \bar{P}_k .

with increasing \bar{P}_k for a fixed $d_{r,k}$. Thus, with increasing SNR, note that the peak center θ_k^* decreases only polynomially, i.e., θ_k^* converges to 0 only as \bar{P}_k^{-2} .

C.3.1 Upper and Lower Bounds

Since $\theta_k \in [0, 1]$, we can lower bound $P_o^{(k)}$ as

$$P_o^{(k)} \geq \Pr \left\{ \log \left(1 + \frac{|A_{d,k}|^2 \bar{P}_k}{d_{d,k}^\gamma} + \frac{|A_{d,r}|^2 P_r}{d_{d,r}^\gamma} \right) < R_k \right\} = P_{o,2 \times 1} \quad (\text{C.49})$$

where $P_{o,2 \times 1}$ is the outage probability of a 2×1 MIMO channel. On the other hand, for any θ_k , $P_o^{(k)}(\theta_k)$ can be upper bounded as

$$P_o^{(k)}(\theta_k) \leq \Pr \left\{ \theta_k \log \left(1 + \frac{|A_{d,k}|^2 \bar{P}_k}{d_{d,k}^\gamma} \right) < R_k \right\} = P_{o,1}(f) \quad (\text{C.50})$$

$$P_o^{(k)}(\theta_k) \leq \Pr \left\{ \bar{\theta}_k \log \left(1 + \frac{|A_{d,k}|^2 \bar{P}_k}{d_{d,k}^\gamma} + \frac{|A_{d,r}|^2 \bar{P}_r}{d_{d,r}^\gamma} \right) < R_k \right\} = P_{o,2}(f) \quad (\text{C.51})$$

Thus, averaging over all θ_k , we have

$$P_o^{(k)} = \mathbb{E} P_o^{(k)}(\theta_k) \leq \mathbb{E} \min(P_{o,1}(\theta_k), P_{o,2}(\theta_k)) = P_{UB}^{(k)} \quad (\text{C.52})$$

Without any loss of generality, we assume that $\bar{P}_k / d_{d,k}^\gamma \neq \bar{P}_r / d_{d,r}^\gamma$ for all k and θ_k . As a result, the weighted sum of the i.i.d. complex Gaussian $A_{d,t}$, $t \in \mathcal{K}$, simplifies to a *hypoexponential* distribution, i.e., a distribution characterized by a weighted sum of exponential distributions. Then, from Lemma C.2, we have

$$P_{o,1}(\theta_k) \leq \frac{(2^{R_k/\theta_k} - 1)d_{d,k}^\gamma}{\bar{P}_k} \quad (\text{C.53})$$

$$P_{o,2}(\theta_k) \leq \frac{(2^{R_k/\bar{\theta}_k} - 1)^2 d_{d,k}^\gamma d_{d,r}^\gamma}{2\bar{P}_k \bar{P}_r} \quad (\text{C.54})$$

and thus the upper bound, $P_{UB}^{(k)}$, in (C.52) simplifies as

$$P_{UB}^{(k)} = \mathbb{E} \min \left(\frac{(2^{R_k/\theta_k} - 1)d_{d,k}^\gamma}{\bar{P}_k}, \frac{(2^{R_k/\bar{\theta}_k} - 1)^2 d_{d,k}^\gamma d_{d,r}^\gamma}{2\bar{P}_k \bar{P}_r} \right) \quad (\text{C.55})$$

From (C.55), we see that for a fixed \bar{P}_k , P_r , and $d_{j,k}$ for all j, k , $P_{o,2}(\theta_k)$ dominates for small θ_k while $P_{o,1}(\theta_k)$ dominates as θ_k approaches 1. Further, observe that $P_{o,2 \times 1} = P_{o,2}(\theta_k = 0)$ and thus (C.54) also provides an upper bound for $P_{o,2 \times 1}$.

In general, the expression in (C.55) is not easy to evaluate analytically. We exploit the functional form of $p(\theta_k)$ to develop an approximation for P_{UB} for the case where R_k does not scale with SNR, i.e., the multiplexing gain is 0. Our approximation results from simplifying $p(\theta_k)$ as discrete distribution with two elements $\theta_k = \theta_k^*$ and $\theta_k = 1$. We justify this simplification from the observations made earlier on the distribution $p(\theta_k)$. Thus, we write

$$P_{UB} \sim \frac{(2^{R_k/\bar{\theta}_k^*} - 1)^2 d_{d,k}^\gamma d_{d,r}^\gamma}{2\bar{P}_k P_r^*} \cdot (1 - p(\theta_k = 1)) + \frac{(2^{R_k} - 1)^2 d_{d,k}^\gamma d_{d,r}^\gamma}{\bar{P}_k^2} \quad (\text{C.56})$$

$$\leq \frac{K(2^R - 1)^2 d_{d,k}^\gamma d_{d,r}^\gamma}{2\bar{P}_k^2} \simeq K P_{o,2 \times 1} \quad (\text{C.57})$$

where $\bar{\theta}_k^* = 1 - \theta_k^*$, $P_r^* = P_r / \bar{\theta}_k^*$, $p(\theta_k = 1)$ is given by (C.43), and

$$K = \left(\frac{(2^{R/(1-\theta_k^*)} - 1)^2 \bar{P}_k}{(2^R - 1)^2 P_r^*} + \frac{2d_{r,k}^\gamma}{d_{d,r}^\gamma} \right). \quad (\text{C.58})$$

C.4 Two-hop Cooperative Network – Outage Analysis under DDF

Recall that the DDF outage probability for the two-hop cooperative network is

$$P_o^{(k)} = \Pr(I_{2,DF}^c < R_k) \quad (\text{C.59})$$

where $I_{2,DF}^c$ is

$$I_{2,DF}^c(\theta_k) = \theta_k \log(1 + |h_{d,k}|^2 \bar{P}_k) + \bar{\theta}_k \log\left(1 + |h_{d,k}|^2 \bar{P}_k + \sum_{j \in \mathcal{C}_k} |h_{d,j}|^2 \frac{\bar{P}_j}{\bar{\theta}_k}\right) \quad (\text{C.60})$$

and θ_k is

$$\theta_k = \min\left(1, \max_{j \in \mathcal{C}_k} \left(\frac{R_k}{\log(1 + |h_{j,k}|^2 \bar{P}_k)}\right)\right). \quad (\text{C.61})$$

As in Appendix C.3, we first derive the probability distribution $p(\theta_k)$. Expanding $h_{j,k}$ as $a_{j,k}/d_{j,k}^{\gamma/2}$, we see that $\theta_k = 0$ only if $d_{j,k} = 0$ for all $j \in \mathcal{C}_k$. In general, however, the probability distribution of θ_k is given as

$$p(\theta_k) = \begin{cases} f_c(\theta_k, R_k) \cdot g_c(\theta_k, R_k) & 0 \leq \theta_k < 1 \\ 1 - \exp\left(\frac{-(2^R - 1)d_{r,k}^{\gamma}}{\bar{P}_k}\right) & \theta_k = 1 \end{cases} \quad (\text{C.62})$$

where

$$f_c(\theta_k, R_k) = \exp\left(\frac{-2^{R_k/\theta_k} \left(\sum_{j \in \mathcal{C}_k} d_{j,k}^{\gamma}\right)}{\bar{P}_k}\right) \cdot R_k \ln 2 \quad (\text{C.63})$$

$$g_c(\theta_k, R_k) = \exp\left(\frac{R_k \ln 2}{\theta_k}\right) \cdot \frac{\left(\sum_{j \in \mathcal{C}_k} d_{j,k}^{\gamma}\right)}{\theta_k^2 \bar{P}_k}. \quad (\text{C.64})$$

Comparing (C.44) and (C.45) with (C.63) and (C.64) respectively, we see that the two functions are the same when the distance $d_{r,k}$ in the half-duplex relay channel is replaced by the sum of the distances between user k and every user in \mathcal{C}_k . Thus, $p(\theta_k)$ exhibits the same functional form discussed in Appendix C.3.

C.4.1 Upper and Lower Bounds

For ease of exposition, we denote the $L_k - 1$ nodes in \mathcal{C}_k as j_2, j_3, \dots, j_L and write $\mathcal{S}_k = \mathcal{C}_k \cup \{k\}$ to denote the set of all transmitters transmitting in the fraction $\bar{\theta}_k$. From

(C.59) and (C.60), we can lower bound $P_o^{(k)}$ as

$$P_o^{(k)} \geq \Pr \left\{ \log \left(1 + \frac{|A_{d,k}|^2 \bar{P}_k}{d_{d,k}^\gamma} + \sum_{j \in \mathcal{C}_k} \frac{|A_{d,j}|^2 \bar{P}_j}{d_{d,j}^\gamma} \right) < R_k \right\} = P_{o, L_k \times 1}(R_k) \quad (\text{C.65})$$

where $P_{o, L_k \times 1}(R_k)$ is the outage probability of a $L_k \times 1$ distributed MIMO channel transmitting at a rate R_k . Note that the i^{th} transmit antenna, $i \in \mathcal{S}$, of this MIMO channel is at a distance $d_{d,i}$ from the destination. As in Appendix C.3, we assume that $\bar{P}_k / d_{d,k}^\gamma \neq \bar{P}_j / (d_{d,j}^\gamma \bar{\theta}_k)$ for all $k \in \mathcal{K}$, $j \in \mathcal{C}_k$, and θ_k which enables us to simplify the weighted sum of i.i.d exponential random variables in (C.65) as a hypoexponential distribution. For a fixed R_k , we upper bound $P_o^{(k)}$ as

$$P_o^{(k)} = \mathbb{E} P_o^{(k)}(\theta_k) \leq \mathbb{E} \min(P_{o,1}(\theta_k), P_{o,2}(\theta_k)) \quad (\text{C.66})$$

where, using Lemma C.2 we write

$$P_{o,1}(\theta_k) = \Pr \left(\log \left(1 + \frac{|A_{d,k}|^2 \bar{P}_k}{d_{d,k}^\gamma} \right) < \frac{R_k}{\theta_k} \right) \quad (\text{C.67})$$

$$\leq \frac{(2^{R_k/\theta_k} - 1) \left(\sum_{j \in \mathcal{C}_k} d_{d,j}^\gamma \right)}{\bar{P}_k} \quad (\text{C.68})$$

$$P_{o,2}(\theta_k) = \Pr \left(\log \left(1 + \frac{|A_{d,k}|^2 \bar{P}_k}{d_{d,k}^\gamma} + \sum_{j \in \mathcal{C}_k} \frac{|A_{d,j}|^2 \bar{P}_j}{d_{d,j}^\gamma \bar{\theta}_k} \right) < \frac{R_k}{\theta_k} \right) \quad (\text{C.69})$$

$$\leq \frac{(2^{R_k} - 1)^{L_k} (\theta_k)^{L_k-1}}{(L_k!)} \left(\prod_{j \in \mathcal{S}_k} \frac{d_{d,j}^\gamma}{\bar{P}_j} \right) \quad (\text{C.70})$$

$$= \frac{(2^{R_k} - 1)^{L_k} (\theta_k)^{L_k-1}}{(L_k!) (\bar{P}_k)^{L_k}} \left(\prod_{j \in \mathcal{S}_k} \frac{d_{d,j}^\gamma}{\lambda_j} \right) \quad (\text{C.71})$$

with $\lambda_j = \bar{P}_j / \bar{P}_k$ for all j .

Substituting (C.68) and (C.71) in (C.66), we thus write

$$P_o^{(k)} \leq P_{UB} = \mathbb{E} \min \left(\frac{(2^{R_k/\theta_k} - 1) d_{d,k}^\gamma}{\bar{P}_k}, \frac{(2^{R_k} - 1)^{L_k} (\theta_k)^{L_k-1}}{(L_k!) (\bar{P}_k)^{L_k}} \prod_{j \in \mathcal{S}_k} \frac{d_{d,j}^\gamma}{\lambda_j} \right) \quad (\text{C.72})$$

As in the outage analysis for the half-duplex relay channel, it is not easy to compute P_{UB} analytically. However, since the functional form of $p(\theta_k)$ is the same that for the

half-duplex relay channel detailed in Appendix C.3, we similarly approximate $p(\theta_k)$ by a discrete distribution with two elements, $\theta_k = \theta_k^*$ and $\theta_k = 1$ where

$$\theta_k^* = \arg \max_{\theta_k} p(\theta_k). \quad (\text{C.73})$$

We thus have

$$P_{UB} \leq \frac{\left(2^{R_k/\bar{\theta}_k^*} - 1\right)^{L_k} (\theta_k)^{L_k-1}}{(L_k!) (\bar{P}_k)^{L_k}} \prod_{j \in S_k} \frac{d_{d,j}^\gamma}{\lambda_j} + \frac{(2^{R_k} - 1)^2 d_{d,k}^\gamma \left(\sum_{j \in C_k} d_{j,k}^\gamma\right)}{\bar{P}_k^2}. \quad (\text{C.74})$$

C.5 Multi-hop Cooperative Network – Outage Analysis under DDF

Recall that the DDF outage probability for the multi-hop cooperative network is

$$P_o^{(k)} = \Pr(I_{2,DF}^c < R_k) \quad (\text{C.75})$$

where $I_{2,DF}^c$ is

$$I_{2,DF}^c(\theta_k) = \theta_{k,1} \log(1 + |h_{d,k}|^2 \bar{P}_k) + \sum_{l=2}^{L_k} \theta_{k,l} \log\left(1 + \sum_{j=1}^l |h_{d,\pi_k(j)}|^2 \frac{\bar{P}_{\pi_k(j)}}{\bar{\theta}_{k,j}}\right). \quad (\text{C.76})$$

Recall that we write $\pi_k(\cdot)$ to denote a permutation on \mathcal{C}_k such that user $\pi_k(l)$ begins its transmissions in the fraction $\theta_{k,l}$, for all $l = 2, 3, \dots, L_k$. Recall further that $\pi_k(1) = k$ and $\pi_k(i:j) = \{\pi_k(i), \pi_k(i+1), \dots, \pi_k(j)\}$. We choose the fraction $\theta_{k,l}$ small enough to ensure that at least one node, denoted as $\pi_k(l+1)$, decodes the message from user k . Thus the fraction $\theta_{k,l}$, for $l = 1, 2, \dots, L_k - 1$, is given as

$$\theta_{k,l} = \begin{cases} \min_{j \in \mathcal{C}_k} \min \left\{ 1, \left\lceil \frac{R_k}{\log(1 + |h_{m,j}|^2 \bar{P}_k)} \right\rceil \right\} & l = 1 \\ \min_{j \in \mathcal{C}'_k(l)} \min \left\{ 1, \left\lceil \frac{R_k - \sum_{m=1}^{l-1} \theta_{k,m} \log(1 + \sum_{i=1}^m |h_{j,\pi_k(i)}|^2 \bar{P}_{\pi_k(i)} / \bar{\theta}_{k,i})}{\log(1 + \sum_{i=1}^l |h_{j,\pi_k(i)}|^2 \bar{P}_{\pi_k(i)} / \bar{\theta}_{k,i})} \right\rceil \right\} & 2 \leq l \leq \bar{L}_k \end{cases} \quad (\text{C.77})$$

where $\bar{L}_k = L_k - 1$, $\bar{\theta}_{k,l}$ is defined in (4.44) and

$$\mathcal{C}'_k(l) = \mathcal{C}_k \setminus \{\pi_k(i)\}_{i=2}^l. \quad (\text{C.78})$$

Finally, we have

$$\theta_{k,L_k} = 1 - \sum_{l=1}^{L_k-1} \theta_{k,l}. \quad (\text{C.79})$$

In general, computing the probability distribution of $p(\theta_{k,l})$ is not straightforward. However, we present simple upper and lower bounds on $P_o^{(k)}$ that require computing $p(\theta_{k,l})$ for specific values of $\theta_{k,l}$. To this end, we make the following observations on the distribution of $\theta_{k,l}$. Consider $\theta_{k,1}$. From (C.77), we have

$$\theta_{k,1} = \min_{j \in \mathcal{C}_k} \min \left\{ 1, \left\lceil \frac{R_k}{\log(1 + |h_{j,k}|^2 \bar{P}_k)} \right\rceil \right\} \quad (\text{C.80})$$

Without evaluating the probability distribution of $\theta_{k,1}$, comparing (C.61) and (C.77), we can see that $\theta_{k,1}$ is at most as large of θ_k for the two-hop case and thus one can expect the $\theta_{k,1}^*$ at which its distribution peaks is smaller than that for the two-hop cooperative network. Further, one can compute $p(\theta_{k,1} = 1)$ as

$$p(\theta_{k,1}) |_{\theta_{k,1}=1} = \Pr \left(\min_{j \in \mathcal{C}_k} \{ R_k / \log(1 + |h_{j,k}|^2 \bar{P}_k) \} \geq 1 \right) \quad (\text{C.81})$$

$$= \prod_{j \in \mathcal{C}_k} \left\{ 1 - \exp \left(\frac{-(2^{R_k} - 1) d_{j,k}^\gamma}{\bar{P}_k} \right) \right\} \quad (\text{C.82})$$

$$\leq \left(\frac{(2^{R_k} - 1)^{L_k-1} \left(\prod_{j \in \mathcal{C}_k} d_{j,k}^\gamma \right)}{\bar{P}_k^{L_k-1}} \right). \quad (\text{C.83})$$

One can similarly argue that, for all $l > 1$, the fraction $\theta_{k,l}$ is at most as large as the two-hop fraction θ_k . This is because the node $\pi_k(l+1)$ reliably decodes in the fraction $\theta_{k,l}$ after it has collected sufficient energy from the transmissions of user k and the users $\pi_k(m)$, for all $1 \leq m \leq l-1$. Further, one can bound $\theta_{k,l}$ as

$$\theta_{k,l} \leq \left\{ \min_{j \in \mathcal{C}'_k(l)} \min \left\{ 1, \left\lceil \frac{R_k}{\log(1 + \sum_{m=1}^l |h_{j,\pi_k(m)}|^2 \bar{P}_{\pi_k(m)}/\bar{\theta}_{k,m})} \right\rceil \right\} \right\} \quad l > 1 \quad (\text{C.84})$$

$$p(\theta_{k,l})|_{\theta_{k,l}=1} \leq \Pr \left(\min_{j \in \mathcal{C}'_k(l)} \left\{ \frac{R_k}{\log \left(1 + \sum_{m=1}^l |h_{j,\pi_k(m)}|^2 \bar{P}_{\pi_k(m)} / \bar{\theta}_{k,m} \right)} \right\} \geq 1 \right) \quad (\text{C.85})$$

$$\leq (2^{R_k} - 1)^{(L_k-1)} \left(\prod_{j \in \mathcal{C}'_k(l)} \prod_{m=1}^l \frac{d_{j,\pi_k(m)}^\gamma \bar{\theta}_{k,m}}{\bar{P}_{\pi_k(m)}} \right) \quad (\text{C.86})$$

$$= \frac{(2^{R_k} - 1)^{(L_k-l) \cdot l}}{\bar{P}_k^{(L_k-l) \cdot l}} \left(\prod_{j \in \mathcal{C}'_k(l)} \prod_{m=1}^l \frac{d_{j,\pi_k(m)}^\gamma \bar{\theta}_{k,m}}{\lambda_{\pi_k(m)}} \right) \quad (\text{C.87})$$

where (C.86) results from applying lemma (C.2) and the fact that the minimum in (C.85) is taken over random variables that for all j are independent. Note that as l increases, $|\mathcal{C}'_k(l)|$, the cardinality of $\mathcal{C}'_k(l)$, decreases and thus the product $l \cdot |\mathcal{C}'_k(l)|$ increases from $L_k - 1$ to a maximum of $L_k^2/4$ ($(L_k^2 - 1)/4$) for even (odd) L_k and then decreases to $L_k - 1$. Thus, the smallest power of \bar{P}_k is $L_k - 1$. We will use this property in developing an upper bound for $P_o^{(k)}$.

C.5.1 Upper and Lower Bounds

From (C.75) and (C.76), we lower bound $P_o^{(k)}$ as

$$P_o^{(k)} \geq \Pr \left\{ \log \left(1 + \sum_{j=1}^{L_k} \frac{|a_{d,\pi_k(j)}|^2 \bar{P}_{\pi_k(j)}}{d_{d,k}^\gamma} \right) < R_k \right\} = P_{o,L_k \times 1}(R_k) \quad (\text{C.88})$$

where, as before, $P_{o,L_k \times 1}(R_k)$ is the outage probability of a $L_k \times 1$ distributed MIMO channel transmitting at a rate R_k . Further, as before, we assume that $\bar{P}_k / d_{d,k}^\gamma \neq \bar{P}_{\pi_k(l)} / (d_{d,j}^\gamma \bar{\theta}_{k,l})$ for all $\theta_{k,l} \in [0, 1]$, $k \in \mathcal{K}$, and $j \in \mathcal{C}_k$. Then, using lemma C.2, we can write the weighted sum of i.i.d exponential random variables in (C.88) as a hypoexponential distribution. For a fixed R_k , we upper bound $P_o^{(k)}$ as

$$P_o^{(k)} = \mathbb{E} P_o^{(k)}(\underline{\theta}_k) \leq \mathbb{E} \min(P_{o,1}(\underline{\theta}_k), P_{o,2}(\underline{\theta}_k), \dots, P_{o,L_k}(\underline{\theta}_k)) = \mathbb{E} \min_{l \in \mathcal{K}}(P_{o,l}(\underline{\theta}_k)) \quad (\text{C.89})$$

where, for all $l = 1, 2, \dots, L_k$, we have

$$P_{o,l}(\underline{\theta}_k) = \Pr \left(\log \left(1 + \sum_{j=1}^l |h_{d,\pi_k(j)}|^2 \bar{P}_{\pi_k(j)} / \bar{\theta}_{k,j} \right) < \frac{R_k}{\theta_{k,l}} \right) \quad (\text{C.90})$$

$$\leq \frac{(2^{R_k/\theta_{k,l}} - 1)^l}{(l!) (\bar{P}_k)^l} \left(\prod_{j=1}^l \frac{d_{d,\pi_k(j)}^\gamma \bar{\theta}_{k,j}}{\lambda_{\pi_k(j)}} \right). \quad (\text{C.91})$$

Note that the bound in (C.91) follows from applying lemma C.2 with $\lambda_{\pi_k(j)} = \bar{P}_{\pi_k(j)} / \bar{P}_k$ for all $\pi_k(j) \in \mathcal{C}_k$.

As with the previous outage analyses, here too we approximate the bounds by simplifying $p(\theta_{k,l})$ for all $l = 1, 2, \dots, L_k - 1$ as a discrete distribution taking values $\theta_{k,l}^*$ and 1 where $\theta_{k,l}^* = \arg \max_{\theta_{k,l}} p(\theta_{k,l})$. Further, for the case where $\theta_{k,l}^*$ is small for all l , we see that the exponential terms in (C.91) compare as

$$2^{R_k/\theta_{k,L_k}^*} < 2^{R_k/\theta_{k,l}^*} \quad \text{for all } 1 \leq l \leq L_k - 1 \quad (\text{C.92})$$

where

$$\theta_{k,L_k}^* = 1 - \sum_{l=1}^{L_k-1} \theta_{k,l}^*. \quad (\text{C.93})$$

Thus, we have

$$P_{UB} \leq P_{o,L_k}(\underline{\theta}_k^*) + \sum_{l=1}^{L_k-1} P_{o,l}(\underline{1}) \cdot p(\theta_{k,l} = 1) \quad (\text{C.94})$$

$$= P_{o,L_k}(\underline{\theta}_k^*) + P_{o,1}(\theta_{k,1} = 1) \cdot p(\theta_{k,l} = 1) \quad (\text{C.95})$$

$$= \frac{(2^{R_k/\bar{\theta}_{k,L_k}^*} - 1)^{L_k}}{(L_k!) (\bar{P}_k)^{L_k}} \prod_{j=\pi_k(1)}^{\pi_k(L_k)} \frac{d_{d,j}^\gamma \bar{\theta}_{k,j}^*}{\lambda_j} + \frac{(2^{R_k} - 1)^{L_k} \left(\prod_{j \in \mathcal{C}_k} d_{j,k}^\gamma \right) d_{d,k}^\gamma}{\bar{P}_k^{L_k}}. \quad (\text{C.96})$$

where in (C.95) we used (C.87) and (C.91) to restrict attention to terms where the exponent of \bar{P}_k is less than or equal to L_k and define

$$\bar{\theta}_{k,j}^* = \sum_{l=j}^{L_k} \theta_{k,l}^*. \quad (\text{C.97})$$

Thus, we see that for a cooperative multi-hop network, DDF achieves the maximum diversity of L_k irrespective of the network geometry.

Appendix D

Degraded Gaussian MARC : Concavity Properties

D.1 Concavity of $I_{d,\mathcal{S}}$

We recall the DF bounds in (5.17), for all $\mathcal{S} \subseteq \mathcal{K}$, as

$$R_{\mathcal{S}} \leq I_{d,\mathcal{S}} = C \left(\frac{\sum_{k \in \mathcal{S}} P_k}{N_d} + \frac{\left(1 - \sum_{k \in \mathcal{S}^c} \beta_k\right) P_r}{N_d} + 2 \sum_{k \in \mathcal{S}} \sqrt{(1 - \alpha_k) \beta_k \frac{P_k}{N_d} \frac{P_r}{N_d}} \right). \quad (\text{D.1})$$

We show that $I_{d,\mathcal{S}}$ is a concave function of $\underline{\beta}_{\mathcal{S}}$ for a fixed $\underline{\beta}_{\mathcal{S}^c}$. Observe that since β_k are power fractions, we have

$$\sum_{k \in \mathcal{K}} \beta_k \leq 1. \quad (\text{D.2})$$

We fix the vector $\underline{\beta}_{\mathcal{S}^c}$ such that

$$\sum_{k \in \mathcal{S}^c} \beta_k = 1 - c \quad (\text{D.3})$$

$$\sum_{k \in \mathcal{S}} \beta_k \leq c. \quad (\text{D.4})$$

where $c \in [0, 1)$. To verify the concavity of $I_{d,\mathcal{S}}$ as a function of $\underline{\beta}_{\mathcal{S}}$, we assume that $\underline{\alpha}_{\mathcal{S}} \neq \underline{1}$. We simplify $I_{d,\mathcal{S}}$ in (D.1) subject to (D.3) as

$$I_{d,\mathcal{S}} = \frac{1}{2} \log \left(K_0 + 2 \sum_{k \in \mathcal{S}} K_k \sqrt{\beta_k} \right) \quad (\text{D.5})$$

where

$$K_0 = 1 + \frac{\sum_{k \in \mathcal{S}} P_k}{N_d} + \frac{P_r(1-c)}{N_d} \quad (\text{D.6})$$

$$K_k = \sqrt{(1 - \alpha_k) \frac{P_k}{N_d} \frac{P_r}{N_d}} \quad k \in \mathcal{S}.$$

We now show that $I_{d,\mathcal{S}}$ is a concave function of $\underline{\beta}_{\mathcal{S}}$ by determining its gradient with respect to β_k for all $k \in \mathcal{S}$. We write the gradient of $I_{d,\mathcal{S}}$ as the vector

$$\nabla I_{d,\mathcal{S}} = [\partial I_{d,\mathcal{S}} / \partial \beta_k]_{k \in \mathcal{S}} \quad (\text{D.7})$$

$$= \frac{1}{K_s} \begin{bmatrix} \frac{K_1}{\sqrt{\beta_1}} & \frac{K_2}{\sqrt{\beta_2}} & \cdots & \frac{K_{|\mathcal{S}|}}{\sqrt{\beta_{|\mathcal{S}|}}} \end{bmatrix}^T \quad (\text{D.8})$$

where K_0 and K_k are defined in (D.6) and

$$K_s = 2 \left(K_0 + 2 \sum_{k \in \mathcal{S}} K_k \sqrt{\beta_k} \right). \quad (\text{D.9})$$

We write the Hessian of $I_{d,\mathcal{S}}$ as the matrix

$$\nabla^2 I_{d,\mathcal{S}} = [\partial^2 I_{d,\mathcal{S}} / \partial \beta_k \partial \beta_m]_{k,m \in \mathcal{S}} \quad (\text{D.10})$$

$$= \frac{-1}{K_s} \text{diag}(\underline{v}) - \underline{z}\underline{z}^T \quad (\text{D.11})$$

where

$$\underline{z} = \frac{2}{K_s} \nabla I_{d,\mathcal{S}} \quad (\text{D.12})$$

$$\underline{v} = \begin{bmatrix} \frac{K_1}{2\beta_1^{3/2}} & \frac{K_2}{2\beta_2^{3/2}} & \cdots & \frac{K_{|\mathcal{S}|}}{2\beta_{|\mathcal{S}|}^{3/2}} \end{bmatrix}. \quad (\text{D.13})$$

To show that $I_{d,\mathcal{S}}$ is concave, we need to show that [74, 3.1.4]

$$\underline{x}^T \nabla^2 I_{d,\mathcal{S}} \underline{x} \leq 0 \quad \text{for all } \underline{x} \in \mathcal{R}^K. \quad (\text{D.14})$$

Substituting (D.11) in (D.14), we have

$$\underline{x}^T \nabla^2 I_{d,\mathcal{S}} \underline{x} = \frac{-1}{K_s} \sum_{k \in \mathcal{S}} \left(\frac{x_k^2 K_k}{2\beta_k^{3/2}} \right) - (\underline{x}^T \cdot \underline{z})^2 \quad (\text{D.15})$$

$$\leq 0 \quad (\text{D.16})$$

where the inequality (D.16) follows from the non-negativity of K_k and β_k for all k with equality if and only if $\underline{x} = \underline{0}$.

We now determine a $\underline{\beta}_{\mathcal{S}}$ that maximizes $I_{d,\mathcal{S}}$ subject to (D.3). Since $I_{d,\mathcal{S}}$ is a continuous concave function of $\underline{\beta}_{\mathcal{S}} \in [0, \infty)^{|\mathcal{S}|}$, it is also concave over the convex region in (D.4) and achieves its maximum at a $\underline{\beta}_{\mathcal{S}}^*$ where

$$\left. \frac{\partial I_{d,\mathcal{S}}}{\partial \beta_k} \right|_{\beta_k^*} = 0 \quad \text{for all } k \in \mathcal{S}. \quad (\text{D.17})$$

Using Lagrange multiplier rule, we find that a $\underline{\beta}_{\mathcal{S}}^*$ that maximizes $I_{d,\mathcal{S}}$ subject to (D.3) has entries

$$\beta_k^* = \begin{cases} \frac{c(1-\alpha_k)P_k}{\sum_{k \in \mathcal{S}} (1-\alpha_k)P_k} & k \in \mathcal{S} \end{cases} . \quad (\text{D.18})$$

Relaxing the constraint in (D.3) to (D.2), we write the first and second partial derivatives of $I_{d,\mathcal{S}}$ with respect to β_k , for all $k \in \mathcal{S}^c$, as

$$\frac{\partial I_{d,\mathcal{S}}}{\partial \beta_k} = \frac{-P_r/N_d}{K_s} < 0 \quad (\text{D.19})$$

$$\frac{\partial^2 I_{d,\mathcal{S}}}{\partial \alpha_k^2} = \frac{-2(P_r/N_d)^2}{K_s^2}. \quad (\text{D.20})$$

where K_s is defined in (D.9). Thus, from (D.19) we see that $I_{d,\mathcal{S}}$ decreases monotonically with β_k for all $k \in \mathcal{S}^c$. Further from (D.16) and (D.20) we conclude that $I_{d,\mathcal{S}}$ is a concave function of β_k for all $k \in \mathcal{K}$.

Finally, one can similarly show that for a fixed $\underline{\beta}_{\mathcal{K}}$, the first and second derivatives of with respect to α_k , for all $k \in \mathcal{K}$, are

$$\frac{\partial I_{d,\mathcal{S}}}{\partial \alpha_k} = \begin{cases} \frac{-G_k}{(1-\alpha_k)^{3/2}K_s} & k \in \mathcal{S} \\ 0 & k \notin \mathcal{S} \end{cases} \quad (\text{D.21})$$

$$\frac{\partial^2 I_{d,\mathcal{S}}}{\partial \alpha_k^2} = \begin{cases} \frac{-3G_k}{(1-\alpha_k)^{5/2}K_s} - \frac{2G_k^2}{(1-\alpha_k)^3K_s^2} < 0 & k \in \mathcal{S} \\ 0 & k \notin \mathcal{S} \end{cases} \quad (\text{D.22})$$

where K_0 and K_s are defined in (D.6) and (D.9) respectively and

$$G_k = \sqrt{\beta_k \frac{P_k}{N_d} \frac{P_r}{N_d}}. \quad (\text{D.23})$$

Thus, we see that $I_{d,\mathcal{S}}$, for all $\mathcal{S} \subseteq \mathcal{K}$, is a concave function of α_k for all $k \in \mathcal{K}$.

Rate Region for a fixed $\underline{\alpha}_{\mathcal{K}}$: For any choice of a non-zero $\underline{\alpha}_{\mathcal{K}}$ and a $\underline{\beta}_{\mathcal{K}}$ subject to (D.2), the rate region satisfying (D.1) for all \mathcal{S} is a polytope. For the case where $\underline{\alpha}_{\mathcal{K}} = \underline{1}$ since there are no gains achieved from coherent combining in (D.1), we set $\underline{\beta}_{\mathcal{K}} = \underline{0}$ and obtain a polytope.

We next consider the case where where $\underline{\alpha}_{\mathcal{K}} \neq \underline{1}$. Since there is at least one k for which $\alpha_k < 1$, gains from coherent combining at the destination are maximized

by choosing $\underline{\beta}_{\mathcal{K}}$ to satisfy (D.2) with equality. For a fixed of $\underline{\alpha}_{\mathcal{K}}$, we then write the rate region at the destination as a union over all polytopes, one for each choice of $\underline{\beta}_{\mathcal{K}}$ satisfying

$$\sum_{k=1}^K \beta_k = 1. \quad (\text{D.24})$$

Observe that for $\underline{\beta}_{\mathcal{K}}^*$ with entries given by (D.18), the bound $I_{d,\mathcal{S}}$ is maximized. In Fig D.1, we illustrate the rate region for a two-user degraded Gaussian MARC with the SNR $P_1/N_d = P_2/N_d$ chosen as -10 dB, $\underline{\alpha} = (.5, .5)$, and five choices of $\underline{\beta}_{\mathcal{K}}$. Observe that the maximum single-user rate R_1 is achieved by setting β_1 to 1 though this value does not maximize R_2 or $R_1 + R_2$. For all other (β_1, β_2) such as $(.85, .15)$, as β_1 decreases and β_2 increases, R_1 decreases while R_2 increases achieving its maximum at $\beta_2 = 1$. The bound on the sum rate $R_1 + R_2$ increases from $(\beta_1, \beta_2) = (1, 0)$, achieves its maximum at $(\beta_1^*, \beta_2^*) = (.5, .5)$, and then decreases as β_2 approaches 1. The resulting region at the destination is then a union over all polytopes, each resulting from a unique choice of $\underline{\beta}_{\mathcal{K}}$.

D.2 $B_{r,\mathcal{S}}$ vs. $\underline{\gamma}_{\mathcal{K}}$

We show that the function $B_{r,\mathcal{S}}$ in (5.83) is a concave function of $\underline{\gamma}_{\mathcal{S}}$ for a fixed $\underline{\gamma}_{\mathcal{S}^c}$ and for all $\mathcal{S} \subseteq \mathcal{K}$. Recall the expression for $B_{r,\mathcal{S}}$ as

$$B_{r,\mathcal{S}} = C \left(\sum_{k \in \mathcal{S}} \frac{P_k}{N_r} - \frac{\left(\sum_{k \in \mathcal{S}} \sqrt{\gamma_k P_k} \right)^2}{N_r \left(1 - \sum_{k \in \mathcal{S}^c} \gamma_k \right)} \right) \quad (\text{D.25})$$

where we assume that

$$\sum_{k \in \mathcal{S}^c} \gamma_k = 1 - c < 1. \quad (\text{D.26})$$

Observe that $B_{r,\mathcal{S}}$ is maximized when $c = 1$, i.e., $\gamma_k = 0$ for all $k \in \mathcal{S}$, and minimized for $c = 0$. Further, comparing $B_{r,\mathcal{S}}$ and $I_{d,\mathcal{S}}$, one can see that for

$$\gamma_k = \begin{cases} P_k / (\sum_{k \in \mathcal{S}} P_k) & k \in \mathcal{S} \\ 0 & k \in \mathcal{S}^c \end{cases} \quad (\text{D.27})$$

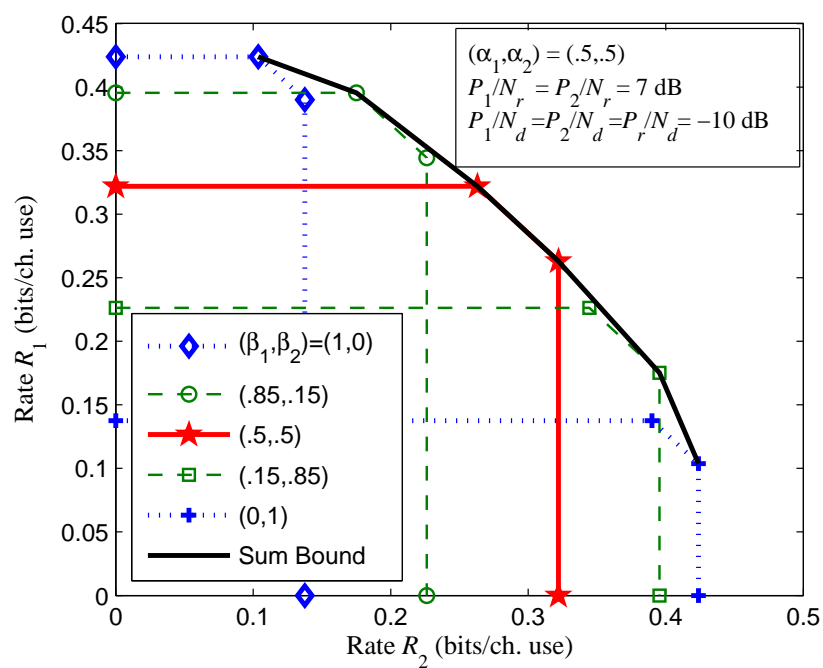


Figure D.1: Rate region achieved at the destination for a two-user MARC and $\alpha_1 = \alpha_2 = .5$.

$B_{r,\mathcal{S}}$ achieves its minimum, i.e., $B_{r,\mathcal{S}} = 0$.

We let

$$x = \left(\sum_{k \in \mathcal{S}} \sqrt{\gamma_k \lambda_k} \right) \quad (\text{D.28})$$

where, as defined for DF case 5.4, we have

$$P_{\max} = \max_{k \in \mathcal{K}} P_k \quad \text{and} \quad \lambda_k = P_k / P_{\max}. \quad (\text{D.29})$$

Substituting (D.28) in the expression for $B_{r,\mathcal{S}}$ in (D.25), we have

$$B_{r,\mathcal{S}} = C \left(\sum_{k \in \mathcal{S}} \frac{P_k}{N_r} - \frac{x^2 P_{\max}}{N_r c} \right). \quad (\text{D.30})$$

Differentiating $B_{r,\mathcal{S}}$ with respect to x we have

$$\frac{dB_{r,\mathcal{S}}}{dx} = \frac{-2P_{\max}}{N_r c} \cdot \left(1 + \sum_{k \in \mathcal{S}} \frac{P_k}{N_r} - \frac{x^2 P_{\max}}{N_r c} \right)^{-1} \quad (\text{D.31})$$

$$\frac{d^2 B_{r,\mathcal{S}}}{dx^2} = \frac{-2P_{\max}}{N_r c} \cdot \frac{\left(1 + \sum_{k \in \mathcal{S}} \frac{P_k}{N_r} + \frac{x^2 P_{\max}}{N_r c} \right)}{\left(1 + \sum_{k \in \mathcal{S}} \frac{P_k}{N_r} - \frac{x^2 P_{\max}}{N_r c} \right)^2} \quad (\text{D.32})$$

$$< 0 \quad (\text{D.33})$$

where the strict inequality in (D.33) follows since all terms in (D.32) are positive. Thus, we see that $B_{r,\mathcal{S}}$ is a concave function of x .

References

- [1] E. Telatar, "Capacity of multi-antenna Gaussian channels," *Europ. Trans. Telecommunications*, vol. 10, pp. 585–595, Nov. 1999.
- [2] G. J. Foschini and M. J. Gans, "On limits of wireless communications in a fading environment when using multiple antennas," *Wireless Personal Communications: Kluwer Academic*, vol. 6, no. 3, pp. 311–355, Mar. 1998.
- [3] A. Sendonaris, E. Erkip, and B. Aazhang, "User cooperation diversity - part I: System description," *IEEE Trans. Commun.*, vol. 51, no. 11, pp. 1927–1938, Nov. 2003.
- [4] G. Kramer, I. Marić, and R. D. Yates, "Cooperative communications," foundations and Trends in Networking, now Publishers Inc., to appear 2007.
- [5] E. C. van der Meulen, "Three-terminal communication channels," *Adv. Applied Probability*, vol. 3, pp. 120–154, 1971.
- [6] T. Cover and A. El Gamal, "Capacity theorems for the relay channel," *IEEE Trans. Inform. Theory*, vol. 25, no. 5, pp. 572–584, Sept. 1979.
- [7] F. M. J. Willems, "Informationtheoretical Results for the Discrete Memoryless Multiple Access Channel," Ph.D. dissertation, Doctor in de Wetenschappen Proefschrift, Katholieke Universiteit Leuven, Leuven, Belgium, Oct. 1982.
- [8] A. B. Carleial, "Multiple-access channels with different generalized feedback signals," *IEEE Trans. Inform. Theory*, vol. 28, no. 6, pp. 841–850, Nov. 1982.
- [9] J. N. Laneman, D. N. C. Tse, and G. Wornell, "Cooperative diversity in wireless networks: efficient protocols and outage behavior," *IEEE Trans. Inform. Theory*, vol. 50, no. 12, pp. 3062–3080, Dec. 2004.
- [10] G. Kramer, M. Gastpar, and P. Gupta, "Cooperative strategies and capacity theorems for relay networks," *IEEE Trans. Inform. Theory*, vol. 51, no. 9, pp. 3027–3063, Sept. 2005.
- [11] A. Host-Madsen and J. Zhang, "Capacity bounds and power allocation for the wireless relay channel," *IEEE Trans. Inform. Theory*, vol. 51, no. 6, pp. 2020–2040, June 2005.
- [12] L.-L. Xie and P. R. Kumar, "A network information theory for wireless communication: scaling laws and optimal operation," *IEEE Trans. Inform. Theory*, vol. 50, no. 5, pp. 748–767, May 2004.
- [13] M. A. Khojastepour, A. Sabharwal, and B. Aazhang, "On the capacity of 'cheap' relay networks," in *37th Annual Conf. Information Sciences and Systems*, Baltimore, MD, Mar. 2003.

- [14] K. Azarian, H. El Gamal, and P. Schniter, "On the achievable diversity-multiplexing tradeoff in half-duplex cooperative channels," *IEEE Trans. Inform. Theory*, vol. 51, no. 12, pp. 4152–4172, Dec. 2005.
- [15] M. Yuksel and E. Erkip, "Cooperative wireless systems: A diversity-multiplexing tradeoff perspective," Aug. 2007, to appear in the *IEEE Trans. Inform. Theory*.
- [16] A. S. Avestimehr and D. N. C. Tse, "Outage capacity of the fading relay channel in the low SNR regime," 2006, submitted to the *IEEE Trans. Inform. Theory*.
- [17] P. Gupta and P. R. Kumar, "The capacity of wireless networks," *IEEE Trans. Inform. Theory*, vol. 46, no. 2, pp. 388–404, Mar. 2000.
- [18] —, "Towards an information theory of large networks: An achievable rate region," *IEEE Trans. Inform. Theory*, vol. 49, no. 8, pp. 1877–1894, Aug. 2003.
- [19] S. Mathur, L. Sankaranarayanan, and N. B. Mandayam, "Coalitional games in receiver cooperation for spectrum sharing," in *Proc. 40th Annual Conference on Inform. Sciences and Systems (CISS)*, Princeton, NJ, Mar. 2006.
- [20] —, "Coalitional games in gaussian interference channels," in *Proc. 2006 IEEE Intl. Symp. Inform. Theory*, Seattle, WA, July 2006.
- [21] O. Ileri, S.-C. Mau, and N. B. Mandayam, "Pricing for enabling forwarding in self-configuring ad hoc networks," *IEEE JSAC*, vol. 23, no. 1, pp. 151–162, Jan. 2005.
- [22] H. Nama, "Resource allocation in cooperative and non-cooperative energy-constrained wireless networks," Ph.D. dissertation, Rutgers, The State University of New Jersey, North Brunswick, NJ, 2007. [Online]. Available: <http://www.winlab.rutgers.edu/~hithesh>
- [23] K. Martinez, R. Ong, and J. Hart, "Glacsweb: a sensor network for hostile environments," in *Proc. 1st Annual IEEE Conference on Sensor and Ad Hoc Communications and Networks*, Santa Clara, CA, Oct. 2004. [Online]. Available: <http://envisense.org/glacsweb/index.html>
- [24] G. Kramer and A. J. van Wijngaarden, "On the white Gaussian multiple-access relay channel," in *Proc. 2000 IEEE Int. Symp. Inform. Theory*, Sorrento, Italy, June 2000, p. 40.
- [25] B. Aazhang and J. R. Cavallaro, "Multitier wireless communications," *Wireless Personal Communications*, vol. 17, no. 2-3, pp. 323–330, June 2001.
- [26] L. Sankaranarayanan, G. Kramer, and N. B. Mandayam, "Capacity theorems for the multiple-access relay channel," in *Proc. 42nd Annual Allerton Conf. on Commun., Control, and Computing*, Monticello, IL, Sept. 2004, pp. 1782–1791.

- [27] —, “Hierarchical wireless networks: Capacity theorems using the constrained multiple-access relay channel model,” in *Proc. 38th Annual Asilomar Conf. Signals, Systems, and Computers*, Pacific Grove, CA, Nov. 2004, invited paper.
- [28] —, “Hierarchical sensor networks: Capacity theorems and cooperative strategies using the multiple-access relay channel model,” in *Proc. First IEEE Conference on Sensor and Ad Hoc Communications and Networks*, Santa Clara, CA, Oct. 2004.
- [29] R. G. Gallager, *Information Theory and Reliable Communication*. New York: John Wiley, 1968.
- [30] T. M. Cover and J. A. Thomas, *Elements of Information Theory*. New York: Wiley, 1991.
- [31] G. Kramer, “Models and theory for relay channels with receive constraints,” in *42nd Annual Allerton Conf. on Commun., Control, and Computing*, Monticello, IL, Sept. 2004.
- [32] H. G. Eggleston, *Convexity*. London: Cambridge University Press, 1958.
- [33] G. Kramer, M. Gastpar, and P. Gupta, “Capacity theorems for wireless relay channels,” in *Proc. 41st Annual Allerton Conf. on Commun., Control, and Computing*, Monticello, IL, Oct. 2003, pp. 1074–1083.
- [34] A. D. Wyner and J. Ziv, “The rate-distortion function for source coding with side information at the decoder,” *IEEE Trans. Inform. Theory*, vol. 22, no. 1, pp. 1–11, Jan. 1976.
- [35] L.-L. Xie and P. R. Kumar, “An achievable rate for the multiple-level relay channel,” *IEEE Trans. Inform. Theory*, vol. 51, no. 4, pp. 1348–1358, Apr. 2005.
- [36] A. Furuskar and K. Johansson, “An infrastructure cost evaluation of single- and multi-access networks with heterogeneous user behavior,” in *IEEE Vehicular Tech. Conf.*, Stockholm, Sweden, May 2005.
- [37] R. S. Cheng and S. Verdu, “Gaussian multiple-access channels with intersymbol interference: Capacity region and multiuser water-filling,” *IEEE Trans. Inform. Theory*, vol. 39, pp. 773–785, May 1993.
- [38] M. R. Aref, “Information flow in relay networks,” Ph.D. dissertation, Stanford University, Stanford, CA, Oct. 1980.
- [39] M. Sikora, J. N. Laneman, M. Haenggi, D. J. Costello, and T. E. Fuja, “Bandwidth- and power-efficient routing in linear wireless networks,” *IEEE Trans. Inform. Theory*, vol. 52, no. 6, pp. 2624–2633, June 2006.
- [40] C.-M. Zeng, F. Kuhlmann, and A. Buzo, “Achievability proofs of some multiuser channel coding theorems using backward decoding,” *IEEE Trans. Inform. Theory*, vol. 35, no. 6, pp. 1160–1165, Nov. 1989.

- [41] J. N. Laneman and G. Kramer, "Window decoding for the multiaccess channel with generalized feedback," in *Proc. 2004 IEEE Int. Symp. Inform. Theory*, Chicago, IL, June 27 - July 2, 2004, p. 281.
- [42] B. Rimoldi and R. Urbanke, "A rate-splitting approach to the Gaussian multiple access channel," *IEEE Trans. Inform. Theory*, vol. 42, no. 2, pp. 364–375, Mar. 1996.
- [43] A. Grant, B. Rimoldi, R. Urbanke, and P. Whiting, "Rate-splitting multiple access for discrete memoryless channels," *IEEE Trans. Inform. Theory*, vol. 47, no. 3, pp. 873–890, Mar. 2001.
- [44] A. Schrijver, *Combinatorial Optimization: Polyhedra and Efficiency*. New York: Springer-Verlag, 2003.
- [45] L. Sankaranarayanan, G. Kramer, and N. B. Mandayam, "Cooperation vs. hierarchy: An information-theoretic comparison," in *Proc. Int. Symp. Inf. Theory*, Adelaide, Australia, Sept. 2005, pp. 411–415.
- [46] L.-L. Xie and P. R. Kumar, "A multi-relay scheme for the multi-source multicast network," in *Proc. 2006 IEEE Intl. Symp. Inform. Theory*, Seattle, WA, July 2006, pp. 2383–2387.
- [47] —, "Multi-source, multi-destination, multi-relay wireless networks," Aug. 2006, this issue.
- [48] I. Maric and R. Yates, "Forwarding strategies for Gaussian parallel-relay networks," in *Proc. 2004 IEEE Int. Symp. Inform. Theory*, Chicago, IL, June 2004.
- [49] L. Sankaranarayanan, G. Kramer, and N. B. Mandayam, "Cooperative diversity in wireless networks: A geometry-inclusive analysis," in *Proc. 43rd Annual Allerton Conf. on Commun., Control, and Computing*, Monticello, IL, Sept. 2005.
- [50] Atheros Communications, "Power consumption and energy efficiency comparisons of wlan products," www.atheros.com/pt/whitepapers/atheros_power_whitepaper.pdf.
- [51] W. Heinzelman, A. Chandrakasan, and H. Balakrishnan, "Energy-efficient routing protocols for wireless microsensor networks," in *Proc. 33rd Hawaii Intl. Conf. Systems and Sciences*, Maui, HA, Jan. 2000, pp. 1–10.
- [52] L. Zheng and D. N. C. Tse, "Diversity and multiplexing: A fundamental tradeoff in multiple-antenna channels," *IEEE Trans. Inform. Theory*, vol. 49, no. 5, pp. 1073–1096, May 2003.
- [53] D. Chen, K. Azarian, and J. Laneman, "A case for amplify-and-forward relaying in the block-fading multi-access channel," Jan. 2007, submitted to the *IEEE Trans. Inform. Theory*.

- [54] J. N. Laneman, "Network coding gain of cooperative diversity," in *Proc. IEEE Military Comm. Conf. (MILCOM)*, Monterey, CA, Nov 2004.
- [55] —, "Limiting analysis of outage probabilities for diversity schemes in fading channels," in *Proc. IEEE Global Comm. Conf. (GLOBECOM)*, San Francisco, CA, Dec 2003.
- [56] D. Chen and J. N. Laneman, "The diversity-multiplexing tradeoff of the multi-access relay channel," in *Proc. 40th Annual Conference on Inform. Sciences and Systems (CISS)*, Princeton, NJ, Mar. 2006.
- [57] E. J. Duarte-Melo and M. Liu, "Data-gathering wireless sensor networks: organization and capacity," *Computer Networks (COMNET): Special Issue on Wireless Sensor Network*, vol. 43, no. 4, pp. 519–537, Nov. 2003.
- [58] L. Sankaranarayanan, G. Kramer, and N. B. Mandayam, "Offset encoding for multiaccess relay channels," Aug. 2006, to appear, *IEEE Trans. Inform. Theory*.
- [59] R. U. Nabar, H. Bölcskei, and F. W. Kneubühler, "Fading relay channels: Performance limits and space-time signal design," *IEEE JSAC Special issue on Fundamental Performance Limits of Wireless Sensor Networks*, 2003, accepted for publication.
- [60] T. H. Cormen, C. E. Leiserson, and R. L. Rivest, *Introduction to Algorithms*. Cambridge, MA: The MIT Press, 1990.
- [61] S. Verdú, "Spectral efficiency in the wideband regime," *IEEE Trans. Inform. Theory*, vol. 48, no. 6, pp. 1319–1343, June 2006.
- [62] A. Reznik, S. R. Kulkarni, and S. Verdú, "Capacity and optimal resource allocation in the degraded Gaussian relay channel with multiple relays," in *Proc. 40th Annual Allerton Conf. on Commun., Control, and Computing*, Monticello, IL, Oct. 2002.
- [63] A. El Gamal and M. Aref, "The capacity of the semideterministic relay channel," *IEEE Trans. Inform. Theory*, vol. 28, no. 3, p. 536, May 1982.
- [64] Y. Liang and V. Veeravalli, "Gaussian orthogonal relay channel: Optimal resource allocation and capacity," *IEEE Trans. Inform. Theory*, vol. 51, no. 9, pp. 3284–3289, Sept. 2005.
- [65] A. E. Gamal and S. Zahedi, "Capacity of relay channels with orthogonal components," 2006, accepted for publication *IEEE Trans. Inform. Theory*.
- [66] A. E. Gamal and N. Hassanpour, "Capacity theorems for the relay-without-delay channels," in *Proc. 43rd Annual Allerton Conf. on Commun., Control, and Computing*, Monticello, IL, Sept. 2005.

- [67] —, “Relay without delay,” 2006, submitted to the IEEE Trans. Inform. Theory.
- [68] G. Kramer, M. Gastpar, and P. Gupta, “Information-theoretic multi-hopping for relay networks,” in *International Zurich Seminar on Communications*, ETH Zurich, Switzerland, Feb. 2004, pp. 192–195.
- [69] V. Poor, *An Introduction to Signal Detection and Estimation*, 2nd. Ed. Springer, 1994.
- [70] Y. Liang and V. Veeravalli, “Resource allocation for wireless relay channels,” in *Proc. 38th Annual Asilomar Conf. Signals, Systems, and Computers*, Pacific Grove, CA, Nov. 2004.
- [71] J. A. Thomas, “Feedback can at most double Gaussian multiple access channel capacity,” *IEEE Trans. Inform. Theory*, vol. 33, no. 5, pp. 711–716, Sept. 1987.
- [72] I. Csiszár and J. Körner, *Information Theory: Coding Theorems for Discrete Memoryless Systems*. Budapest: Akadémiai Kiadó, 1981.
- [73] D. R. Cox, *Renewal Theory*. London: Methuen’s Monographs on Applied Probability and Statistics, 1967.
- [74] S. Boyd and L. Vandenberghe, *Convex Optimization*. Cambridge, UK: Cambridge University Press, 2004.

Curriculum Vitae

Lalitha Sankar

- 2007** PhD in Electrical and Computer Engineering, Rutgers - The State University of New Jersey
- 1994** M.S. in Electrical Engineering from University of Maryland, Baltimore County, Baltimore, MD
- 1992** B.Tech. in Engineering Physics from Indian Institute of Technology, Bombay, India
-
- 2003-2007** Graduate Research Assistant, WINLAB, Rutgers - The State University of New Jersey
- 2002-2003** Graduate Teaching Assistant, WINLAB, Rutgers - The State University of New Jersey
- 1996-2002** Senior Member of Technical Staff, Advanced Communications Technology Group, AT&T Shannon Labs, AT&T, Florham Park, NJ
- 1995-1996** Member of Technical Staff, AT&T Microelectronics, Allentown, PA
- 1994-1995** Advanced Engineer, Engineering R&D, Polaroid Corporation, Cambridge, MA
-
- 2007** L. Sankar, G. Kramer, and N. Mandayam, "Offset Encoding for Multiaccess Relay Channels," accepted, *IEEE Trans. Inform. Theory*, May 2007.
- 2006** S. Mathur, L. Sankaranarayanan, and N. Mandayam, "Coalitional games in cooperative radio networks," *Asilomar Conference on Signals, Systems, and Computers*, Pacific Grove, CA, Nov. 2007.
- S. Mathur, L. Sankaranarayanan, and N. Mandayam, "Coalitional games in Gaussian interference channels," *IEEE International Symposium on Information Theory*, Seattle, WA, Jul. 2007.
- S. Mathur, L. Sankaranarayanan, and N. Mandayam, "Coalitional games in receiver cooperation for spectrum sharing," *Conference on Information Systems and Sciences*, Princeton, NJ, Mar. 2007.

- 2005** L. Sankaranarayanan, G. Kramer, and N. Mandayam, "Cooperative Diversity in Wireless Networks: A Geometry-inclusive analysis," *Allerton Conference on Communications, Control, and Computing*, Monticello, IL, Sep. 2005.
- L. Sankaranarayanan, G. Kramer, and N. Mandayam, "Cooperation vs. Hierarchy: An Information-theoretic comparison," *International Symposium on Information Theory*, Adelaide, Australia, Sep. 2005.
- 2004** L. Sankaranarayanan, G. Kramer, and N. Mandayam, "Hierarchical Wireless Networks: Capacity Bounds using the Constrained Multiaccess relay channel model," *Asilomar Conference on Signals, Systems, and Computers*, Pacific Grove, CA, Nov. 2004.
- L. Sankaranarayanan, G. Kramer, and N. Mandayam, "Hierarchical Sensor Networks: Capacity Bounds and Cooperative Strategies using the Multiaccess relay channel model," *IEEE SECON Conference on Sensor and Ad Hoc Communications and Networks*, Santa Clara, CA, Oct. 2004.
- L. Sankaranarayanan, G. Kramer, and N. Mandayam, "Capacity Theorems for the Multiaccess relay channel," *Allerton Conference on Communications, Control, and Computing*, Monticello, IL, Sep. 2004.